APPENDIX A

QUESTIONNAIRE SURVEY AND RESULTS

TABLE OF CONTENTS

LIST OF FIGURES

LIST OF TABLES

A.1 INTRODUCTION

This appendix provides additional information and results from the questionnaire survey distributed to 52 different state transportation agencies described in Chapter 3. Twenty-nine of the fifty-two agencies responded. Among the agencies responding, thirteen reported no or minimal use of precast-prestressed bridge deck panels (full or partial-depth). Results from the sixteen states that reported using precast-prestressed panels are fully described in this appendix. Comments from the agencies reporting non-usage of this system are also included.

A.2 METHODOLOGY OF QUESTIONNAIRE SURVEY

A.2.1 Cover letter

The cover letter included with the questionnaire survey form is shown below.

Dear Sir or Madam:

The Missouri University of Science and Technology, under the Missouri Department of Transportation (MoDOT), is conducting a project investigation entitled "**Spalling Solution of Precast-Prestressed Bridge Deck Panels.**" The objectives of this research project are to investigate the problems and develop a cost-effective mitigation solution to the current concrete deterioration problems found in the existing partial-depth precast-prestressed concrete panels, as well as review improved design options for new construction for the panels that are currently used by the Missouri Department of Transportation.

MoDOT has been using the partial-depth precast paneling system since the early 1970's. Since then several bridge decks have been inspected and found to have rusted embedded steel reinforcement and concrete spalling issues in deck panels. MoDOT has contracted a research project with Missouri University of Science and Technology to investigate the cause and development of solutions including alternate design options for these panels.

The enclosed questionnaire is intended to generate ideas about the main cause(s) of the panel deterioration and gather ideas about ways to mitigate it. In addition, this questionnaire is aimed at compiling a list of important issues and parameters that need to be considered for possibly developing new design specifications for MoDOT.

We realize that you may receive many inquiries like this and that they take up a lot of your time. We, therefore, sincerely appreciate your efforts in sharing your department's experience with others who can benefit from it. At the completion of this project and with approval of MoDOT, a copy of research project report will be shared with you.

Sincerely,

Abdeldjelil Belarbi, Ph.D., P.E.
Principal Investigator

Lesley H. Sneed, Ph.D., P.E.
Co-Principal Investigator

A.2.2 Questionnaire survey form

A total number of twenty questions were included in the survey form. The questionnaire survey is shown below.

Questionnaire Survey

Bridge Research Program

Sponsored by

The Missouri Department of Transportation

SPALLING SOLUTION OF PRECAST-PRESTRESSED CONCRETE BRIDGE DECK PANELS

Conducted by

Missouri University of Science and Technology (Missouri S&T)

Please return this survey to:

Abdeldjelil Belarbi, PhD, PE
Distinguished Professor
Missouri University of Science and Technology
323 Butler-Carlton Hall
1401 North Pine Street
Rolla, MO 65409-1050
Email: belarbi@mst.edu
Fax: (573) 202-2117

PURPOSE OF THE QUESTIONNAIRE

This research is sponsored by Missouri Department of Transportation (MoDOT) and is being conducted by Missouri University of Science and Technology (Missouri S&T). The purpose of this survey is to collect objective data with regard to spalling problems observed in the soffit of the precast-prestressed concrete bridge deck panels and to request information about field data and/or research studies related to this issue. Your input will assist in the development of a detailed report and research summary that will compile the research findings and provide directions for future application and design approach.

GENERAL INFORMATION

Organization: __________

Respondent's name: __________

Position/Title: __________

Address: __________

Tel: __________ Fax: __________ E-mail: __________

PART I: DOCUMENTS REQUESTED

1. If possible, please provide us with a copy of design guidelines and specifications for construction of precast-prestressed concrete bridge deck panels in use by your organization.
2. Please complete the survey on the following pages. If it is more convenient, please call us at (573) 341-4478 to discuss this questionnaire.

PART II: BRIDGE DECK SYSTEMS

1. Has your DOT ever used a precast-prestressed paneling system for bridge decks? ☐ Yes ☐ No

   (If no, please go to question 2. If yes, please proceed to question 3.)

2. If your agency has never used the precast-prestressed concrete deck panels, why? Have you ever considered the use of this system? (Please skip to question 20.)

   ____

3. Which precast-prestressed concrete deck panel is primarily used in your state?

	Percentage of Panels
☐ Full-Depth Precast Panel	______ %
☐ Partial-Depth Precast Panel	______ %

4. What are the dimensions of the precast concrete bridge deck panels used?

   ____

5. When did your DOT first start to use precast concrete panels as bridge deck? How old are the bridges that have these components? __________

6. What type of reinforcement has been used in the concrete deck panels?

   ☐ Mild reinforcement ☐ Epoxy coated reinforcing steel ☐ Prestressing reinforcement
   ☐ Fiber reinforced polymer (FRP) reinforcing bars ☐ Other: __________

7. What is the specified 28-day compressive strength of concrete for the precast bridge deck panels?
☐ ≤ 4000 psi ☐ 6000 psi ☐ 8000 psi ☐ 10,000 psi Other: ____________

8. Has your DOT updated design guidelines for these deck systems? If so, please describe the main changes and the reasons for the changes. ____________

PART IIA: PARTIAL-DEPTH PANELS

9. What is the specified compressive strength of concrete for the cast-in-place (CIP) concrete topping slab? ☐ ≤ 3500 psi ☐ 4000 psi ☐ 5000 psi ☐ Other: ____________

10. What are the types and lengths of the curing process for the cast-in-place (CIP) concrete?

Procedures:	Duration:
☐ Moist curing method	____________ Days
☐ Liquid membrane curing compound method	____________ Days
☐ Waterproof cover method	____________ Days
☐ Other: ____________	____________ Days

11. How are panel joints constructed?
☐ Compressible filler ☐ None ☐ Other: ____________

PART IIB: FULL-DEPTH PANELS

12. How are panel joints constructed?
☐ Compressible filler ☐ None ☐ Other: ____________

PART III: PROBLEMS OBSERVED IN PRECAST CONCRETE DECK PANELS

13. Please indicate which of the following problems (if any) have been observed with these systems.

☐ Transverse cracks over the topping concrete at the location of joints
☐ Longitudinal cracks in CIP concrete topping along the girder line
☐ Cracks in the bottom side of panels
☐ Seepage at the joints
☐ Efflorescence in deck panels
☐ Rust stains of deck panels along the direction of prestressed tendons
☐ Concrete spalling at the joints
☐ Corrosion of reinforcement at the joints
☐ None
☐ Other: ____________

14. What, if any, attempts have been made to mitigate these problems?

- ☐ Linseed oil
- ☐ Epoxy injection
- ☐ Total deck surface treatment
- ☐ Shotcrete
- ☐ Deck crack pouring
- ☐ Chip seal
- ☐ Deck replacement
- ☐ None
- ☐ Other: ______________________

15. How frequently are deicing procedures typically used, and what is the typical deicing solution material makeup?

Deicing Solution:	Frequency:
☐ Conventional road salt	______ Per/year
☐ Chloride salts	______ Per/year
☐ Organic products	______ Per/year
☐ Nitrogen products	______ Per/year
☐ Abrasives	______ Per/year
☐ Other: ______	______ Per/year
☐ None	Never

16. How frequently are the deck joints (either panel to panel in the case of full-depth precast panels or contraction joints in concrete CIP topping) maintained, and what are the maintenance tactics?

Tactic:	Frequency:
☐ Hot pour sealing	______ Per/year
☐ Silicone sealing	______ Per/year
☐ Polytite sealing	______ Per/year
☐ Other: ______	______ Per/year
☐ None	Never Per/year

17. Which type of girder is used to support the precast concrete deck panel?

	Percentage of girders:
☐ Steel girders	______ %
☐ Prestressed concrete girders	______ %

PART IV: MITIGATIONS & NEWLY-DEVELOPED TECHNOLOGIES

18. If your DOT has experienced any of the above mentioned problems, do you have specific mitigation or repair methods to resolve them? If available please list below.
☐ Yes ☐ No Please explain: ______________________

19. Does your DOT have specific guidelines for the repair of deteriorated precast concrete deck panels? ☐ Yes ☐ No

20. Would your agency be willing to share any report related to the repair/mitigation of spalling and corrosion-related issues in your concrete bridge system? ☐ Yes ☐ No

A.3 Survey Results

This section presents the results of questionnaire survey with respect to each question.

A.3.1 Part II: Bridge deck system

A.3.1.1 Questions 1 & 2: Usage of a precast-prestressed paneling system

Table A-1 lists the 16 responding state agencies that reported use of precast-prestressed paneling systems. Table A-2 lists the 13 responding state agencies that reported non-usage of this system and includes corresponding comments received by those agencies.

Table A-1 State Agencies Reporting Use of Precast-Prestressed Paneling Systems

No.	State
1	Alaska
2	Arkansas
3	Colorado
4	Florida
5	Georgia
6	Hawaii
7	Iowa
8	Kansas
9	Kentucky
10	Michigan
11	Minnesota
12	Missouri
13	Nebraska
14	Oklahoma
15	Tennessee
16	Texas

Table A-2 State Agencies Reporting Non-Usage of Precast-Prestressed Paneling Systems and Related Comments

No.	State	Comments
1	Delaware	We have considered it in a couple of instances but found alternative solutions.
2	Idaho	Generally our contractors are not acquainted with deck panels. We have heard that there can be issues with workmanship and (partial-depth) grout strip (camber strip) with contractors who are not familiar with this approach.
3	Louisiana	In Louisiana, even though we have a detail for P/C P/S Concrete Bridge Deck Panels under Optional Span Detail, this type of deck is seldom used. A very high percentage of our deck are SIP or wood formwork in place. If the Empirical Design method is used, P/S P/C Concrete Bridge Deck Panels are not used.
4	Maine	We have used some partial-depth precast deck panels. However, their uses have been limited because it is difficult for bridge maintenance inspectors to look at the cast in place portion of deck over time. I am not aware of any spalling problems with these deck panels.
5	Maryland	We have only used once for a temporary measure. The panels are no longer in service. We don't use because the end ride surface isn't as good as a cast-in-place deck.
6	Montana	Not cost effective without need for rapid construction.
7	New Mexico	We have only used precast deck panels. Have yet to use prestressed panels but hope to in the near future.
8	North Dakota	We tried in 1978 and contractor had difficulty installing and ended up with bad ride. Program was discontinued.- was a one time research project.
9	Oregon	Your questionnaire seems to be geared towards those agencies that have a history of precast deck panels. Oregon does not have any significant history with precast deck panels. Therefore, we do not have any specifications for deck panels or any standardized repair procedures. For this reason, I would like to just mention a few things about our direction rather than send you a mostly blank questionnaire. We are in the early stages of our own research. We are looking at precast concrete deck panels (possibly prestressed) as a way to improve abrasion resistance. At this point we are still working on optimizing a concrete mix to meet the objective of improved abrasion resistance. Should we be able to show significant improvement in abrasion resistance, we then intend to place precast panels on a trial bridge. Oregon's interest is focused on full-depth panels. We are not considering partial-depth panels. We have not settled on the compressive strength we intend to require, but are expecting to fall somewhere between 6,000 and 8,000 psi. We will likely use prestressing strand and black steel in our precast deck panels. We are interested in evaluating FRP reinforcing bars for some applications, but are not considering them in precast panels. We are also evaluating various curing options, but are likely to settle on a combination of steam curing and liquid curing compound.
10	Pennsylvania	No comment
11	South Dakota	There has not been much interest from our local contractors to utilize them and not many critical sites where formwork construction time or removal are a big issue. We have also had concern over reflective cracking at panel joints/edges through topping slab.
12	Vermont	We do have a section in our prestress specifications that covers the production of them. It could possibly be the designers in our structures section are not aware of the systems or familiar enough with them. They may also be concerned of reflective cracking at the joints.
13	Wyoming	We have considered the system only. We have not chose to utilize them at this time.

A.3.1.2 Question 3: Type of precast-prestressed concrete deck panel

Table A-3 Type of PPC Panels

No.	State	Percentage of Panels	
		Full-Depth	Partial-Depth
1	Alaska	33	66
2	Arkansas	100	0
3	Colorado	95	5
4	Florida		
5	Georgia	100	0
6	Hawaii	100	0
7	Iowa	83.33	16.67
8	Kansas	100	0
9	Kentucky	100	0
10	Michigan	100	
11	Minnesota	100	0
12	Missouri	90	10
13	Nebraska	0	100
14	Oklahoma	100	
15	Tennessee	100	0
16	Texas	100	0

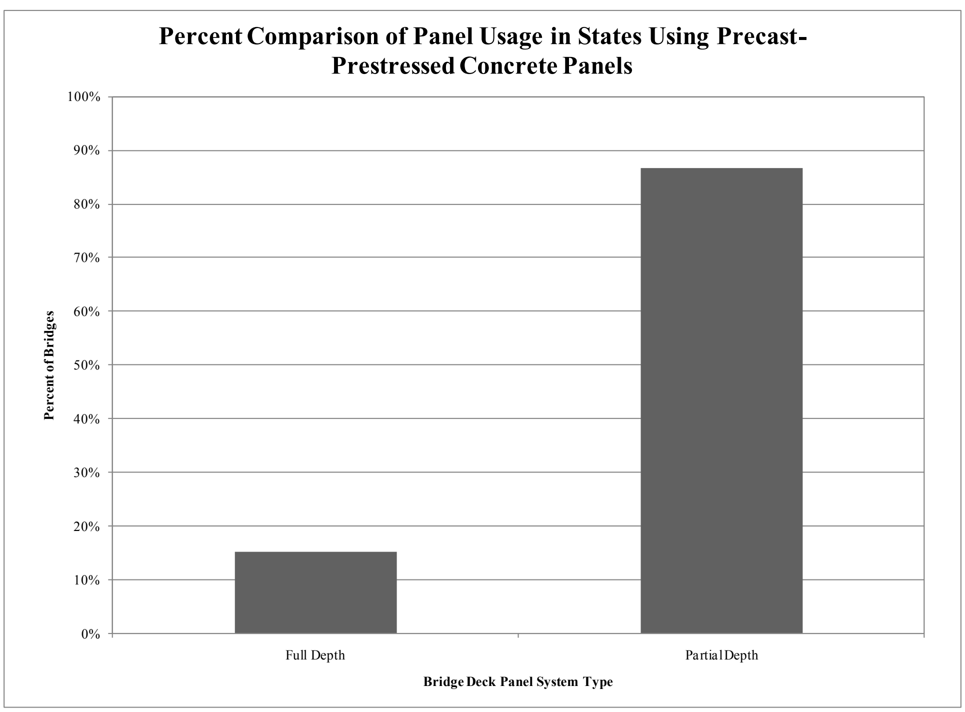

Figure A-1 Survey Results of Question 3

A.3.1.3 Question 4: Panel Dimensions

Table A-4 Thickness of Panels

No.	State	Panel Thickness (in.)
1	Alaska	8
2	Arkansas	No response
3	Colorado	No response
4	Florida	No response
5	Georgia	6
6	Hawaii	3.5
7	Iowa	3.5
8	Kansas	3
9	Kentucky	No response
10	Michigan	No response
11	Minnesota	3.5
12	Missouri	3
13	Nebraska	No response
14	Oklahoma	4
15	Tennessee	3.5
16	Texas	4

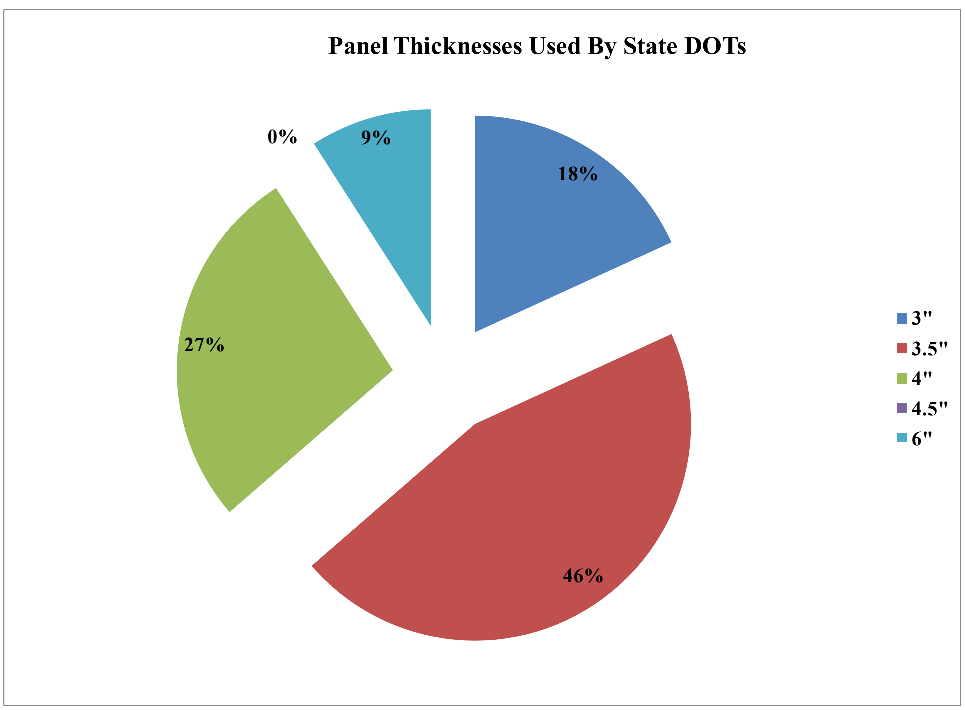

Figure A-2 Survey Results of Question 4

A.3.1.4 Question 5: Panel Age

Table A-5 Age of Panels

No.	State	Age (year)
1	Alaska	20
2	Arkansas	0
3	Colorado	16
4	Florida	40
5	Georgia	28
6	Hawaii	14
7	Iowa	25
8	Kansas	20
9	Kentucky	10
10	Michigan	NA
11	Minnesota	8
12	Missouri	35
13	Nebraska	5
14	Oklahoma	15
15	Tennessee	33
16	Texas	25

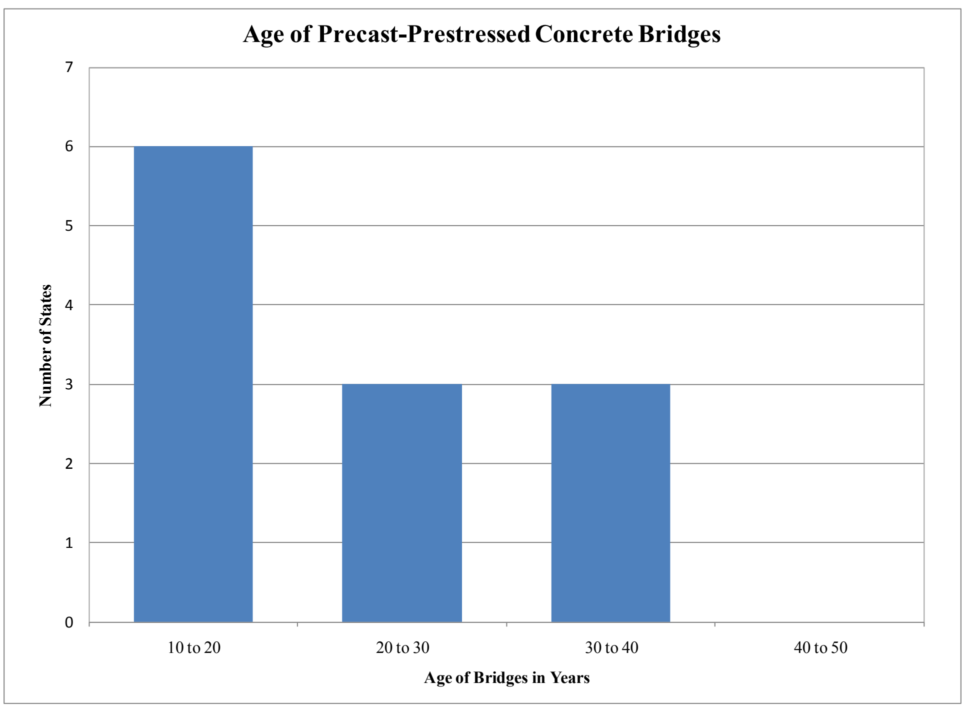

Figure A-3 Survey Results of Question 5

A.3.1.5 Question 6: Reinforcement Type

Table A-6 Types of Panel Reinforcement

No.	State	Mild Reinforcement	Epoxy Coated Reinforcing Steel	Prestressing Reinforcement	FRP Reinforcing Bars
1	Alaska	O	O		
2	Arkansas		O		
3	Colorado	O			O
4	Florida	O			
5	Georgia	O			O
6	Hawaii	O			O
7	Iowa	O	O		O
8	Kansas	O	O		
9	Kentucky	O	O		
10	Michigan		O		
11	Minnesota	O	O	O	
12	Missouri	O			
13	Nebraska	O	O		
14	Oklahoma	O		O	
15	Tennessee	O			
16	Texas	O			

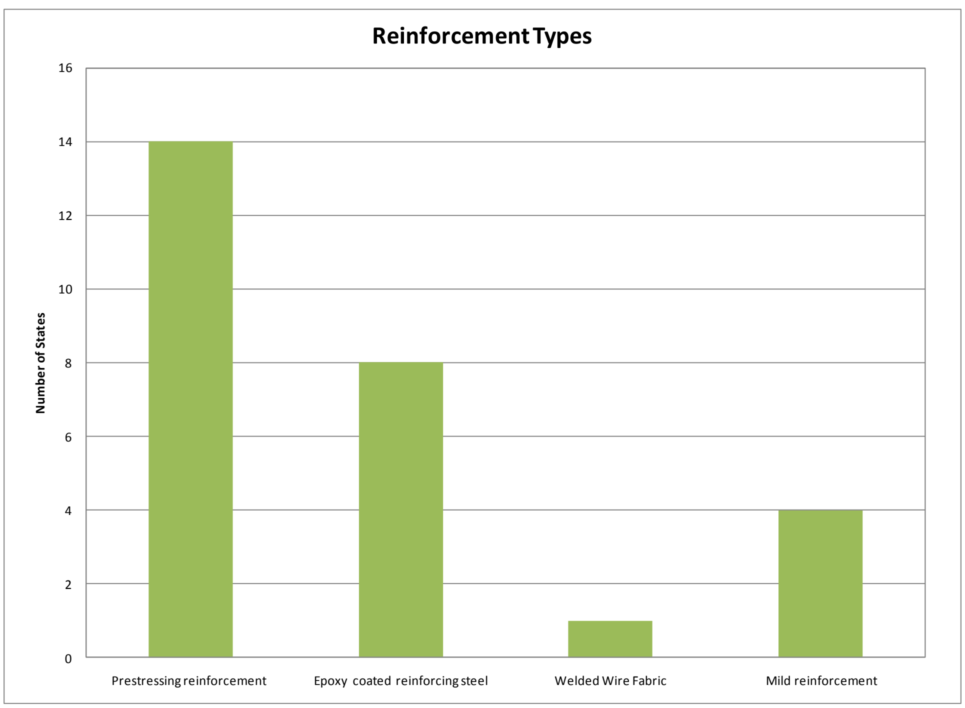

Figure A-4 Survey Results of Question 6

A.3.1.6 Question 7: Specified Compressive Strength of Precast Panel

Table A-7 Specified Compressive Strength of Panel

No.	State	≤ 4,000 psi	≤ 6,000 psi	≤ 8,000 psi	≤ 10,000 psi
1	Alaska		6,000		
2	Arkansas		5,800		
3	Colorado		5,000		
4	Florida				
5	Georgia		5,000		
6	Hawaii		6,000		
7	Iowa				10,000
8	Kansas	4,000			
9	Kentucky				
10	Michigan	4,000			
11	Minnesota		6,000		
12	Missouri		6,000		
13	Nebraska			8,000	
14	Oklahoma		5,000		
15	Tennessee	4,000			
16	Texas		5,000		

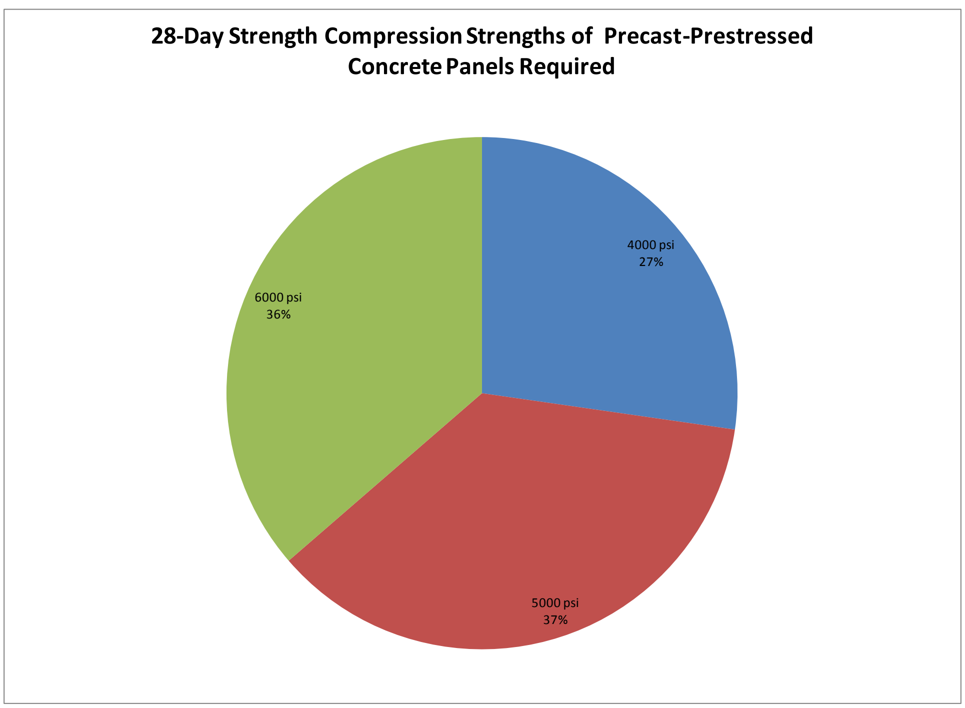

Figure A-5 Survey Results of Question 7

A.3.1.7 Question 8: Design Guidelines

Table A-8 Updated Design Guidelines

No.	State	Yes	No	Comments
1	Alaska	O		Full-depth, precast deck planks (sometimes prestressed) were originally used to replace worn glue-lam timber decks at remote locations. These deck planks are not stressed longitudinally and were intended as a more durable version of the older timber deck system
2	Arkansas		O	
3	Colorado		O	
4	Florida		O	
5	Georgia	O		(Used partial-depth panels a lot in time period 1980-1995; however, the contractors stopped using them) Took them out of specifications
6	Hawaii		O	
7	Iowa	O		Set 28 day strength of panels to 10000 psi
8	Kansas	O		LRFD Loads
9	Kentucky		O	
10	Michigan		O	
11	Minnesota	O		We used information from MoDOT
12	Missouri	O		Panel thickness reduced from 3.5" to 3" to increase top concrete thickness from 5" to 5.5" to reduce reflective cracking at the joints where panels meet. Concrete strength rose from 5000 psi to 6000 psi in order to provide corrosion protection to the strands. Min. joint filler increased 3/4" to 1" to permit better consolidation and firm bearing
13	Nebraska		O	
14	Oklahoma		O	
15	Tennessee	O		We updated standard for the support system during panel placement and deck pours. Previously, the bituminous strips supporting panels were placed on beam flanges. This becomes unwieldy when correcting for camber and grade differences. We now require support outside the flanges as shown
16	Texas		O	

A.3.1.8 Question 9: Concrete Strength of CIP Topping Concrete

Table A-9 Compressive Strength of Concrete for CIP Topping Concrete

No.	State	≤ 3,500 psi	≤ 4,000 psi	≤ 5,000 psi	Other
1	Alaska				5,800
2	Arkansas			5,000	
3	Colorado				
4	Florida	3,500			
5	Georgia		4,000		
6	Hawaii	3,500			
7	Iowa		4,000		
8	Kansas			5,000	
9	Kentucky		4,000		
10	Michigan		4,000		
11	Minnesota		4,000		
12	Missouri				
13	Nebraska		4,000		
14	Oklahoma		4,000		
15	Tennessee		4,000		
16	Texas				5,800

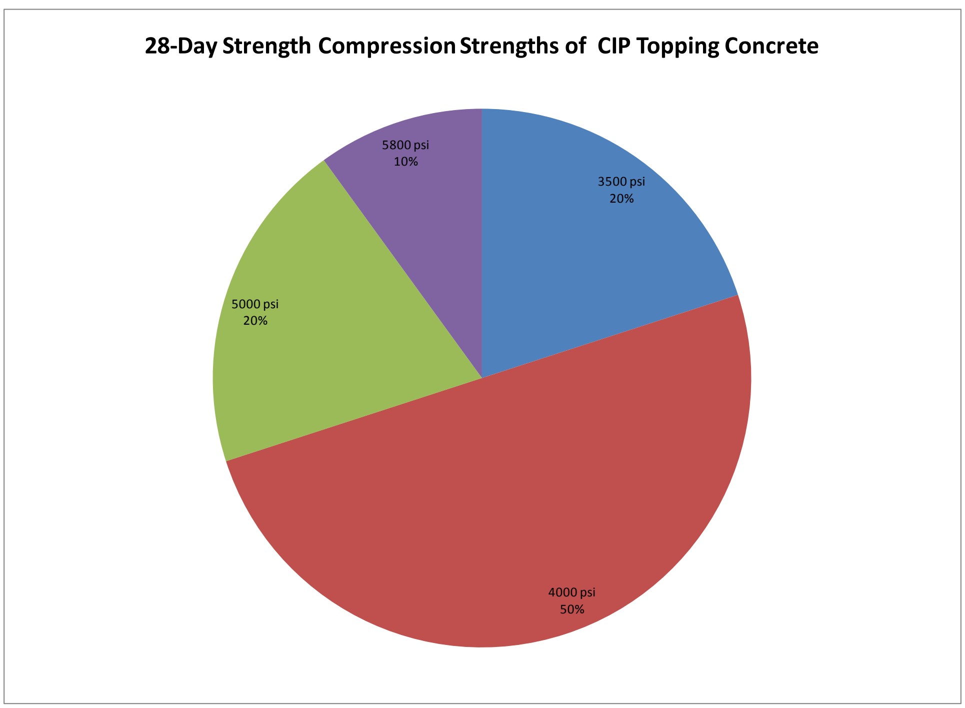

Figure A-6 Survey Results of Question 9

A.3.1.9 Question 10: Curing

Table A-10 Types and Lengths of Curing for CIP Topping Concrete

No.	State	Moist Curing	Liquid Membrane Curing Compound	Waterproof Cover	Others
1	Alaska				No response
2	Arkansas	14 days			
3	Colorado		O	O	
4	Florida				No response
5	Georgia	5 days		5 days	
6	Hawaii	7 days	7 days		
7	Iowa			4 days	
8	Kansas	7 days			
9	Kentucky	O			
10	Michigan	7 days			
11	Minnesota	7 days			
12	Missouri	7 days	9 days		
13	Nebraska				No response
14	Oklahoma	7 days			
15	Tennessee	5 days	O		
16	Texas	8 days		10 days	

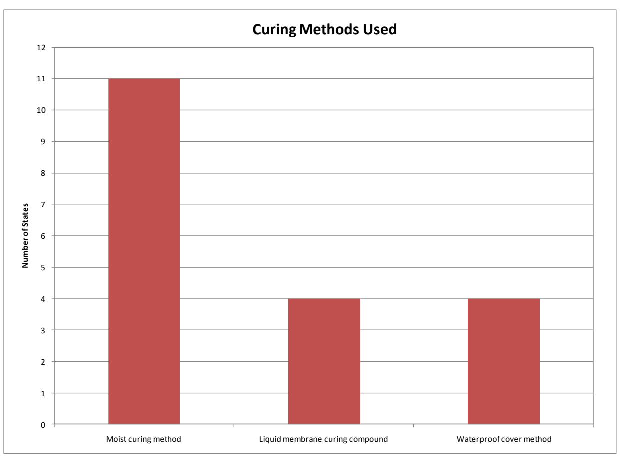

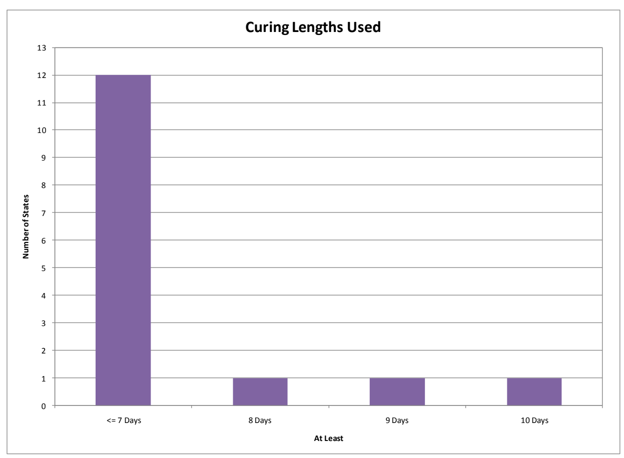

Figure A-7 Survey Results of Question 10

A.3.1.10 Questions 11 & 12: Construction of Deck Joint

Table A-11 Panel Joints of Partial-Depth Panels

No.	State	Compressive Filler	CIP Concrete	Tight Fit	Butt Joints	None
1	Alaska					O
2	Arkansas					O
3	Colorado					O
4	Florida					O
5	Georgia					O
6	Hawaii	O*				
7	Iowa		O			
8	Kansas	O				
9	Kentucky					O
10	Michigan					O
11	Minnesota			O		
12	Missouri	O				
13	Nebraska					O
14	Oklahoma					O
15	Tennessee				O**	
16	Texas					O

*Edges of panels are beveled to slightly above the bottom with compressible filler placed to seal the joint prior to placement of topping.
**Transverse cracking is inevitable as wet concrete will shrink differentially than beams or in this case, beams and deck panels. If decks are placed full depth, cracks occur every 4 ft, with panels, every 8 ft.

Table A-12 Panel Joints of Full-Depth Panels

No.	State	Compressive Filler	CIP Concrete	Grouted to Female Joints
1	Alaska	O		
2	Arkansas			
3	Colorado			O
4	Florida			
5	Georgia			
6	Hawaii			
7	Iowa		O	
8	Kansas			
9	Kentucky			
10	Michigan			
11	Minnesota			
12	Missouri			
13	Nebraska	O		
14	Oklahoma			
15	Tennessee			
16	Texas			

A.3.2 Part III: Problems observed in precast concrete deck panels

A.3.2.1 Question 13: Observed problems

Table A-13 Problem Description

No.	Observed Problems
1	Transverse cracks in CIP
2	Longitudinal cracks in CIP
3	Cracks in the bottom side of panels
4	Seepage at the Joints
5	Efflorescence at the joints
6	Rust stains of deck panels along tendons
7	Concrete spalling at the joints
8	Corrosion of Reinforcement

Table A-14 Observed Problems in Precast Concrete Deck System

No.	State	1	2	3	4	5	6	7	8
1	Alaska				O				
2	Arkansas								
3	Colorado	O		O	O	O			
4	Florida		O						
5	Georgia								
6	Hawaii								
7	Iowa								
8	Kansas	O	O						
9	Kentucky								
10	Michigan	O	O	O	O				
11	Minnesota	O	O						
12	Missouri	O	O	O	O		O	O	O
13	Nebraska								
14	Oklahoma	O							
15	Tennessee								
16	Texas	O	O						
Sum		***7***	***6***	***3***	***4***	***1***	***1***	***1***	***1***

A.3.2.2 Question 14: Mitigation methods

Table A-15 Description of Mitigation Methods

No.	Observed Problems
1	Polymer overlay
2	Epoxy injection
3	Deck replacement
4	Deck crack pouring
5	Chip seal
6	HMWMA
7	Water-proofing membrane w/asphalt overlay
8	Concrete sealer
9	Total deck surface treatment
10	Linseed oil

Table A-16 Mitigation Methods for Observed Problems

No.	State	1	2	3	4	5	6	7	8	9	10
1	Alaska							O			
2	Arkansas										
3	Colorado		O		O					O	
4	Florida		O	O							
5	Georgia										
6	Hawaii										
7	Iowa										
8	Kansas	O									
9	Kentucky										
10	Michigan										
11	Minnesota				O						
12	Missouri			O		O			O	O	O
13	Nebraska										
14	Oklahoma						O				
15	Tennessee										
16	Texas				O	O					
Sum		***1***	***2***	***2***	***3***	***2***	***1***	***1***	***1***	***2***	***1***

A.3.2.3 Question 15: Deicing procedure

Table A-17 Frequency of Deicing Procedures and Materials (per year)

No.	State	Conventional Road salt	Chloride salts	Brine solution	Abrasives	Magnetism Chloride	None
1	Alaska						O
2	Arkansas						O
3	Colorado				1		
4	Florida						O
5	Georgia	1				1	
6	Hawaii						O
7	Iowa	varies	O				
8	Kansas	10	40				
9	Kentucky	15	15				
10	Michigan	O					
11	Minnesota	20	20				
12	Missouri	30					
13	Nebraska		O				
14	Oklahoma	2	10				
15	Tennessee	10		15			
16	Texas	varies					

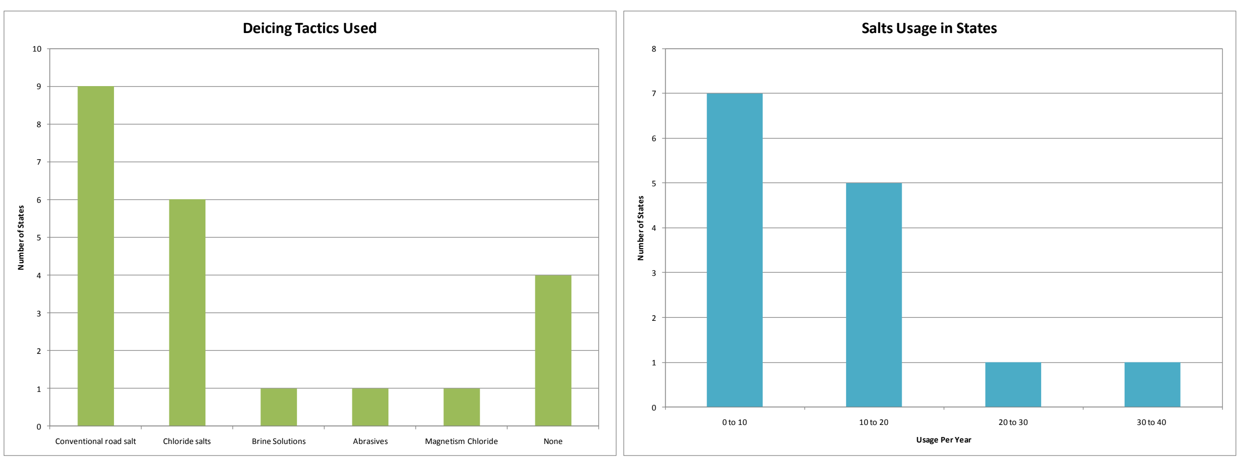

Figure A-8 Survey Results of Question 15

A.3.2.4 Question 16: Maintenance of deck joints

Table A-18 Period of Maintenance of Deck Joints and Materials (years)

No.	State	Silicon sealing	Hot pour sealing	Methacrylate resin treatment	None
1	Alaska	5			
2	Arkansas				O
3	Colorado			O	
4	Florida				O
5	Georgia	0.1			
6	Hawaii				O
7	Iowa		O		
8	Kansas				O
9	Kentucky				O
10	Michigan				O
11	Minnesota	2-3			
12	Missouri		O		
13	Nebraska				O
14	Oklahoma	At construction			
15	Tennessee				O
16	Texas				O

A.3.2.5 Question 17: Girder types

Table A-19 Types of Girders Supporting Precast Concrete Deck Panels (%)

No.	State	Steel Girders	Prestressed Concrete Girders	Other
1	Alaska	100		
2	Arkansas	100		
3	Colorado	10	90	
4	Florida		100	
5	Georgia		100	
6	Hawaii		100	
7	Iowa	20	80	
8	Kansas	5	10	85
9	Kentucky	100		
10	Michigan		100	
11	Minnesota		100	
12	Missouri	40	60	
13	Nebraska	100		
14	Oklahoma	50	50	
15	Tennessee	30	50	20
16	Texas	5	95	

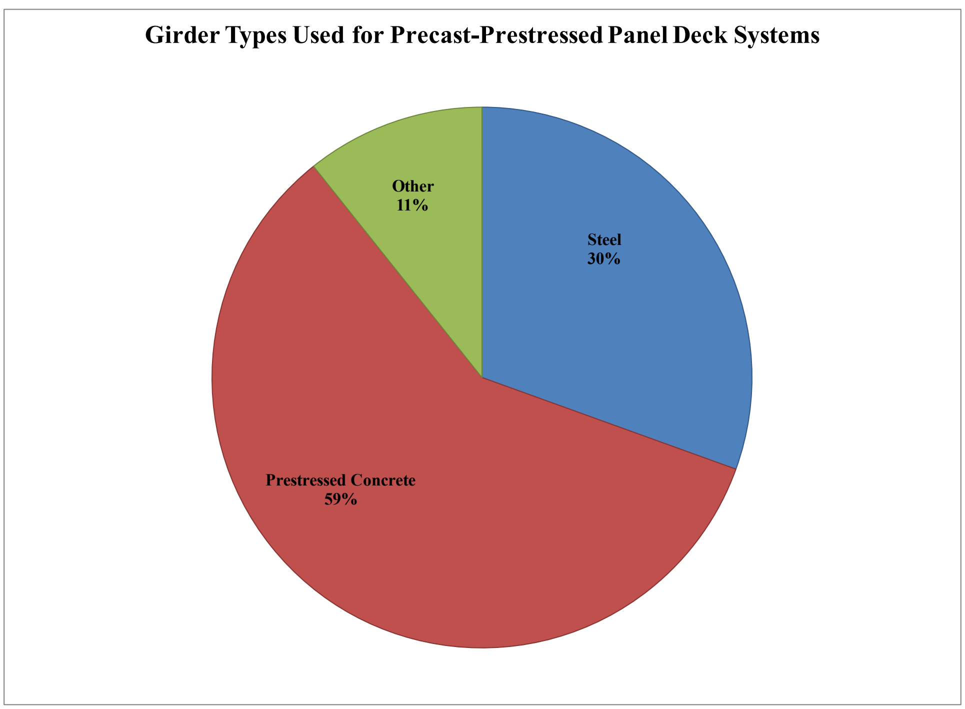

Figure A-9 Survey Results of Question 17

APPENDIX B

FIELD INVESTIGATIONS

TABLE OF CONTENTS

LIST OF FIGURES

LIST OF TABLES

B.1 INTRODUCTION

This appendix provides data obtained during the field investigation of Bridge A4709 described in Chapter 4.

B.2 CONTENTS

Tables B-1 and B-2 present the half-cell potential and resistivity data from Bridge A4709 respectively. Table B-3 presents calibrated rebound hammer compressive strength values from panels on Bridge A4709. Table B-4 summarizes core depth, reinforcement encountered, bottom surface type, chloride ion content, and carbonation depth data from cores taken from Bridge A4709. Figure B-1 show visual inspection data observed from the bottom surface of the bridge deck, respectively including efflorescence, water staining, spalling, and discoloration line locations. Figure B-2 shows visual inspection data observed from the top surface of the bridge deck, including crack maps and drain locations. Photos of cores taken from Bridge A4709 are shown in Figure B-3.

Table B-1 Half-cell Potential Data from Bridge A4709

Panel	Potential Difference (mV)*	Tendon Description	Corrosion
D23-22	-583	Fully exposed and fractured	probable
	-524	Fully exposed and fractured	probable
	-538	Fully exposed and fractured	probable
	-497	Fully exposed and fractured	probable
	-514	Fully exposed and fractured	probable
	-454	Partially exposed	probable
	-460	Partially exposed	probable
	-388	Partially exposed	probable
	-365	Partially exposed	probable
D22-23	-600	Partially exposed	probable
	-635	Partially exposed	probable
	-479	Partially exposed	probable
	-300	Partially exposed	probable
D23-24	-445	Fully exposed, not fractured	probable
	-362	Fully exposed, not fractured	probable
	-383	Fully exposed, not fractured	probable
	-320	Fully exposed, not fractured	probable
	-560	Fully exposed, not fractured	probable
	-517	Fully exposed, not fractured	probable
	-570	Fully exposed, not fractured	probable
	-675	Fully exposed, not fractured	probable
D24-23	-395	Partially exposed	probable
	-407	Partially exposed	probable
	-376	Partially exposed	probable
	-320	Partially exposed	probable
D23-24	-445	Partially exposed	probable
	-410	Partially exposed	probable
	-420	Partially exposed	probable
	-400	Partially exposed	probable
	-436	Partially exposed	probable

*Potential difference levels less than -500 mV correspond to corrosion levels producing visible evidence of corrosion; -350 to -500 mV corresponds to a 95% chance of corrosion; -200 to -350 corresponds to a 50% chance of corrosion; and more than -200 corresponds to 5% chance of reinforcement being corroded

Table B-2 Resistivity Data from Bridge A4709

Panel	Resistivity (kΩcm)	Current %	Reliable*	Corrosion Probability
A24-25	47	100	yes	unlikely
A24-25	35	90	yes	unlikely
A24-25	99	20	no	-
A24-25	23	100	yes	unlikely
A24-25	13	100	yes	unlikely
A24-25	77	42	no	-
A23-24	55	50	yes	unlikely
A23-24	30	100	yes	unlikely
A23-24	56	100	yes	unlikely
A23-24	63	100	yes	unlikely
A23-24	51	100	yes	unlikely
A22-23	38	36	no	-
A22-23	42	61	yes	unlikely
A22-23	34	100	yes	unlikely
A22-23	18	100	yes	unlikely
A22-23	62	48	no	-
B24-25	0	-	-	-
B23-24	0	-	-	-
B22-23	0	-	-	-
C24-25	29	100	yes	unlikely
C24-25	47	60	yes	unlikely
C24-25	99	47	no	-
C23-24	77	41	no	-
C23-24	49	81	yes	unlikely
C23-24	21	78	yes	unlikely
C23-24	39	52	yes	unlikely
C23-24	46	48	no	-
C23-24	95	42	no	-
C23-24	87	28	no	-
C23-24	50	51	yes	unlikely
C23-24	59	55	yes	unlikely
C22-23	51	64	yes	unlikely
D24-25	99	100	yes	unlikely
D24-25	99	72	yes	unlikely
D24-25	99	98	yes	unlikely
D24-25	99	100	yes	unlikely
D24-25	75	100	yes	unlikely
D24-25	56	100	yes	unlikely
D24-25	16	100	yes	unlikely

D24-25	36	79	yes	unlikely
D24-25	36	60	yes	unlikely
D24-25	38	65	yes	unlikely
D24-25	26	89	yes	unlikely
D24-25	53	42	no	-
D23-24	21	61	yes	unlikely
D23-24	68	50	yes	unlikely
D23-24	99	38	no	-
D23-24	18	61	yes	unlikely
D22-23	41	44	no	-
D22-23	33	100	yes	unlikely
D22-23	21	100	yes	unlikely
D22-23	10	100	yes	possible
D22-23	14	76	yes	unlikely
D22-23	23	100	yes	unlikely
D22-23	16	100	yes	unlikely
D12-13	64	66	yes	unlikely
D12-13	85	66	yes	unlikely
D12-13	99	76	yes	unlikely
D12-13	53	82	yes	unlikely
D12-13	99	48	no	-
D12-13	99	20	no	-
D12-13	99	32	no	-
D12-13	99	10	no	-
D12-13	99	27	no	-
D12-13	99	20	no	-
D12-13	99	42	no	-
D12-13	99	45	no	-
C11-12	99	60	yes	unlikely
C11-12	99	80	yes	unlikely
C11-12	99	68	yes	unlikely
C11-12	99	100	yes	unlikely
C11-12	51	100	yes	unlikely
C11-12	55	75	yes	unlikely
C11-12	37	-	no	-
C11-12	84	-	no	-
C12-13	0	-	-	-
C13-14	0	-	-	-
B13-14	0	-	-	-
B12-13	0	-	-	-
B11-12	0	-	-	-

A11-12	55	95	yes	unlikely
A11-12	99	32	no	-
A11-12	30	100	yes	unlikely
A11-12	54	100	yes	unlikely
A11-12	66	100	yes	unlikely
A11-12	52	100	yes	unlikely
A11-12	29	100	yes	unlikely
A12-13	99	10	no	-
A12-13	99	18	no	-
A13-14	99	12	no	-
A13-14	99	10	no	-

* A reading with a current percentage between 50% and 100% indicates a reliable reading, between 20% and 50% indicates the value is not exact and any readings below 20% indicate a very poor connection between the four-prong probe and the concrete of interest (IAEA 2002).

Table B-3 Rebound Hammer Compressive Strength Values for Each Panel from Bridge A4709

Panel Number	Average compressive strength calibrated with panel results (psi)[1]
A23-A24	6350
D24-D25[3]	7520
D23-D24[3]	7590
B25-B26	7650
C26-C27[3]	7810
C24-C25[3]	7930
A26-A27	7970
C23-C24[3]	8020
A25-A26	8150
B26-B27	8120
A24-A25	7630
B24-B25	8170
B23-B24	8200
D25-D26[3]	8350
A11-A12	8420
C13-C14	8420
C25-C26[3]	8450
B13-B14	8610
A13-A14	8310
C12-C13[2]	8590
B12-B13	8640
A12-A13	8640
C14-C15	8780
B14-B15	8830
D14-D15	8870
D13-D14	9210
D12-D13[2]	9260

[1]Values reported are the average of 10 readings
[2] Panels with one cracked and/or spalled edge
[3] Panels with two cracked and/or spalled edges

Table B-4 Summary of Core Data from Bridge A4709

Core ID	Depth of core (in.)	Depth of reinforcement encountered (in.)	Bottom surface of core	Sampling Depths (in.)	lb Cl-/yd^3	Corrosion Possibility	Carbonation Depth (mm)
C-1	4.5	4.5	broken	3	0.332	Not Likely	1 mm
C-2	5.5	None	smooth	3	0.224	Not Likely	1 mm or less
				4	1.445	Possible	
C-3	6.125	None	smooth	3	2.610	Possible	1 mm
				4	2.614	Possible	
				5	1.377	Possible	
C-4	3.125	3.125	broken	2	0.643	Not Likely	less than 1 mm
C-5	6.5	None	broken	3	0.257	Not Likely	less than 1 mm
				4	0.363	Not Likely	
				5	0.115	Not Likely	
C-6	6.625	3.875	broken	3	0.263	Not Likely	1-2 mm
				4	0.100	Not Likely	
				5	0.252	Not Likely	
C-7	6.5	4.75	smooth	3	0.279	Not Likely	1- 2 mm
				4	0.181	Not Likely	
				5	0.268	Not Likely	
C-8	6.375	4.5	smooth	3	0.221	Not Likely	1 mm, 11 mm at large void
				4	0.183	Not Likely	
				5	0.212	Not Likely	
C-9	7	6.875	broken	3	0.189	Not Likely	1 mm, 11 mm in crack
				4	0.328	Not Likely	
				5	0.230	Not Likely	
C-10	7.125	4.25	broken	3	6.532	Possible	less than 1 mm
				4	5.393	Possible	
				5	6.051	Possible	

Figure B-1 Visual Inspection Data from the Bottom Surface of the Bridge Deck – Bridge

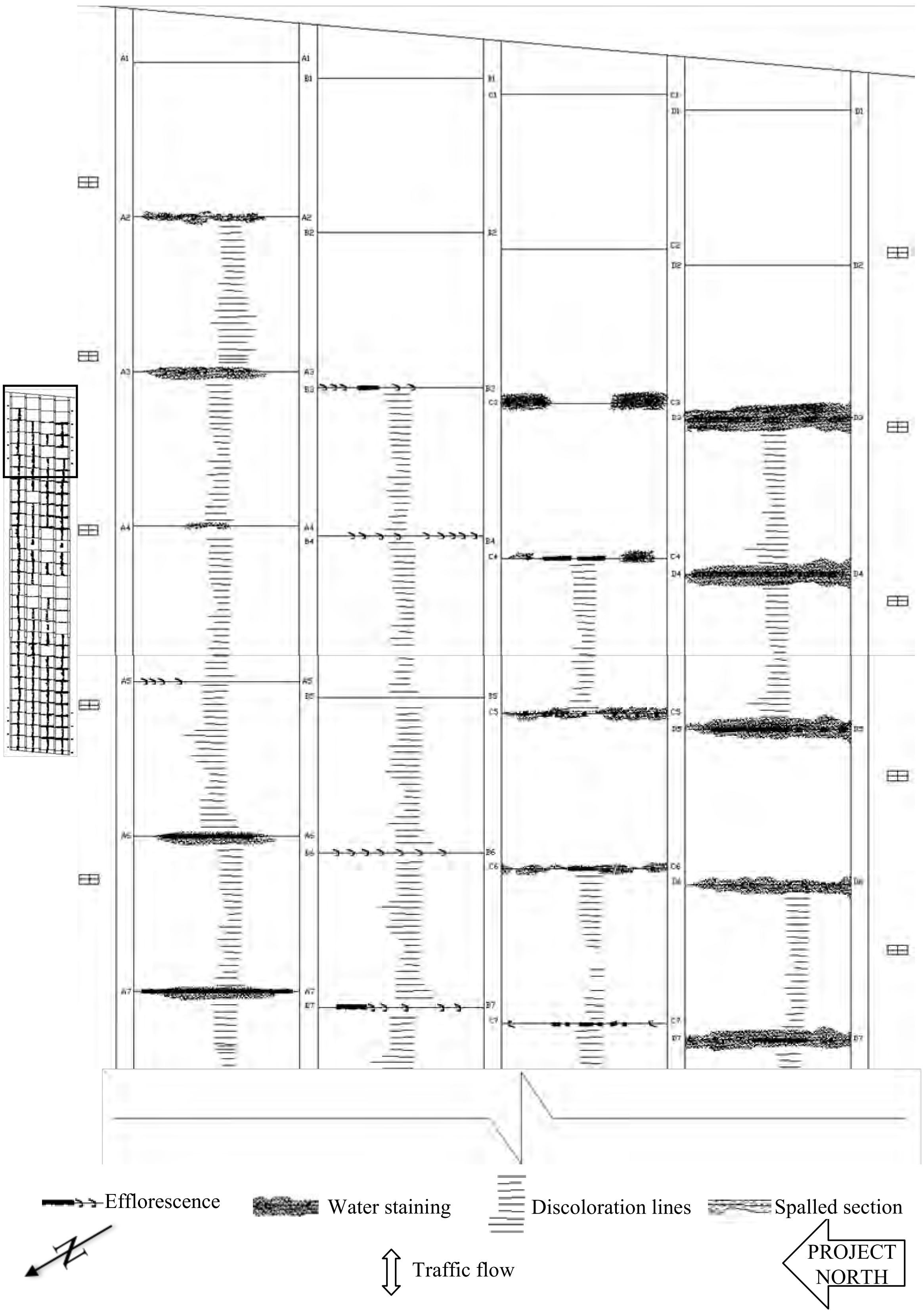

Figure B-1 Visual Inspection Data from the Bottom Surface of the Bridge Deck – Bridge A4709 (Cont.)

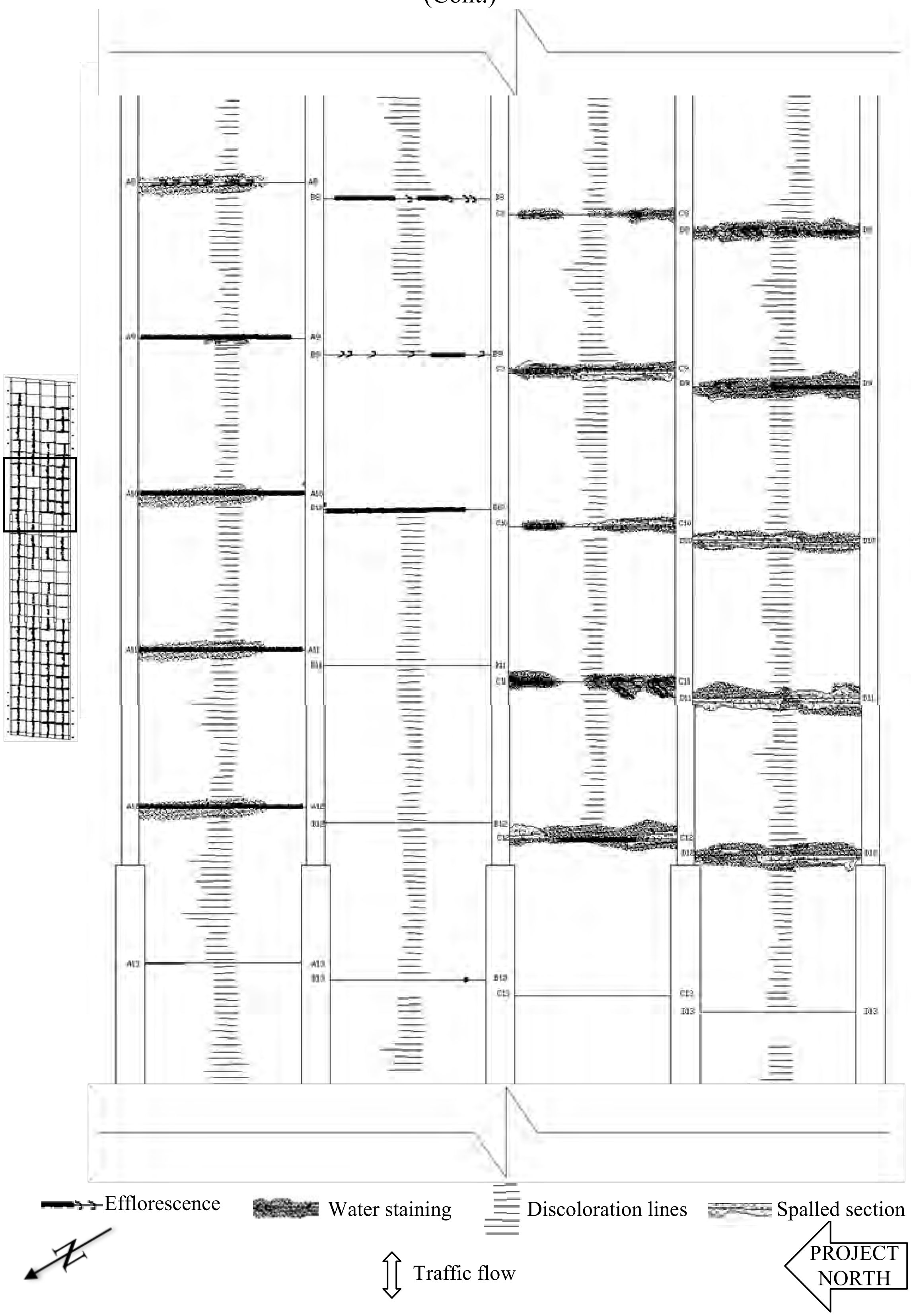

Figure B-1 Visual Inspection Data from the Bottom Surface of the Bridge Deck – Bridge A4709 (Cont.)

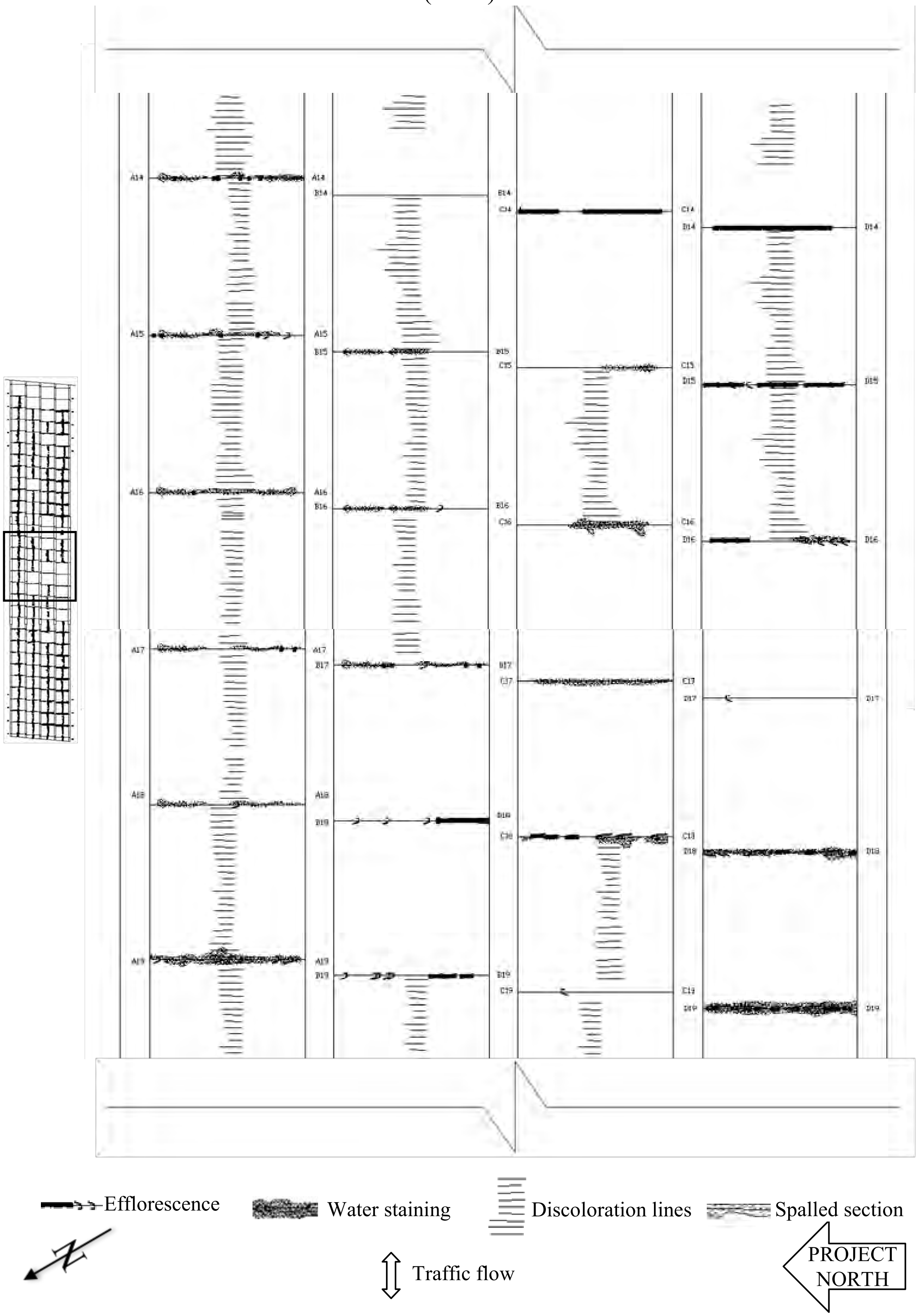

Figure B-1 Visual Inspection Data from the Bottom Surface of the Bridge Deck – Bridge A4709 (Cont.)

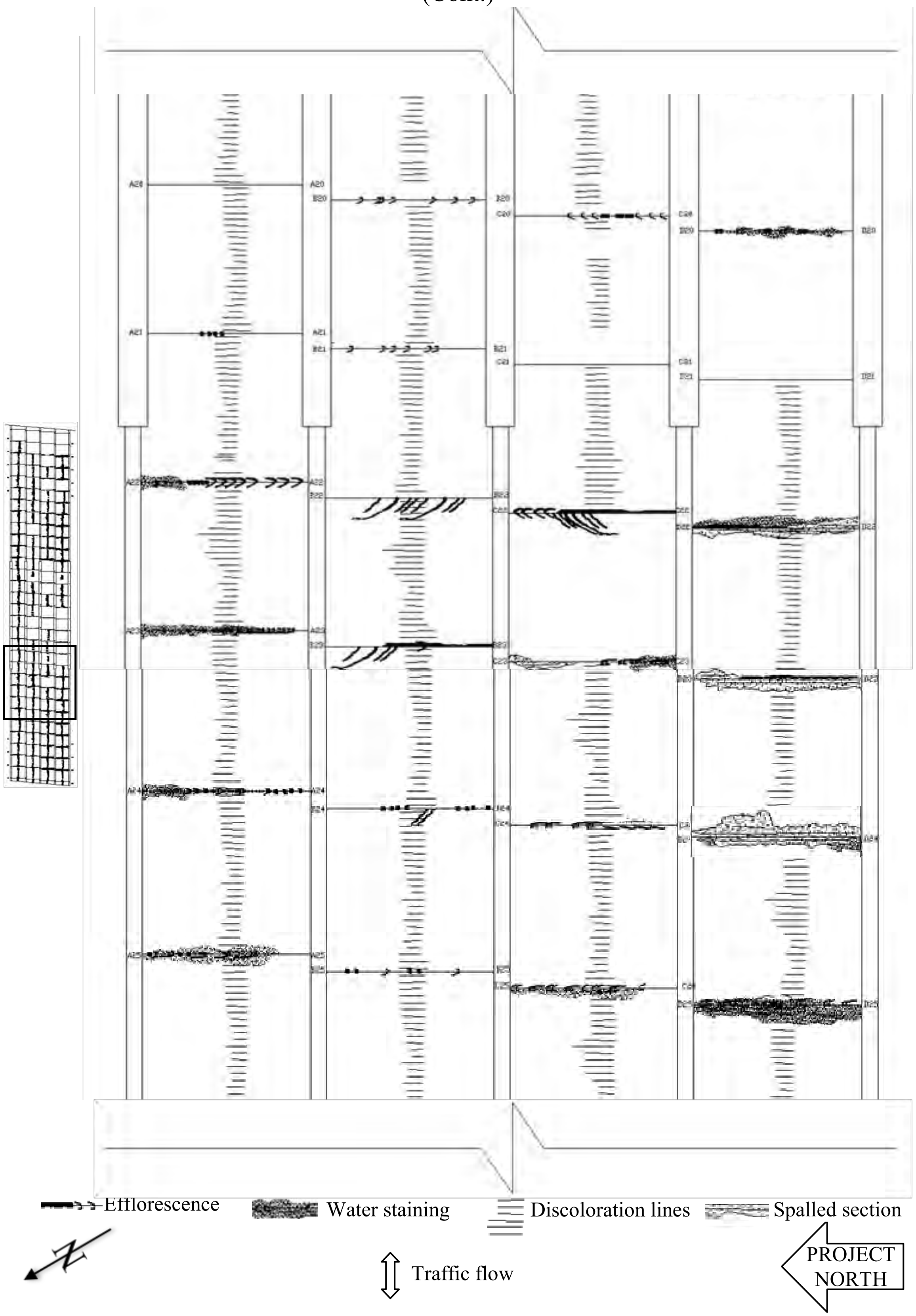

Figure B-1 Visual Inspection Data from the Bottom Surface of the Bridge Deck – Bridge A4709 (Cont.)

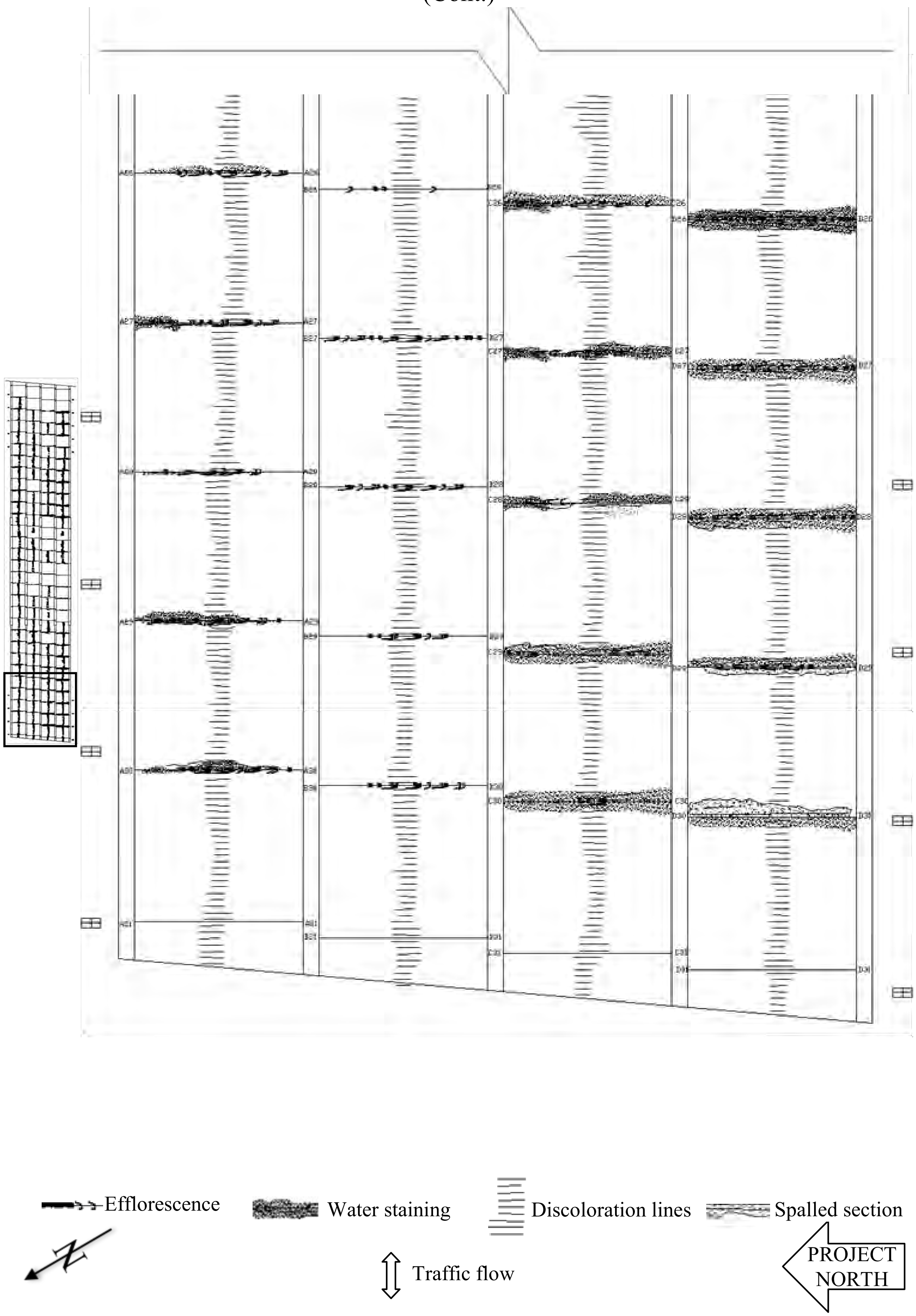

Figure B-2 Visual Inspection Data from the Top Surface of the Bridge Deck - Crack Map and Drain Locations – Bridge A4709A4709

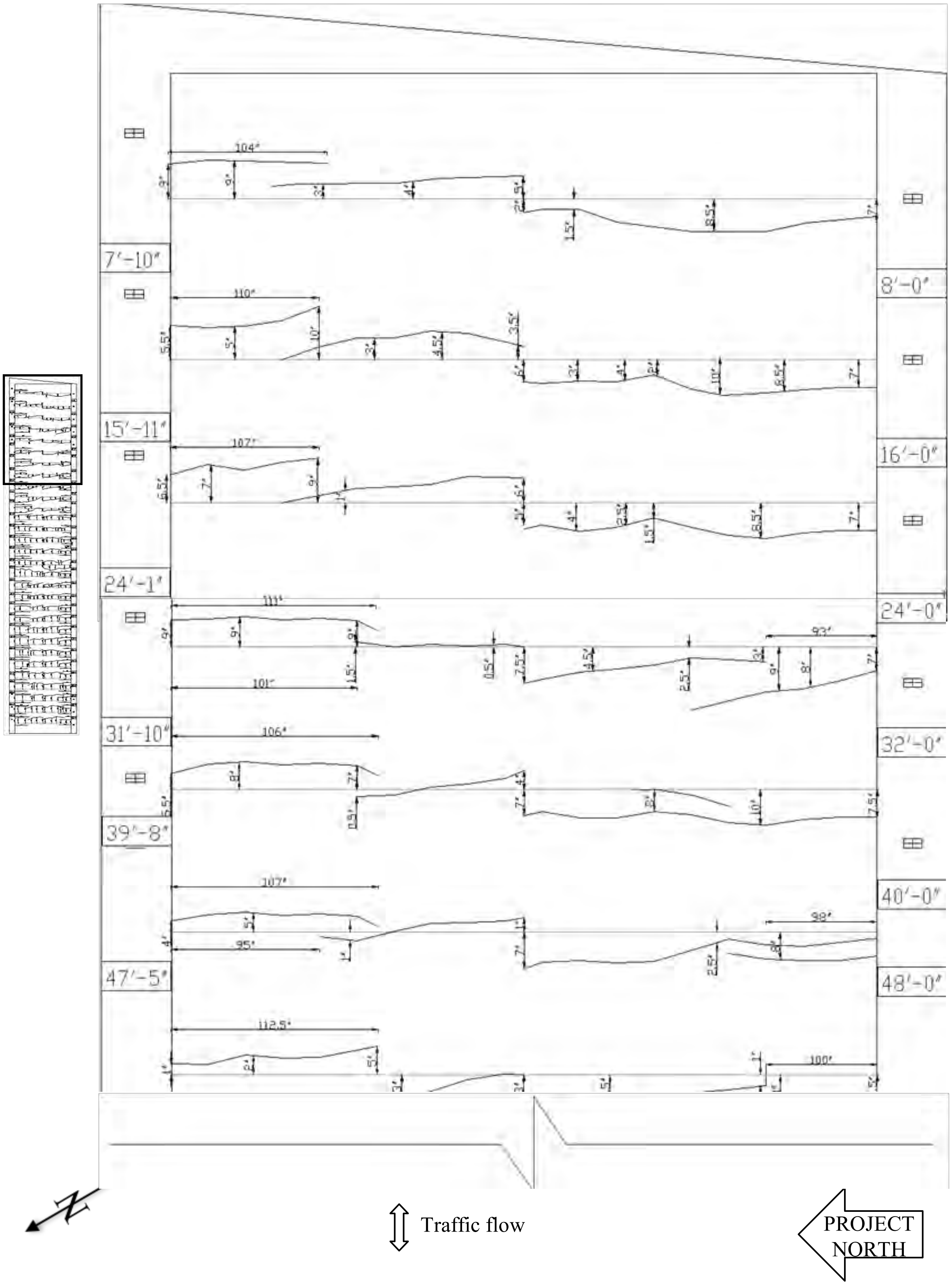

Figure B-2 Visual Inspection Data from the Top Surface of the Bridge Deck - Crack Map and Drain Locations – Bridge A4709 (Cont.)

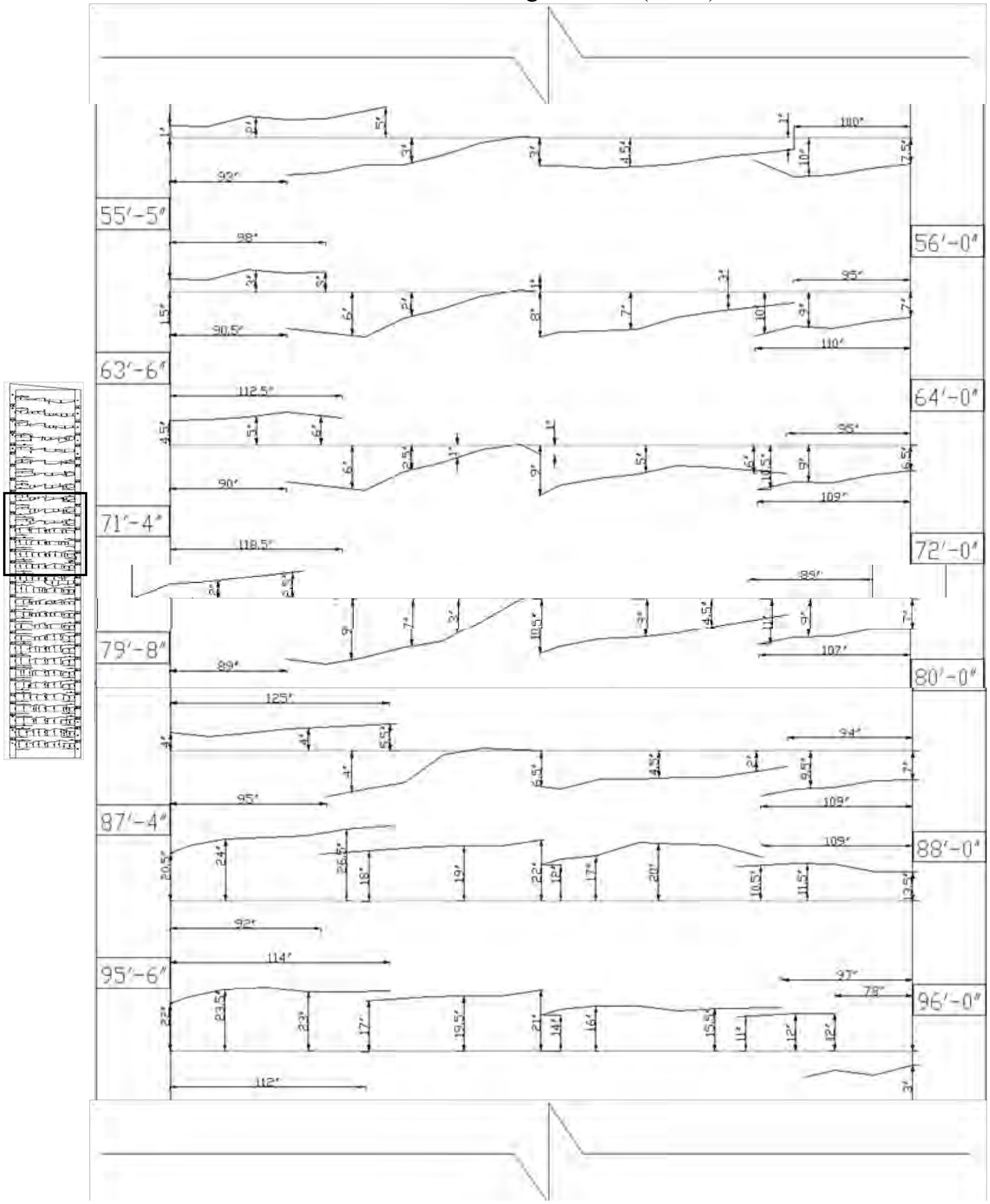

Traffic flow

PROJECT NORTH

Figure B-2 Visual Inspection Data from the Top Surface of the Bridge Deck - Crack Map and Drain Locations – Bridge A4709 (Cont.)

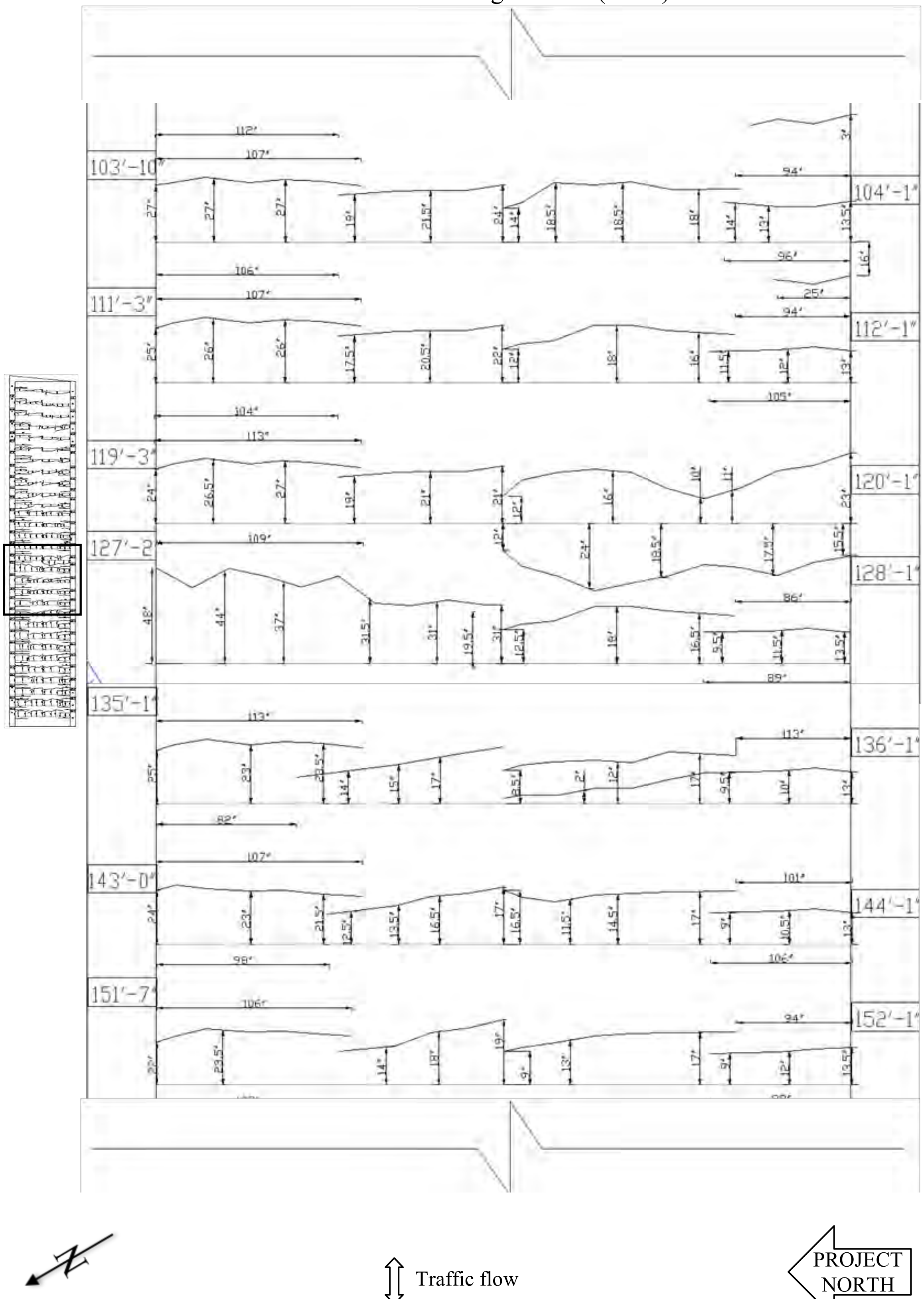

Figure B-2 Visual Inspection Data from the Top Surface of the Bridge Deck - Crack Map and Drain Locations – Bridge A4709 (Cont.)

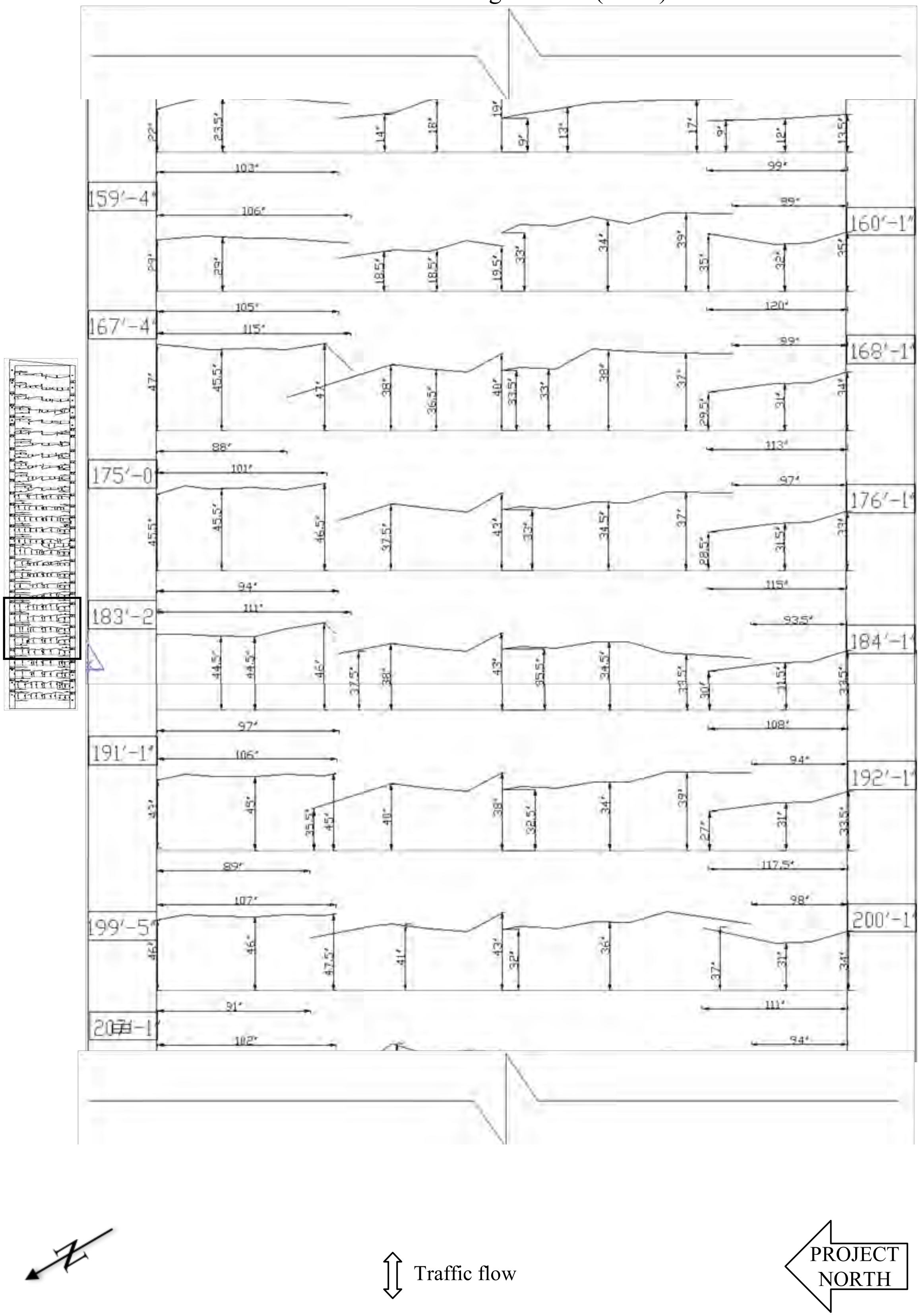

Figure B-2 Visual Inspection Data from the Top Surface of the Bridge Deck - Crack Map and Drain Locations – Bridge A4709 (Cont.)

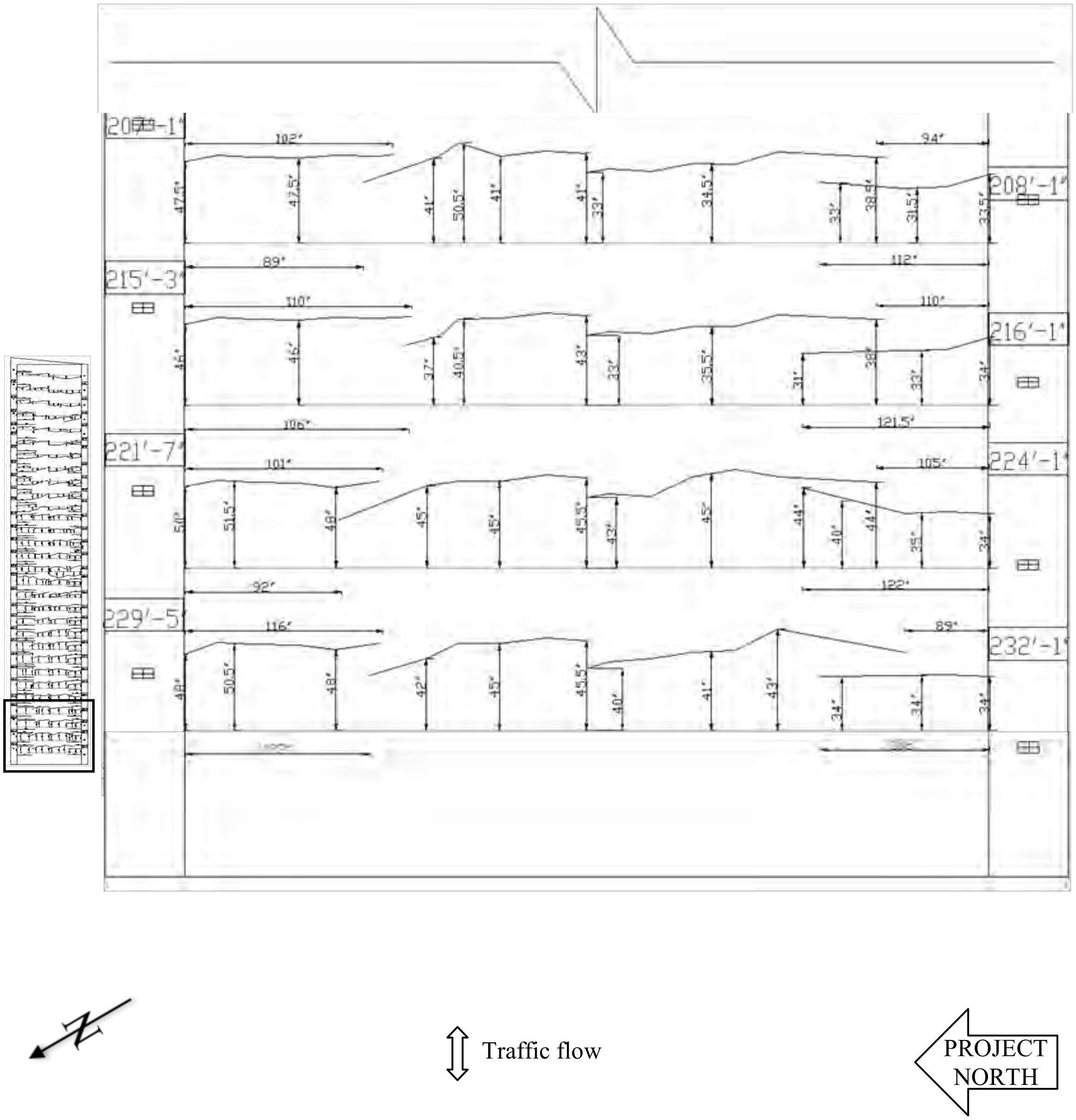

Figure B-3 Photos of Cores Including Lengths and Bottom Type from Bridge A4709

Core C-1: 4.5” long (broken)

Core C-2: 5.5” long (smooth)

Core C-3: 6.125” long (smooth)

Core C-4: 6.125” long (smooth)

Core C-5: 6.5” long (broken)

Core C-6: 6.625” long (broken)

Figure B-3 Photos of Cores Including Lengths and Bottom Type from Bridge A4709 (Cont.)


Core C-7: 6.5" long (smooth)	Core C-8: 6.375" long (smooth)


Core C-9: 7" long (broken)	Core C-10: 7.125" long (broken)

APPENDIX C

EXPERIMENTS

TABLE OF CONTENTS

LIST OF FIGURES

LIST OF TABLES

C.1 INTRODUCTION

This appendix provides information about the experiments discussed in Chapter 5 including mechanical properties of materials used and test specimen construction (Section C.2), test setup (Section C.3), and individual test specimen results (Sections C.4 and C.5).

C.2 TEST SPECIMENS

C.2.1 Specimen Materials

Specified and as-built material properties of the specimens tested in this study are discussed in the following sections. Concrete is discussed in Section C.2.1.1, and reinforcement is discussed in Section C.2.1.2

C.2.1.1 Concrete

The concrete mixtures used in the specimen construction were provided by Coreslab Structures in Marshall, MO. The concrete mixture designs selected for this study were based on Coreslab Structure's standard concrete mixture design that is used to construct precast slab panels provided to MoDOT in accordance with current MoDOT specifications for this type of construction. This concrete mixture is referred to herein as "normal concrete." The aggregates used in the concrete mixture were from aggregates local to the region. The specified compressive strength of the standard concrete mixture at 28 days is 6000 psi.

Variations of the standard concrete mixture were used in this study to examine various test parameters, as explained in Section 5.1. Six different types of concrete were used which include the addition of fibers and varying levels of corrosion inhibitor and NaCl: normal concrete, normal concrete with NaCl, normal concrete with corrosion inhibitor, normal concrete with both NaCl and MCI corrosion inhibitor, normal concrete with fibers, and normal concrete with fibers and NaCl. Fibers were type Master Fiber F 70 (fibrillated micro synthetic fiber) from Master Builders. Corrosion inhibitor was MCI from Cortec Corporation. NaCL solution was provided by Master Builders. The concrete mixture proportions are given in Table C-1.

Ten 4x8 in. cylinders were cast for each different type of concrete to examine the evolution of the concrete compressive strengths. For each type of concrete, compressive strength was tested in uniaxial compression with three 4x8 in. cylinders (unless noted otherwise) seven and 28 days after the concrete was cast, as well as on the day unit panels were tested. Cylinders were capped with sulfur caps prior to testing. Additional cylinders were tested for compressive strength by Coreslab Structures to determine the compressive strength after one day for the purpose of form removal. The compression cylinders were tested in a 600-kip Forney® testing machine in the Civil Engineering Materials Laboratory at Missouri S&T. The loading rate for the compressive strength tests was 565 lb/sec. Flexural beams (6x6x24 in.) were also tested on the same date in the Civil Engineering Materials Laboratory at Missouri S&T. Flexural beams were tested in a 600-kip Forney® at a rate of 30 lbs/sec. All loading rates were within the limits prescribed in ASTM C293 (2008).

Mechanical properties of concrete and the date at which each property was tested are presented in Table C- 2.

C.2.1.2 Reinforcement

Three types of prestressed reinforcement were used in the experiments to examine various test parameters, as explained in Section 5.1. Steel strand was 3/8 in. diameter, 7-wire, Grade 270 low-relaxation conforming to ASTM A 416 (2010). Epoxy-coated strand was 3/8 in. diameter, 7-wire, Grade 270 low-relaxation grit-impregnated conforming to ASTM A 882 (2010). Epoxy-coated strand was type Flo-Bond manufactured by Sumiden Wire Products Corporation. Carbon fiber reinforced polymer (CFRP) tendons were No. 3 reinforcing bar. CFRP tendons were type Aslan 200 manufactured by Hughes Bros.

Other types of reinforcement used in the experiments include reinforcing bars, used as shrinkage and temperature reinforcement, and fibers. Reinforcing bars were No. 3 epoxy-coated reinforcing bar. Fibers were type Master Fiber F 70 (fibrillated micro synthetic fiber) from Master Builders as discussed in Section C.2.1.

All reinforcement of a given type used to construct the test specimens on a given day came from a single producer and from a single heat of material.

Yield and breaking strengths of the steel strand were determined in accordance with ASTM A 370 (2010) with uniaxial tension tests from samples that were from the same heat as the strand used in fabricating the specimens. Tension tests were conducted in a 200 kip 4-pole MTS®880 testing machine under displacement control. The testing machine had a precision of 10 lbs and 0.0001 in. Coupons were tested at a single continuous loading rate of 1,930 lbs/min. Figure C- 1 shows typical load-strain relationships obtained from the tensile coupons for each of the steel strand types used in the specimens. Prestressed reinforcement material properties, including measured and reported by the manufacturer, are shown in Table C- 3. Measured values represent the average of three tensile coupons tested for each strand.

C.2.2 Specimen Construction

Construction of the specimens by a precast concrete manufacturer, including the use of local materials and standard concrete mixtures, was decided so that the specimens tested would be representative of components used in service. This decision was based on feedback from the MoDOT project TAP members.

Two general types of test specimens were used in the experiments in this study: corrosion specimens and unit panel specimens. The test specimens were constructed at Coreslab Structures precast concrete plant in Marshall, MO on two separate dates. All of the corrosion specimens and four of the unit panels were cast on December 29, 2009. The remaining eight unit panels were cast on March 12, 2010. All specimens were transported to the High Bay Structures Laboratory at Missouri S&T within seven days of casting, where they were stored until they were tested. Specimens were stored in conditioned space. Construction of the unit panel specimens is described in Section C.2.2.1, and construction of the durability specimens is described in Section C.2.2.2.

C.2.2.1 Unit Panel Specimens

Twelve unit panels of six types were constructed comprised of the following prestressed reinforcement types (2 panels each): steel strand with normal concrete, steel strand with normal concrete and fibers, steel and epoxy-coated steel strand with normal concrete, steel and epoxy-coated steel strand with normal concrete and fibers, steel strand and CFRP bars with normal concrete, steel strand and CFRP bars with normal concrete and fibers. The rational for the different panel types is explained in Section 5.2.1.

Four unit panel specimens were cast at Coreslab Structures in Marshall, MO on December 29, 2009 along with the corrosion specimens (see Section C.3.1). The first four unit panels consisted of panels with steel strand only. The remaining eight unit panel specimens were cast together at the same facility on March 12, 2010. The remaining eight panels included epoxy-coated steel strand and CFRP tendons. Figure C-5 shows the prestressed reinforcement in the casting bed prior to concrete placement.

Tendons were prestressed in the prestressing beds prior to the application of strain gages. This was in an attempt to ensure the bond between the strain gage and tendon would remain intact during the fabrication process. All strain gages were installed the day prior to casting the specimens. Figure C-6 shows the strain gages applied to the prestressed reinforcement. Strain gage types and locations are discussed in Section C.3.1.1.

Prestressing steel strands were pretensioned to achieve jacking force of 17.2 kips. The force in the tendon was measured with the jack, and the measured elongation was compared to the theoretical elongation. Standard prestressing anchorages were used for the uncoated and epoxy-coated prestressing strand. For the epoxy-coated strand, the epoxy was removed before anchoring the strand. For the CFRP tendons, a specialized splice system designed by Hughes Bros. was used to splice the two CFRP tendons to a single 0.6 in. diameter strand on the one end, and to two epoxy-coated strands on the other end. Figure C-7 shows the splice system anchorage system and set-up.

The formwork was blown out with an air compressor immediately before casting the concrete. Care was taken not to disturb the integrity of the strain gages during concrete placement. Concrete was batched on site at the Coreslab Structures precast plant and was placed and consolidated using normal procedures. Concrete was moist-cured using wet burlap applied to the top surface of each specimen. For both cast dates, four project representatives were present at the precast plant to observe the concrete placement.

C.2.2.2 Durability Specimens

Durability specimens were constructed at Coreslab structures in Marshall, MO on December 29, 2009. Two types of corrosion specimens were constructed, non-prestressed corrosion specimens and prestressed corrosion specimens, as explained in Section 5.3.2.

Custom new wood formwork was designed and constructed by Coreslab Structures to form the non-prestressed corrosions specimens. The reinforcement was placed within the specimen forms and supported with plastic-tipped steel chairs. Prior to placing the reinforcement, the weight of the reinforcement was measured to facilitate the gravimetric study based on the loss of steel weight due to corrosion. Figure C-3 shows the formwork and reinforcement prior to casting.The prestressed corrosion specimens were constructed in the same casting bed used for the casting of full-size unit panels by adding block-outs to achieve the dimensions required. Figure C-4 shows the formwork prior to casting. Prestressing steel strands were pretensioned to achieve jacking force of 17.2 kips. The force in the tendon was measured with the jack, and the measured elongation was compared to the theoretical elongation. Standard prestressing anchorages were used for the uncoated and epoxy-coated prestressing strand.

The formwork was blown out with an air compressor immediately before casting the concrete. Concrete was batched on site at the Coreslab Structures precast plant and was placed and consolidated using normal procedures. Concrete was moist-cured using wet burlap applied to the top surface of each specimen. Four project representatives were present at the precast plant to observe the concrete placement.

C.3 TEST SETUP

C.3.1 Unit Panel Specimens

C.3.1.1 Instrumentation

C.3.1.1.1 Strain Gages

Uniaxial electrical resistance strain gages (Vishay Micro-Measurements Type EA-06-125BT-120/LE) were attached to the tendons at locations selected to study the variation of longitudinal tensile strains along the length of the reinforcement. Tendons were pretentioned prior to gage installation. Uniaxial electrical resistance strain gages (Tokyo Sokki Kenkyujo Co., Ltd. TML Type PL-60-11) were attached to the top and bottom surface of the concrete to study the longitudinal strain in the extreme tension and compression fibers. Concrete surface strain gage locations were selected such that they would correspond to locations where tendon strain gages were located to study the strain distribution at that section. Because the unit panel specimens were pretensioned, precompression strain was not accounted for in concrete surface gage measurements. Locations of all strain gages are shown in Figure C-8. All strain gages were installed per the manufacturer's recommendations.

C.3.2 Durability Specimens

C.3.2.1 Corrosion initiation specimens

Figure C-110 shows the dimensions and specimen numbers for the 27 specimens included in the corrosion initiation test. The test specimens were subjected to wet/dry cycles during a test period of six months. Two main measurements were conducted at different time intervals. The half-cell potential test was performed according to ASTM C876 (1991) every two weeks during the test period using a Canin Corrosion Analyzing Instrument manufactured by Proceq. Figure C-111 shows a typical half-cell potential measurement. In addition, visual inspection was also conducted every two weeks together with half-cell potential test to observe the deterioration levels of concrete. The chloride content test was performed every two months. Two month testing was performed by MoDOT. Four and six month testing was performed by Missouri S&T according to ASTM C1218 (1999) using the Rapid Chloride Test (RCT) instrument. Finally, a gravimetric study was conducted according to ASTM G1-03 after six months. Cleaning, preparing, and evaluating of corrosion specimens followed this recommendation. Based on ASTM G1-03, rust on the corroded steel tendons was removed by scrubbing with a nonmetallic bristle brush. Cleaned steel tendons were placed into a muriatic acid solution for further cleaning as shown in Figure C-112. The weights of steel tendons were measured before concrete casting and after testing.

C.3.2.1 Accelerated corrosion specimens

Figure C-113 shows the dimensions and specimen numbers for the 18 specimens included in the accelerated corrosion test. The specimens were subjected to 0.4 mA electrical current for six months. Weekly visual inspection was conducted to observe and record deterioration during the test period. A gravimetric study was also performed to measure the steel loss due to the accelerated corrosion process. Steel tendon losses were used to estimate the corrosion rate.

C.4 UNIT PANEL EXPERIMENT RESULTS

The experimental results and behavior of each unit panel specimen are described in the sections that follow. Specimens subjected to monotonic static loading are presented in Sections C.4.1 through C.4.6. Specimens subjected to fatigue loading are presented in Sections C.4.7 through C.4.11.

C.4.1 Panel ST-NC-SL

C.4.1.1 Failure and Cracking Behavior

Panel ST-NC-SL was tested to failure on 3/05/10, 65 days after the concrete was cast. Flexural cracks first developed on the extreme tension face, which increased in length and number with increasing applied load. Cracks were first observed on the side face at an applied load of 16.94 kips and displacement of 0.8 inch. The initial cracks started to appear at locations near the edge of the spreader beam location. As the applied displacement (and corresponding applied load) was increased, additional flexural cracks appeared and existing cracks propagated upward. The panel failed by concrete crushing as the failure crack penetrated the flexural compression zone completely at the location of the spreader beam. As a result of the loss of load carrying capacity associated with the destruction of the flexural compression zone, the applied load dropped to 16.94 kips. The maximum load and corresponding displacement were 22.08 kips and 2.14 in., respectively. Upon attempt to maintain and increase the load level, further deformation was imposed on the specimen. Thus the failure load for Panel ST-NC-SL corresponds to an applied load of 22.08 kips. Figure C-9 shows the post-failure state of the panel after the spreader beam was removed.

C.4.1.2 Load-displacement

Figure C- 10 shows the measured displacement along the length the panel length at Grids E, E’, and F for various load levels, including cracking and maximum loads (13.92 kips and 22.08 kips, respectively). The cracking load was determined based on the change in behavior in the load displacement relationship from Figure C- 11, as well as the change in load-strain relationship discussed in Section C.4.1.3. Note that the cracking load determined in this manner is slightly lower than the load corresponding to when flexural cracks were first observed as discussed in Section C.4.1.1. Displacements measured at Grids E, E’, and F are similar (within 4%) at each load level with the exception of the failure load, where the displacement measured at Grid E was slightly higher (5%) than Grids E’ and F. Figure C- 11 shows the applied load-displacement response for all locations.

Figure C-12 shows the measured displacements along width of panel at Grids 1, 2, and 3. At each load level, displacements measured at different locations along the width of the panel were similar (within 10%), which indicates that the load applied by the actuator was uniformly distributed along width at the panel midspan by the spreader beam.

C.4.1.3 Load-strain

Figure C-13 shows the applied load-tendon strain relationship. Note that the relationship shown does not account for the effects of precompression (ref. Section C.3.1.1.1). In the figure, compression strain is shown as negative while tension strain is shown as positive. Tendon strains measured at all locations are negligible for applied load less than 13.92 kips. For applied load greater than 13.92 kips tensile strains measured in the tendons along midspan (-2 locations in the figure) increase linearly with increasing applied load, indicated that the neutral axis is shifting upwards and that the section has cracked. At quarter span (1- and -3 locations in the figure), the tendon strains are almost zero during the entire test. This change in behavior at this load level is consistent with the change in behavior of the load-displacement relationship described in Section C.4.1.2.

Figure C-14 shows the applied load-concrete surface strain relationship. Note that the relationship shown does not account for the effects of precompression (ref. Section C.3.1.1.1). (Also note that gage E-B-3 was not working and was not plotted in the figure.) The load-strain relationship for the concrete surface at midspan (-2 locations in Figure C-14) has a bilinear behavior, with a greater slope when the applied load is less than the cracking load and a lesser slope when load is greater than the cracking load. At quarter span (-1 and -3 locations), the the surface strains increase linearly until the maximum load is achieved. Concrete surface gages along Grid 2 on the bottom surface of the panel stopped working after flexural cracks occurred at the gage location; thus measured strain in these locations is reported only until the respective gage stopped working.

The strain distribution within the section at various locations is shown in Figure C-15. Note that the relationship shown does not account for the effects of precompression (ref. Section C.3.1.1.1). For each location, Figure C-15 shows strains measured on the top and bottom concrete surfaces and the corresponding strain measured in the tendon at different load levels, including cracking and failure loads (13.92 kips and 22.08 kips, respectively). Concrete surface gages along Grid 2 on the bottom surface of the panel stopped working after flexural cracks occurred at the gage location; thus, measured strain in these locations is reported only until the respective gage stopped working.

C.4.2 Panel ST-FRC-SL

C.4.2.1 Failure and Cracking Behavior

Panel ST-FRC-SL was tested to failure on 3/19/10, 79 days after the concrete was cast. Flexural cracks first developed on the extreme tension face, which increased in length and number with increasing applied load. Cracks were first observed on the side face at an applied load of 17.07 kips and displacement of 0.8 in. The initial cracks started to appear at locations near the edge of the spreader beam location. As the applied load was increased, additional flexural cracks appeared and existing cracks propagated upward. Failure occurred as the failure crack penetrated the flexural compression zone completely at the location of the spreader beam. As a result of the loss of load carrying capacity associated with the destruction of the flexural compression zone, the applied load dropped to 9.64 kips. Upon attempt to maintain and increase the load level, further deformation was imposed on the specimen. The maximum load of 20.25 kips was not able to be recovered; thus the failure load for Panel ST-FRC-SL corresponds to an applied load of 20.25 kips with a corresponding displacement of 1.65 in. Figure C-16 shows the post-failure state of the panel after the spreader beam was removed. The failure crack was located near the east side of the spreader beam on the top surface of the panel and extended the entire width of the panel.

During the test, cracks were marked on the side faces of the panel at discrete load increments until the failure load was achieved. Figure C-17shows the progression of cracking from an applied load of 17.07 kips (shortly after first observed flexural cracking occurred) to the maximum load of 20.25 kips.

C.4.2.2 Load-displacement

Figure C-18 shows the measured displacement along the length the panel length at Grids E, E', and F for various load levels, including cracking and maximum loads (13.79 kips and 20.25 kips, respectively). The cracking load was determined based on the change in behavior in the load displacement relationship from Figure C-18, as well as the change in load-strain relationship discussed in Section C.4.2.3. Note that the cracking load determined in this manner is slightly lower than the load corresponding to when flexural cracks were first observed as discussed in Section C.4.2. Displacements measured at Grids E, E', and F are similar (within 5%) at each load level. Figure C-19 shows the applied load-displacement response for all locations.

Figure C-20 shows the measured displacements along width of panel at Grids 1, 2, and 3. At each load level, displacements measured at different locations along the width of the panel were similar (within 10%), which indicates that the load applied by the actuator was uniformly distributed along width at the panel midspan by the spreader beam.

C.4.2.3 Load-strain

Figure C-21 shows the applied load-tendon strain relationship. Note that the relationship shown does not account for the effects of precompression (ref. Section C.3.1.1.1). In the figure, compression strain is shown as negative while tension strain is shown as positive. Tendon strains measured at all locations are negligible for applied load less than 13.79 kips. For applied load greater than 13.79 kips tensile strains measured in the tendons along Grid 2 increase linearly with increasing applied load, indicated that the neutral axis is shifting upwards and that the section has cracked. This change in behavior at this load level is consistent with the change in behavior of the load-displacement relationship described in Section C.4.2.2.

Figure C-22 shows the applied load-concrete surface strain relationship. Note that the relationship shown does not account for the effects of precompression (ref. Section C.3.1.1.1). (Also note that gage A-T-3 was not working and was not plotted in the figure.) Concrete surface gages along Grid 2 on the bottom surface of the panel stopped working after flexural cracks occurred at the gage location; thus measured strain in these locations is reported only until the respective gage stopped working.

The strain distribution within the section at various locations is shown in Figure C-23. Note that the relationship shown does not account for the effects of precompression (ref. Section C.3.1.1.1). For each location, Figure C-23 shows strains measured on the top and bottom concrete surfaces and the corresponding strain measured in the tendon at different load levels, including cracking and failure loads (13.79 kips and 20.25 kips, respectively). Concrete surface gages along Grid 2 on the bottom surface of the panel stopped working after flexural cracks occurred at the gage location; thus, measured strain in these locations is reported only until the respective gage stopped working.

C.4.3 Panel ECST-NC-SL

C.4.3.1 Failure and Cracking Behavior

Panel ECST-NC-SL was tested to failure on 4/08/10, 28 days after the concrete was cast. Flexural cracks first developed on the extreme tension face, which increased in length and number with increasing applied load. Cracks were first observed on the side face at an applied load of 17.00 kips and displacement of 0.7 in. The initial cracks started to appear at locations near the edge of the spreader beam location. As the applied displacement (and corresponding applied load) was increased, additional flexural cracks appeared and existing cracks propagated upward. Additional longitudinal splitting cracks were evident on the panel side surfaces as shown in Figure C-24. Failure occurred as the failure crack penetrated the flexural compression zone completely at the location of the spreader beam. As a result of the loss of load carrying capacity associated with the destruction of the flexural compression zone, the applied load dropped to 8.2 kips. Upon attempt to maintain and increase the load level, further deformation was imposed on the specimen. The deformation of the panel increased, but the maximum load of 18.50 kips was not able to be recovered; thus the failure load for Panel ECST-NC-SL corresponds to an applied load of 18.50 kips with a corresponding displacement of 1.05 in. Figure C-24 shows the post-failure state of the panel after the spreader beam was removed.

During the test, cracks were marked on the side faces of the panel at discrete load increments until the failure load was achieved. Figure C-25 shows the progression of cracking from an applied load of 17.00 kips (shortly after first observed flexural cracking occurred) to the maximum load of 18.50 kips.

C.4.3.2 Load-displacement

Figure C-26 shows the measured displacement along the length the panel length at Grids E, E’, and F for various load levels, including cracking and maximum loads (14.19 kips and 18.49 kips, respectively). The cracking load was determined based on the change in behavior in the load displacement relationship from Figure C-26, as well as the change in load-strain relationship discussed in Section C.4.3.3. Note that the cracking load determined in this manner is slightly lower than the load corresponding to when flexural cracks were first observed as discussed in Section C.4.3.1. Displacements measured at Grids E, E’, and F are similar (within 5%) at each load level. Figure C-27 shows the applied load-displacement response for all locations.

Figure C-28 shows the measured displacements along width of panel at Grids 1, 2, and 3. At each load level, displacements measured at different locations along the width of the panel at Grids 2 and 3 were similar (within 10%), which indicates that the load applied by the actuator was uniformly distributed along width at the panel midspan by the spreader beam. At Grid 1, the displacement measured at Grid F larger than at Grid E by 17% at the maximum load.

C.4.3.3 Load-strain

Figure C-29 shows the applied load-tendon strain relationship. Note that the relationship shown does not account for the effects of precompression (ref. Section C.3.1.1.1). In the figure, compression strain is shown as negative while tension strain is shown as positive. Tendon strains measured at all locations are negligible for applied load less than 14.19 kips. For applied load greater than 14.19 kips tensile strains measured in the tendons along Grid 2 increase linearly with increasing applied load, indicated that the neutral axis is shifting upwards and that the section has cracked. This change in behavior at this load level is consistent with the change in behavior of the load-displacement relationship described in Section C.4.3.2.

Figure C-30 shows the applied load-concrete surface strain relationship. Note that the relationship shown does not account for the effects of precompression (ref. Section C.3.1.1.1). Concrete surface gage A-B-2 along Grid 2 on the bottom surface of the panel stopped working after flexural cracks occurred at the gage location; thus measured strain in this location is reported only until the respective gage stopped working.

The strain distribution within the section at various locations is shown in Figure C-31. Note that the relationship shown does not account for the effects of precompression (ref. Section C.3.1.1.1). For each location, Figure C-31 shows strains measured on the top and bottom concrete surfaces and the corresponding strain measured in the tendon at different load levels, including cracking and failure loads (14.19 kips and 18.49 kips, respectively). Concrete surface gage A-B-2 along Grid 2 on the bottom surface of the panel stopped working after flexural cracks occurred at the gage location; thus measured strain in this location is reported only until the respective gage stopped working.

C.4.4 Panel ECST-FRC-SL

C.4.4.1 Failure and Cracking Behavior

Panel ECST-FRC-SL was tested to failure on 4/12/10, 32 days after the concrete was cast. Flexural cracks first developed on the extreme tension face, which increased in length and number with increasing applied load. Cracks were first observed on the side face at an applied load of 15.80 kips and applied displacement of 0.5 in. The initial cracks started to appear at locations near the edge of the spreader beam location. As the applied displacement (and corresponding applied load) was increased, additional flexural cracks appeared and existing cracks propagated upward. Failure occurred as the failure crack penetrated the flexural compression zone completely at the location of the spreader beam. As a result of the loss of load carrying capacity associated with the destruction of the flexural compression zone, the applied load dropped to 16.70 kips. Upon attempt to maintain and increase the load level, further deformation was imposed on the specimen. The maximum load of 21.20 kips was not able to be recovered; thus the failure load for Panel ECST-FRC-SL corresponds to an applied load of 21.20

kips with a corresponding displacement of 1.70 in Figure C-32 shows the post-failure state of the panel after the spreader beam was removed.

During the test, cracks were marked on the side faces of the panel at discrete load increments until the failure load was achieved. Figure C-33 shows the progression of cracking from an applied load of 15.80 kips (shortly after first observed flexural cracking occurred) to the maximum load of 20.20 kips.

C.4.4.2 Load-displacement

Figure C-34 shows the measured displacement along the length the panel length at Grids E, E', and F for various load levels, including cracking and maximum loads (14.25 kips and 21.20 kips, respectively). The cracking load was determined based on the change in behavior in the load displacement relationship from Figure C-34 as well as the change in load-strain relationship discussed in Section C4.4.3. Note that the cracking load determined in this manner is slightly lower than the load corresponding to when flexural cracks were first observed as discussed in Section C.4.4.1. Displacements measured at Grids E, E', and F are similar (within 5%) at each load level with the exception of the failure load, where the displacement measured at Grid E was slightly higher (10%) than Grids E' and F. Figure C-35 shows the applied load-displacement response for all locations.

Figure C-36 shows the measured displacements along width of panel at Grids 1, 2, and 3. For each load level, displacements measured at different locations along the width of the panel were similar (within 12%), which indicates that the load applied by the actuator was uniformly distributed along width at the panel midspan by the spreader beam.

C.4.4.3 Load-strain

Figure C-37 shows the applied load-tendon strain relationship. Note that the relationship shown does not account for the effects of precompression (ref. Section C.3.1.1.1). (Also note that gages A-2, E-2, and F-3 were not working and were not plotted in the figure.) In the figure, compression strain is shown as negative while tension strain is shown as positive. Tendon strains measured at all locations are negligible for applied load less than 14.25 kips. For applied load greater than 14.25 kips tensile strains measured in the tendons along Grid 2 increase linearly with increasing applied load, indicated that the neutral axis is shifting upwards and that the section has cracked. This change in behavior at this load level is consistent with the change in behavior of the load-displacement relationship described in Section C.4.4.2.

Figure C-38 shows the applied load-concrete surface strain relationship. Note that the relationship shown does not account for the effects of precompression (ref. Section C.3.1.1.1). Concrete surface gages along Grid 2 on the bottom surface of the panel stopped working after flexural cracks occurred at the gage location; thus, measured strain in these locations is reported only until the respective gage stopped working.

The strain distribution within the section at various locations is shown in Figure C-39. Note that the relationship shown does not account for the effects of precompression (ref. Section C.3.1.1.1). For each location, Figure C-39 shows strains measured on the top and bottom concrete surfaces and the corresponding strain measured in the tendon at different load levels, including cracking and failure loads (14.25 kips and 21.20 kips, respectively). Concrete surface gages along Grid 2 on the bottom surface of the panel stopped working after flexural cracks occurred at the gage location; thus measured strain in these locations is reported only until the respective gage stopped working.

C.4.5 Panel CFRPT-NC-SL

C.4.5.1 Failure and Cracking Behavior
Panel CFRPT-NC-SL was tested to failure on 4/13/10, 33 days after the concrete was cast. Cracks were first observed on the side face at an applied load of 18.8 kips. The initial cracks started to appear at locations near the edge of the spreader beam location. As the applied displacement (and corresponding applied load) was increased, additional flexural cracks appeared and existing cracks propagated upward. Failure occurred as the failure crack penetrated the flexural compression zone completely at the location of the spreader beam. As a result of the loss of load carrying capacity associated with the destruction of the flexural compression zone, the applied load gradually dropped to 15.9 kips. Upon attempt to maintain and increase the load level, further deformation was imposed on the specimen. The maximum load of 21.15 kips was not able to be recovered; thus the failure load for Panel CFRPT-NC-SL corresponds to an applied load of 21.15 kips with a corresponding displacement of 1.38 in. Figure C-40 shows the post-failure state of the panel after the spreader beam was removed.

During the test, cracks were marked on the side faces of the panel at discrete load increments until the failure load was achieved. Figure C-41 shows the progression of cracking from an applied load of 18.45 kips (shortly after first observed flexural cracking occurred) to the maximum load of 21.05 kips.

C.4.5.2 Load-displacement
Figure C-42 shows the measured displacement along the length the panel length at Grids E, E', and F for various load levels, including cracking and maximum loads (14.99 kips and 21.05 kips, respectively). The cracking load was determined based on the change in behavior in the load displacement relationship from Figure C-42, as well as the change in load-strain relationship discussed in Section C.4.5.3. Note that the cracking load determined in this manner is slightly lower than the load corresponding to when flexural cracks were first observed as discussed in Section C.4.5.1. Displacements measured at Grids E, E', and F are similar (within 5%) at each load level. Figure C-43 shows the applied load-displacement response for all locations.

Figure C-44 shows the measured displacements along width of panel at Grids 1, 2, and 3. For each load level, displacements measured at different locations along the width of the panel were similar (within 5%), which indicates that the load applied by the actuator was uniformly distributed along width at the panel midspan by the spreader beam.

C.4.5.3 Load-strain
Figure C-45 shows the applied load-tendon strain relationship. Note that the relationship shown does not account for the effects of precompression (ref. Section C.3.1.1.1). (Also note that gages A-3, B-2, C-3, D-2, E-1, and E-3 were not working and were not plotted in the figure.) In the figure, compression strain is shown as negative while tension strain is shown as positive. Tendon

strains measured at all locations are negligible for applied load less than 14.99 kips. For applied load greater than 14.99 kips, tensile strains measured in the tendons along Grid 2 increase linearly with increasing applied load, indicated that the neutral axis is shifting upwards and that the section has cracked. This change in behavior at this load level is consistent with the change in behavior of the load-displacement relationship described in Section C.4.5.2.

Figure C-46 shows the applied load-concrete surface strain relationship. Note that the relationship shown does not account for the effects of precompression (ref. Section C.3.1.1.1). Concrete surface gages along Grid 2 on the bottom surface of the panel stopped working after flexural cracks occurred at the gage location; thus measured strain in these locations is reported only until the respective gage stopped working.

The strain distribution within the section at various locations is shown in Figure C-47. Note that the relationship shown does not account for the effects of precompression (ref. Section C.3.1.1.1). For each location, Figure C-47 shows strains measured on the top and bottom concrete surfaces and the corresponding strain measured in the tendon at different load levels, including cracking and failure loads (14.99 kips and 21.05 kips, respectively). Concrete surface gages along Grid 2 on the bottom surface of the panel stopped working after flexural cracks occurred at the gage location; thus measured strain in these locations is reported only until the respective gage stopped working.

C.4.6 Panel CFRPT-FRC-SL

C.4.6.1 Failure and Cracking Behavior

Panel CFRPT-FRC-SL was tested to failure on 4/19/10, 39 days after the concrete was cast. Cracks were first observed on the side face at an applied load of 16.72 kips and displacement of 0.7 in. The initial cracks started to appear at locations near the edge of the spreader beam location. As the applied displacement (and corresponding applied load) was increased, additional flexural cracks appeared and existing cracks propagated upward. Failure occurred as the failure crack penetrated the flexural compression zone completely at the location of the spreader beam. As a result of the loss of load carrying capacity associated with the destruction of the flexural compression zone, the applied load dropped to 17.3 kips. Upon attempt to maintain and increase the load level, further deformation was imposed on the specimen. The maximum load of 20.70 kips was not able to be recovered; thus the failure load for Panel CFRPT-FRC-SL corresponds to an applied load of 20.70 kips and corresponding displacement of 1.75 in. Figure C-48 shows the post-failure state of the panel after the spreader beam was removed.

During the test, cracks were marked on the side faces of the panel at discrete load increments until the failure load was achieved. Figure C-49 shows the progression of cracking from an applied load of 16.72 kips (shortly after first observed flexural cracking occurred) to the maximum load of 20.70 kips.

C.4.6.2 Load-displacement

Figure C-50 shows the measured displacement along the length the panel length at Grids E, E’, and F for various load levels, including cracking and maximum loads (14.06 kips and 20.70 kips, respectively). The cracking load was determined based on the change in behavior in the load displacement relationship from Figure C-50, as well as the change in load-strain relationship discussed in Section C.4.6.3. Note that the cracking load determined in this manner is slightly lower than the load corresponding to when flexural cracks were first observed as discussed in Section C.4.6.1. Displacements measured at Grids E, E', and F are similar (within 5%) at each load level. Figure C-51 shows the applied load-displacement response for all locations.

Figure C-52 shows the measured displacements along width of panel at Grids 1, 2, and 3. At each load level, displacements measured at different locations along the width of the panel were similar (within 5%), which indicates that the load applied by the actuator was uniformly distributed along width at the panel midspan by the spreader beam.

C.4.6.3 Load-strain

Figure C-53 shows the applied load-tendon strain relationship. Note that the relationship shown does not account for the effects of precompression (ref. Section C.3.1.1.1). (Also note that gage E-2 was not working and was not plotted in the figure.) In the figure, compression strain is shown as negative while tension strain is shown as positive. Tendon strains measured at all locations are negligible for applied load less than 14.06 kips. For applied load greater than 14.06 kips, tensile strains measured in the tendons along Grid 2 increase linearly with increasing applied load, indicated that the neutral axis is shifting upwards and that the section has cracked. This change in behavior at this load level is consistent with the change in behavior of the load-displacement relationship described in Section C.4.6.2.

Figure C-54 shows the applied load-concrete surface strain relationship. Note that the relationship shown does not account for the effects of precompression (ref. Section C.3.1.1.1). Concrete surface gages along Grid 2 on the bottom surface of the panel stopped working after flexural cracks occurred at the gage location; thus measured strain in these locations is reported only until the respective gage stopped working.

The strain distribution within the section at various locations is shown in Figure C-55. Note that the relationship shown does not account for the effects of precompression (ref. Section C.3.1.1.1). For each location, Figure C-55 shows strains measured on the top and bottom concrete surfaces and the corresponding strain measured in the tendon at different load levels, including cracking and failure loads (14.06 kips and 20.70 kips, respectively). Concrete surface gages along Grid 2 on the bottom surface of the panel stopped working after flexural cracks occurred at the gage location; thus measured strain in these locations is reported only until the respective gage stopped working.

C.4.7 Panel ST-NC-FL

C.4.7.1 Failure and Cracking Behavior

Panel ST-NC-FL was tested under fatigue loading during the period between 5/26/10 and 6/14/10. The panel was subjected to two million cycles with the loading protocol described in Section 5.2.3.3. The panel was subjected to post-fatigue quasi-static load test until failure on 6/14/10, 148 days after the concrete was cast. No flexural cracks were observed during the cyclic loading process since the loading was within elastic range. In the post-fatigue static load test, flexural cracks first developed on the extreme tension face, which increased in length and numbers with increasing applied load. Cracks were first observed on the side face at an applied load of 18.77 kips and displacement of 1 in. The initial cracks started to appear at locations near the edge of the spreader beam location. As the applied load was increased, additional flexural cracks appeared and existing cracks propagated upward. At the final load stage the panel failed by concrete crushing. Failure occurred as the crack penetrated the flexural compression zone completely at the location of the spreader beam. As a result of the loss of load carrying capacity associated with the destruction of the flexural compression zone, the applied load dropped to 18.33 kips. The maximum load and corresponding displacement was 22.10 kips and 1.76 in., respectively. Upon attempt to regain the load level, further deformation was imposed on the specimen. The maximum load of 22.1 kips was not able to be recovered; thus the failure load for Panel ST-NC-FL corresponds to an applied load of 22.1 kips. Figure C-56 shows the post-failure state of the panel after the spreader beam was removed.

During the test, cracks were marked on the side faces of the panel at discrete load increments until the failure load was achieved. Figure C-57 shows the progression of cracking from an applied load of 18.77 kips (shortly after first observed flexural cracking occurred) to the maximum load of 22.1 kips.

C.4.7.2 Load-displacement

The stiffness degradation of the panel was studied by performing a quasi-static load test up to 0.25 inch after each 500,000 cycles. Panel ST-NC-FL was not subjected to the first two quasi-static load tests (0 cycles and 500,000 cycles). Figure C-58 shows the results of the quasi-static load tests at 1,000,000, 1,500,000, and 2,000,000 cycles at all locations. In Figure C-58, the stiffness degradation was observed to have the same rate in the cycles between 1,000,000 and 1,500,000 and in the cycles between 1,500,000 and 2,000,000. In addition, the stiffness degradation can be observed by the decreased maximum displacement, which affects the overall ductility. Figure C-59 shows the measured displacement along the panel length at Grids E, E’, and F for various load levels, including cracking and maximum loads (13.98 kips and 22.1 kips, respectively). As discussed in the static load test results sections, the cracking load was determined based on the change in behavior of the load-displacement relationship from Figure C-59 as well as the change in load-strain relationship discussed in Section C.4.1.3. Note that the cracking load determined in this manner is lower than the load corresponding to when side cracks were first observed as discussed in Section C.4.1.1. Displacements measured at Grids E, E’, and F are similar (within 3%) at each load level with the exception of the failure load. Figure C-60 shows the applied load-displacement response for all locations.

C.4.7.3 Load-strain

Figure C-61 shows the applied load-tendon strain relationship. In the figure, compression strain is shown as negative while tension strain is shown as positive. Tendon strains measured at all locations are negligible for applied load less than 13.98 kips. For applied load greater than 13.98 kips, tendon strains measured along Grid 2 increased linearly with increasing applied load, indicating that the neutral axis is shifting upwards and that the section has cracked. This change in behavior at this load level is consistent with the change in behavior of the load-displacement relationship described in Section C.4.7.2.

Figure C-62 shows the applied load-concrete surface strain relationship. Concrete surface gages along Grid 2 on the bottom surface of the panel stopped working after flexural cracks occurred at the gage location; thus measured strain in this location is reported only until the respective gage stopped working.

The strain distribution within the section at various locations is shown in Figure C-63. For each location, Figure C-63 shows strains measured on the top and bottom concrete surfaces and the corresponding strain measured in the tendon at different load levels, including cracking and failure loads (13.98 kips and 22.1 kips, respectively). Concrete surface gages along Grid 2 on the bottom surface of the panel stopped working after flexural cracks occurred at the gage location; thus measured strain in this location is reported only until the respective gage stopped working.

Figure C-64 shows the strain distribution within the section at various locations. For each location, Figure C-64 shows strains measured on the top and bottom concrete surfaces and the corresponding strain measured in the tendon at the maximum load for different number of cycles. The maximum load ranged between 8 kips and 12 kips. The measured strains in all locations are reported only for the working gages at the maximum load level.

C.4.8 Panel ST-FRC-FL

C.4.8.1 Failure and Cracking Behavior

Panel ST-FRC-FL was tested under fatigue loading during the period between 7/8/10 and 7/15/10. The panel was subjected to two million cycles with the loading protocol described in Section 5.2.3.3. The panel was subjected to a post-fatigue quasi-static load test until failure immediately after two million load cycles. The static load test was conducted on 7/16/10, 190 days after the concrete was cast. No flexural cracks were observed during the cyclic loading process since the loading was within elastic range. In the post fatigue static load test, flexural cracks first developed on the extreme tension face, which increased in length and number with increasing applied load. Cracks were first observed on the side face at an applied load of 15.33 kips and displacement of 0.45 in. The initial cracks started to appear at locations near the edge of the spreader beam location. As the applied load was increased, additional flexural cracks appeared and existing cracks propagated upward. As observed in the static load test, at the final load stage the panel failed by concrete crushing by means failure occurred as the crack penetrated the flexural compression zone completely at the location of the spreader beam. As a result of the loss of load carrying capacity associated with the destruction of the flexural compression zone, the applied load dropped to 17.18 kips. The maximum load and corresponding displacement was 20.7 kips and 1.63 in., respectively. Upon attempt to maintain and increase the load level, further deformation was imposed on the specimen. The maximum load of 20.7 kips was not able to be recovered; thus the failure load for Panel ST-FRC-FL corresponds to an applied load of 20.7 kips. Figure C-65 shows the post-failure state of the panel after the spreader beam was removed.

During the post fatigue static load test, cracks were marked on the side faces of the panel at discrete load increments until the failure load was achieved. Figure C-66 shows the progression of cracking from an applied load of 15.33 kips (shortly after first observed flexural cracking occurred) to the maximum load of 20.7 kips.

C.4.8.2 Load-displacement

The stiffness degradation of the panel was studied by performing a quasi-static load test up to 0.25 inch after each 500,000 cycles. Panel ST-FRC-FL was subjected to a total of five quasi-static load tests before the cyclic loading began and after each 500,000 cycles (0, 500,000, 1,000,000, 1,500,000, and 2,000,000 cycles). Figure C-67 shows the applied load and displacement relationships for the quasi-static load tests at all locations. The figure shows major stiffness degradation in the cycles between 0 and 500,000 and the cycles between 1,500,000 and 2,000,000 cycles. At the final load stage, the stiffness degradation was observed by the decreased maximum displacement, which affects the overall ductility. Figure C-68 shows the measured displacement along the panel length at Grids E, E', and F for various load levels, including cracking and maximum loads (14 kips and 20.7 kips, respectively). As discussed in the static load test section, the cracking load was determined based on the change in behavior of the load-displacement relationship from Figure C-68 as well as the change in load-strain relationship discussed in Section C.4.8.3. Note that the cracking load determined in this manner is slightly lower than the load corresponding to when flexural cracks were first observed as discussed in Section C.4.8.1. Displacements measured at Grids E, E', and F are similar (within 3.5%) at each load level with the exception of the failure load. Figure C-69 shows the applied load-displacement response for all locations.

C.4.8.3 Load-strain

Figure C-70 shows the applied load-tendon strain relationship at the final load stage. In the figure, compression strain is shown as negative while tension strain is shown as positive. Tendon strains measured at all locations are negligible for applied load less than 14.0 kips. For applied load greater than 14.0 kips tensile strains measured in the tendons along Grid 2 increase linearly with increasing applied load, indicating that the neutral axis is shifting upwards and that the section has cracked. This change in behavior at this load level is consistent with the change in behavior of the load-displacement relationship described in Section C.4.8.2. The response of the applied load-tendon strain shows the insignificant effects of two million cycles on the panel behavior.

Figure C-71 shows the applied load-concrete surface strain relationship at the final load stage. Concrete surface gages along Grid 2 on the bottom surface of the panel stopped working after flexural cracks occurred at the gage location; thus measured strain in this location is reported only until the respective gage stopped working.

The strain distribution within the section at various locations at the final loading stage is shown in Figure C-72. For each location, Figure C-72 show strains measured on the top and bottom concrete surfaces and the corresponding strain measured in the tendon at different load levels, including cracking and failure loads (14.0 kips and 20.7 kips, respectively). Concrete surface gages along Grid 2 on the bottom surface of the panel stopped working after flexural cracks occurred at the gage location; thus, measured strain in this location is reported only until the respective gage stopped working.

Figure C-73 shows the strain distribution within the section at various locations. For each location, Figure C-73 shows strains measured on the top and bottom concrete surfaces and the corresponding strain measured in the tendon at the maximum load for different number of cycles. The maximum load after each 500,000 cycles ranged between 8 kips and 12 kips. The measured strains in all locations are reported only for the working gages at the maximum load level.

C.4.9 Panel ECST-NC-FL

C.4.9.1 Failure and Cracking Behavior

Panel ST-NC-FL was tested under fatigue loading on the period between 6/28/10 and 7/7/10. The panel was subjected to two million cycles with the loading protocol described in Section 5.2.3.3. The panel was subjected to static load test until failure immediately after two million load cycles. The static load test was conducted on 7/7/10, 118 days after the concrete was cast. No flexural cracks were observed during the cyclic loading process since the loading was within elastic range. In the post fatigue static load test, flexural cracks first developed on the extreme tension face, which increased in length and number with increasing applied load. Cracks were first observed on the side face at an applied load of 17.18 kips and displacement of 0.65 in. The initial cracks started to appear at locations near the edge of the spreader beam location. As the applied load was increased, additional flexural cracks appeared and existing cracks propagated upward. As observed in the static load test, at the final load stage the panel failed by concrete crushing by means failure occurred as the crack penetrated the flexural compression zone completely at the location of the spreader beam. As a result of the loss of load carrying capacity associated with the destruction of the flexural compression zone, the applied load dropped suddenly to 10.35 kips. The maximum load and corresponding displacement was 19.0 kips and 1.12 in., respectively. Upon attempt to maintain and increase the load level, further deformation was imposed on the specimen. No decrease in the displacement was observed. The maximum load of 19 kips was not able to be recovered; thus the failure load for Panel ST-NC-FL corresponds to an applied load of 19 kips. Figure C-74 shows the post-failure state of the panel after the spreader beam was removed.

During the test, cracks were marked on the side faces of the panel at discrete load increments until the failure load was achieved. Figure C-75 shows the progression of cracking from an applied load of 17.18 kips (shortly after first observed flexural cracking occurred) to the maximum load of 19.00 kips.

C.4.9.2 Load-displacement

The stiffness degradation of the panel was studied by performing a quasi-static load test up to 0.25 inch after each 500,000 cycles. Panel ST-NC-FL was subjected to a total of five quasi-static load tests (0, 500,000, 1,000,000, 1,500,000, and 2,000,000 cycles). Figure C-76 shows the applied load and displacement results of the quasi-static load tests at all locations. The figure shows main stiffness degradation in the cycles between 0 and 500,000 and the cycles between 1,500,000 and 2,000,000 cycles. In addition, the stiffness degradation was observed by the decreased maximum displacement, which affects the overall ductility. Figure C-77 shows the measured displacement along the panel length at Grids E, E’, and F for various load levels, including cracking and maximum loads (15.5 kips and 19.0 kips, respectively). As discussed in the static load test section, the cracking load was determined based on the change in behavior of the load- displacement relationship from Figure C-77, as well as the change in load-strain relationship discussed in Section C.4.9.3. Note that the cracking load determined in this manner is slightly lower than the load corresponding to when flexural cracks were first observed as discussed in Section C.4.9.1. Displacements measured at Grids E, E', and F are similar (within 3.5%) at each load level with the exception of the failure load. Figure C-78 shows the applied load-displacement response for all locations.

C.4.9.3 Load-strain

Figure C-79 shows the applied load-tendon strain relationship. In the figure, compression strain is shown as negative while tension strain is shown as positive. Tendon strains measured at all locations are negligible for applied load less than 15.5 kips. For applied load greater than 15.5 kips tensile strains measured in the tendons along Grid 2 increase linearly with increasing applied load, indicating that the neutral axis is shifting upwards and that the section has cracked. This change in behavior at this load level is consistent with the change in behavior of the load-displacement relationship described in Section C.4.9.2. The response of the applied load-tendon strain shows the insignificant effects of two million cycles on the panel behavior.

Figure C-80 shows the applied load-concrete surface strain relationship. Concrete surface gages along Grid 2 on the bottom surface of the panel stopped working after flexural cracks occurred at the gage location; thus measured strain in this location is reported only until the respective gage stopped working.

The strain distribution within the section at various locations at the final loading stage is shown in Figure C-81. For each location, in Figure C-81 shows strains measured on the top and bottom concrete surfaces and the corresponding strain measured in the tendon at different load levels, including cracking and failure loads (15.5 kips and 19.0 kips, respectively). Concrete surface gage along Grid 2 on the bottom surface of the panel stopped working after flexural cracks occurred at the gage location; thus measured strain in this location is reported only until the respective gage stopped working.

Figure C-82 shows the strain distribution within the section at various locations. For each location, Figure C-82 shows strains measured on the top and bottom concrete surfaces and the corresponding strain measured in the tendon at the maximum load for different number of cycles. The maximum load after each 500,000 cycles ranged between 8 kips and 12 kips. The measured strains in all locations are reported only for the working gages at the maximum load level.

C.4.10 Panel ECST-FRC-FL

C.4.10.1 Failure and Cracking Behavior

Panel ECST-FRC-FL was tested under fatigue loading during the period between 7/28/10 and 8/4/10. No flexural cracks were observed during the cyclic loading process since the loading was within elastic range. The panel was subjected to static load test until failure immediately after two million load cycles. The static load test was conducted on 8/4/10, 143 days after the concrete was cast. No flexural cracks were observed during the cyclic loading process since the loading was within elastic range. In the post fatigue static load test, flexural cracks first developed on the extreme tension face, which increased in length and number with increasing applied load.

Cracks were first observed on the side face at an applied load of 15.71 kips and displacement of 0.50 in. The initial cracks started to appear at locations near the edge of the spreader beam location. As the applied load was increased, additional flexural cracks appeared and existing cracks propagated upward. As observed in the static load test, at the final load stage the panel failed by concrete crushing by means failure occurred as the crack penetrated the flexural compression zone completely at the location of the spreader beam. As a result of the loss of load carrying capacity associated with the destruction of the flexural compression zone, the applied load dropped suddenly to 11.15 kips. The maximum load and corresponding displacement was 19.49 kips and 1.40 in., respectively. Upon attempt to maintain and increase the load level, further deformation was imposed on the specimen. The maximum load of 19.49 kips was not able to be recovered; thus the failure load for Panel ECST-FRC-FL corresponds to an applied load of 19.49 kips. Figure C-83 shows the post-failure state of the panel after the spreader beam was removed.

During the test, cracks were marked on the side faces of the panel at discrete load increments until the failure load was achieved. Figure C-84 shows the progression of cracking from an applied load of 15.71 kips (shortly after first observed flexural cracking occurred) to the maximum load of 19.49 kips.

C.4.10.2 Load-displacement

The stiffness degradation of the panel was studied by performing a quasi-static load test up to 0.25 inch after each 500,000 cycles. Panel ST-NC-FL was subjected to a total of five quasi-static load tests (0, 500,000, 1,000,000, 1,500,000, and 2,000,000 cycles). Figure C-85 shows the applied load and displacement results of the quasi-static load tests at all locations. The figure shows main stiffness degradation in the cycles between 0 and 500,000 and the cycles between 1,500,000 and 2,000,000 cycles. In addition, the stiffness degradation was observed by the decreased maximum displacement, which affects the overall ductility. Figure C-86 shows the measured displacement along the panel length at Grids E, E’, and F for various load levels, including cracking and maximum loads (13.25 kips and 19.49 kips, respectively). As discussed in the static load test section, the cracking load was determined based on the change in behavior of the load- displacement relationship from Figure C-86, as well as the change in load-strain relationship discussed in Section C.4.1.3. Note that the cracking load determined in this manner is slightly lower than the load corresponding to when flexural cracks were first observed as discussed in Section C.4.1.1. Displacements measured at Grids E, E’, and F are similar (within 3%) at each load level with the exception of the failure load. Figure C-87 shows the applied load-displacement response for all locations.

C.4.10.3 Load-strain

Figure C-88 shows the applied load-tendon strain relationship. In the figure, compression strain is shown as negative while tension strain is shown as positive. Tendon strains measured at all locations are negligible for applied load less than 13.25 kips. For applied load greater than 13.25 kips tensile strains measured in the tendons along Grid 2 increase linearly with increasing applied load, indicating that the neutral axis is shifting upwards and that the section has cracked. This change in behavior at this load level is consistent with the change in behavior of the load-displacement relationship described in Section C.4.3.2. The response of the applied load-tendon strain shows the insignificant effects of two million cycles on the panel behavior.

Figure C-89 shows the applied load-concrete surface strain relationship. Concrete surface gages along Grid 2 on the bottom surface of the panel stopped working after flexural cracks occurred at the gage location; thus measured strain in this location is reported only until the respective gage stopped working.

The strain distribution within the section at various locations at the final loading stage is shown in Figure C-90. For each location, Figure C-90 shows strains measured on the top and bottom concrete surfaces and the corresponding strain measured in the tendon at different load levels, including cracking and failure loads (13.25 kips and 19.49 kips, respectively). Concrete surface gage along Grid 2 on the bottom surface of the panel stopped working after flexural cracks occurred at the gage location; thus measured strain in this location is reported only until the respective gage stopped working.

Figure C-91 shows the strain distribution within the section at various locations. For each location, Figure C-91 shows strains measured on the top and bottom concrete surfaces and the corresponding strain measured in the tendon at the maximum load for different number of cycles. The maximum load after each 500,000 cycles ranged between 8 kips and 12 kips. The measured strains in all locations are reported only for the working gages at the maximum load level.

C.4.11 Panel CFRPT-NC-FL

C.4.11.1 Failure and Cracking Behavior

Panel CFRPT-NC-FL was tested under fatigue loading on the period between 6/16/10 and 6/23/10. The panel was subjected to two million cycles with the loading protocol described in Section 5.2.3.3. The panel was subjected to static load test until failure immediately after two million load cycles. The static load test was conducted on 6/25/10, 106 days after the concrete was cast. No flexural cracks were observed during the cyclic loading process since the loading was within elastic range. In the post fatigue static load test, flexural cracks first developed on the extreme tension face, which increased in length and number with increasing applied load. Cracks were first observed on the side face at an applied load of 16.38 kips and displacement of 0.70 in. The initial cracks started to appear at locations near the edge of the spreader beam location. As the applied load was increased, additional flexural cracks appeared and existing cracks propagated upward. As observed in the static load test, at the final load stage the panel failed by concrete crushing by means failure occurred as the crack penetrated the flexural compression zone completely at the location of the spreader beam. As a result of the loss of load carrying capacity associated with the destruction of the flexural compression zone, the applied load dropped to 14.95 kips. The maximum load and corresponding displacement was 17.49 kips and 1.02 in., respectively. Upon attempt to maintain and increase the load level, further deformation was imposed on the specimen. No significant displacement increase was observed. The maximum load of 17.49 kips was not able to be recovered; thus the failure load for Panel CFRPT-NC-FL corresponds to an applied load of 17.49 kips. Figure C-92 shows the post-failure state of the panel after the spreader beam was removed.

During the post fatigue static load test, cracks were marked on the side faces of the panel at discrete load increments until the failure load was achieved. Figure C-93 shows the progression of cracking from an applied load of 16.38 kips (shortly after first observed flexural cracking occurred) to the maximum load of 17.49 kips.

C.4.11.2 Load-displacement

The stiffness degradation of the panel was studied by performing a quasi-static load test up to 0.25 inch after each 500,000 cycles. Panel CFRPT-NC-FL was subjected to a total of five quasi-static load test before the cyclic loading and after each 500,000 cycles (0, 500,000, 1,000,000, 1,500,000, and 2,000,000 cycles). Figure C-94 shows the applied load and displacement results of the quasi-static load tests at all locations. The figure shows major stiffness degradation in the cycles between 0 and 500,000 and the cycles between 1,500,000 and 2,000,000 cycles. In addition, the stiffness degradation was observed by the decreased maximum displacement, which affects the overall ductility. Figure C-95 shows the measured displacement along the panel length at Grids E, E', and F for various load levels, including cracking and maximum loads (13.7 kips and 17.49 kips, respectively). As discussed in the static load test section, the cracking load was determined based on the change in behavior of the load- displacement relationship from Figure C-95, as well as the change in load-strain relationship discussed in Section C.4.11.3. Note that the cracking load determined in this manner is slightly lower than the load corresponding to when flexural cracks were first observed as discussed in Section C.4.11.1. Displacements measured at Grids E, E', and F are similar (within 3.5%) at each load level with the exception of the failure load. Figure C-96 shows the applied load-displacement response for all locations.

C.4.11.3 Load-strain

Figure C-97 shows the applied load-tendon strain relationship at the final load stage. In the figure, compression strain is shown as negative while tension strain is shown as positive. Tendon strains measured at all locations are negligible for applied load less than 13.7 kips. For applied load greater than 13.7 kips tensile strains measured in the tendons along Grid 2 increase linearly with increasing applied load, indicating that the neutral axis is shifting upwards and that the section has cracked. This change in behavior at this load level is consistent with the change in behavior of the load-displacement relationship described in Section C.4.11.3. The response of the applied load-tendon strain shows the insignificant effects of two million cycles on the panel behavior.

Figure C-98 shows the applied load-concrete surface strain relationship at the final load stage. Concrete surface gages along Grid 2 on the bottom surface of the panel stopped working after flexural cracks occurred at the gage location; thus, measured strain in this location is reported only until the respective gage stopped working.

The strain distribution within the section at various locations at the final loading stage is shown in Figure C-99. For each location, Figure C-99 shows strains measured on the top and bottom concrete surfaces and the corresponding strain measured in the tendon at different load levels, including cracking and failure loads (13.7 kips and 17.49 kips, respectively). Concrete surface gages along Grid 2 on the bottom surface of the panel stopped working after flexural cracks occurred at the gage location; thus measured strain in this location is reported only until the respective gage stopped working.

Figure C-100 shows the strain distribution within the section at various locations. For each location, Figure C-100 shows strains measured on the top and bottom concrete surfaces and the corresponding strain measured in the tendon at the maximum load for different number of cycles. The maximum load after each 500,000 cycles ranged between 8 kips and 12 kips. The measured strains in all locations are reported only for the working gages at the maximum load level.

C.4.12 Panel CFRPT-FRC-FL

C.4.12.1 Failure and Cracking Behavior

Panel CFRPT-NC-FL was tested under fatigue loading on the period between 7/20/10 and 7/26/10. The panel was subjected to two million cycles with the loading protocol described in Section 5.2.3.3. The panel was subjected to static load test until failure immediately after two million load cycles. The static load test was conducted on 7/26/10, 134 days after the concrete was cast. No Flexural cracks observed during the cyclic loading process due to the elastic loading range. In the post fatigue static load test, flexural cracks first developed on the extreme tension face, which increased in length and number with increasing applied load. Cracks were first observed on the side face at an applied load of 15.14 kips and displacement of 0.60 in. The initial cracks started to appear at locations near the edge of the spreader beam location. As the applied load was increased, additional flexural cracks appeared and existing cracks propagated upward. As observed in the static load test, at the final load stage the panel failed by concrete crushing by means failure occurred as the crack penetrated the flexural compression zone completely at the location of the spreader beam. As a result of the loss of load carrying capacity associated with the destruction of the flexural compression zone, the applied load dropped to 11.24 kips. The maximum load and corresponding displacement was 17.95 kips and 1.33 in., respectively. Upon attempt to maintain and increase the load level, further deformation was imposed on the specimen. No significant displacement increase was observed. The maximum load of 17.95 kips was not able to be recovered; thus the failure load for Panel CFRPT-FRC-FL corresponds to an applied load of 17.95 kips. Figure C-101 shows the post-failure state of the panel after the spreader beam was removed.

During the post fatigue static load test, cracks were marked on the side faces of the panel at discrete load increments until the failure load was achieved. Figure C-102 shows the progression of cracking from an applied load of 16.38 kips (shortly after first observed flexural cracking occurred) to the maximum load of 17.49 kips.

C.4.12.2 Load-displacement

The stiffness degradation of the panel was studied by performing quasi-static load test up to 0.25 inch after each 500,000 cycles. Panel CFRPT-FRC-FL was subjected to five quasi-static load test before the cyclic loading and after each 500,000 cycles (0, 500,000, 1,000,000, 1,500,000, and 2,000,000 cycles). Figure C-103 shows the applied load and displacement results of the quasi static at all locations. The figure shows major stiffness degradation in the cycles between 0 and 500,000 and the cycles between 1,500,000 and 2,000,000 cycles. In addition, the stiffness degradation was observed by the decreased maximum displacement, which affects the overall ductility. Figure C-104 shows the measured displacement along the panel length at Grids E, E’, and F for various load levels, including cracking and maximum loads (13 kips and 17.95 kips, respectively). As discussed in the static load test section, the cracking load was determined based on the change in behavior of the load- displacement relationship from Figure C-104, as well as the change in load-strain relationship discussed in Section C.4.12.3. Note that the cracking load determined in this manner is slightly lower than the load corresponding to when flexural cracks were first observed as discussed in Section C.4.12.1. Displacements measured at Grids E, E', and F are similar (within 3 %) at each load level with the exception of the failure load. Figure C-105 shows the applied load-displacement response for all locations.

C.4.12.3 Load-strain

Figure C-106 shows the applied load-tendon strain relationship. In the figure, compression strain is shown as negative while tension strain is shown as positive. Tendon strains measured at all locations are negligible for applied load less than 13 kips. For applied load greater than 13 kips tensile strains measured in the tendons along Grid 2 increase linearly with increasing applied load, indicating that the neutral axis is shifting upwards and that the section has cracked. This change in behavior at this load level is consistent with the change in behavior of the load-displacement relationship described in Section C.4.12.2.

Figure C-107 shows the applied load-concrete surface strain relationship. Concrete surface gages along Grid 2 on the bottom surface of the panel stopped working after flexural cracks occurred at the gage location; thus measured strain in this location is reported only until the respective gage stopped working.

The strain distribution within the section at various locations is shown in Figure C-108. For each location, Figure C-108 shows strains measured on the top and bottom concrete surfaces and the corresponding strain measured in the tendon at different load levels, including cracking and failure loads (13 kips and 17.95 kips, respectively). Concrete surface gages along Grid 2 on the bottom surface of the panel stopped working after flexural cracks occurred at the gage location; thus measured strain in this location is reported only until the respective gage stopped working.

Figure C-109 shows the strain distribution within the section at various locations. For each location, Figure C-109 shows strains measured on the top and bottom concrete surfaces and the corresponding strain measured in the tendon at the maximum load for different number of cycles. The maximum load ranged between 8 kips and 12 kips. The measured strains in all locations are reported only for the working gages at the maximum load level.

C.5 DURABILITY EXPERIMENT RESULTS

C.5.1 Corrosion initiation test

C.5.1.1 Visual inspection

The corrosion initiation test was conducted in the Missouri S&T Civil Engineering Materials Laboratory from 1/27/2010 to 8/3/2010. Test specimens were subjected to wet/dry cycles during the test period. Test specimens were submerged in 5% NaCl solution for 4 days then were dried in oven at 104ºF for 3 days. Table C-4, Table C-5, and Table C-6 show the concrete deterioration observed with respect to different edge distance. Efflorescence was observed in all specimens regardless of geometrical and material properties. Rust was observed on most of specimens with 1.5 in. edge distance, while two specimens for each specimen group with 2.5 in. and 3.5 in. edge distances showed rust. Cracking was observed in three specimens with 1.5 in. edge distance, while only one specimen in each specimen group with 2.5 in. and 3.5 in. edge distances showed cracking. All cracks were observed on the surfaces of the specimens only; cracks did not appear to have propagated from the tendon location. In other words, the cracks appeared to be superficial cracks and not corrosion-induced cracks. Thus, it was concluded that the corrosion of the embedded tendons was not enough to cause corrosion-induced cracks.

C.5.1.2 Half-cell potential

Table C-7, Table C-8, and Table C-9 show half-cell potential data collected every two weeks during the test period. The values in the tables can be compared to limiting values reported in ASTM C876-91. Accordingly, corrosion probability is higher than 90% when potential value is higher than -350 mV. Values within the range of -200mV to -350mV indicate a 50% probability of corrosion. For values lower than -200mV, probability is less than 5%. Figure C-114 shows the relationship between potential and time duration for each of the different concrete materials. Figure C-115 shows the relationship between potential and time duration for specimens with different edge distance. Although there are some fluctuations in the data, decreasing edge distance tended to increase the probability of corrosion. From both Figure C-114 and Figure C-115, it can be seen that specimens with corrosion inhibitor tended to have the highest probability of corrosion.

C.5.1.3 Chloride content analysis

Figure C-116 shows the chloride contents at different depths for specimens of the same material but different edge distances, while Figure C-117 shows the chloride contents at different depths for specimens with the same edge distances and different concrete materials. Concrete samples were taken from three locations: 0.5 in. from the surface, mid-depth between surface and steel location, and at the steel location. Although it is somewhat difficult to distinguish the effects of material and edge distance due to the scatter of the data, general observations can be made. Specimens with corrosion inhibitor tended to have the greatest chloride ingress. Specimens with 3.5 in. edge distance tended to show the lowest chloride ingress.

C.5.2 Accelerated corrosion test

C.5.2.1 Visual inspection

Accelerated corrosion test specimens were tested for a six month time duration from 1/29/2010 to 7/8/2010. Table C-10 shows the steel tendons retrieved at the end of test. Corrosion length was measured at both ends of the specimen, and longer length was taken as the corrosion length for the corresponding specimen.

C.5.2.2 Gravimetric study

Steel tendons were retrieved from all test specimens to measure the steel loss after 4,400 hours. The initial weight of the steel tendons was determined on the day the specimens were constructed (12/29/2009). Steel loss, as well as recorded time to corrosion cracking and spalling, is reported in Table C-11. Concrete with fibers showed the longest time for corrosion cracking, while concrete with corrosion inhibitor showed the shortest time. Steel mass loss data were used to estimate the corrosion rate (described in the main body of the report).

Table C- 1 Concrete Mixture Materials and Proportions

Normal concrete, Normal concrete + fibers (12/29/09 Concrete Batch)

	Normal concrete		Normal concrete + fibers	
	Specified	Actual	Specified	Actual
Cement[1] (lbs/cy)	751	748	751	748
Course aggregate[2] (lbs/cy)	1573	1571	1570	1569
Sand[3] (lbs/cy)	1289	1288	1290	1291
Water (lbs/cy)	187	188	185	185
HRWR[6] (oz)	85	86	80	80
Air Entraining Admixture[5] (oz)	37	37	35	35
Fiber[6] (bags/cy)	-	-	1	1
Corrosion inhibitor[7]	-	-	-	-
NaCl[8]	-	-	-	-
Water–cement ratio (w/c)	0.34	0.31	0.34	0.34

Normal concrete, Normal concrete + fibers (3/12/10 Concrete Batch)

	Normal concrete		Normal concrete + fibers	
	Specified	Actual	Specified	Actual
Cement[1] (lbs/cy)	751	751	751	752
Course aggregate[2] (lbs/cy)	1549	1591	1549	1595
Sand[3] (lbs/cy)	1235	1287	1235	1289
Water (lbs/cy)	268	166	268	173
HRWR[6] (oz)	72.02	70.67	72.02	70.67
Air Entraining Admixture[5] (oz)	32	32	32	32
Fiber (bags/cy)	-	-	1.5	1
Corrosion inhibitor[7]	-	-	-	-
NaCl[8]	-	-	-	-
Water–cement ratio (w/c)	0.3656	.321	0.3656	.365

Normal concrete + 3% NaCl, Normal concrete + fibers + 3% NaCl

	Normal concrete + 3% NaCl		Normal concrete + fibers + 3% NaCl	
	Specified	Actual	Specified	Actual
Cement[1] (lbs/cy)	751	750	751	750
Course aggregate[2] (lbs/cy)	1577	1573	1582	1578
Sand[3] (lbs/cy)	1293	1287	1293	1282
Water (lbs/cy)	190	190	190	191
HRWR[6] (oz)	79	81	80	82
Air Entraining Admixture[5] (oz)	35	36	32	32
Fiber (bags/cy)	-	-	1	1
Corrosion inhibitor[7]	-	-	-	-
NaCl[8] (lbs/cy)	22.5	22.5	22.5	22.5
Water–cement ratio (w/c)	0.34	0.34	0.34	0.34

Table C-1 Concrete Mixture Materials and Proportions (Cont.)

Normal concrete + corrosion inhibitor, Normal concrete + corrosion inhibitor + 3% NaCl

	Normal concrete + corrosion inhibitor		Normal concrete + corrosion inhibitor + 3% NaCl	
	Specified	Actual	Specified	Actual
Cement[1] (lbs/cy)	751	748	751	748
Course aggregate[2] (lbs/cy)	1579	1573	1574	1568
Sand[3] (lbs/cy)	1295	1287	1290	1287
Water (lbs/cy)	191	192	187	187
HRWR[6] (oz/cy)	81	83	79	82
Air Entraining Admixture[5] (oz/cy)	37	36	30	31
Fiber (bags/cy)	-	-	-	-
Corrosion inhibitor (oz/cy)[7]	2	3	1	4
NaCl[8] (lbs/cy)	-	-	22.5	22.5
Water–cement ratio (w/c)	0.34	0.34	0.34	0.34

Notes:
1. Cement is ASTM C-150 Type 3 (Ashgrove)
2. Coarse aggregate is ASTM C-33 (Limestone)
3. Fine aggregate is ASTM C-33 (Kaw sand)
4. HRWR is ASTM C-494 (Glenium 7700)
5. Air Entraining Admixture is ASTM C-260 (MB VR standard)
6. Fibers are ASTM C-1116 (Master fiber F70)
7. Corrosion inhibitor is MCI (Cortec Corporation)
8. NaCl is 3% of cement

Table C- 2 Measured Hardened Concrete Properties – Unit Panel Specimens

	ST-NC		ST-FRC		ECT-NC		ECT-FRC		CFRP-NC		CFRP-FRC	
	-SL	-FL	-SL	-FL	-SL	-FL	-SL	-FL	-SL	-FL	-SL	-FL
28-day concrete compr. strength (psi)	6000	6000	6160	6160	5640	5640	7060	7060	5640	5640	7060	5640
Concrete compr. strength at test date (psi)	6360	6380	5580	7710	5900	6200	6460	7600	7000	6040	6390	6080
Modulus of rupture (psi)	600	-	-	855	-	765	-	745	620	-	585	-

Table C- 3 Prestressed Reinforcement Material Properties

	Yield Strength (lbs)		Breaking Strength (lbs)		Elongation (%)	
	Measured	Mill Certification	Measured	Mill Certification	Measured	Mill Certification
Steel strand, 3/8 inch diameter 7-wire Grade 270 ASTM A 416	21450	21,904	23,320	24,404	7.8	7.5
Steel strand, 3/8 inch diameter 7-wire Grade 270 ASTM A 416	22130	21,904	23750	24,404	7.4	7.5
Epoxy-coated steel strand, 3/8 inch diameter 7-wire Grade 270 ASTM A 882	23205	22,438	24,647	24,352	5.1	4.7
CFRP	-	-	-	40,447	-	1.92

Table C- 4 Visual Inspection for Corrosion Initiation Specimens with 1.5 in. Edge Distance

Specimen Designation	Concrete Deterioration		
	Efflorescence	Rust	Cracking
SP1-NC-1	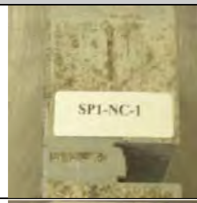	None observed	None observed
SP1-NC-2	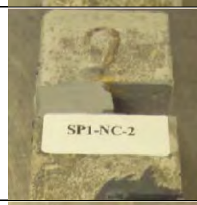		None observed
SP1-NC-3	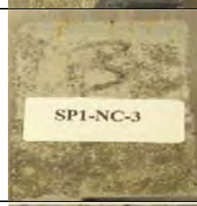		None observed
SP1-CI-1	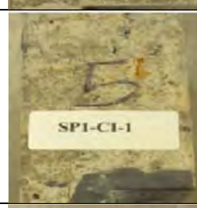		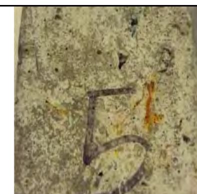
SP1-CI-2	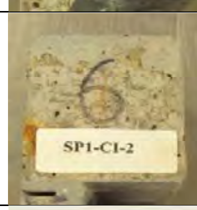	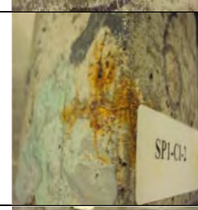	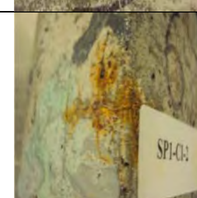
SP1-CI-3	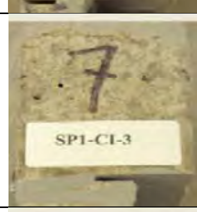		
SP1-FRC-1			
SP1-FRC-2		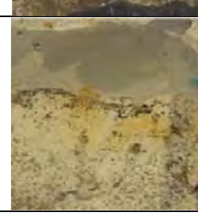	

SP1-FRC-3			

Table C- 5 Visual Inspection for Corrosion Initiation Specimens with 2.5 in. Edge Distance

Specimen Designation	Concrete Deterioration		
	Efflorescence	Rust	Cracking
SP2-NC-5		None observed	None observed
SP2-NC-6		None observed	None observed
SP2-NC-7		None observed	None observed
SP2-CI-5		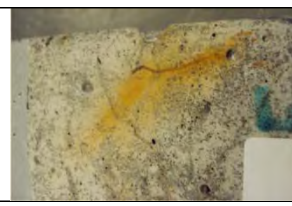	None observed
SP2-CI-6		None observed	None observed
SP2-CI-7			
SP2-FRC-5	None observed	None observed	None observed
SP2-FRC-6	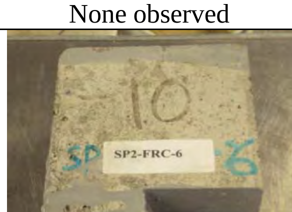	None observed	None observed
SP2-FRC-7		None observed	None observed

Table C- 6 Visual Inspection for Corrosion Initiation Specimens with 3.5 in. Edge Distance

Specimen Designation	Concrete Deterioration		
	Efflorescence	Rust	Cracking
SP3-NC-9		None observed	None observed
SP3-NC-10		None observed	None observed
SP3-NC-11		None observed	None observed
SP3-CI-9			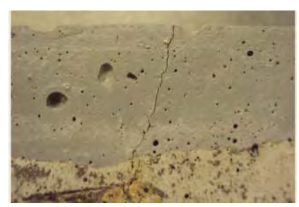
SP3-CI-10			None observed

SP3-CI-11		None observed	None observed
SP3-FRC-9		None observed	None observed
SP3-FRC-10		None observed	None observed
SP3-FRC-11		None observed	None observed

Table C- 7 Half-cell Potential and Resistivity after Two Months

Specimen Label	2 Months specimens - Period and Measurements							
	2 Weeks		4 Weeks		6 Weeks		8 Weeks	
	Potential (mV)	Resistivity (KΩ.cm)	Potential (mV)	Resistivity (KΩ.cm)	Potential (mV)	Resistivity (KΩ.cm)	Potential (mV)	Resistivity (KΩ.cm)
SP1-NC-1	-238.5	5.8	-299.0	19.0	-248.0	13.0	-291.5	14.0
SP1-NC-2	-269.0	5.0	-273.5	11.0	-313.0	11.0	-307.0	17.0
SP1-NC-3	-249.5	12.0	-294.5	36.0	-397.5	11.0	-363.5	19.0
SP1-CI-1	-243.0	14.0	-229.0	19.0	-227.0	8.6	-235.5	17.0
SP1-CI-2	-242.5	7.0	-339.0	14.0	-363.5	14.0	-395.0	20.0
SP1-CI-3	-241.5	10.0	-255.0	12.0	-306.0	11.0	-390.0	17.0
SP1-FRC-1	-344.0	9.0	-369.5	8.5	-356.5	8.1	-350.5	15.0
SP1-FRC-2	-337.5	9.0	-306.5	5.8	-357.5	6.5	-382.5	18.0
SP1-FRC-3	-249.5	7.1	-250.5	9.1	-237.0	7.3	-226.5	15.0
SP2-NC-5	-235.5	17.0	-243.0	16.0	-232.5	29.0	-218.5	32.0
SP2-NC-6	-231.0	15.0	-220.0	12.0	-232.0	14.0	-278.5	28.0
SP2-NC-7	-214.0	13.0	-208.5	18.0	-230.5	19.0	-264.5	33.0
SP2-CI-5	-219.5	10.0	-216.5	12.0	-196.0	11.0	-240.0	19.0
SP2-CI-6	-312.5	21.0	-337.5	18.0	-327.0	16.0	-271.0	25.0
SP2-CI-7	-212.0	18.0	-335.0	13.0	-315.5	15.0	-344.5	23.0
SP2-FRC-5	-255.5	10.0	-328.0	14.0	-321.5	11.0	-318.5	21.0
SP2-FRC-6	-221.5	12.0	-211.0	15.0	-337.0	12.0	-343.0	21.0
SP2-FRC-7	-243.5	15.0	-238.0	15.0	-216.5	14.0	-216.0	26.0
SP3-NC-9	-229.0	18.0	-360.5	23.0	-353.0	25.0	-360.5	37.0
SP3-NC-10	-223.0	16.0	-215.0	20.0	-188.0	28.0	-173.5	45.0
SP3-NC-11	-235.0	15.0	-322.0	18.0	-352.5	23.0	-386.5	35.0
SP3-CI-9	-242.5	20.0	-333.5	17.0	-419.5	24.0	-463.0	29.0
SP3-CI-10	-244.5	15.0	-259.5	18.0	-275.5	25.0	-300.0	30.0
SP3-CI-11	-198.0	17.0	-196.5	20.0	-181.0	20.0	-213.5	32.0
SP3-FRC-9	-215.5	12.0	-218.5	16.0	-244.5	27.0	-303.5	27.0
SP3-FRC-10	-226.0	15.0	-226.5	21.0	-242.0	19.0	-277.0	29.0
SP3-FRC-11	-212.0	15.0	-234.5	18.0	-269.0	19.0	-349.0	29.0

Table C- 8 Half-cell Potential and Resistivity after Four Months

Specimen Label	4 Months specimens - Period and Measurements							
	2 Weeks		4 Weeks		6 Weeks		8 Weeks	
	Potential (mV)	Resistivity (KΩ.cm)	Potential (mV)	Resistivity (KΩ.cm)	Potential (mV)	Resistivity (KΩ.cm)	Potential (mV)	Resistivity (KΩ.cm)
SP1-NC-1	-372.0	31.0	-385.5	34.0	-399.5	19.0	-400.0	54.0
SP1-NC-2	-410.5	14.0	-443.5	11.0	-448.5	13.0	-410.5	20.0
SP1-NC-3	-354.0	15.0	-412.0	11.0	-412.5	9.0	-417.0	16.0
SP1-CI-1	-410.5	9.3	-429.0	12.0	-446.0	9.7	-466.5	14.0
SP1-CI-2	-417.0	6.4	-446.5	5.8	-448.5	5.5	-455.0	9.5
SP1-CI-3	-427.0	6.4	-449.0	6.7	-471.0	8.3	-491.5	12.0
SP1-FRC-1	-385.0	6.3	-390.0	6.6	-420.0	8.0	-398.5	13.0
SP1-FRC-2	-388.5	11.0	-411.0	9.1	-402.5	9.8	-385.0	22.0
SP1-FRC-3	-252.5	10.0	-259.5	10.0	-364.0	11.0	-231.0	17.0
SP2-NC-5	-367.0	17.0	-402.0	16.0	-456.5	20.0	-456.0	29.0
SP2-NC-6	-334.0	19.0	-373.0	17.0	-384.0	21.0	-337.5	31.0
SP2-NC-7	-312.5	14.0	-388.5	14.0	-465.5	16.0	-461.0	24.0
SP2-CI-5	-379.0	19.0	-413.5	16.0	-461.0	22.0	-437.5	30.0
SP2-CI-6	-407.0	14.0	-442.0	12.0	-464.0	14.0	-460.0	19.0
SP2-CI-7	-372.5	12.0	-431.0	11.0	-439.0	12.0	-435.0	17.0
SP2-FRC-5	-352.0	14.0	-350.5	15.0	-381.5	16.0	-400.0	21.0
SP2-FRC-6	-372.0	11.0	-388.5	11.0	-450.0	13.0	-405.5	19.0
SP2-FRC-7	-257.5	13.0	-260.5	12.0	-335.0	15.0	-176.0	21.0
SP3-NC-9	-412.0	18.0	-412.5	22.0	-426.0	22.0	-429.0	33.0
SP3-NC-10	-199.5	27.0	-191.0	23.0	-204.5	24.0	-160.5	44.0
SP3-NC-11	-399.5	24.0	-423.5	18.0	-426.0	25.0	-332.0	27.0
SP3-CI-9	-523.5	17.0	-471.0	15.0	-530.0	19.0	-486.0	24.0
SP3-CI-10	-396.0	20.0	-445.5	18.0	-482.0	20.0	-378.5	30.0
SP3-CI-11	-279.0	19.0	-331.0	19.0	-402.5	23.0	-388.5	37.0
SP3-FRC-9	-356.5	19.0	-351.5	15.0	-352.5	20.0	-368.5	35.0
SP3-FRC-10	-288.0	18.0	-367.5	15.0	-416.0	18.0	-429.0	27.0
SP3-FRC-11	-422.5	20.0	-432.0	18.0	-427.5	20.0	-388.0	31.0

Table C- 9 Half-cell Potential and Resistivity after Six Months

Specimen Label	6 Months specimens - Period and Measurements							
	2 Weeks		4 Weeks		6 Weeks		8 Weeks	
	Potential (mV)	Resistivity (KΩ.cm)	Potential (mV)	Resistivity (KΩ.cm)	Potential (mV)	Resistivity (KΩ.cm)	Potential (mV)	Resistivity (KΩ.cm)
SP1-NC-1	-416.0	19.0	-391.0	20.0	-422.5	18.0	-372.0	54.0
SP1-NC-2	-242.5	8.2	-358.5	10.0	-356.0	11.0	-410.5	20.0
SP1-NC-3	-307.5	10.0	-463.0	13.0	-419.5	12.0	-354.0	11.0
SP1-CI-1	-482.5	12.0	-484.5	11.0	-401.5	10.0	-410.5	14.0
SP1-CI-2	-438.0	4.8	-467.5	3.0	-433.5	5.0	-417.0	8.5
SP1-CI-3	-450.5	12.0	-462.5	11.0	-425.5	12.0	-427.0	12.0
SP1-FRC-1	-361.0	8.0	-455.0	7.0	-469.0	9.0	-385.0	13.0
SP1-FRC-2	-391.5	9.3	-373.5	8.0	-473.0	10.0	-388.5	22.0
SP1-FRC-3	-363.5	14.0	-375.0	13.0	-393.5	15.0	-252.5	17.0
SP2-NC-5	-261.0	21.0	-461.0	20.0	-452.5	21.0	-367.0	29.0
SP2-NC-6	-345.5	17.0	-359.0	16.0	-379.5	15.0	-334.0	31.0
SP2-NC-7	-502.0	13.0	-463.5	12.0	-451.0	11.0	-312.5	24.0
SP2-CI-5	-434.0	21.0	-435.5	20.0	-449.0	18.0	-379.0	30.0
SP2-CI-6	-453.0	11.0	-455.0	12.0	-467.5	13.0	-407.0	19.0
SP2-CI-7	-449.0	13.0	-450.0	11.0	-358.5	10.0	-372.5	17.0
SP2-FRC-5	-435.0	13.0	-444.0	13.0	-467.5	14.0	-352.0	21.0
SP2-FRC-6	-445.0	13.0	-417.0	12.0	-431.0	10.0	-372.0	19.0
SP2-FRC-7	-444.0	13.0	-430.0	10.0	-424.0	9.0	-257.5	21.0
SP3-NC-9	-373.5	17.0	-359.0	15.0	-374.0	18.0	-412.0	33.0
SP3-NC-10	-223.5	18.0	-243.0	19.0	-270.5	17.0	-199.5	44.0
SP3-NC-11	-477.5	21.0	-463.0	20.0	-484.5	18.0	-399.5	27.0
SP3-CI-9	-466.0	17.0	-428.5	18.0	-417.5	17.0	-523.5	24.0
SP3-CI-10	-303.0	20.0	-486.5	19.0	-441.5	21.0	-396.0	30.0
SP3-CI-11	-281.5	28.0	-432.0	26.0	-263.0	25.0	-279.0	37.0
SP3-FRC-9	-380.5	16.0	-386.5	14.0	-392.5	15.0	-356.5	35.0
SP3-FRC-10	-446.0	12.0	-473.5	10.0	-442.0	9.0	-288.0	27.0
SP3-FRC-11	-159.0	17.0	-398.0	15.0	-391.5	16.0	-422.5	31.0

Table C- 10 Visual Inspection for Retrieved Steel Tendons

Specimen Designation	Steel Tendon Deterioration		
	Bottom end	Top end	Overall
SP1-NC-13			
SP1-NC-14			X
SP1-CI-13			
SP1-CI-14			
SP1-FRC-13			
SP1-FRC-14			
SP2-NC-17			
SP2-NC-18			

SP2-CI-17			
SP2-CI-18			
SP2-FRC-17			
SP2-FRC-18			
SP3-NC-21			
SP3-NC-22			
SP3-CI-21			
SP3-CI-22			

SP3-FRC-21			
SP3-FRC-22			

Table C- 11 Recorded Time for Corrosion Cracking and Spalling and Steel Loss

Specimen ID	Initial mass lb (g)	Crack initiation time (hrs)	Spalling time (hrs)	Final mass lb (g)	Mass loss (g)	Ratio of loss (%)
SP1-NC-13	0.312 (141.5)	2304	4440	0.308 (139.7)	1.80	1.3
SP1-NC-14	0.313 (142)	1344	X	0.308 (139.7)	2.30	1.6
SP1-CI-13	0.309 (140.2)	2304	X	0.306 (138.8)	1.40	1.0
SP1-CI-14	0.309 (140.2)	768	4440	0.297 (134.7)	5.50	3.9
SP1-FRC-13	0.312 (141.5)	1344	4440	0.306 (138.8)	2.70	1.9
SP1-FRC-14	0.31 (140.6)	2976	X	0.305 (138.3)	2.30	1.6
SP2-NC-17	0.31(140.6)	3000	X	0.304 (137.9)	2.70	1.9
SP2-NC-18	0.308 (139.7)	No cracks	X	0.302 (137)	2.70	1.9
SP2-CI-17	0.309 (140.2)	1608	X	0.302 (137)	3.20	2.3
SP2-CI-18	0.31(140.6)	No cracks	X	0.309 (140.2)	0.40	0.3
SP2-FRC-17	0.309 (140.2)	2304	X	0.298 (135.2)	5.00	3.6
SP2-FRC-18	0.308 (139.7)	No cracks	X	0.295 (133.8)	5.90	4.2
SP3-NC-21	0.308 (139.7)	3000	X	0.306 (138.6)	0.90	0.6
SP3-NC-22	0.313 (142)	No cracks	X	0.31 (140.6)	1.40	1
SP3-CI-21	0.313 (142)	No cracks	X	0.312 (141.5)	0.50	0.4
SP3-CI-22	0.308 (139.7)	No cracks	X	0.306 (138.8)	0.90	0.6
SP3-FRC-21	0.314 (142.4)	No cracks	X	0.31 (140.6)	1.80	1.3
SP3-FRC-22	0.311 (141.4)	No cracks	X	0.303 (137.4)	3.70	2.6

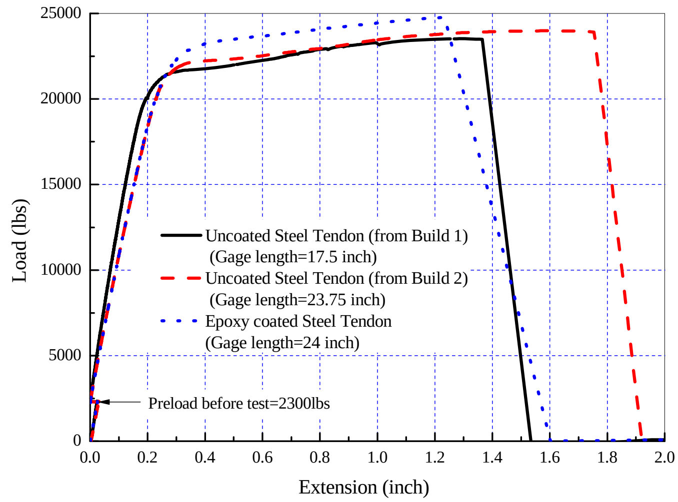

Load-extension relationship for tested tendons

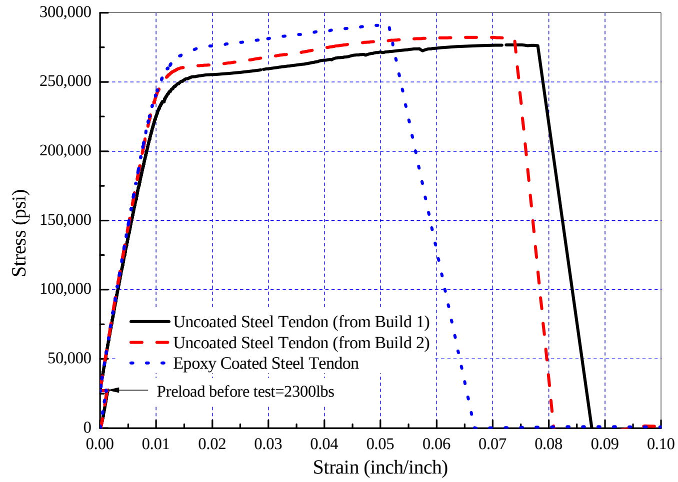

Stress-strain relationship for tested tendons

Note: Epoxy coated steel tendon failed at grips

Figure C- 1 Prestressed Reinforcing Strand Stress-Strain Relationships

Figure C- 2 Non-Prestressed Corrosion Specimen - Formwork and Reinforcement

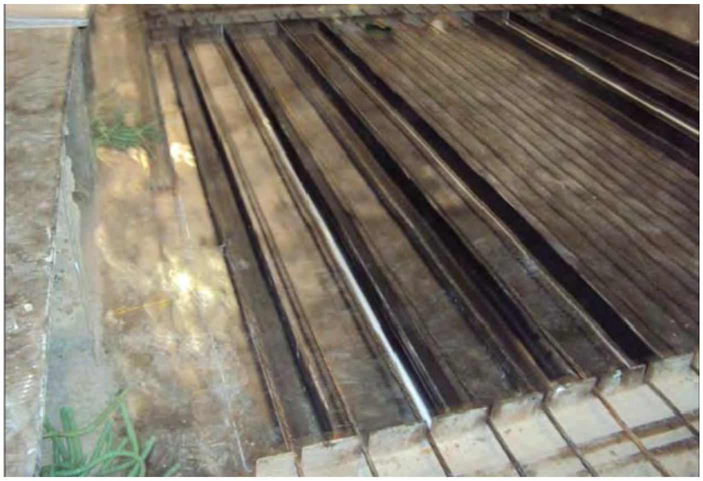
Figure C- 3 Blockouts Provided to Construct Prestressed Corrosion Specimens


Figure C- 4 Prestressed Panel Casting Bed

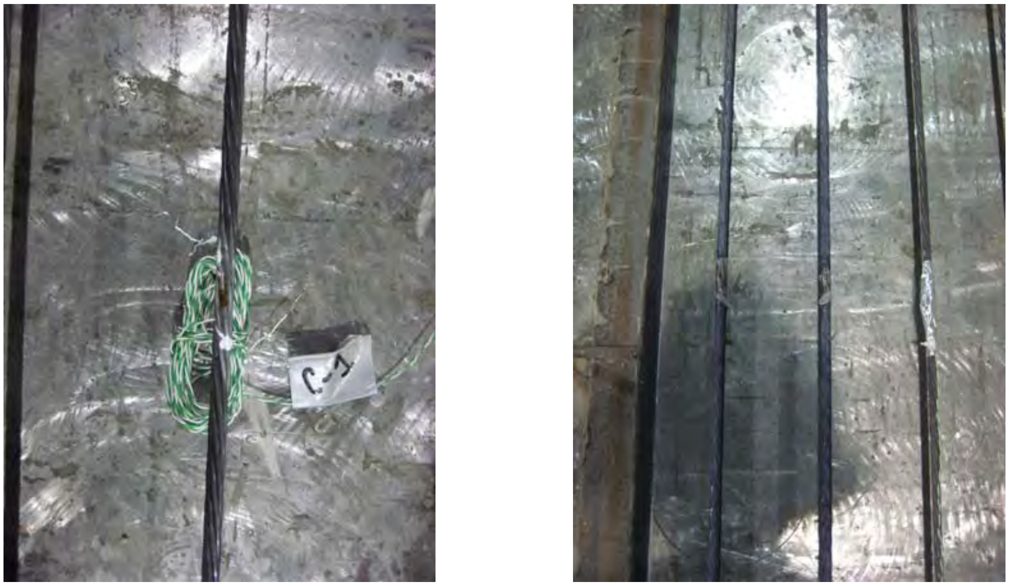

(a) (b)

Figure C- 5 Strain Gages Applied to Prestressed Reinforcement: (a) Steel Strand, (b) Epoxy-Coated Steel Strand

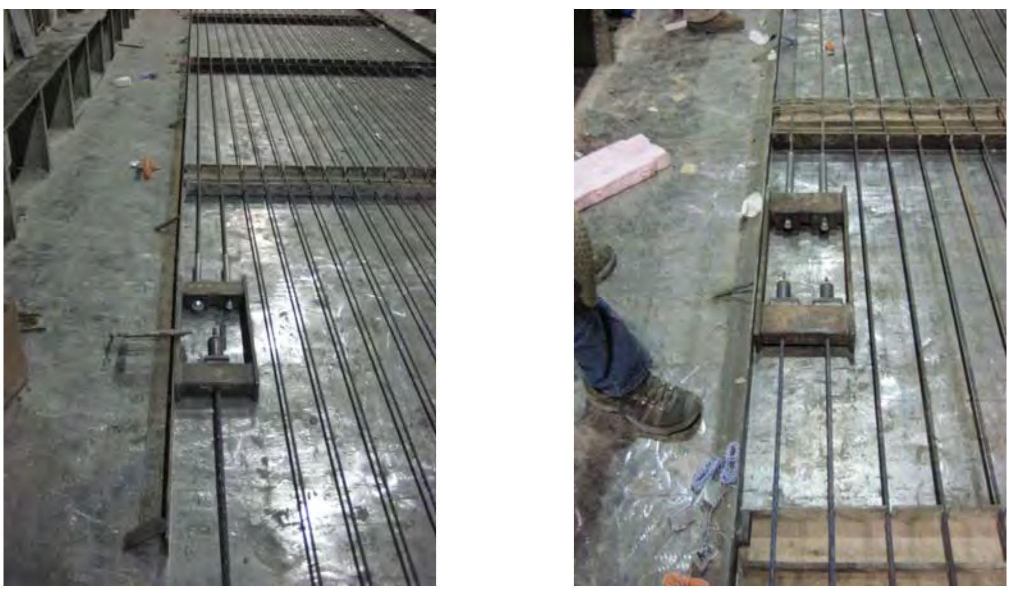

(a) (b)

Figure C- 6 CFRP Prestressed Bar Anchorage Splice: (a) CRFP to 0.6 in. Steel Strand, (b) CRFP to Epoxy-Coated Steel Strand

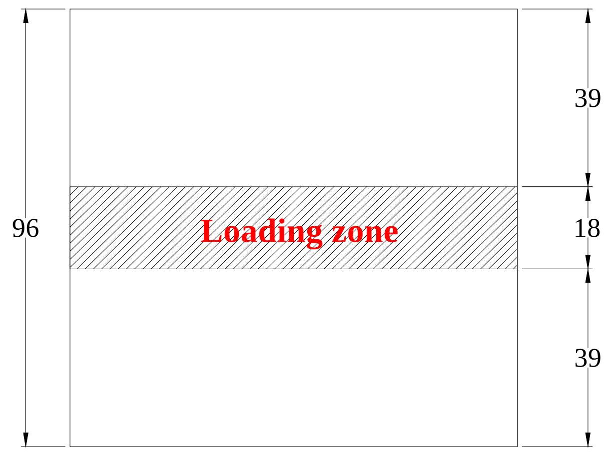

Note: dimensions are in inches

Figure C- 7 Plan View of Panel Loading Zone

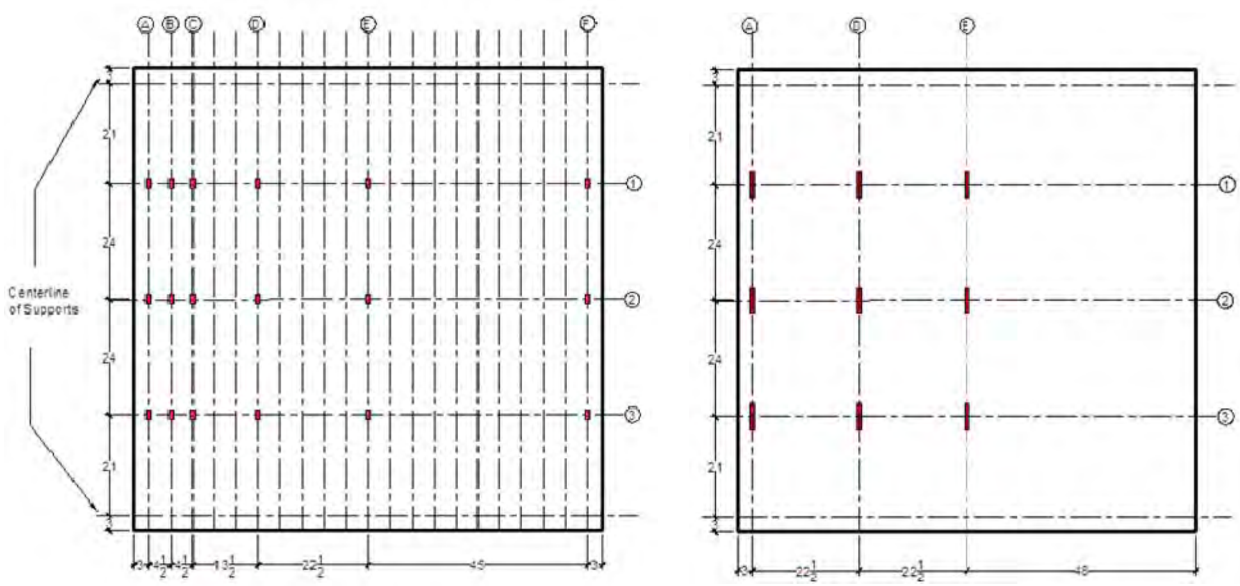

Tendon Strain Gage Layout

Concrete Surface Strain Gage Layout

Note: dimensions are in inches

Figure C- 8 Strain Gage Layout

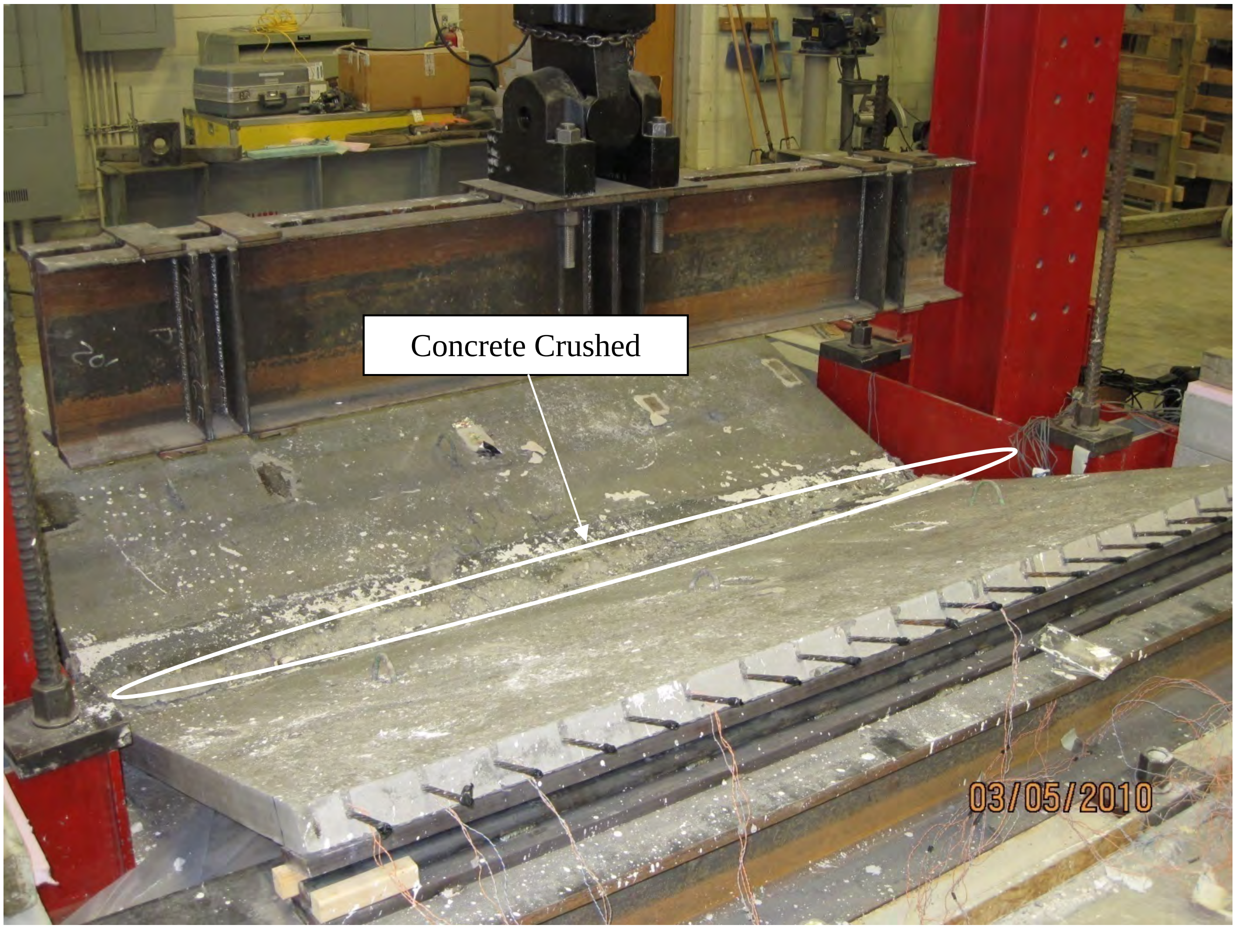

Figure C- 9 Flexural Failure at Midspan by Concrete Crushing of Panel ST-NC-SL

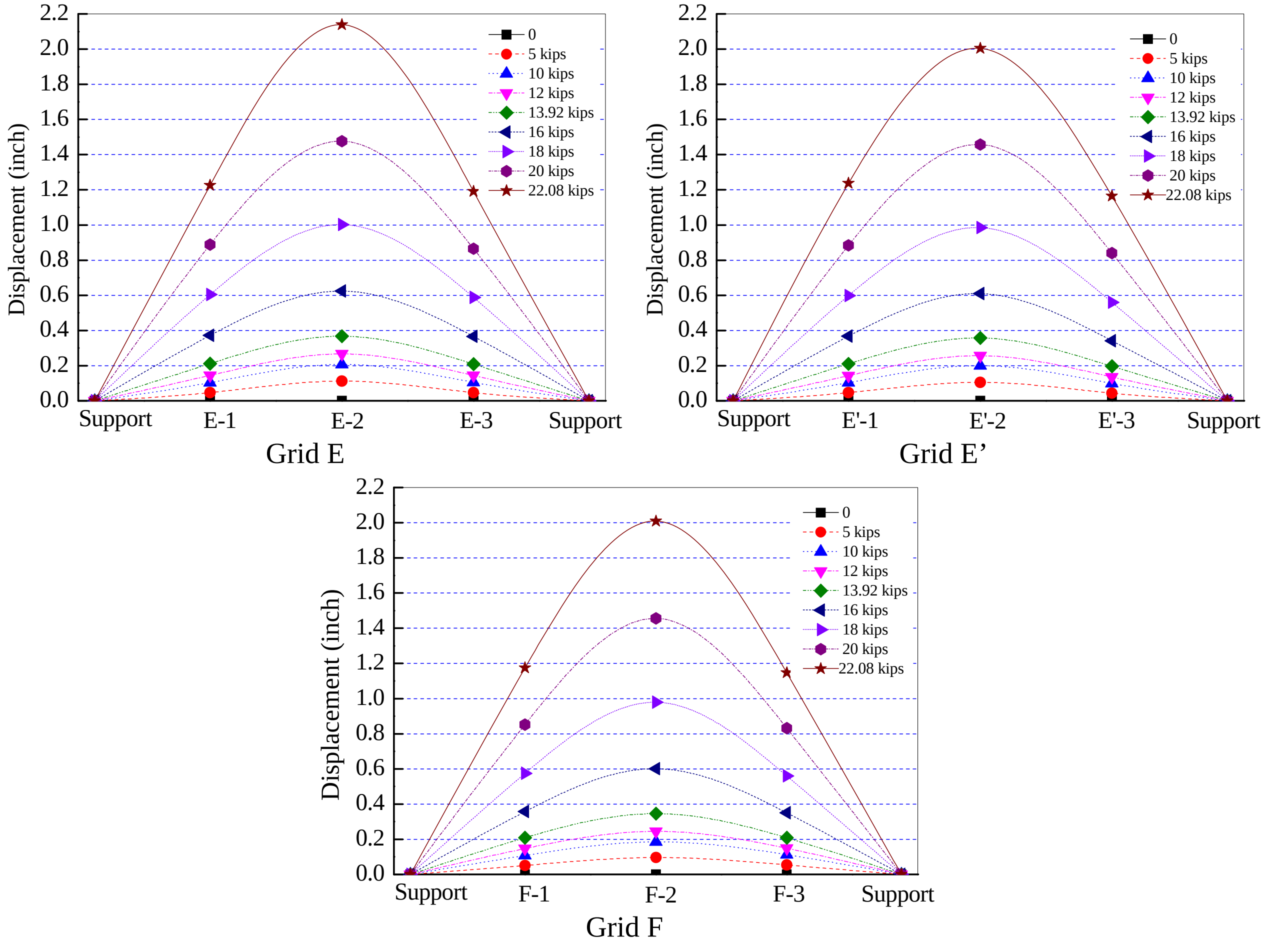

Figure C- 10 Panel ST-NC-SL: Measured Displacement Along Panel Length

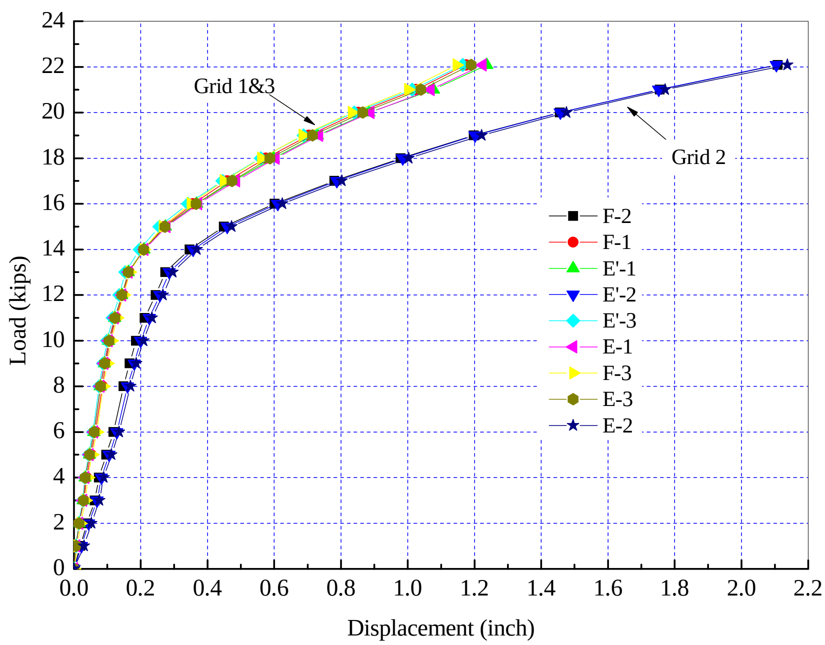

Figure C- 11 Panel ST-NC-SL: Applied Load-Displacement Relationship

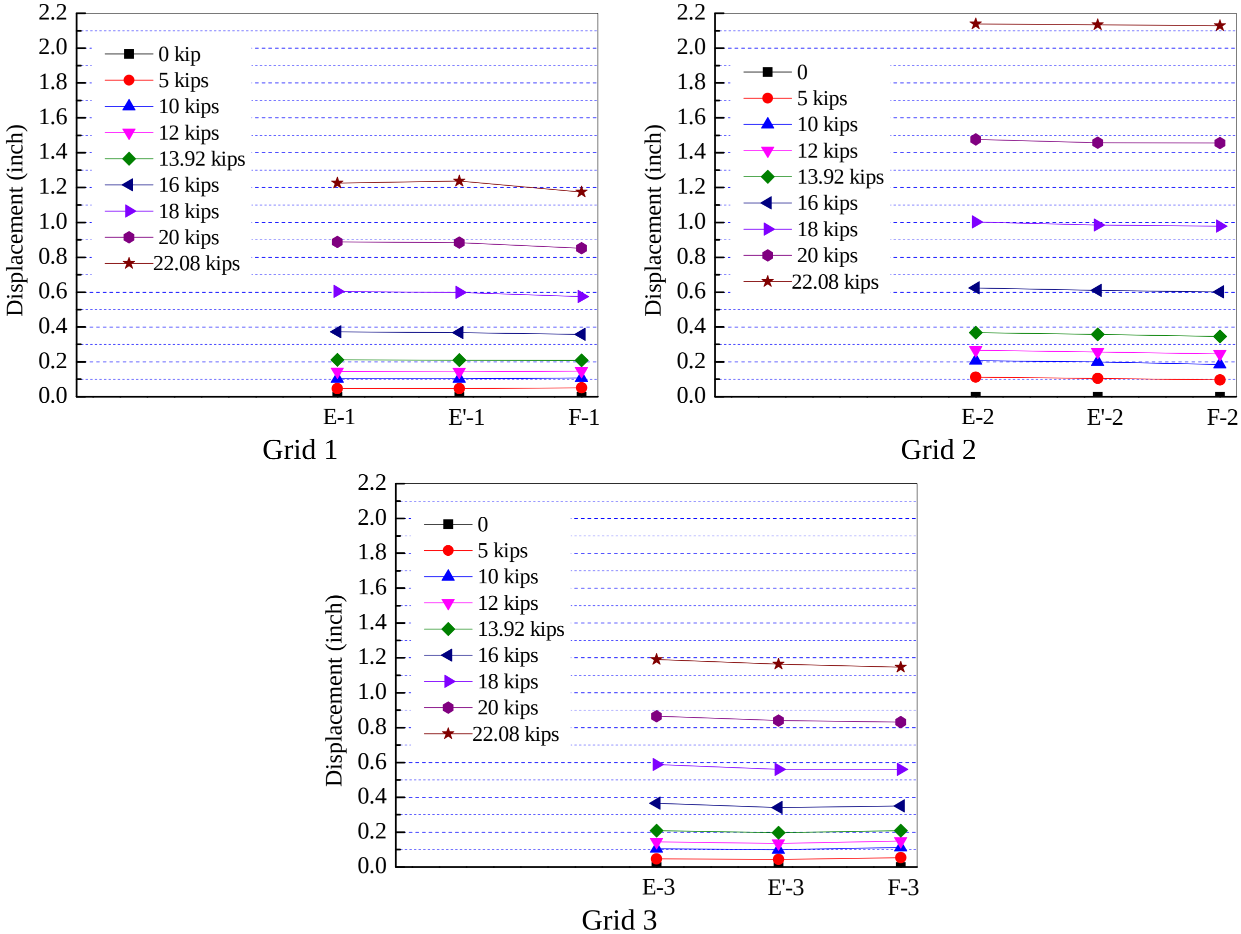

Figure C- 12 Panel ST-NC-SL: Measured Displacement Along Panel Width

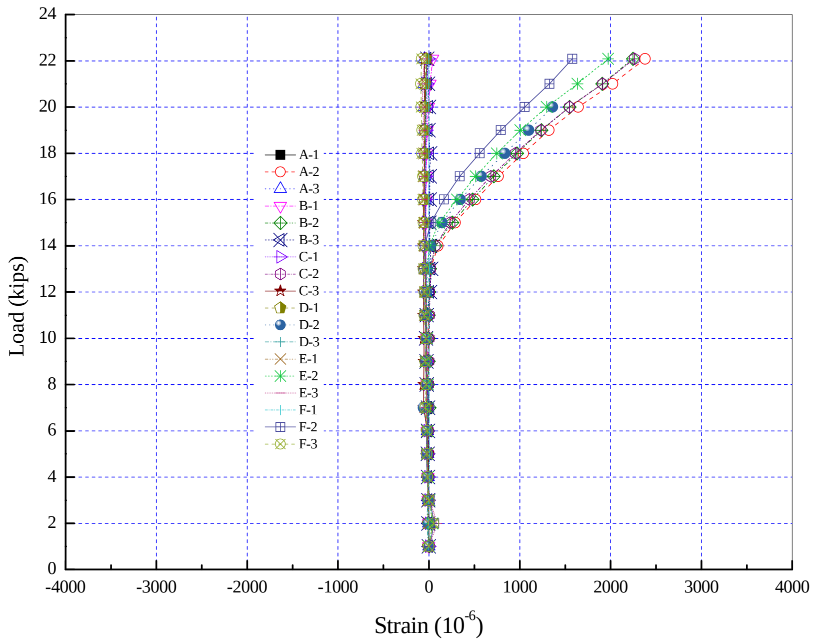

Figure C- 13 Panel ST-NC-SL: Applied Load-Tendon Strain Relationship

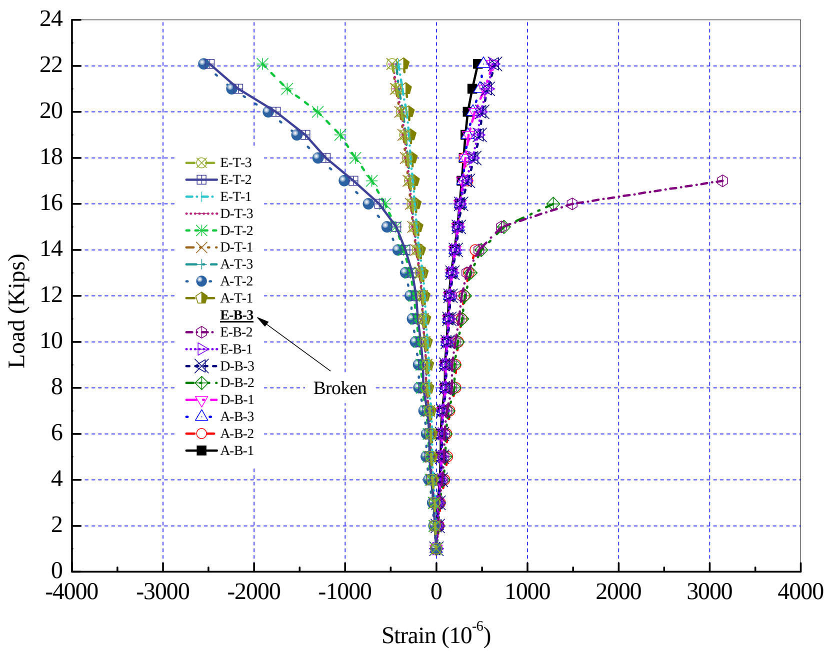

Figure C- 14 Panel ST-NC-SL: Applied Load-Concrete Surface Strain Relationship

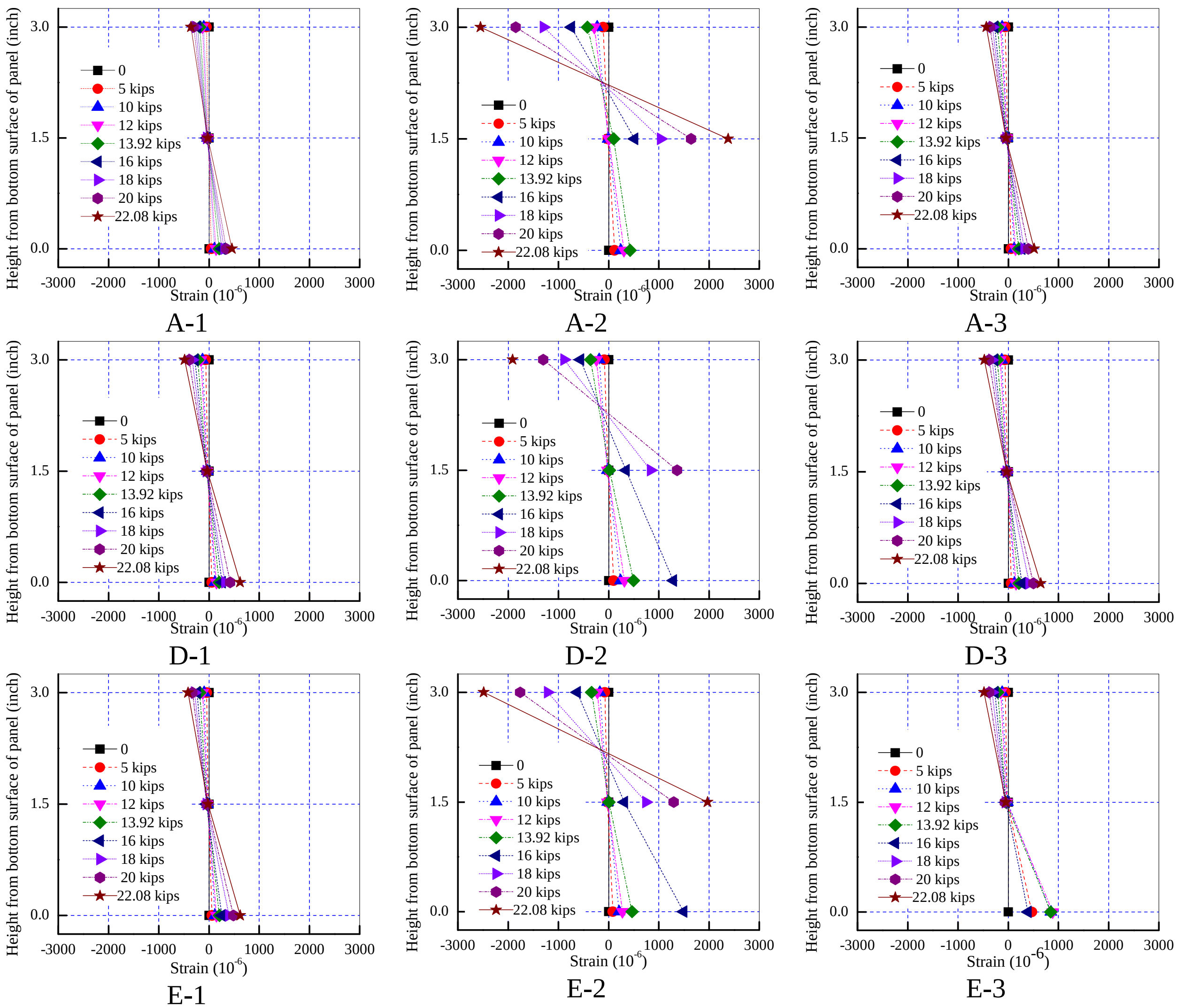

Figure C- 15 Panel ST-NC-SL: Measured Strain Distribution

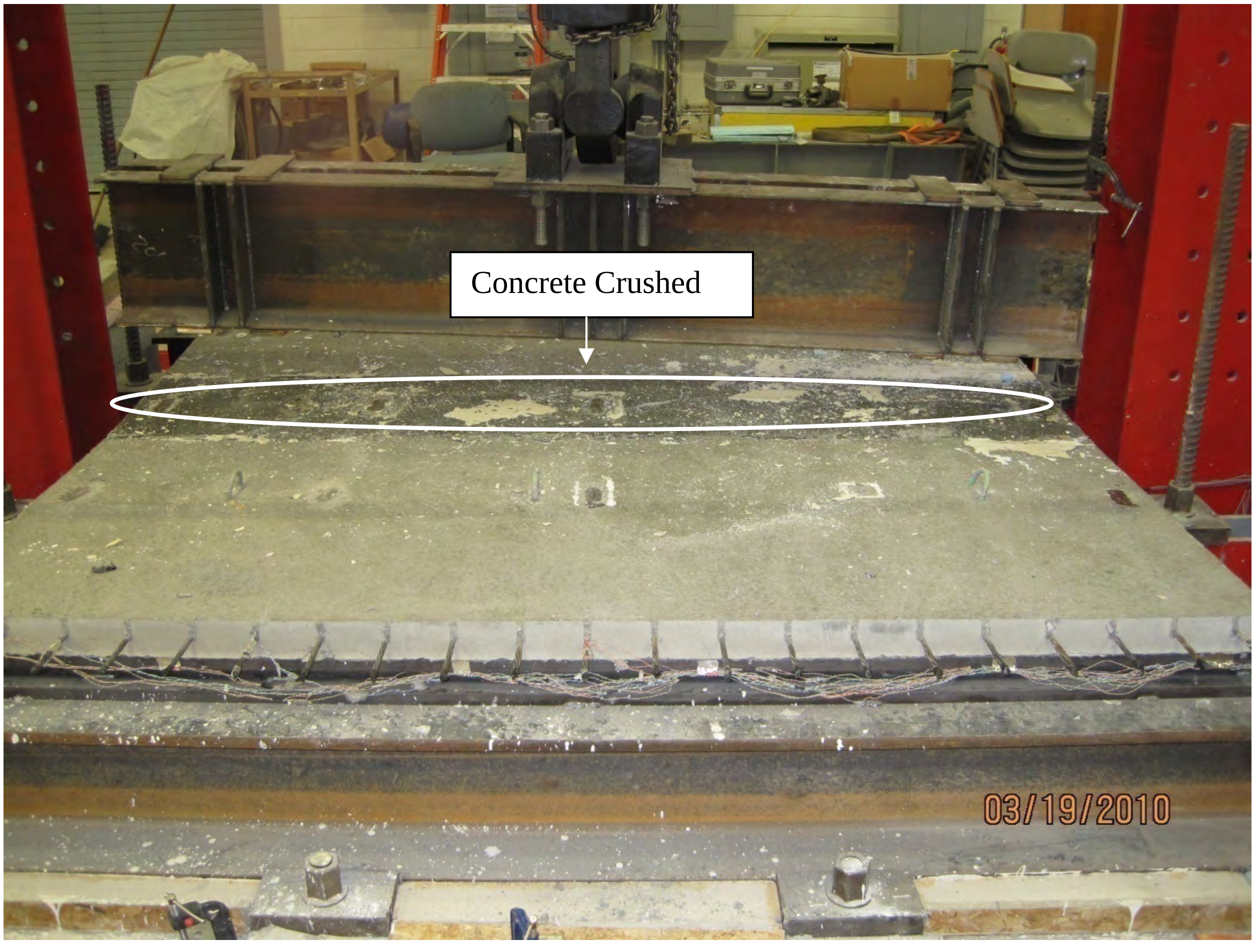

Figure C- 16 Flexural Failure at Midspan by Concrete Crushing of Panel ST-FRC-SL

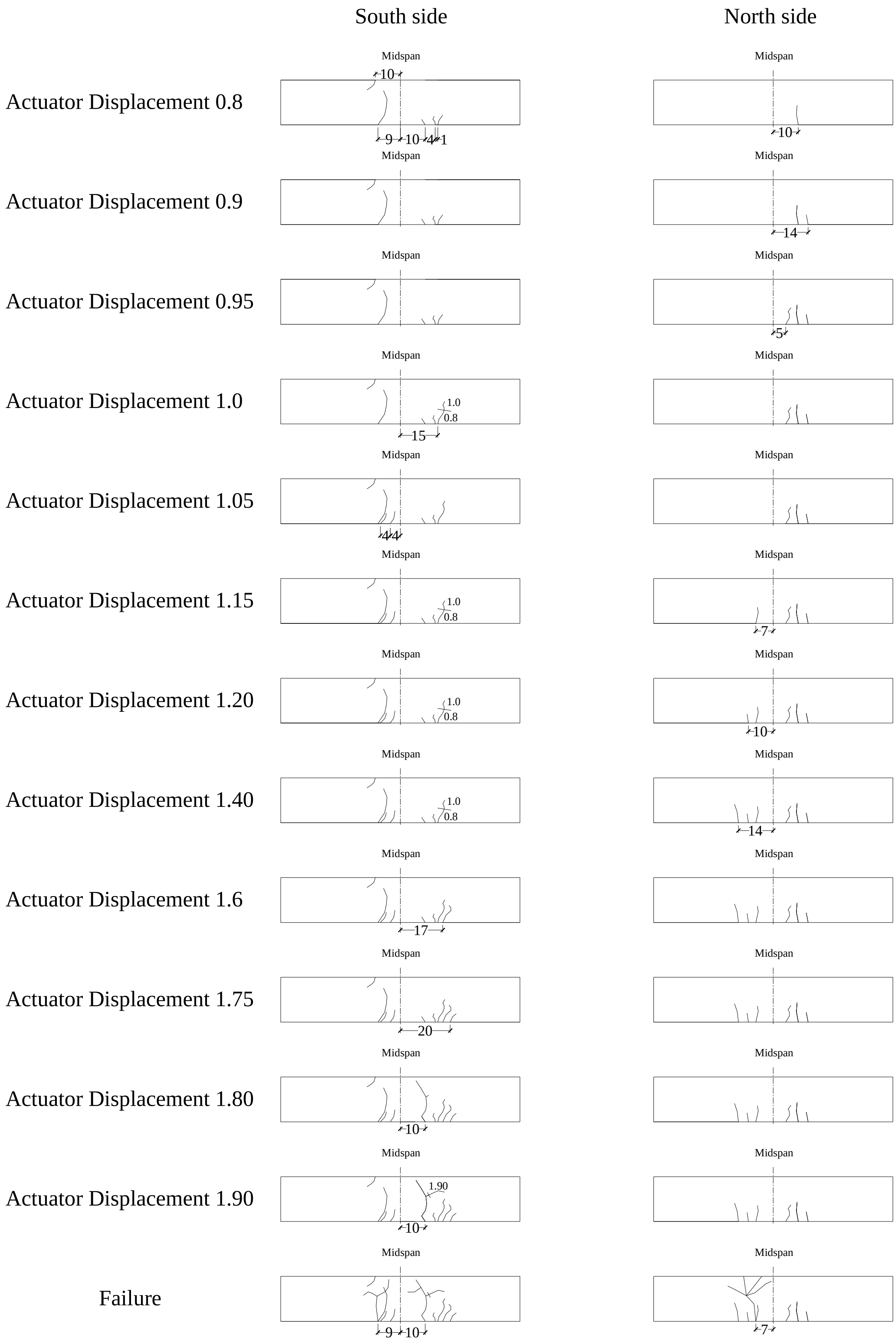

Figure C- 17 Panel ST-FRC-SL: Propagation of Cracking

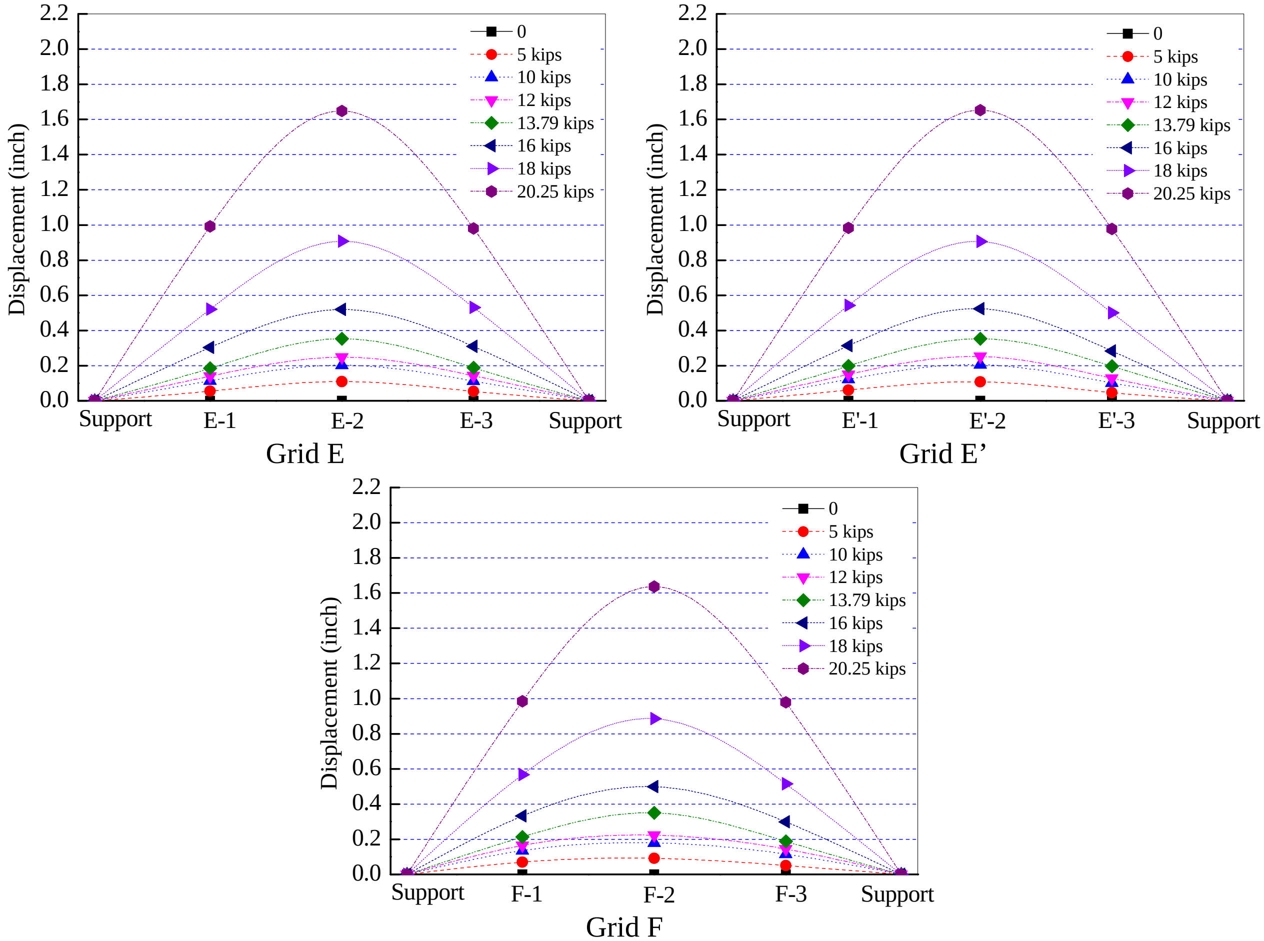

Figure C- 18 Panel ST-FRC-SL: Measured Displacement Along Panel Length

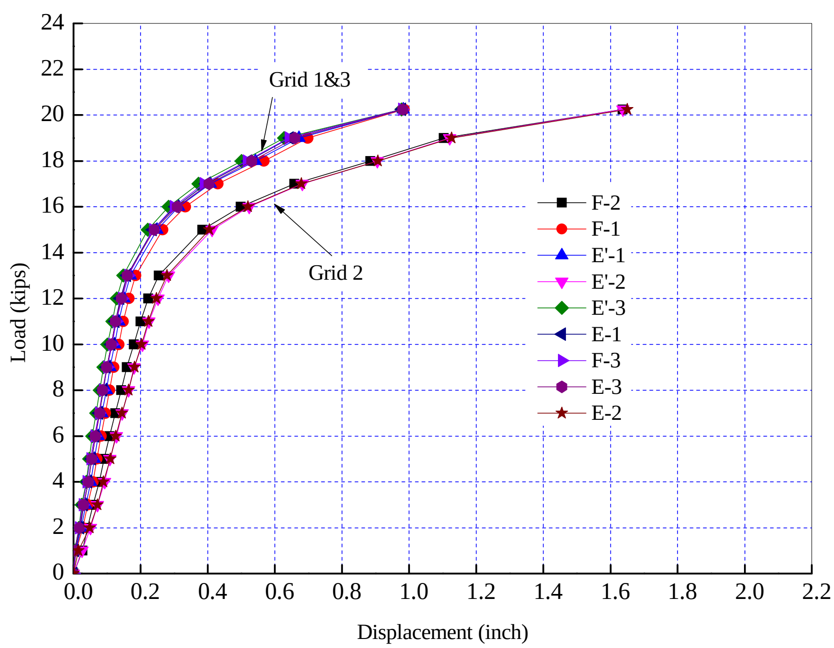

Figure C- 19 Panel ST-FRC-SL: Applied Load-Displacement Relationship

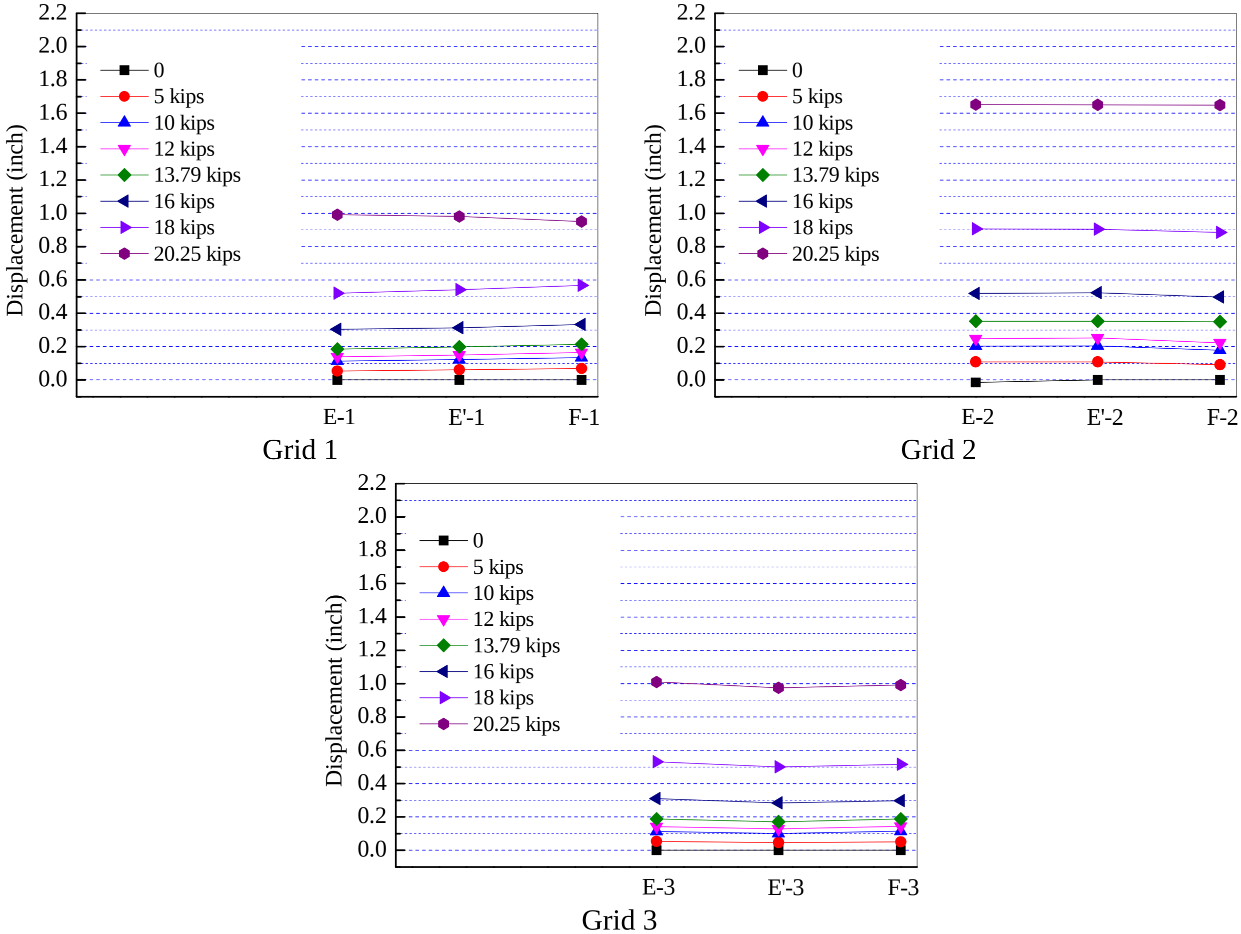

Figure C- 20 Panel ST-FRC-SL: Measured Displacement Along Panel Width

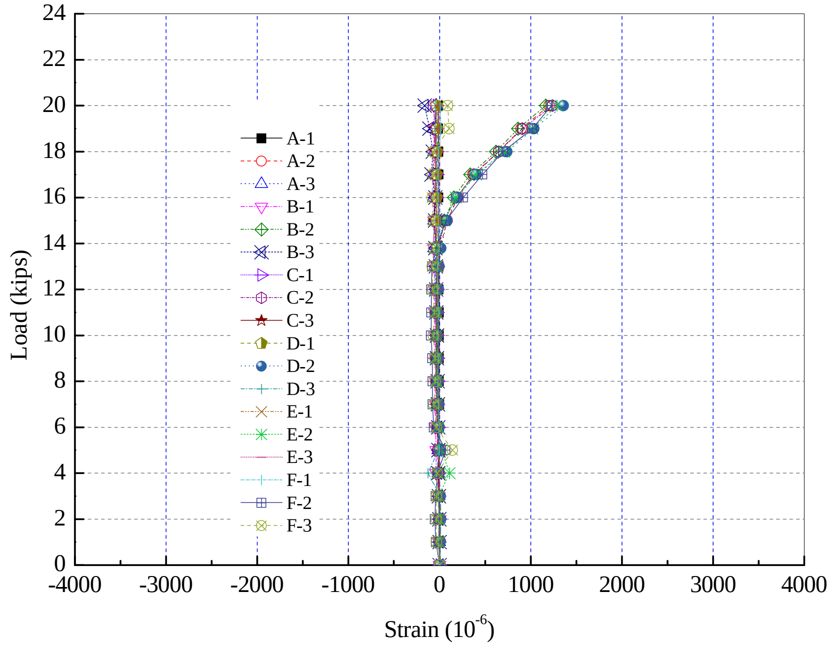

Figure C- 21 Panel ST-FRC-SL: Applied Load-Tendon Strain Relationship

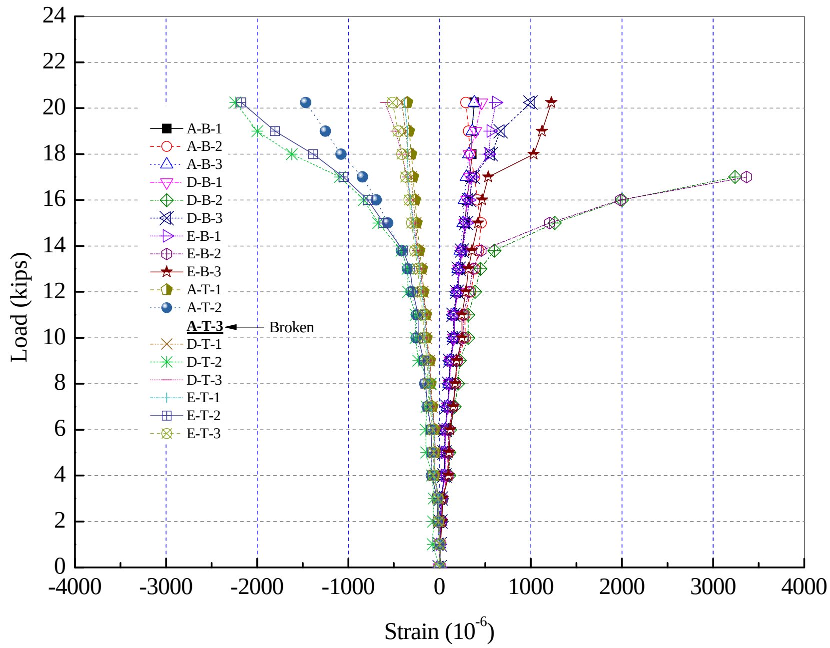

Figure C- 22 Panel ST-FRC-SL: Applied Load-Concrete Surface Strain Relationship

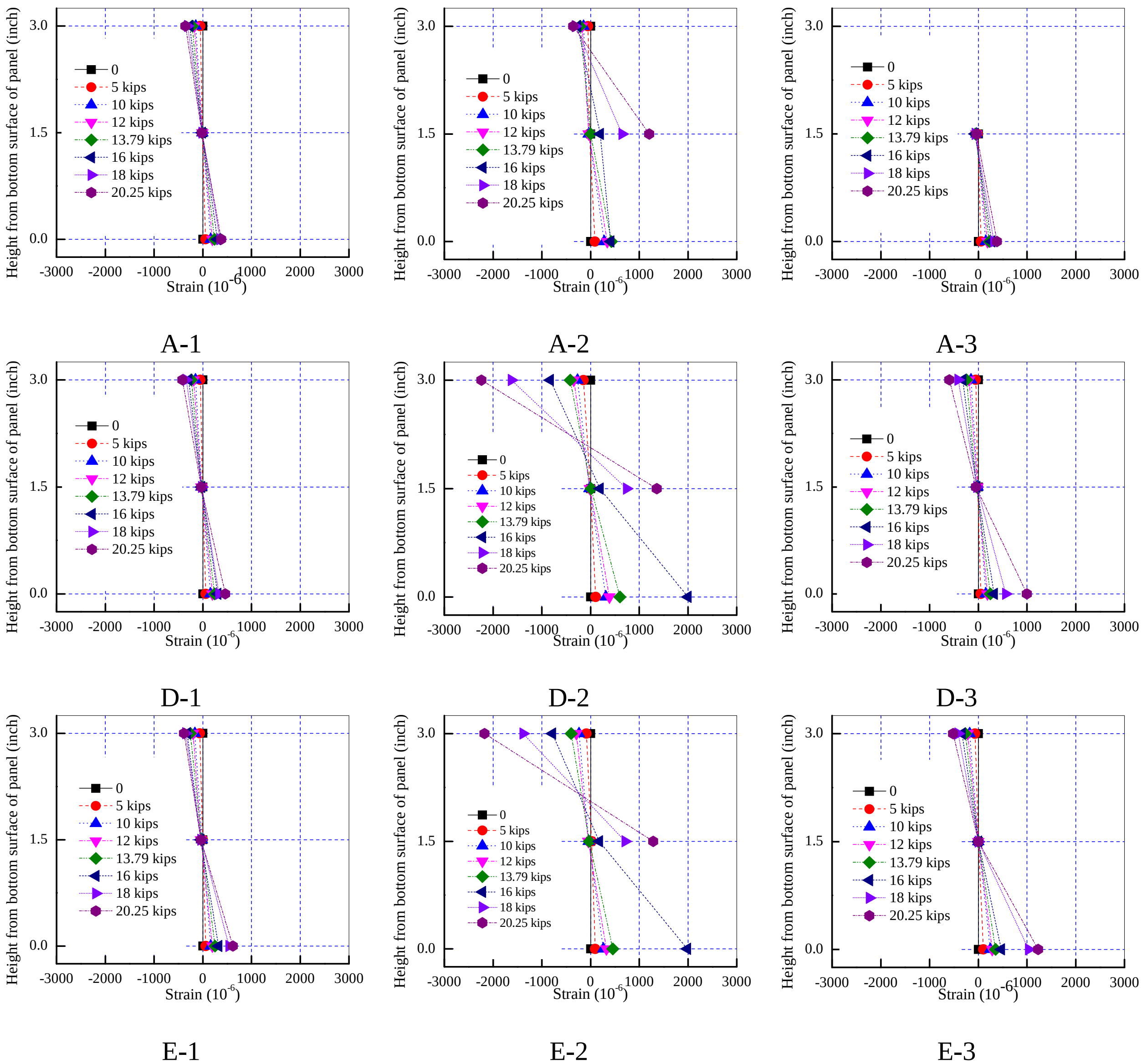

Figure C- 23 Panel ST-FRC-SL: Measured Strain Distribution

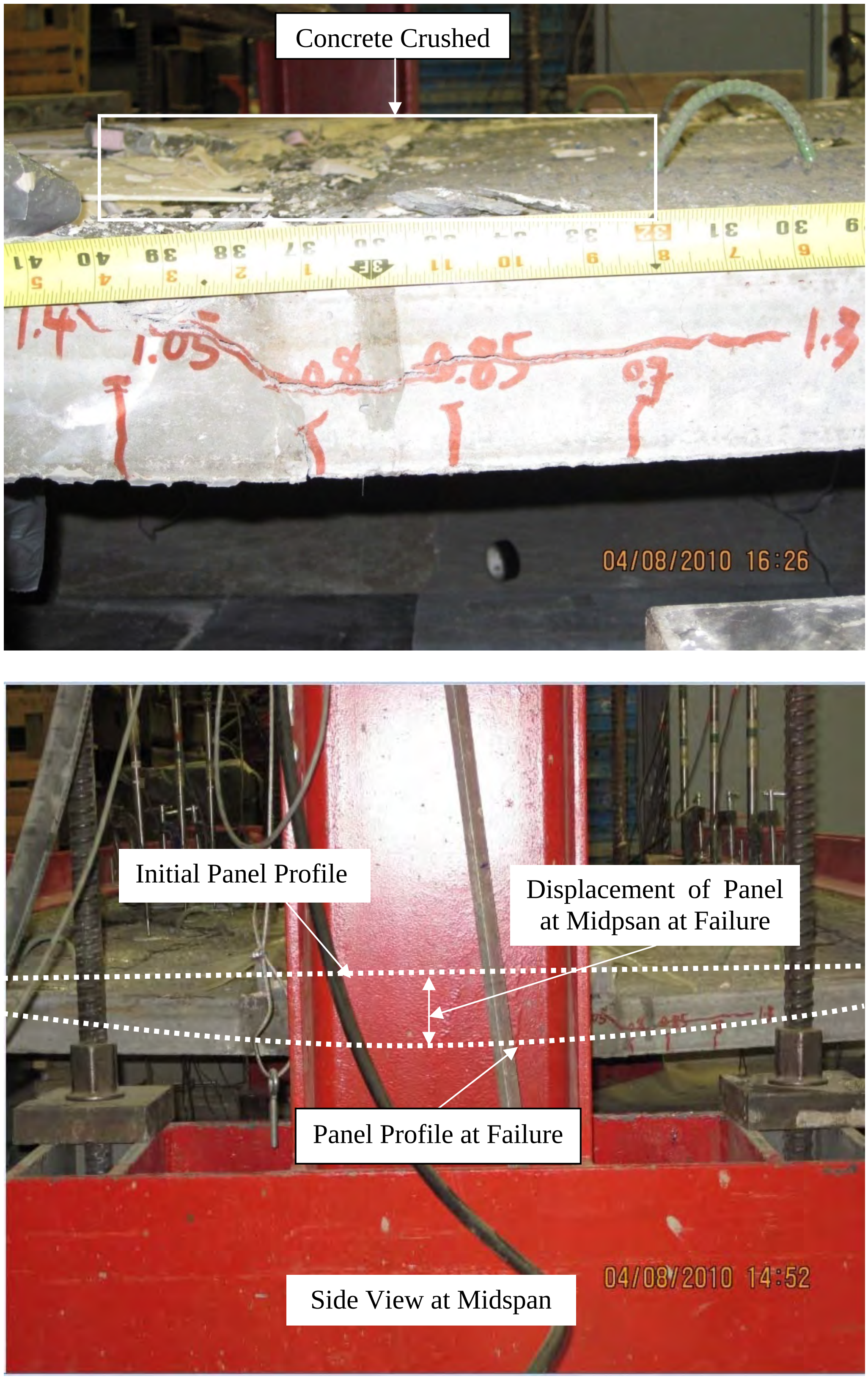

Figure C- 24 Flexural Failure at Midspan by Concrete Crushing of Panel ECST-NC-SL

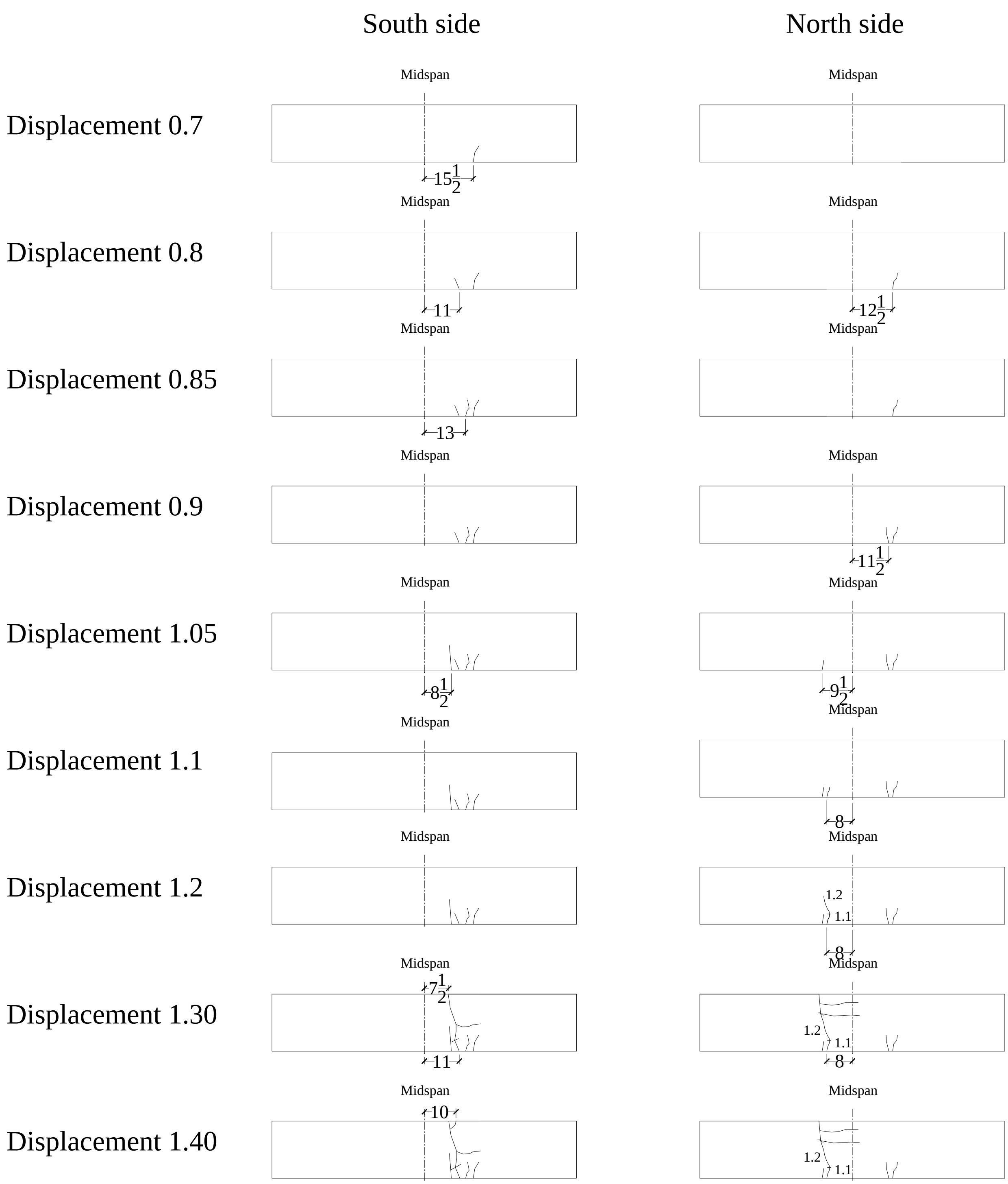

Figure C- 25 Panel ECST-NC-SL: Propagation of Cracking

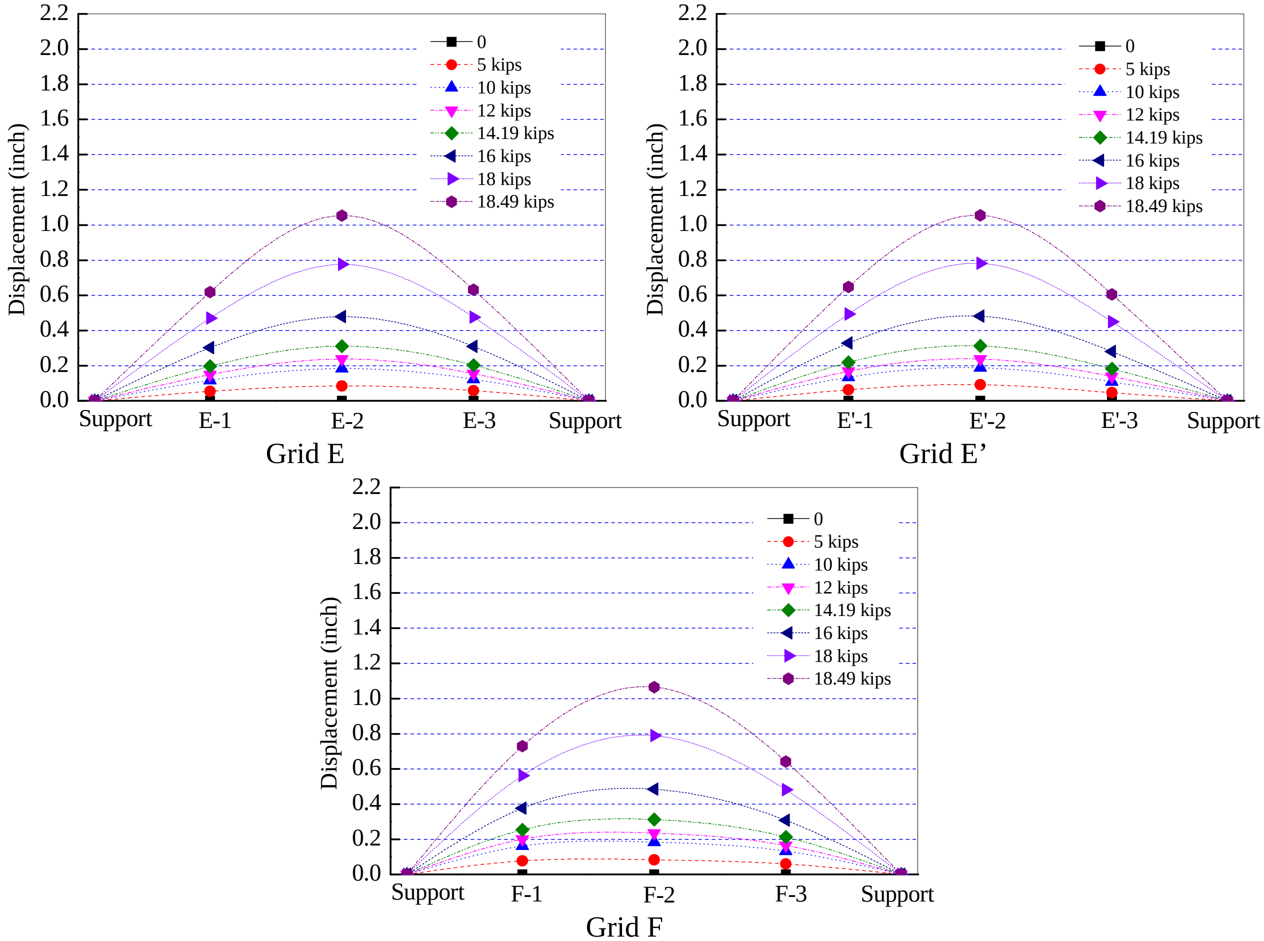

Figure C- 26 Panel ECST-NC-SL: Measured Displacement Along Panel Length

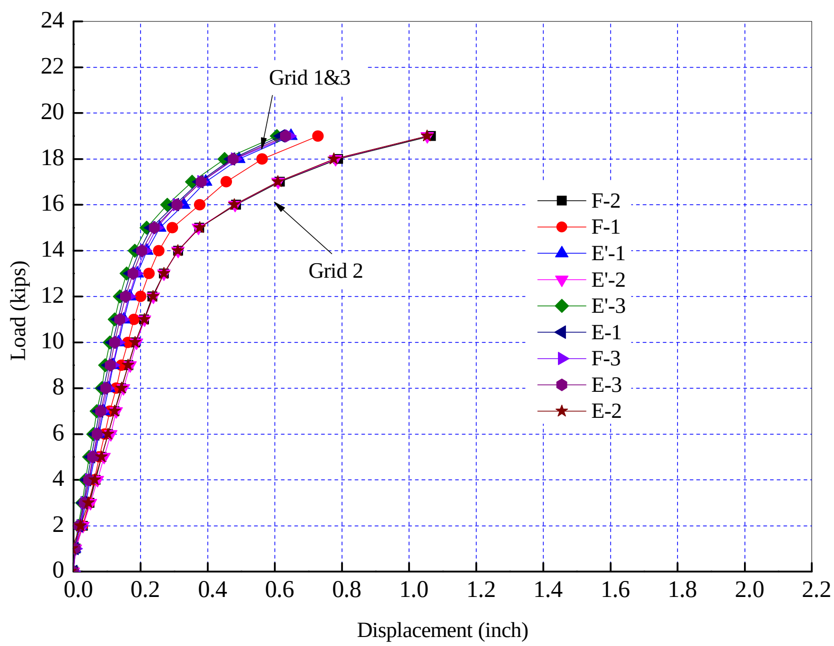

Figure C- 27 Panel ECST-NC-SL: Applied Load-Displacement Relationship

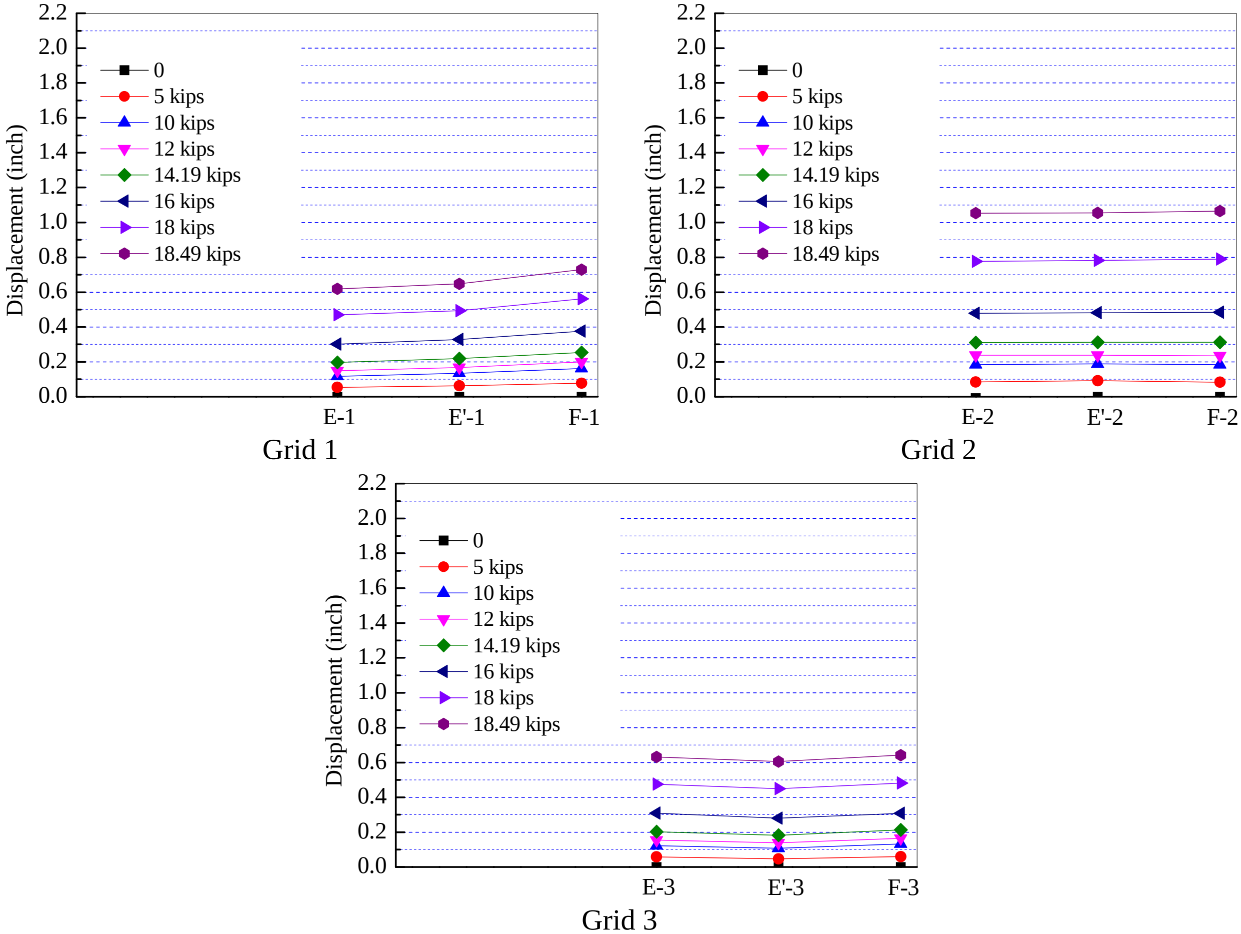

Figure C- 28 Panel ECST-NC-SL: Measured Displacement Along Panel Width

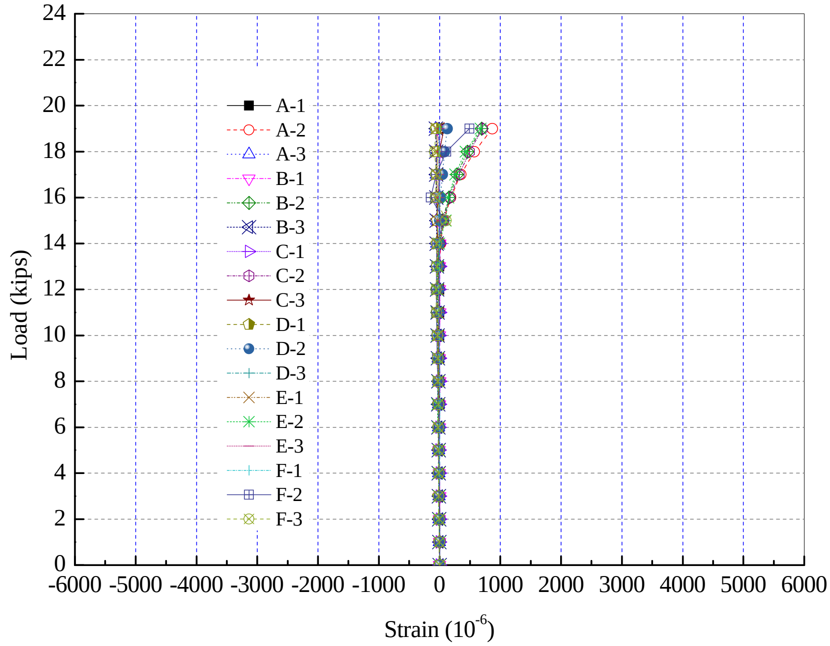

Figure C- 29 Panel ECST-NC-SL: Applied Load-Tendon Strain Relationship

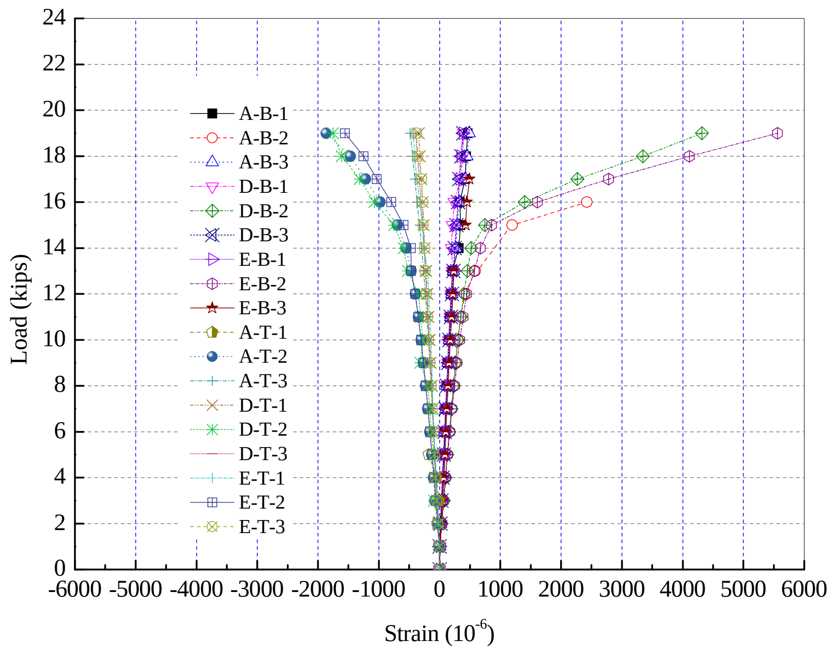

Figure C- 30 Panel ECST-NC-SL: Applied Load-Concrete Surface Strain Relationship

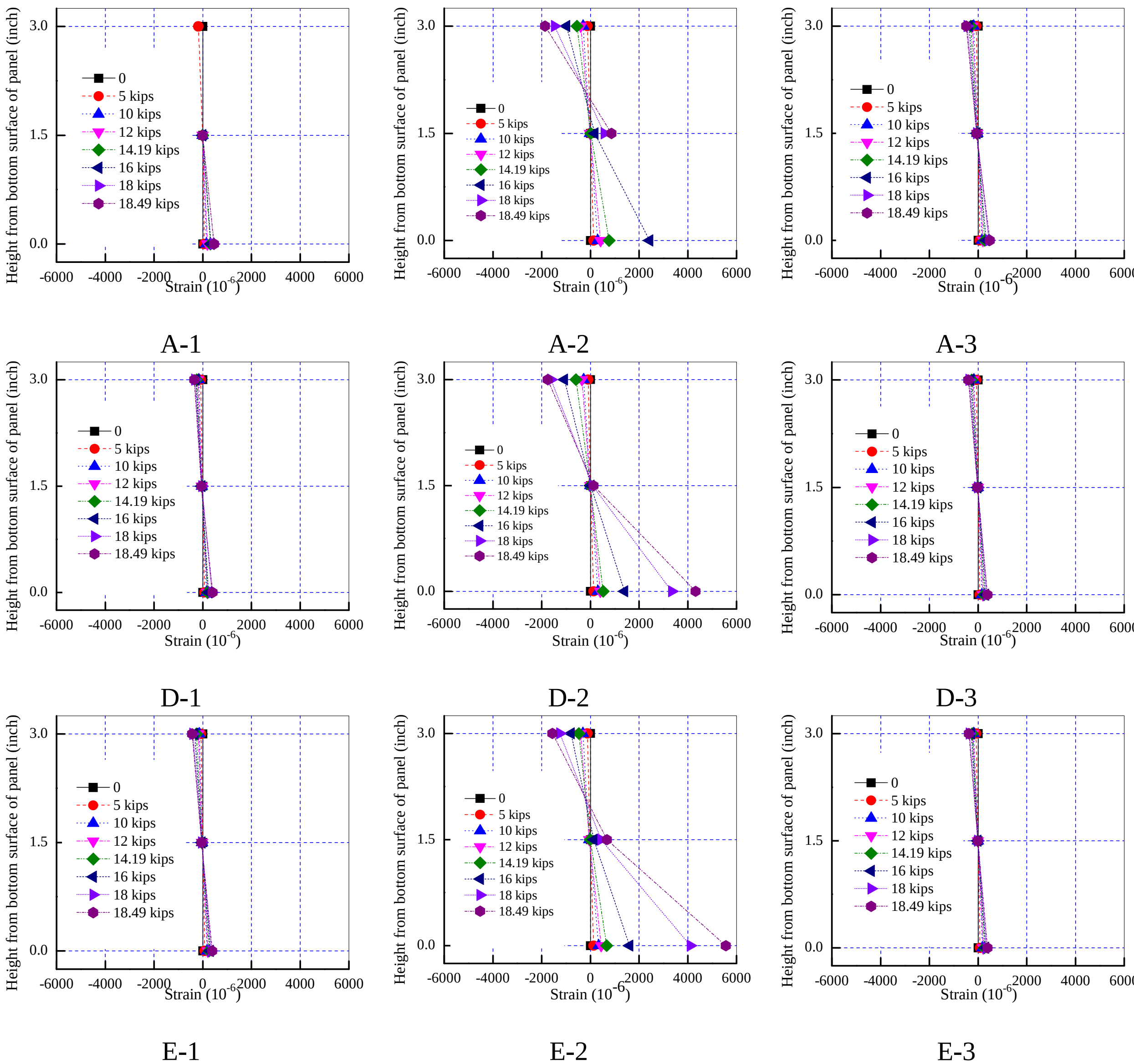

Figure C- 31 Panel ECST-NC-SL: Measured Strain Distribution

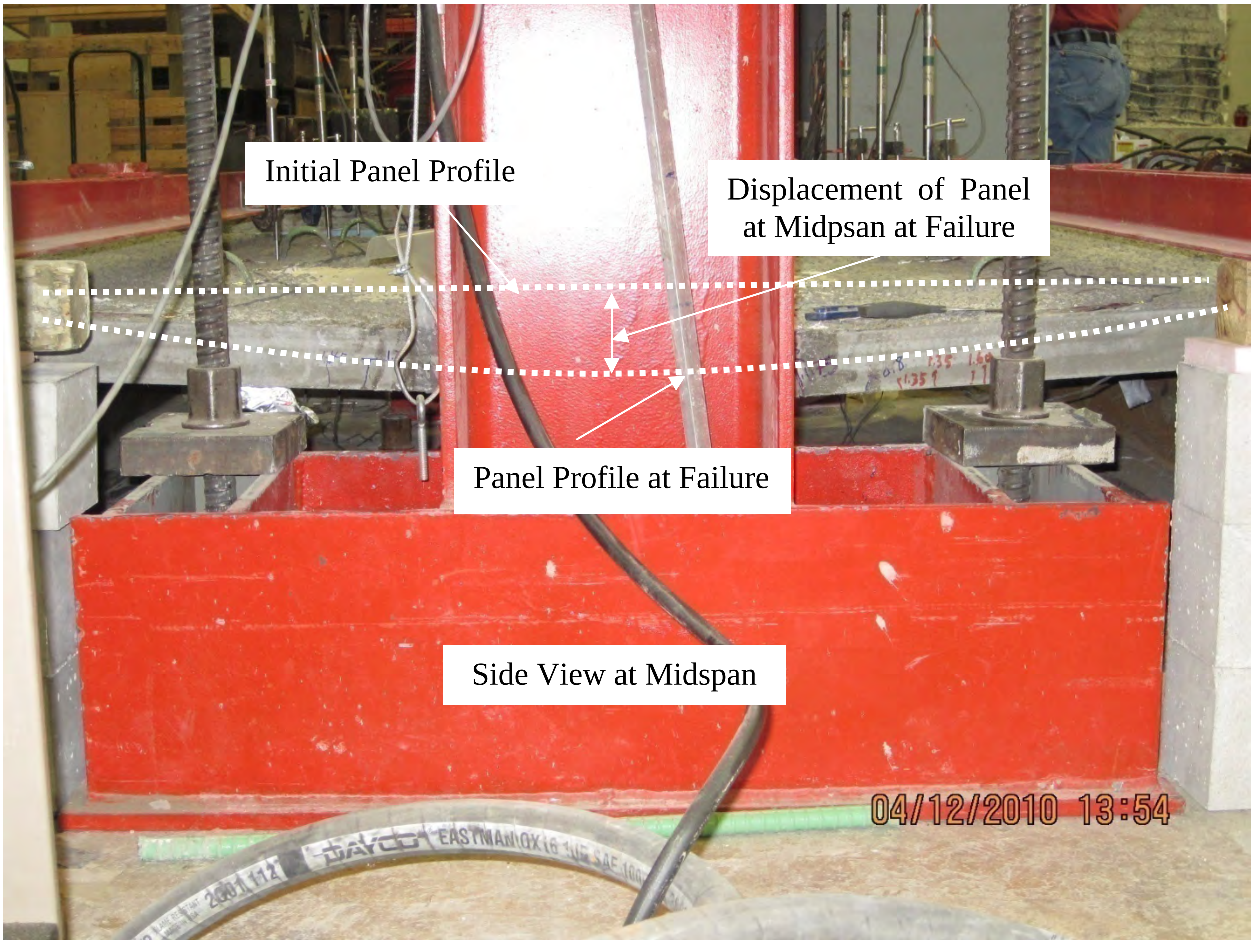

Figure C- 32 Flexural Failure at Midspan by Concrete Crushing of Panel ECST-FRC-SL

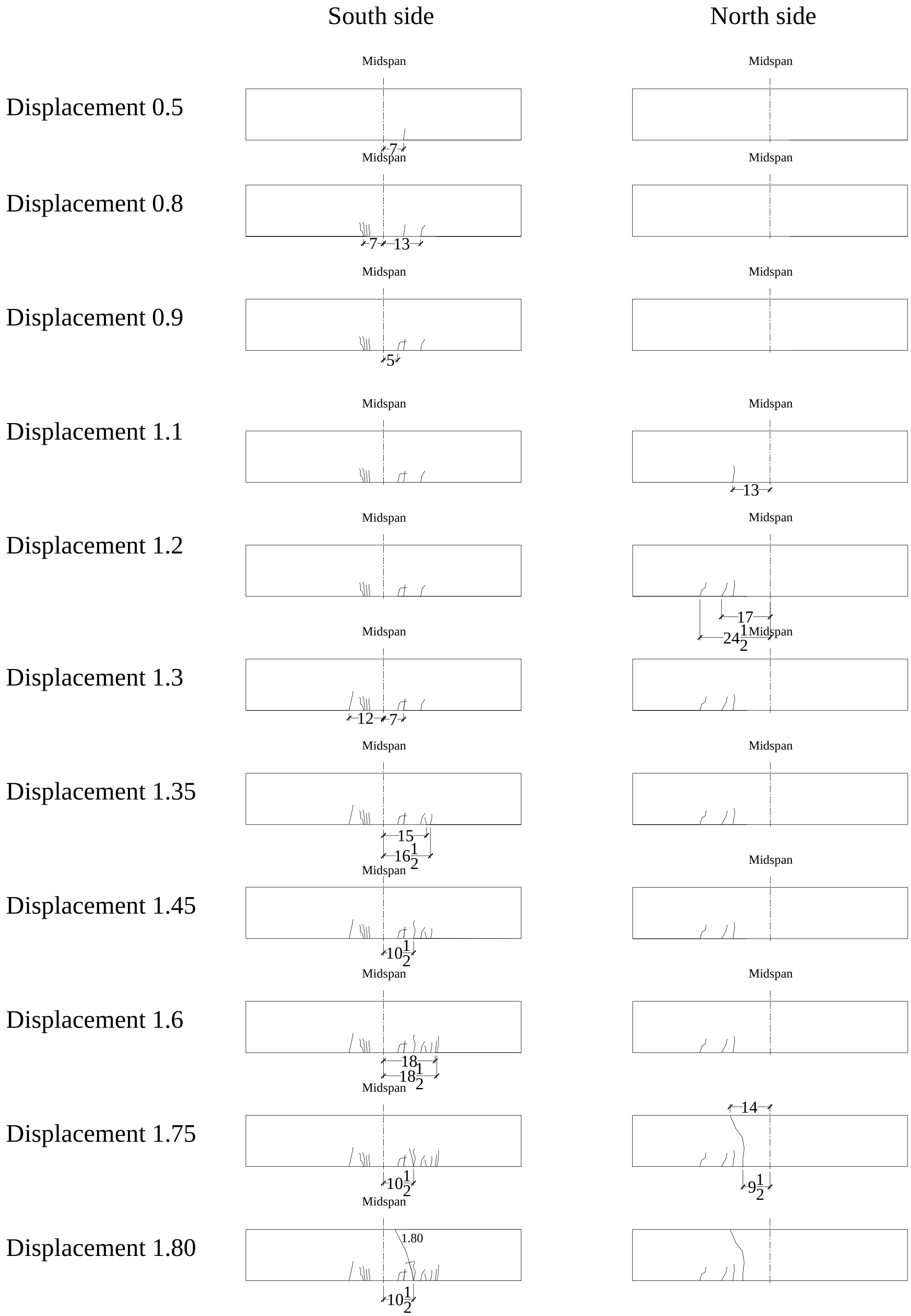

Figure C- 33 Panel ECST-FRC-SL: Propagation of Cracking

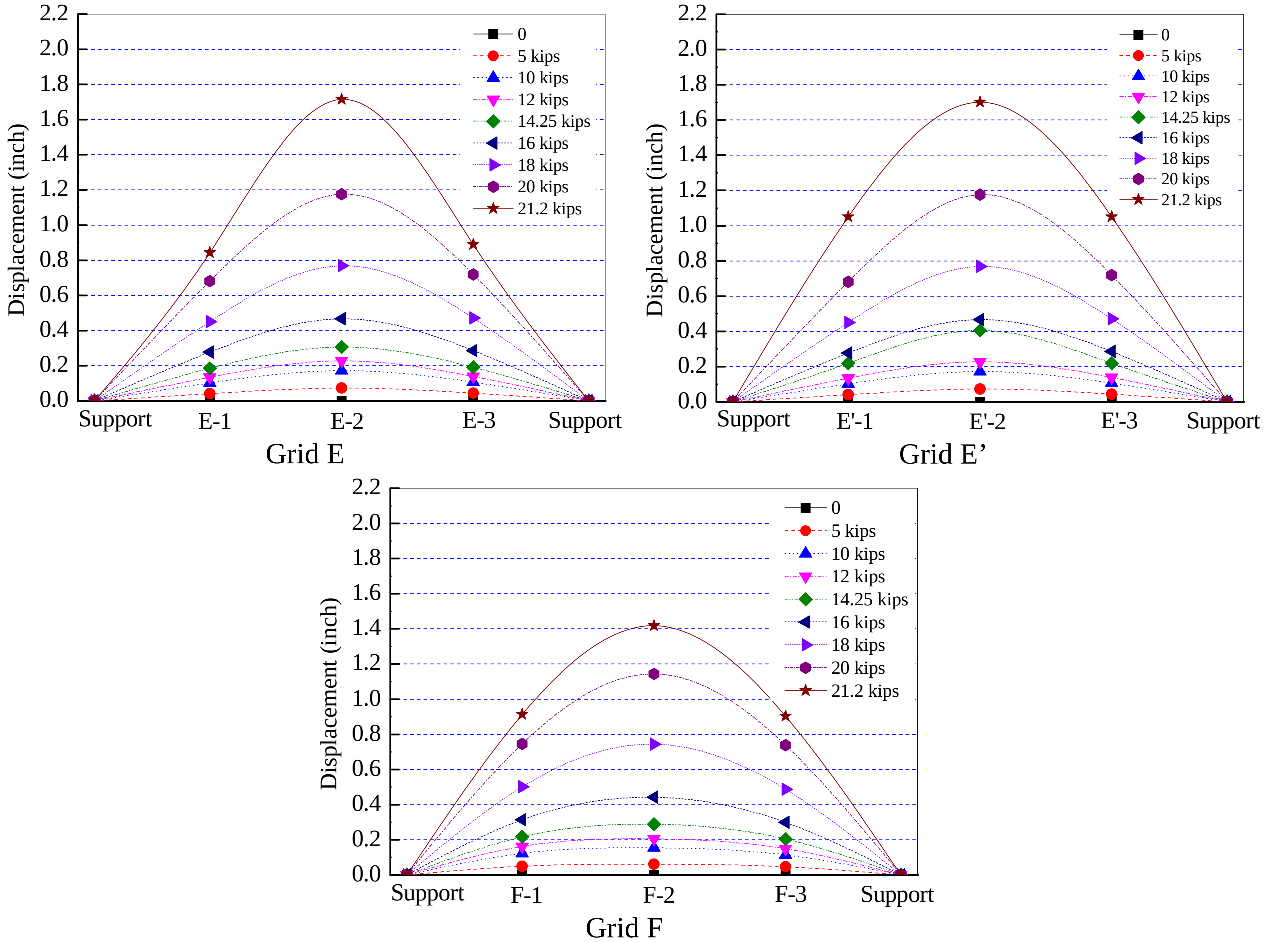

Figure C- 34 Panel ECST-FRC-SL: Measured Displacement Along Panel Length

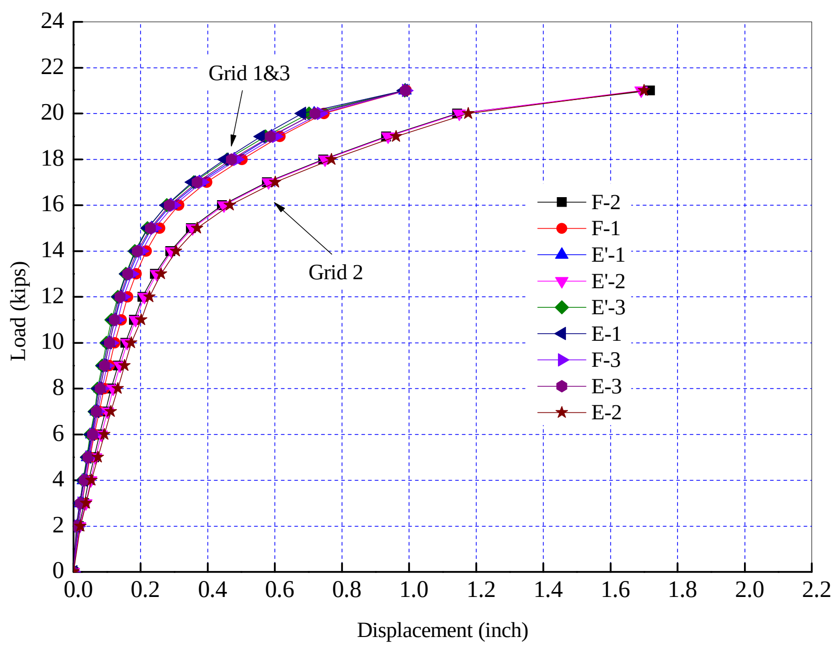

Figure C- 35 Panel ECST-FRC-SL: Applied Load-Displacement Relationship

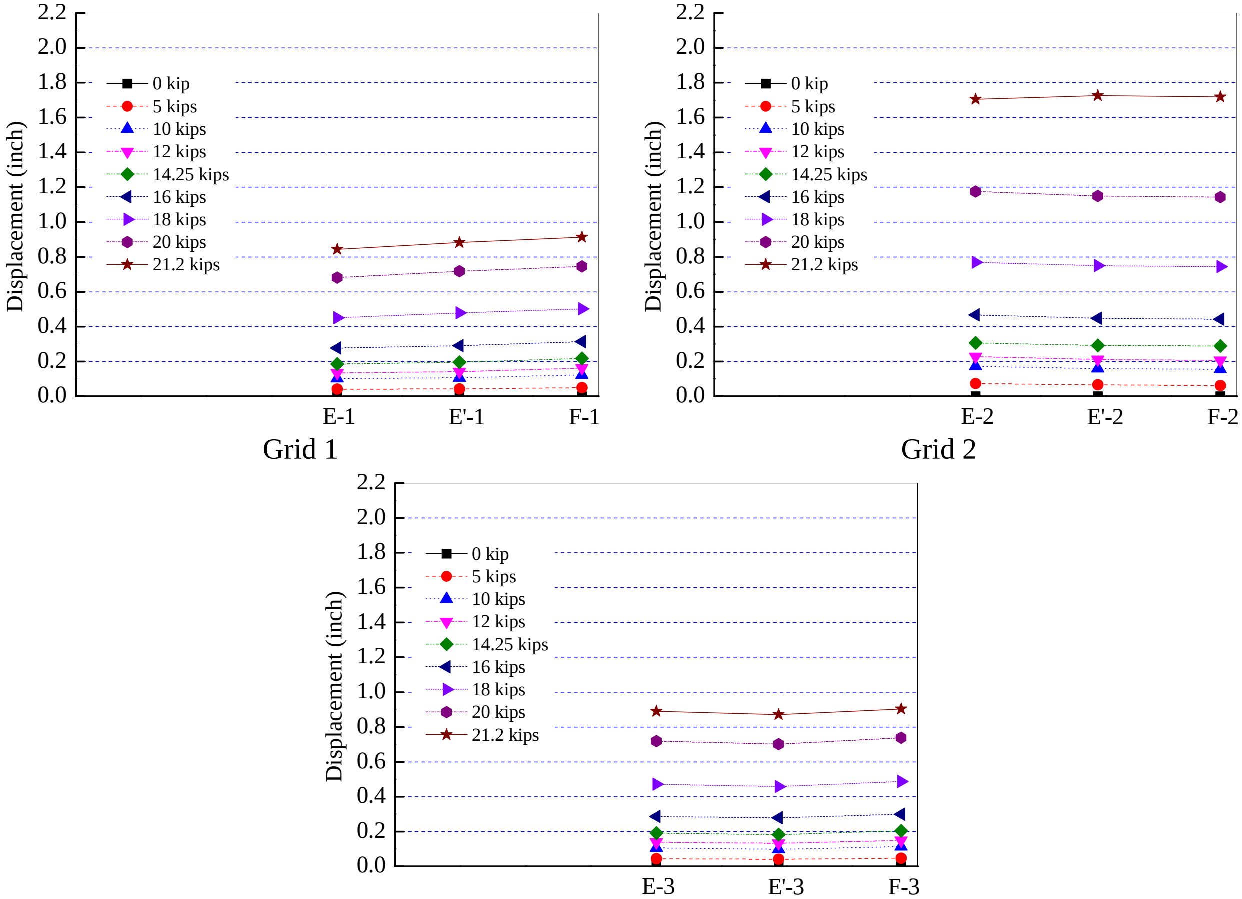

Grid 1

Grid 2

Grid 3

Figure C- 36 Panel ECST-FRC-SL: Measured Displacement Along Panel Width

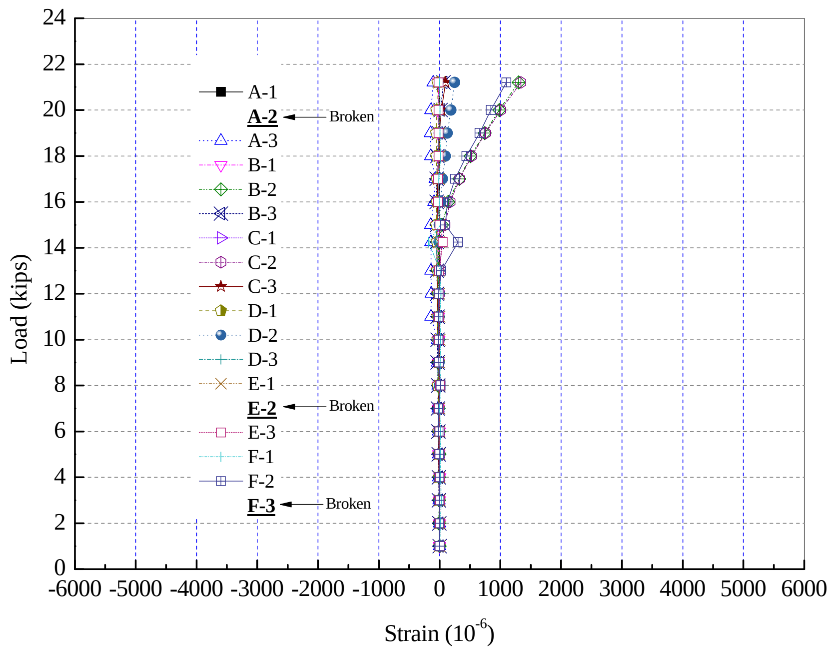

Figure C- 37 Panel ECST-FRC-SL: Applied Load-Tendon Strain Relationship

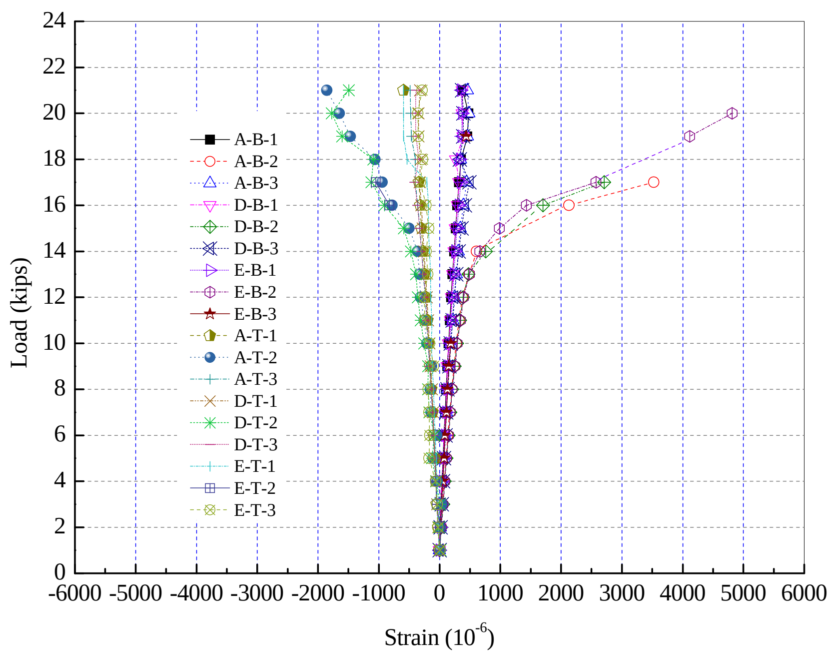

Figure C- 38 Panel ECST-FRC-SL: Applied Load-Concrete Surface Strain Relationship

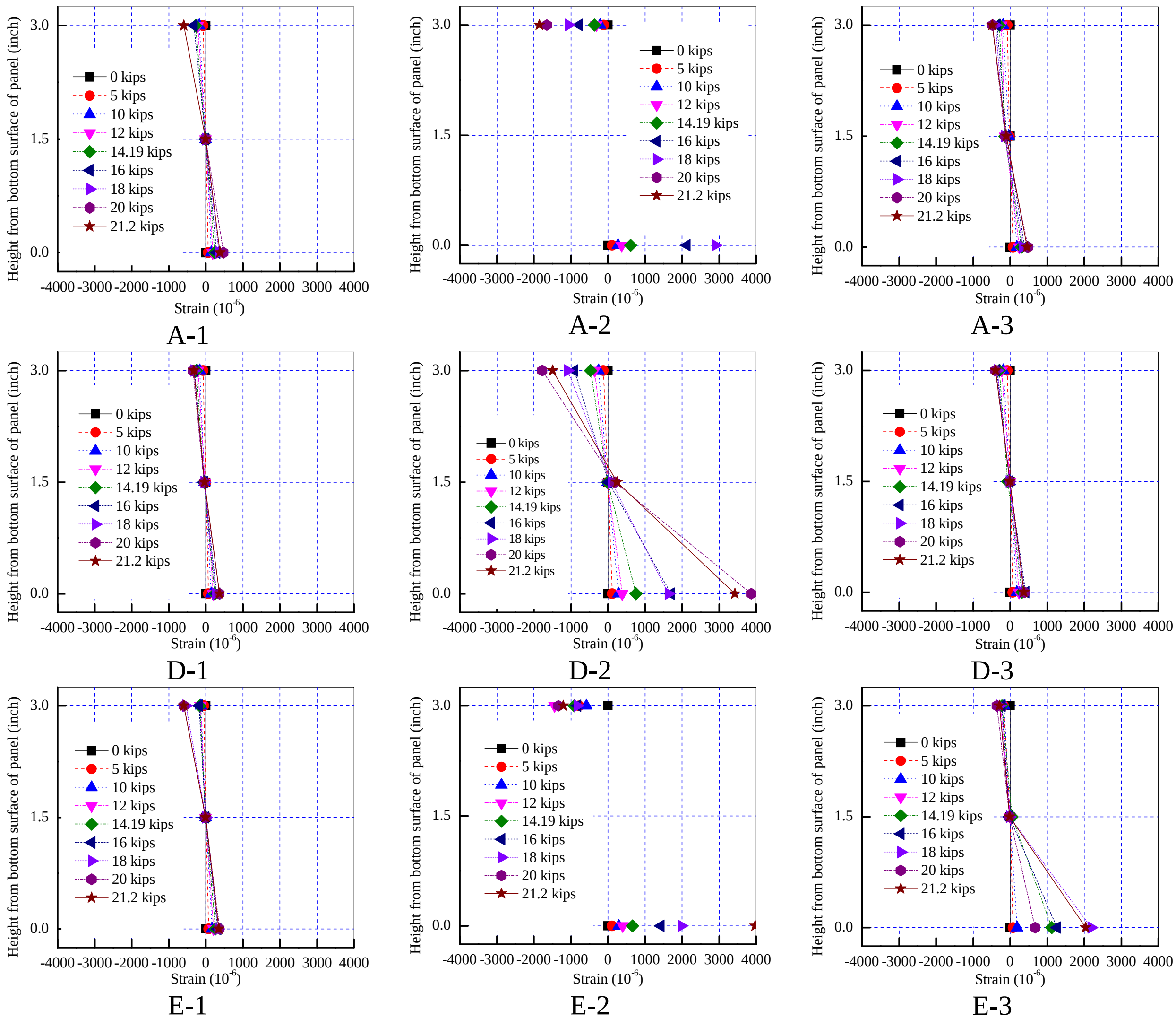

Figure C- 39 Panel ECST-FRC-SL: Measured Strain Distribution

Figure C- 40 Flexural Failure at Midspan by Concrete Crushing of Panel CFRPT-NC-SL

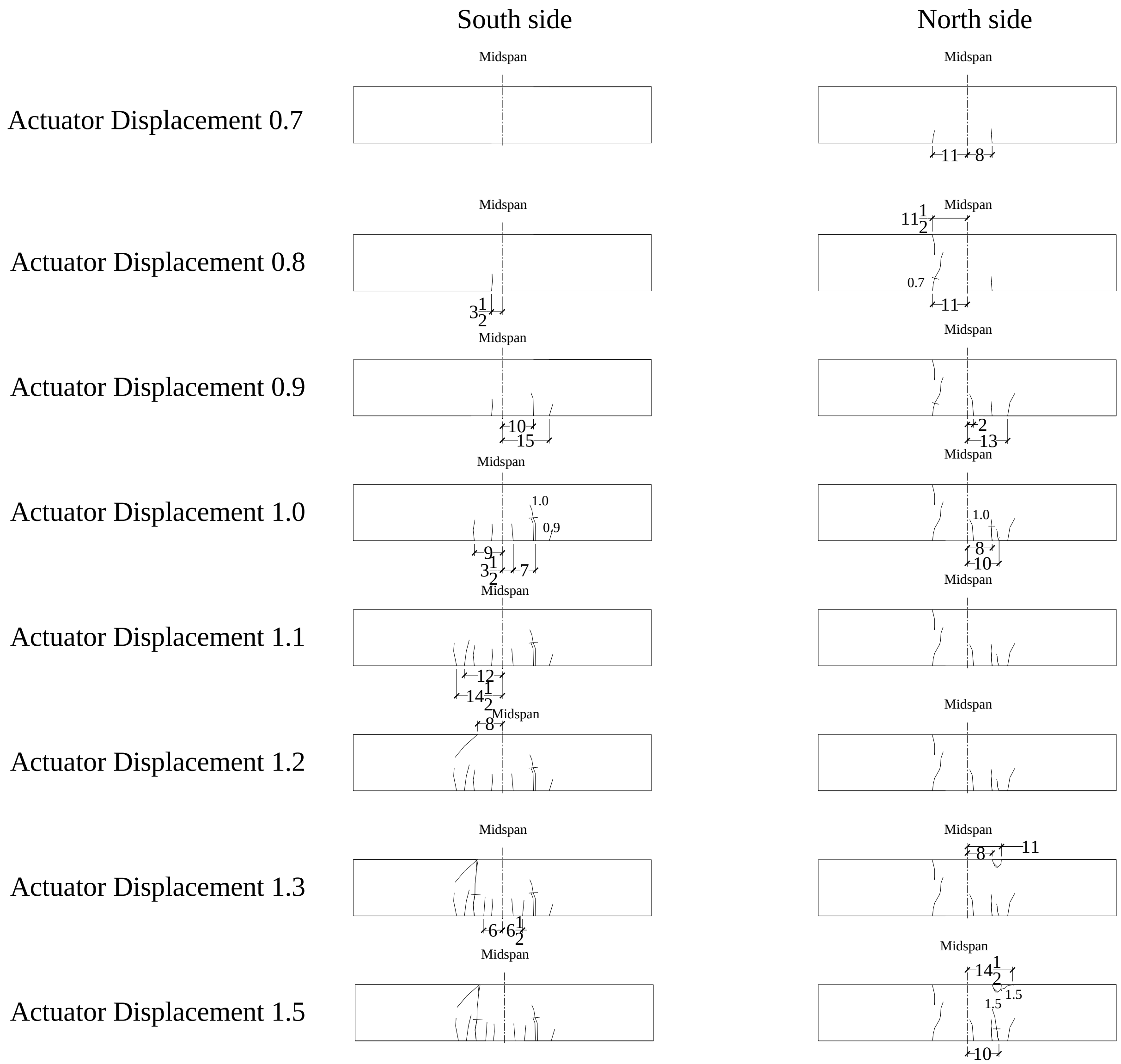

Figure C- 41 Panel CFRPT-NC-SL: Propagation of Cracking

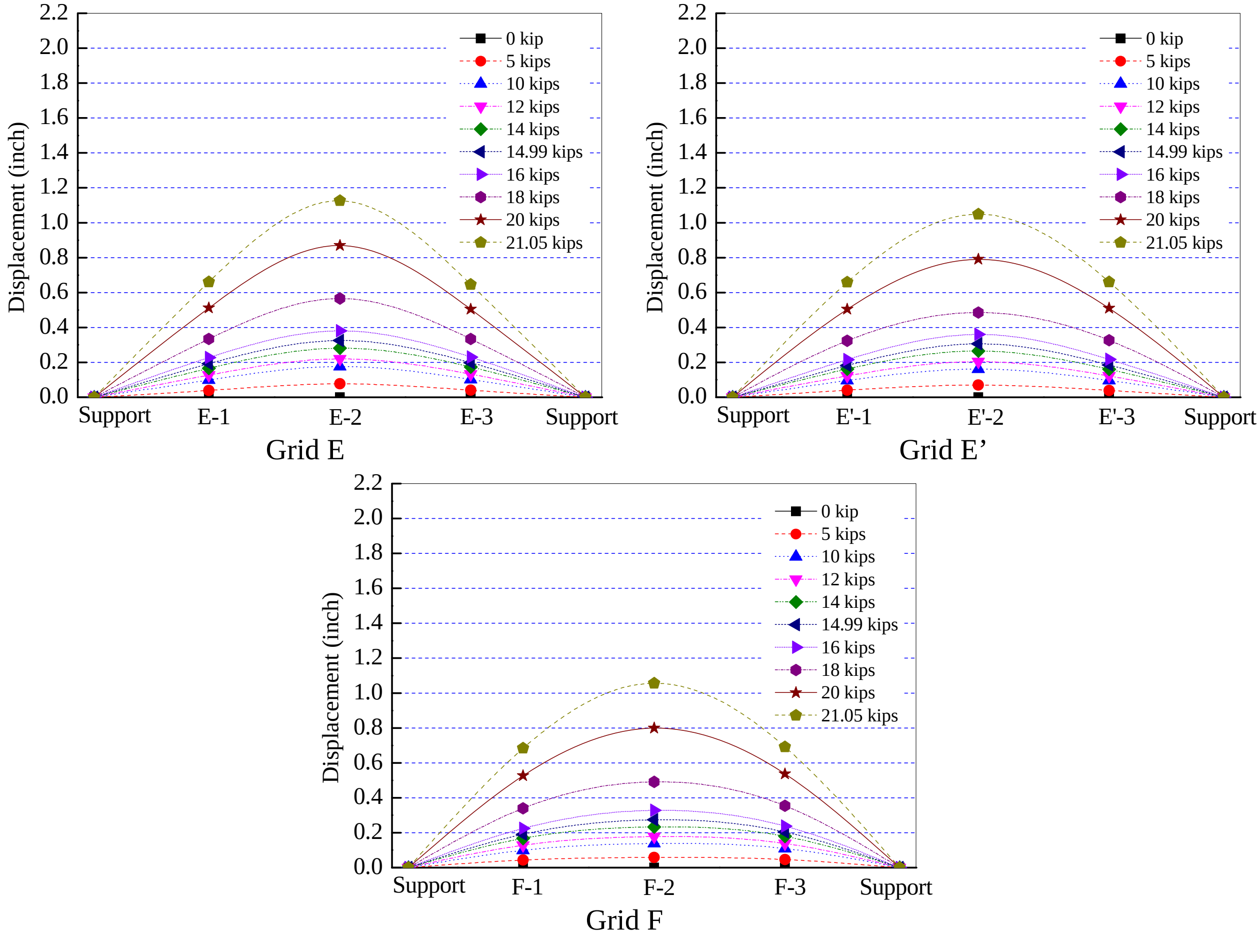

Figure C- 42 Panel CFRPT-NC-SL: Measured Displacement Along Panel Length

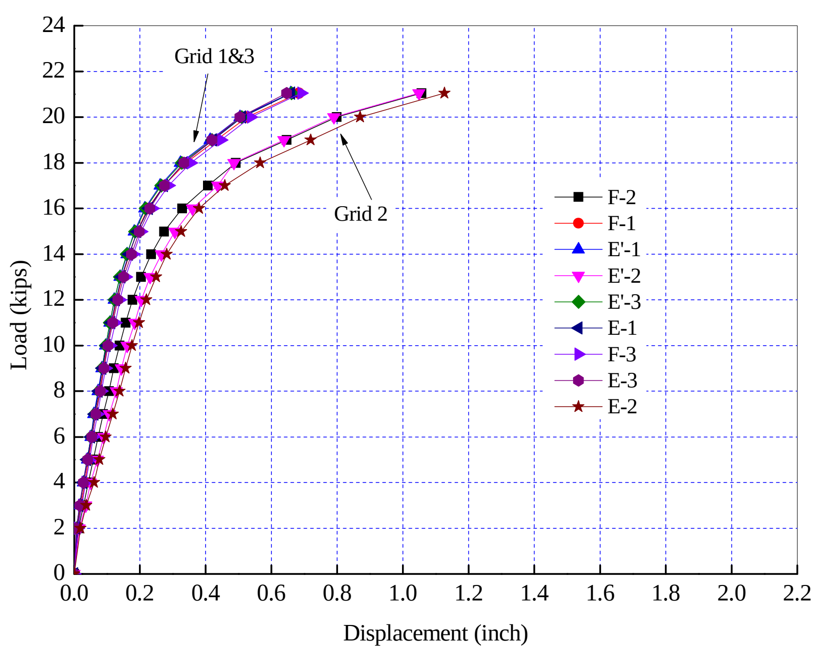

Figure C- 43 Panel CFRPT-NC-SL: Applied Load-Displacement Relationship

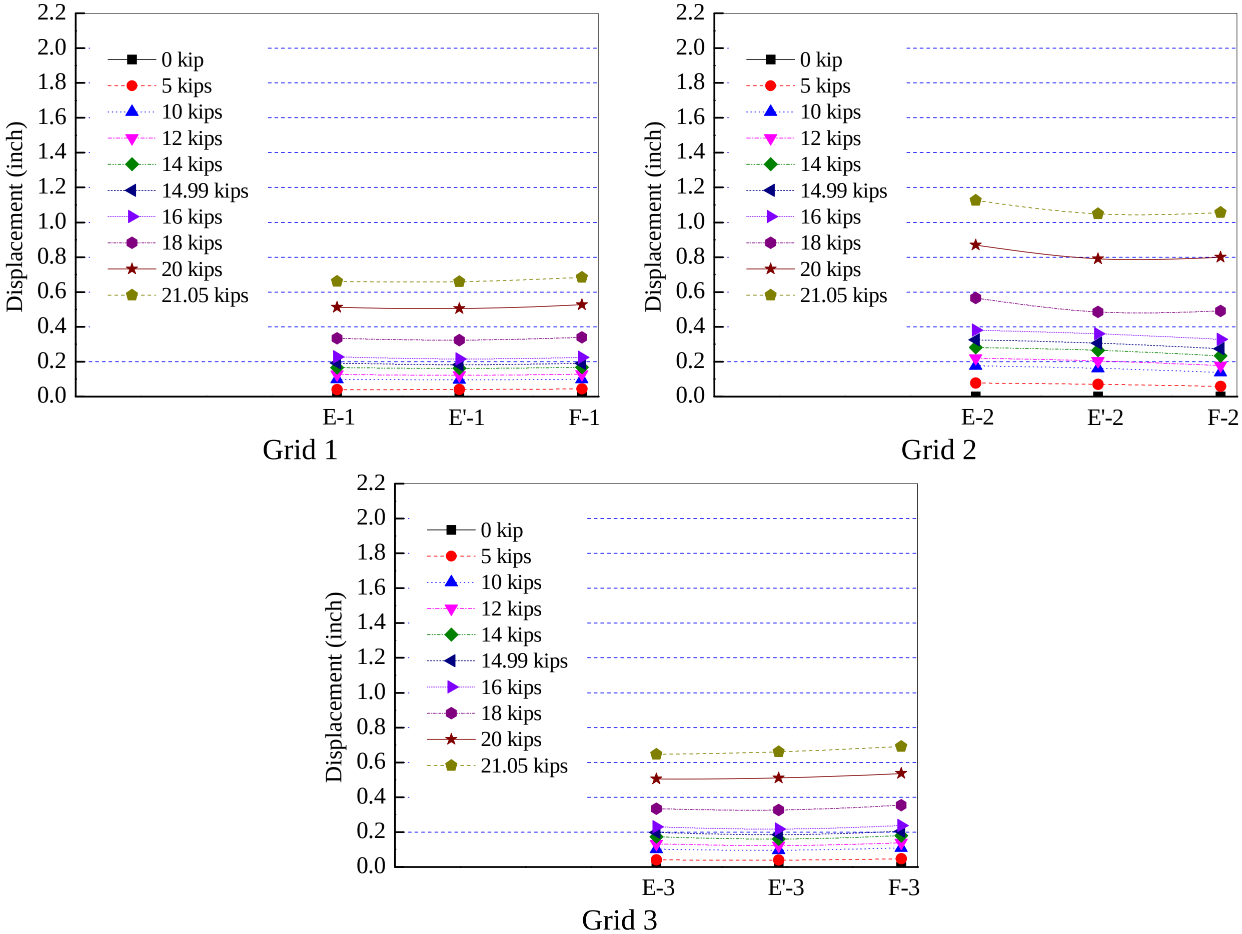

Figure C- 44 Panel CFRPT-NC-SL: Measured Displacement Along Panel Width

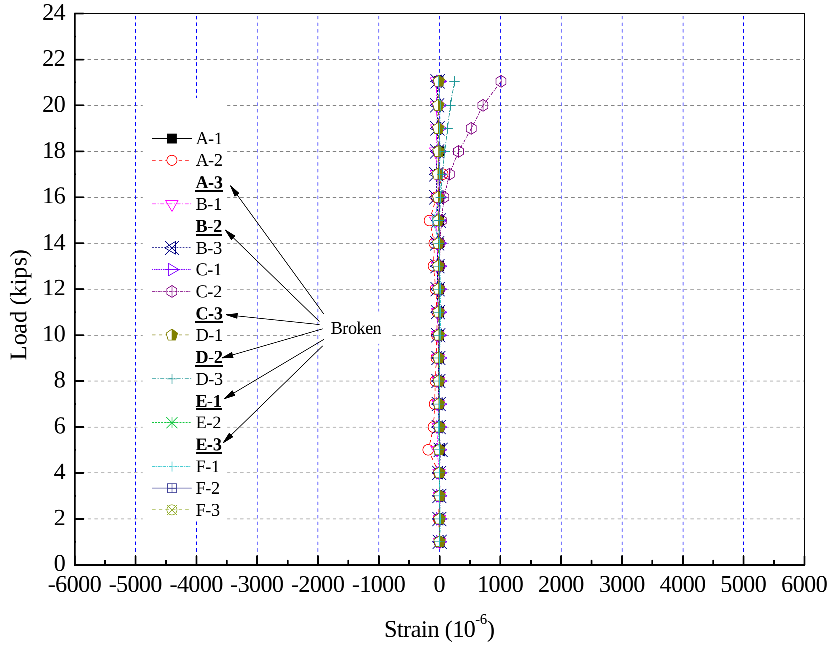

Figure C- 45 Panel CFRPT-NC-SL: Applied Load-Tendon Strain Relationship

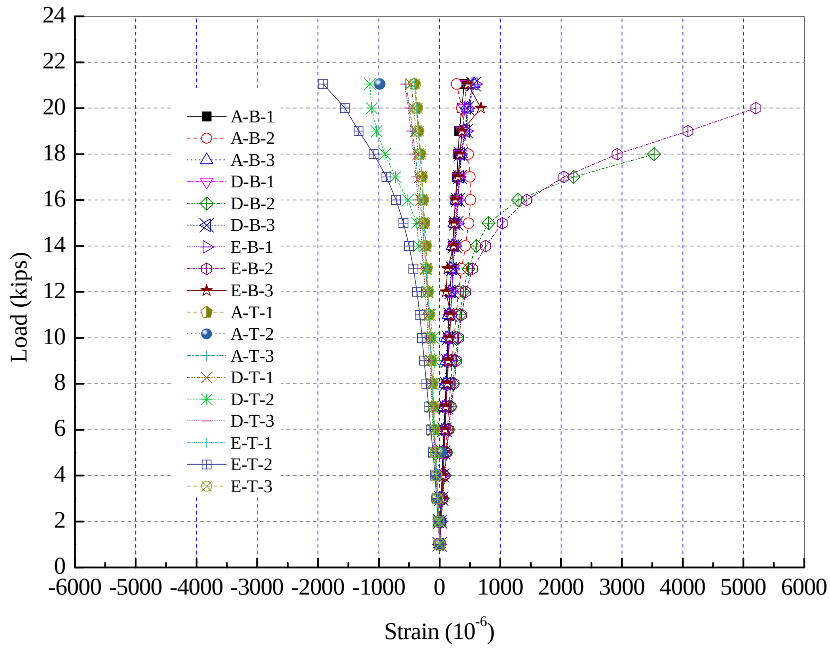

Figure C- 46 Panel CFRPT-NC-SL: Applied Load-Concrete Surface Strain Relationship

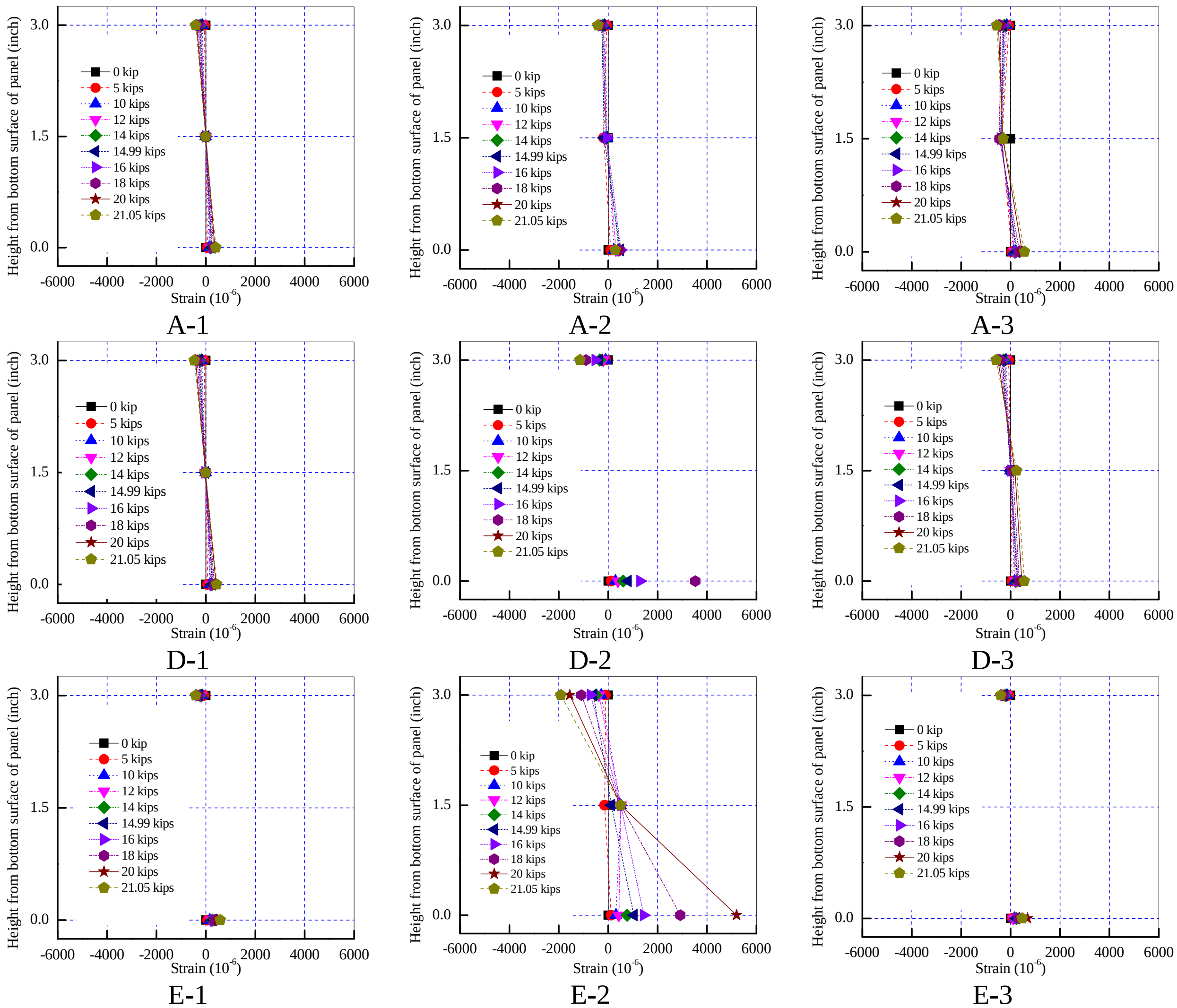

Figure C- 47 Panel CFRT-NC-SL: Measured Strain Distribution

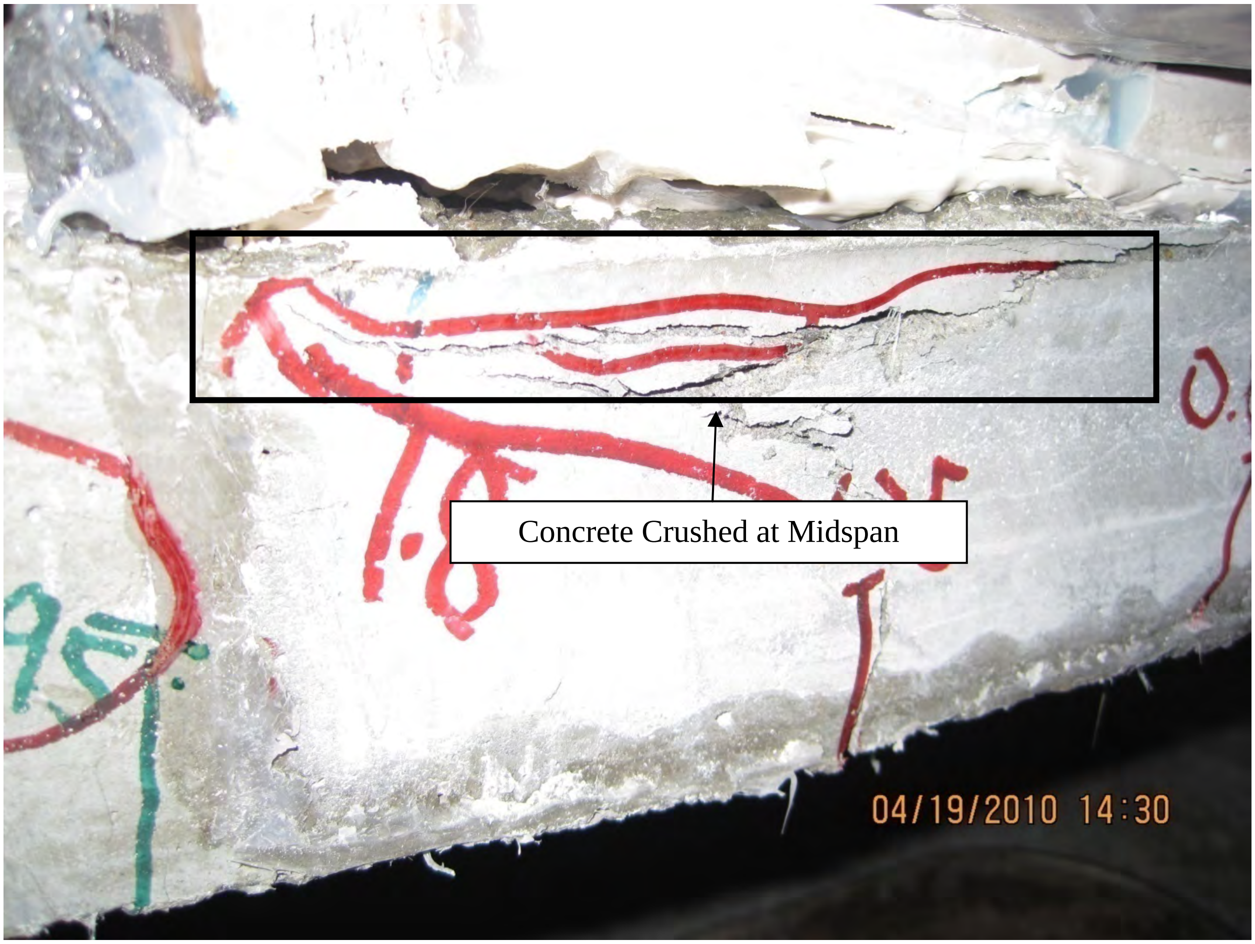

Figure C- 48 Flexural Failure at Midspan by Concrete Crushing of Panel CFRPT-FRC-SL

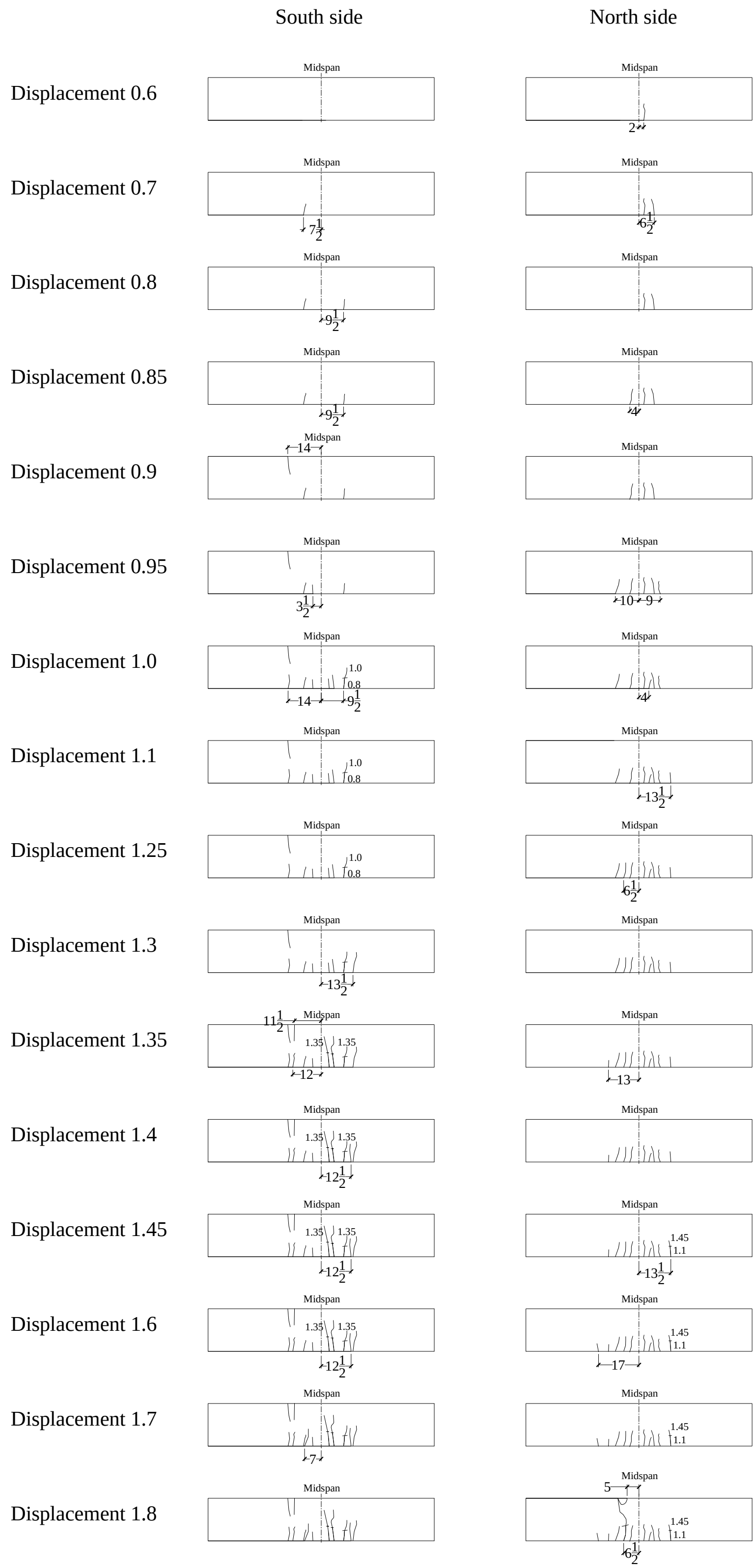

Figure C- 49 Panel CFRPT-FRC-SL: Propagation of Cracking

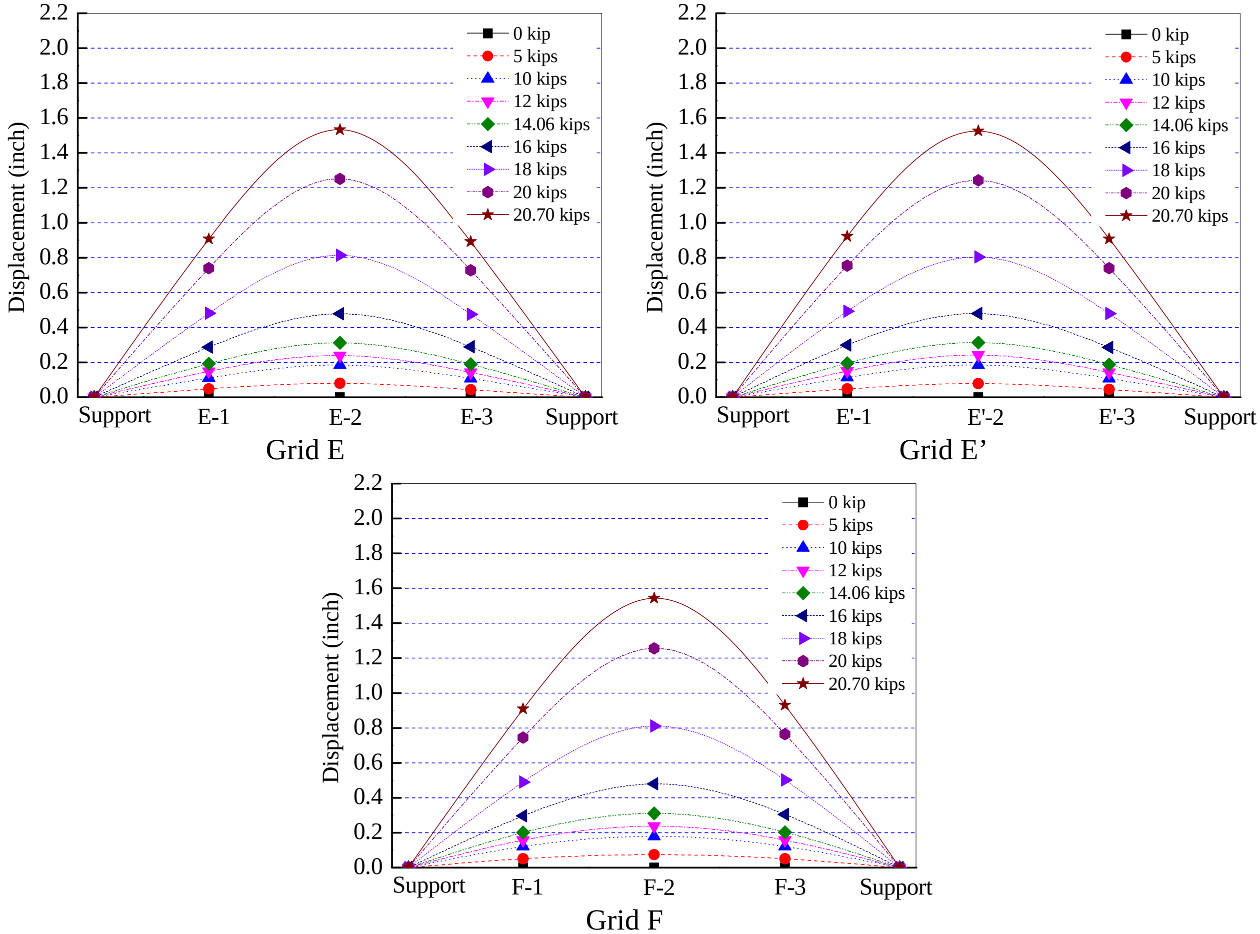

Figure C- 50 Panel CFRT-FRC-SL: Measured Displacement Along Panel Length

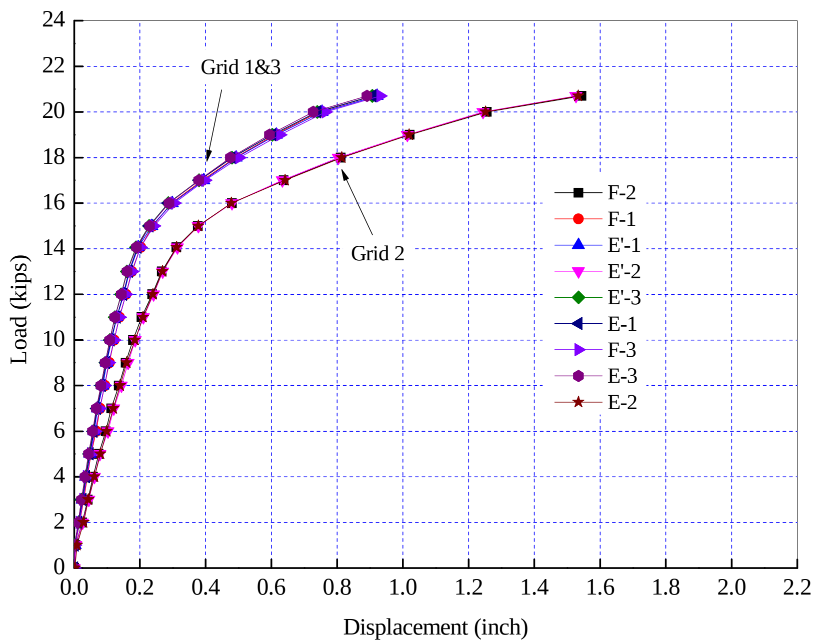

Figure C- 51 Panel CFRP-FRC-SL: Applied Load-Displacement Relationship

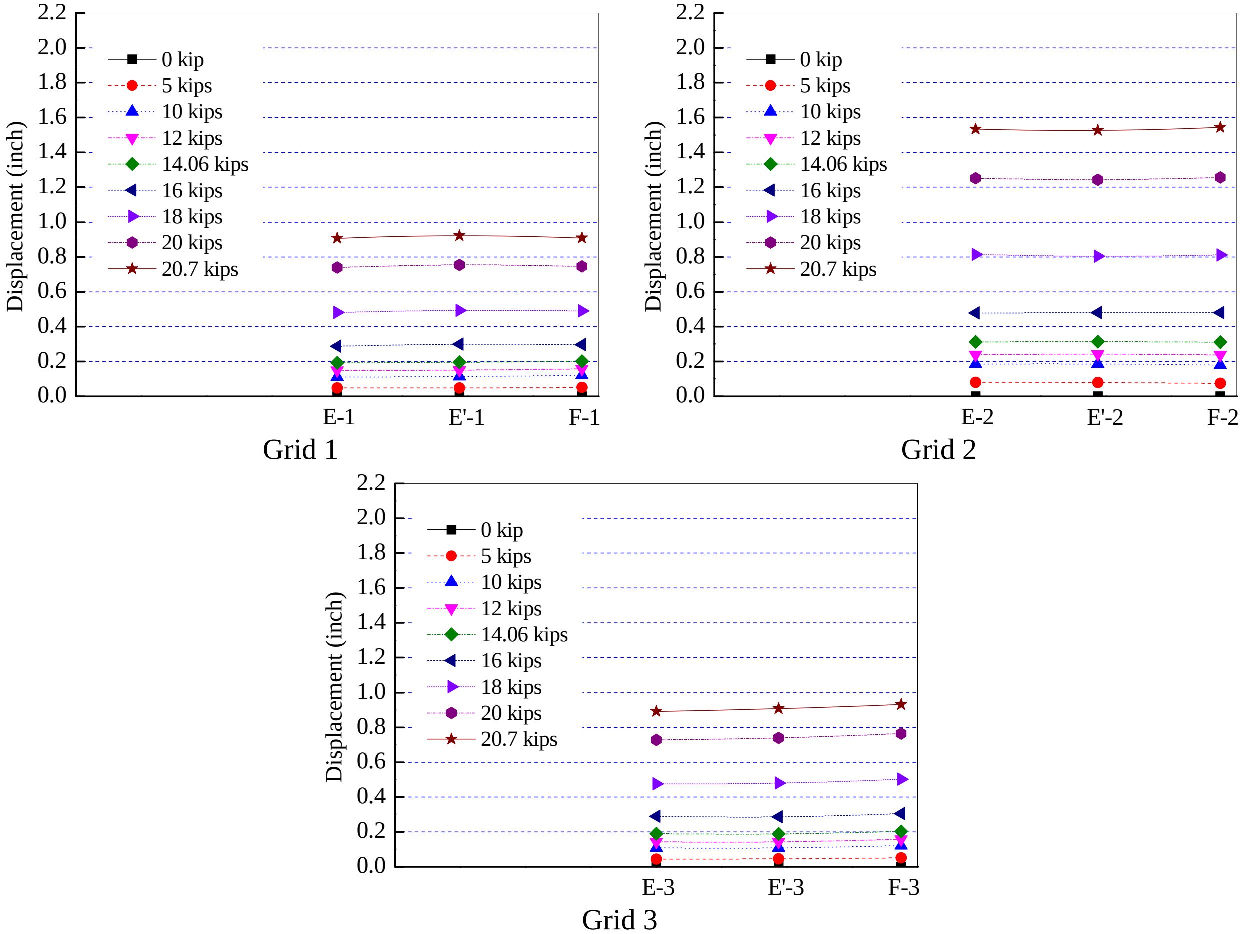

Figure C- 52 Panel CFRPT-FRC-SL: Measured Displacement Along Panel Width

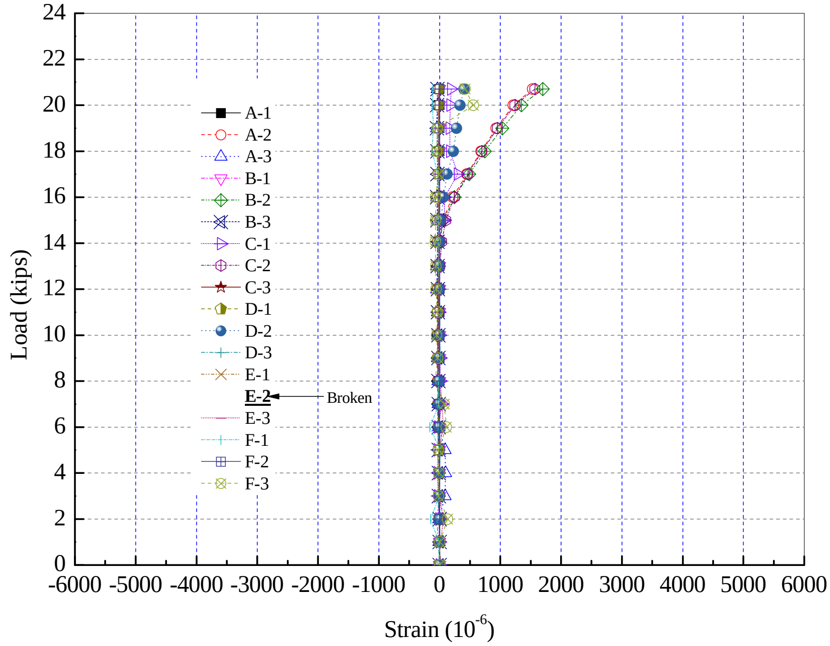

Figure C- 53 Panel CFRPT-FRC-SL: Applied Load-Tendon Strain Relationship

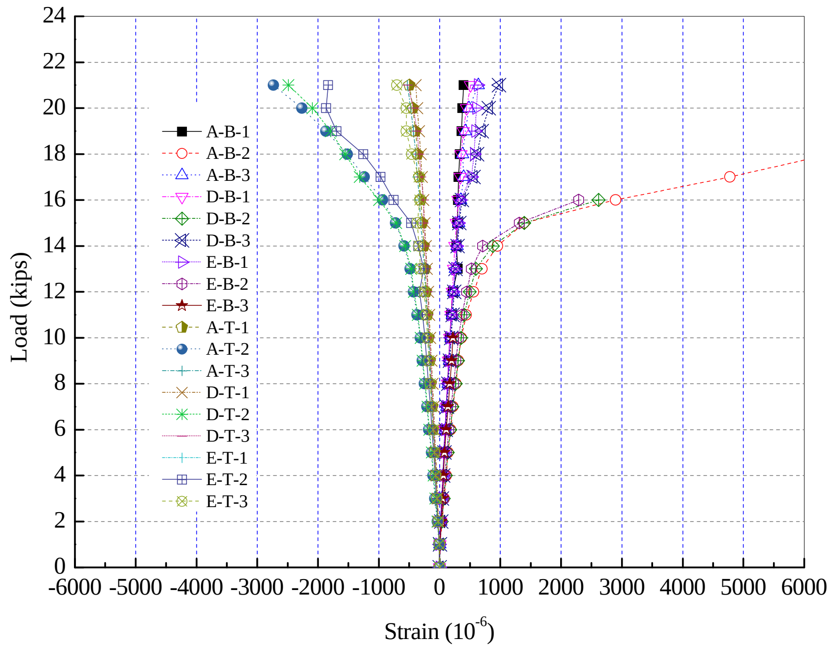

Figure C- 54 Panel CFRPT-FRC-SL: Applied Load-Concrete Surface Strain Relationship

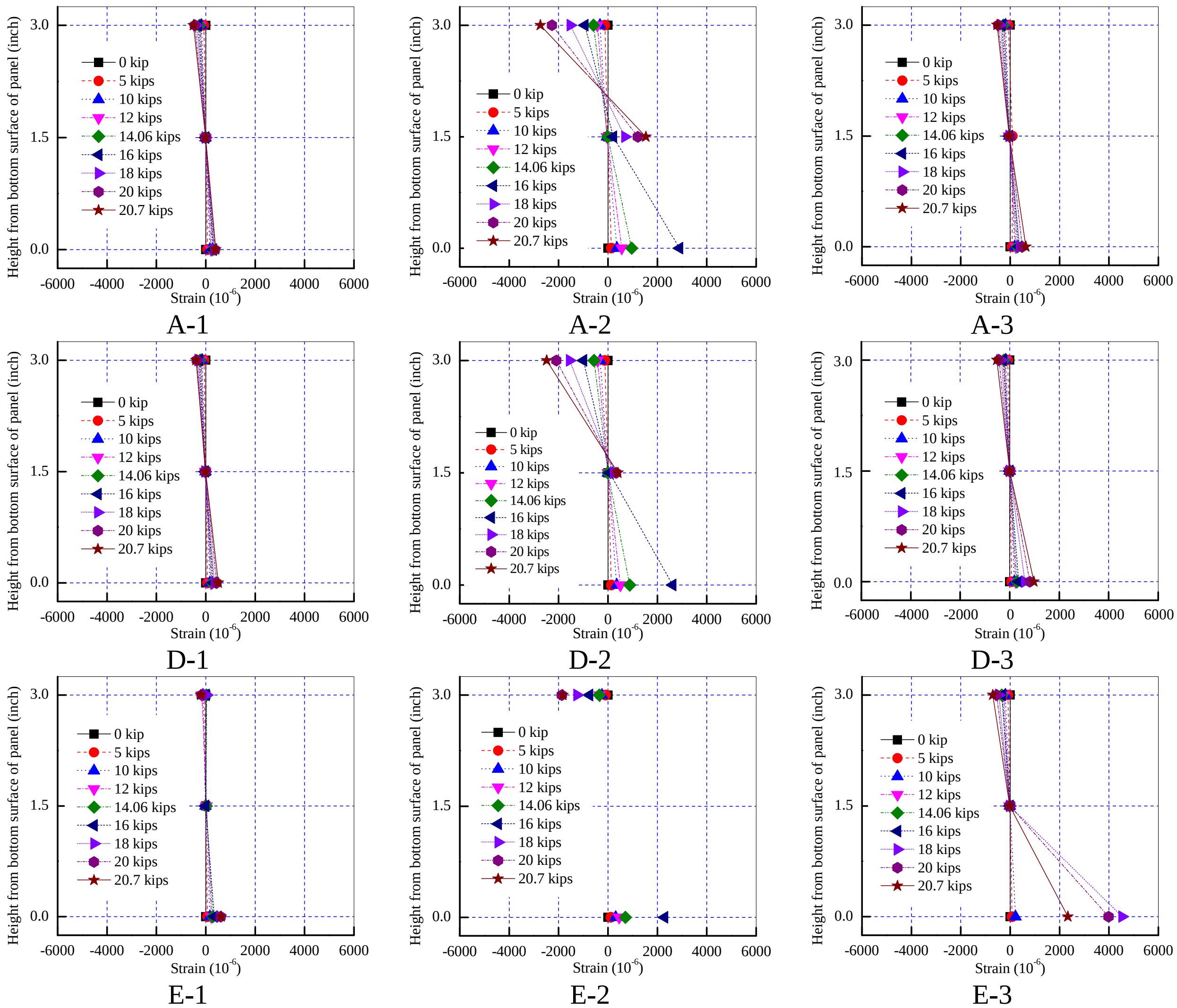

Figure C- 55 Panel CFRPT-FRC-SL: Measured Strain Distribution

Figure C- 56 Flexural Failure at Midspan by Concrete Crushing of Panel ST-NC-FL

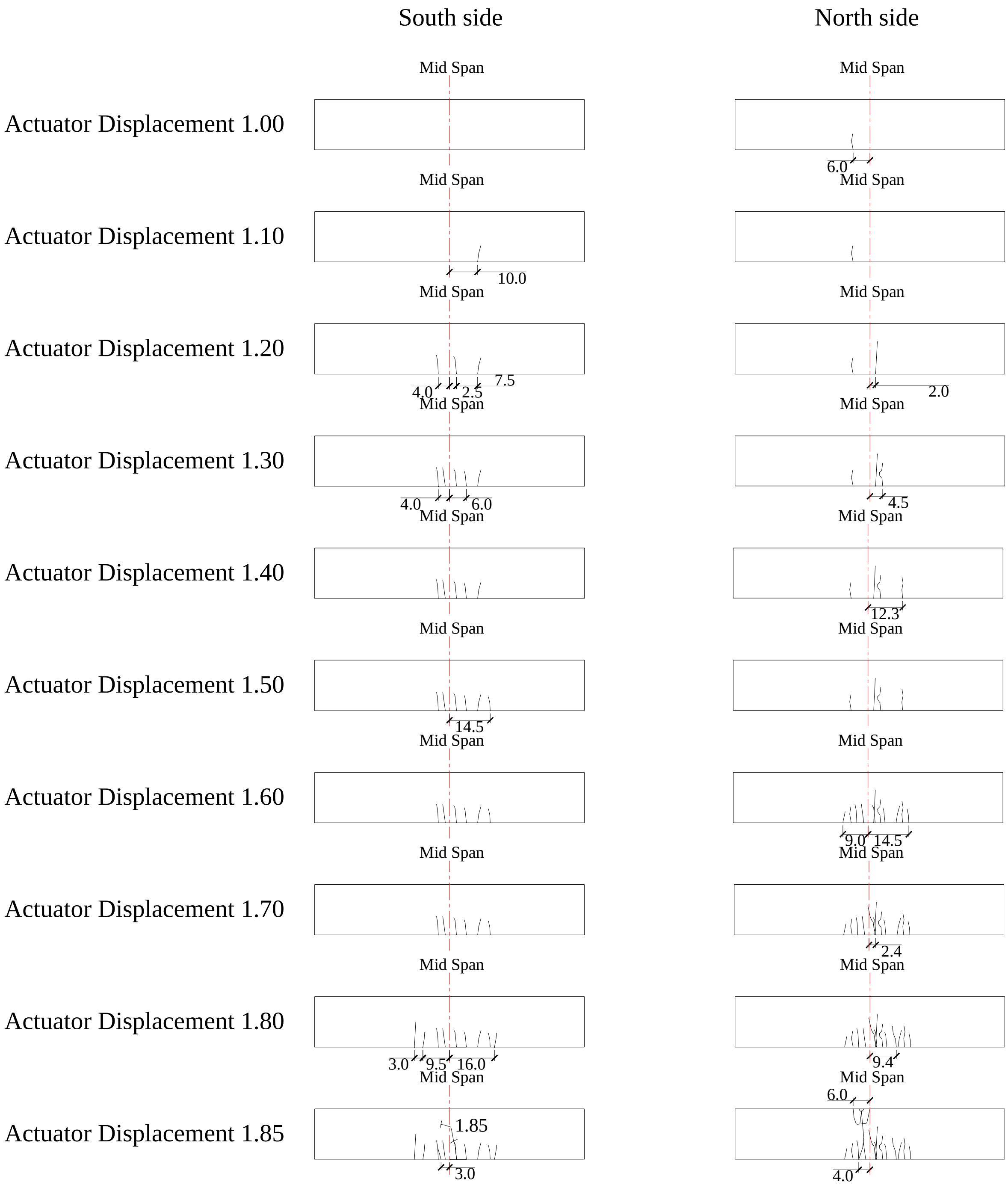

Figure C- 57 Panel ST-NC-FL: Propagation of Cracking

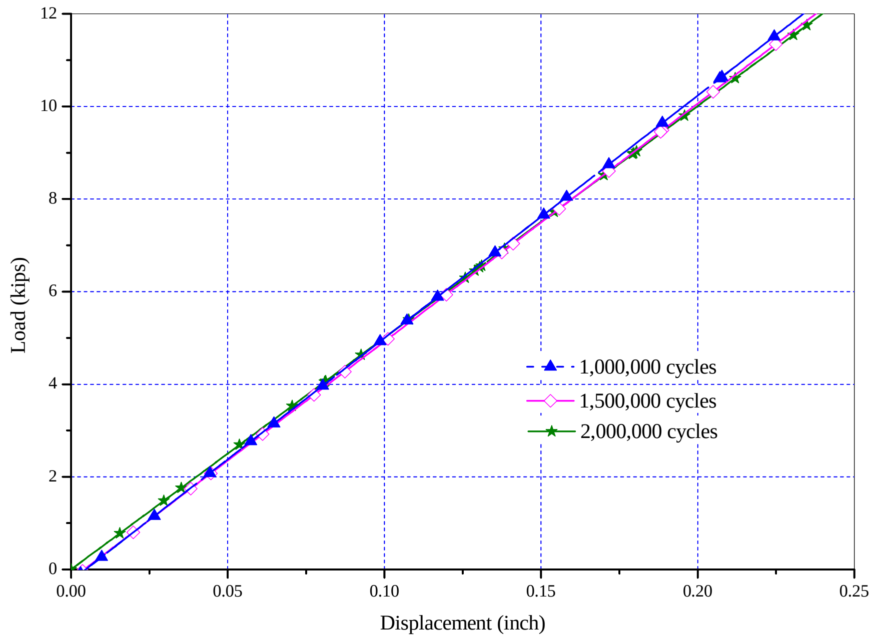

Figure C- 58 Panel ST-NC-FL: Applied Load-Displacement Relationships of the Quasi-Static Load Tests

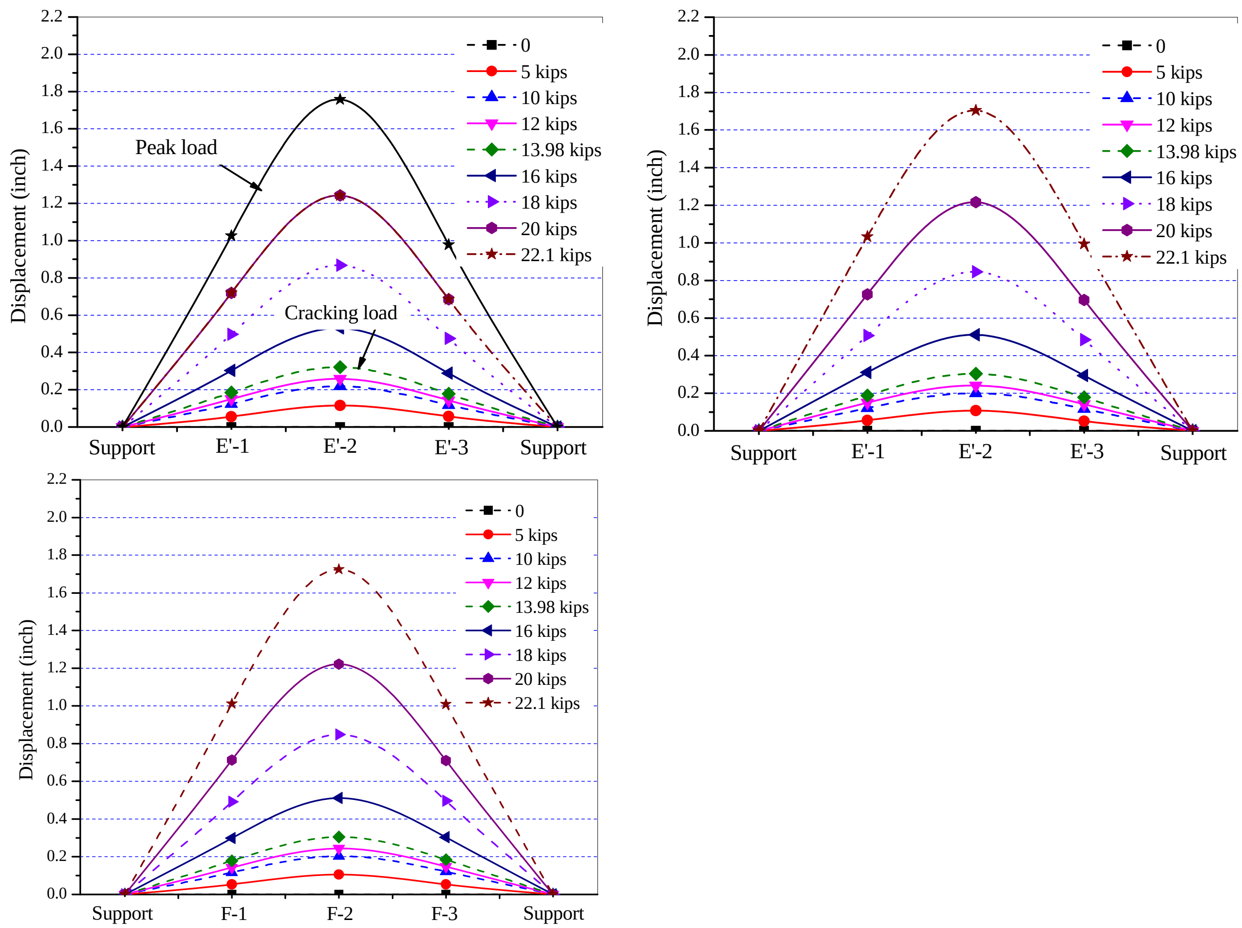

Figure C- 59 Panel ST-NC-FL: Measured Displacement Along Panel Length

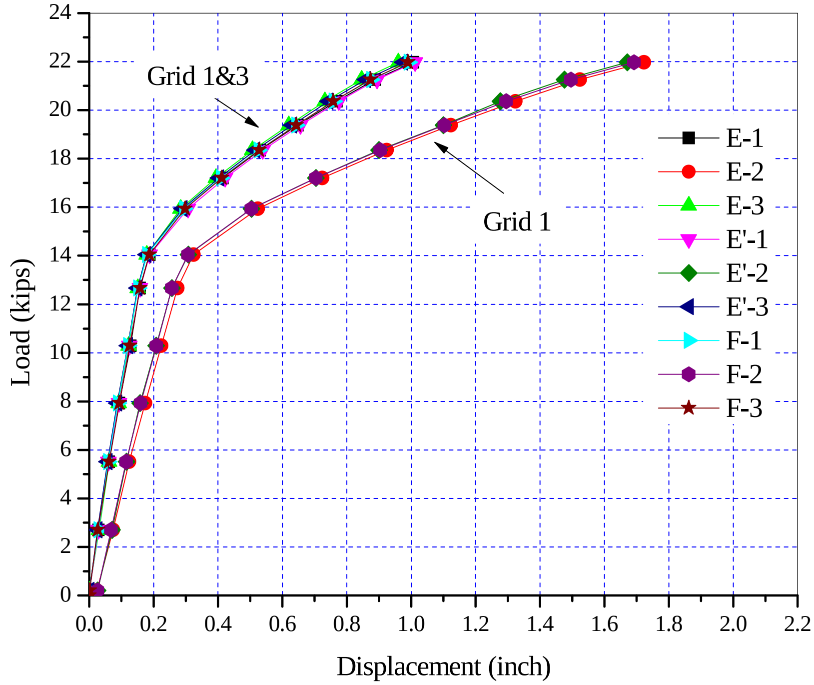

Figure C- 60 Panel ST-NC-FL: Applied Load-Displacement Relationship

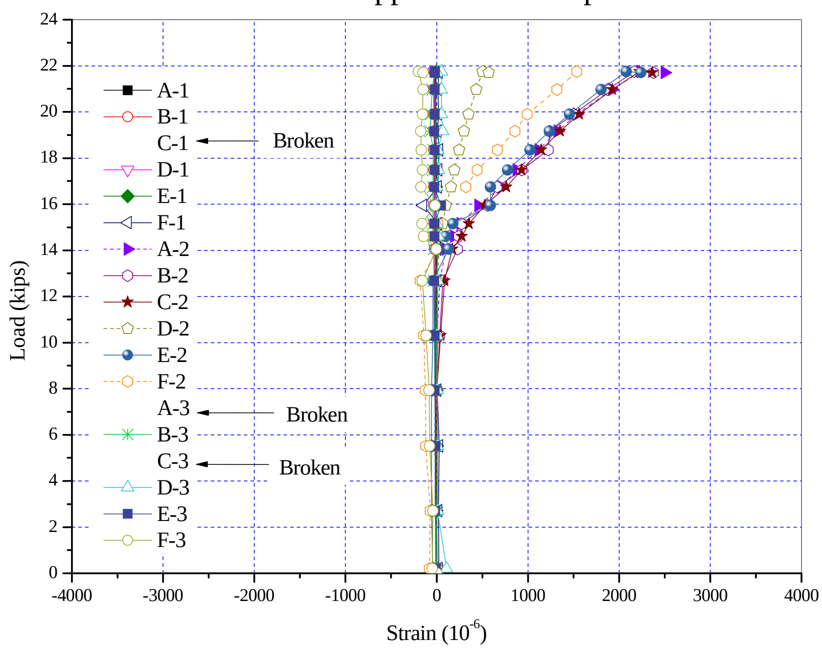

Figure C- 61 Panel ST-NC-FL: Applied Load-Tendon Strain Relationship

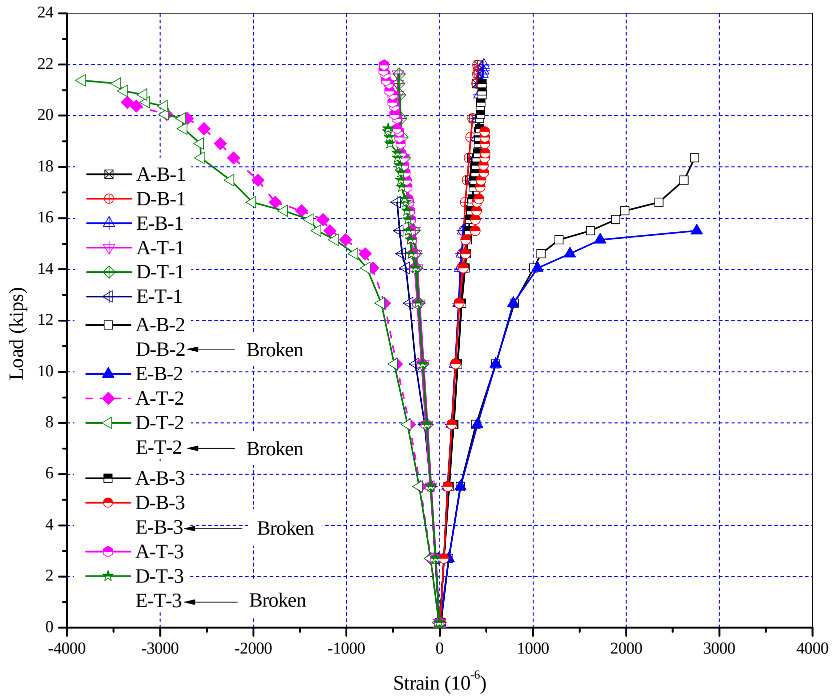

Figure C- 62 Panel ST-NC-FL: Applied Load-Concrete Surface Strain Relationship

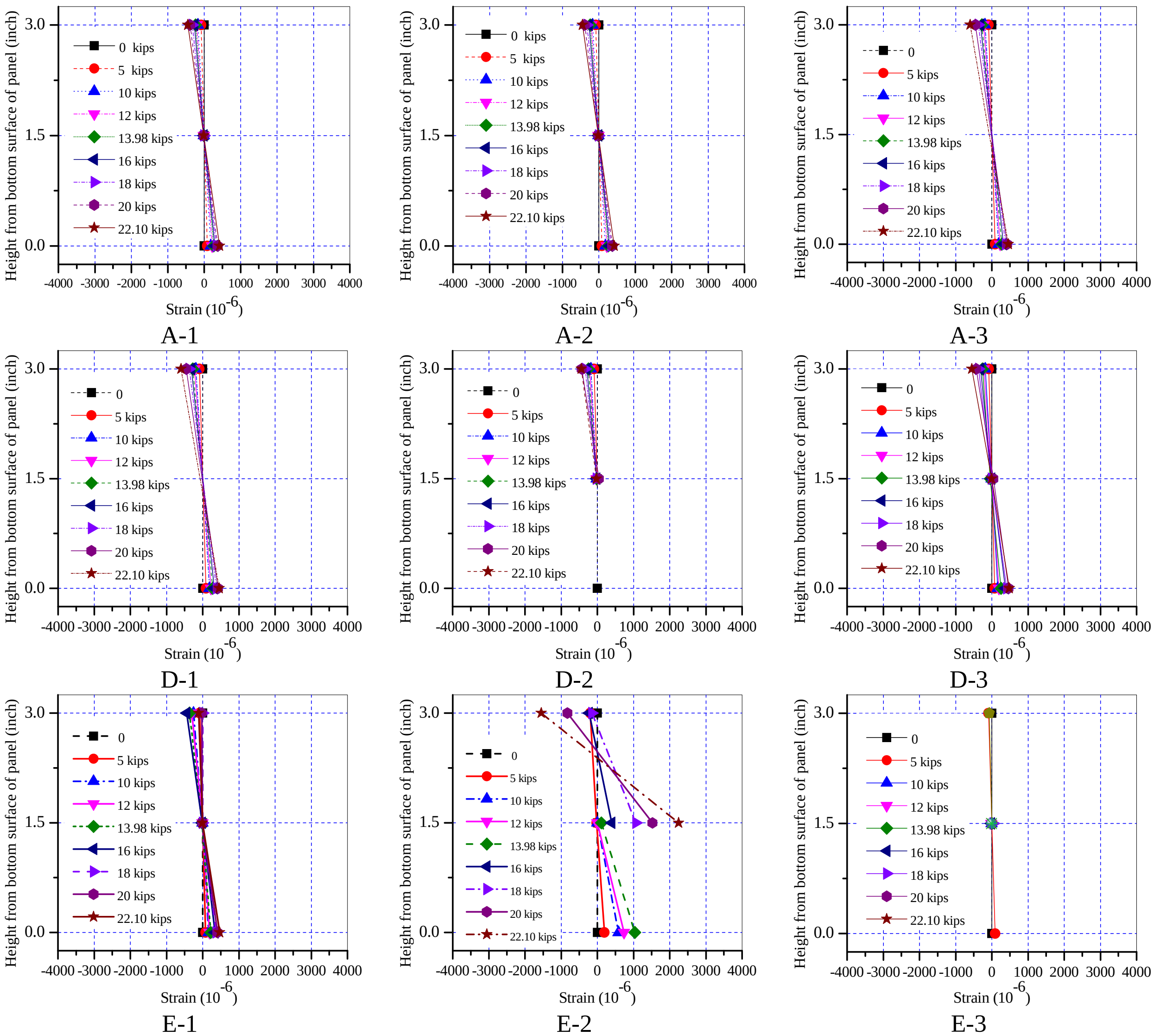

Figure C- 63 Panel ST-NC-FL: Measured Strain Distribution, Post-Fatigue Quasi-Static Test

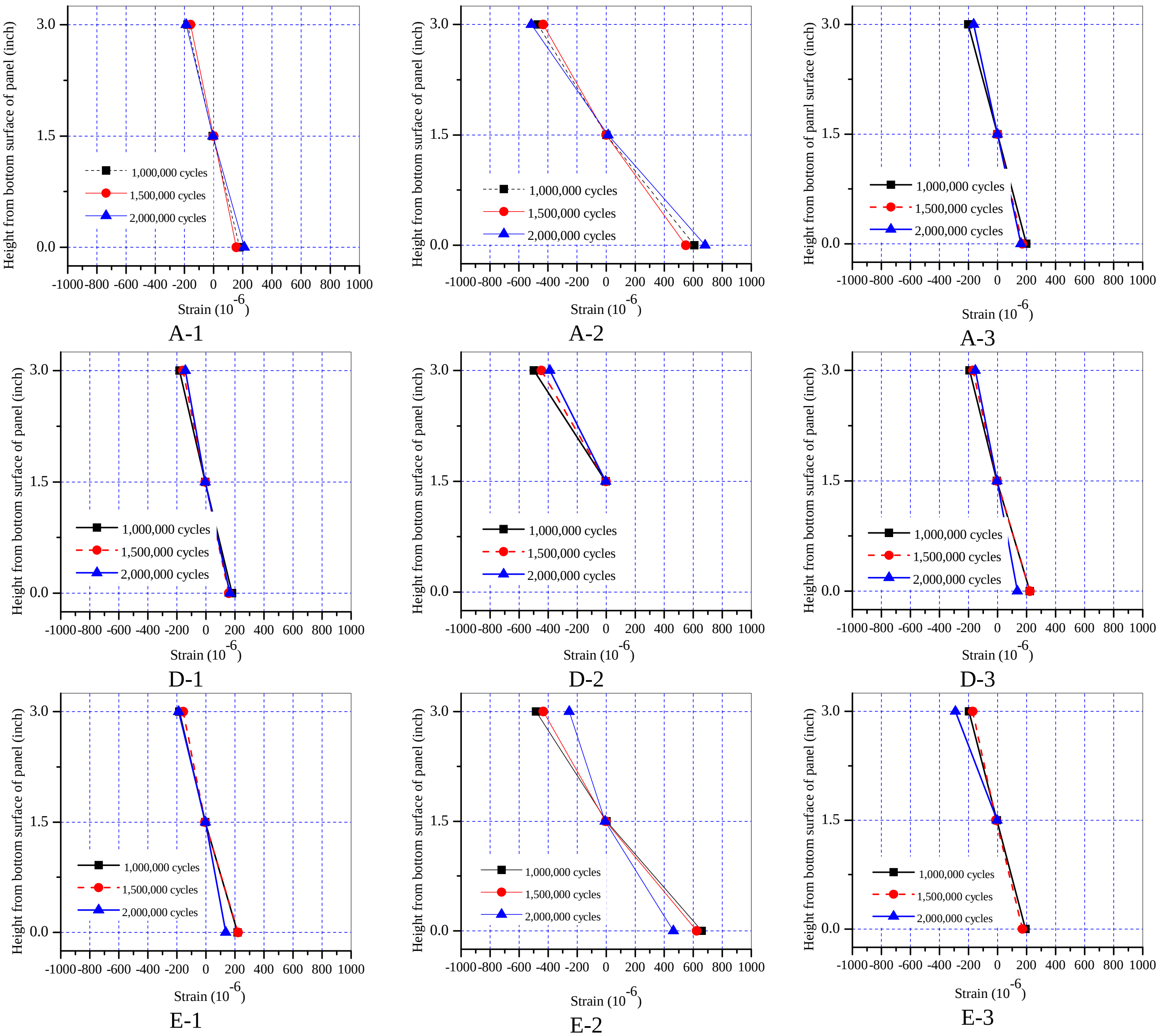

Figure C- 64 Panel ST-NC-FL: Measured Strain Distribution at Various Cycles

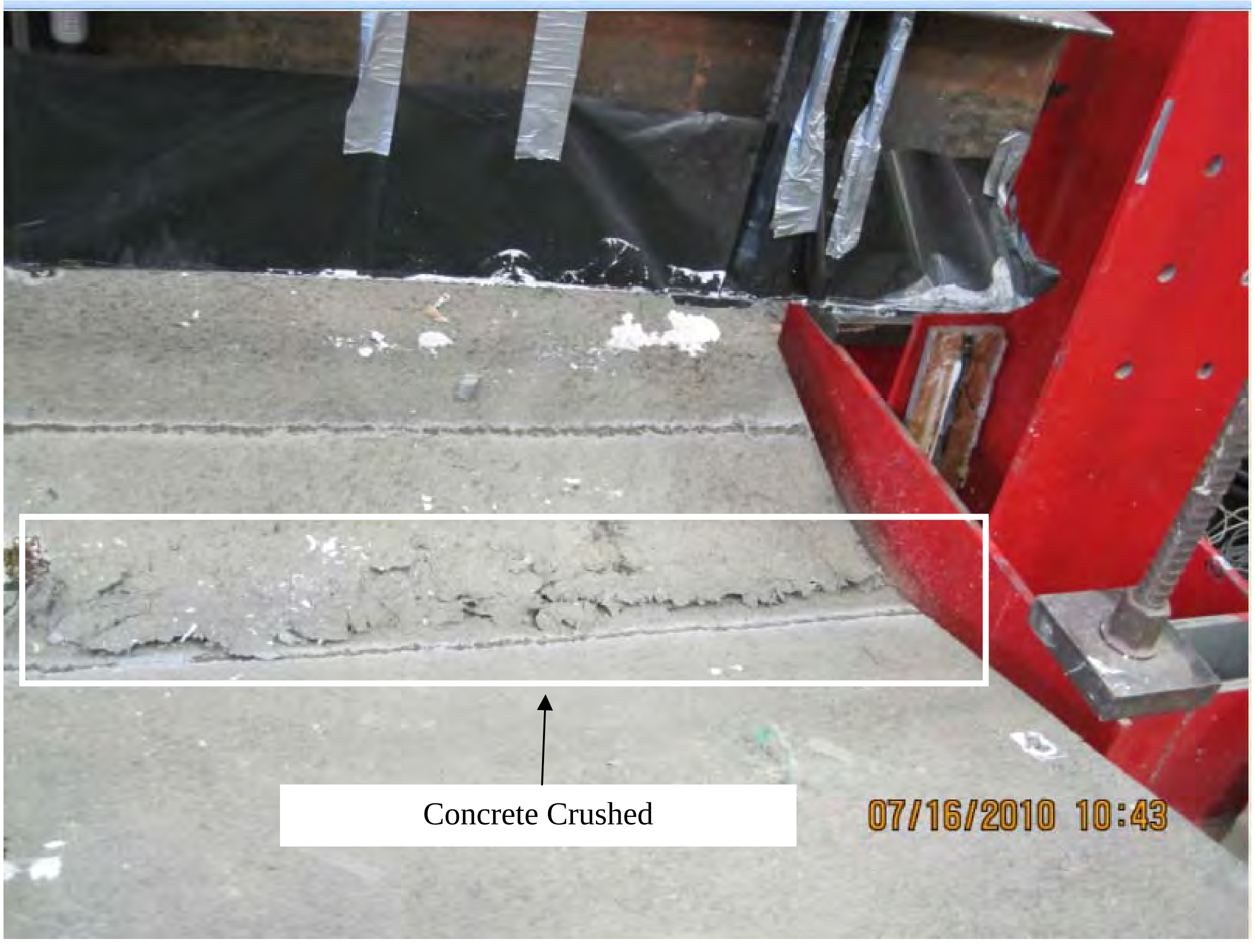

Figure C- 65 Flexural Failure at Midspan by Concrete Crushing of Panel ST-FRC-FL

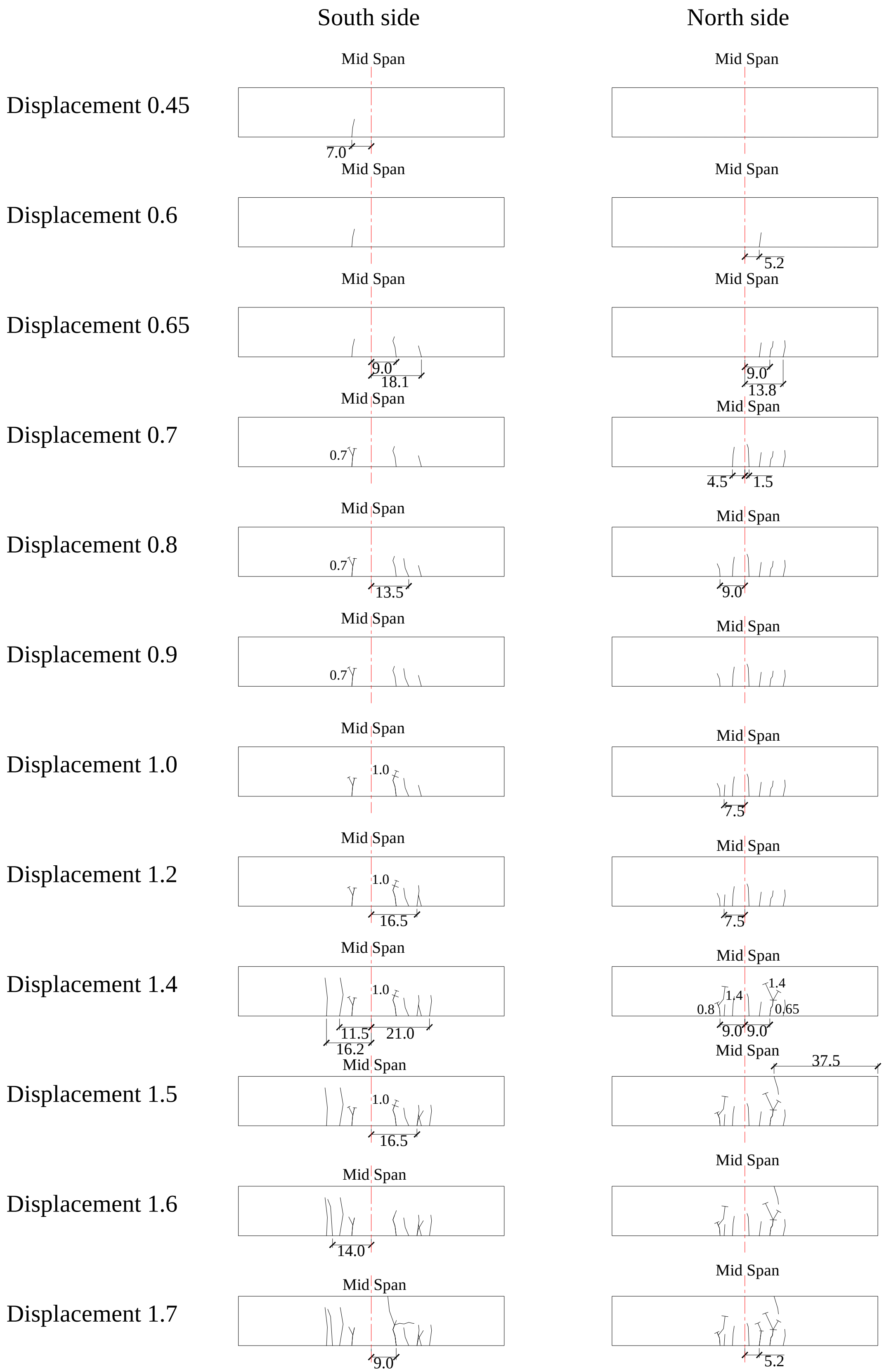

Figure C- 66 Panel ST-FRC-FL: Propagation of Cracking

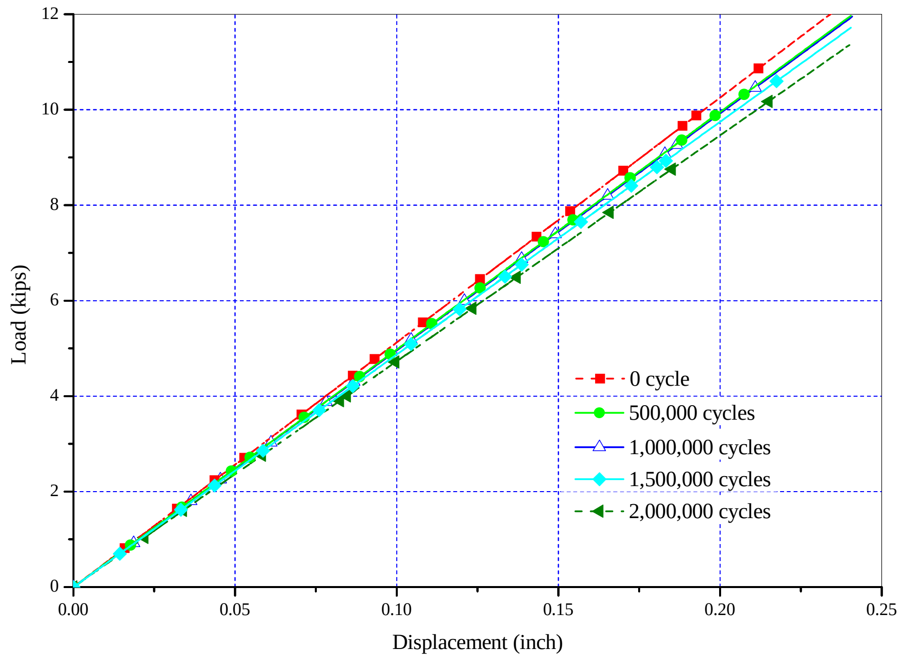

Figure C- 67 Panel ST-FRC-FL: Applied Load-Displacement Relationships of the Quasi-Static Load Tests

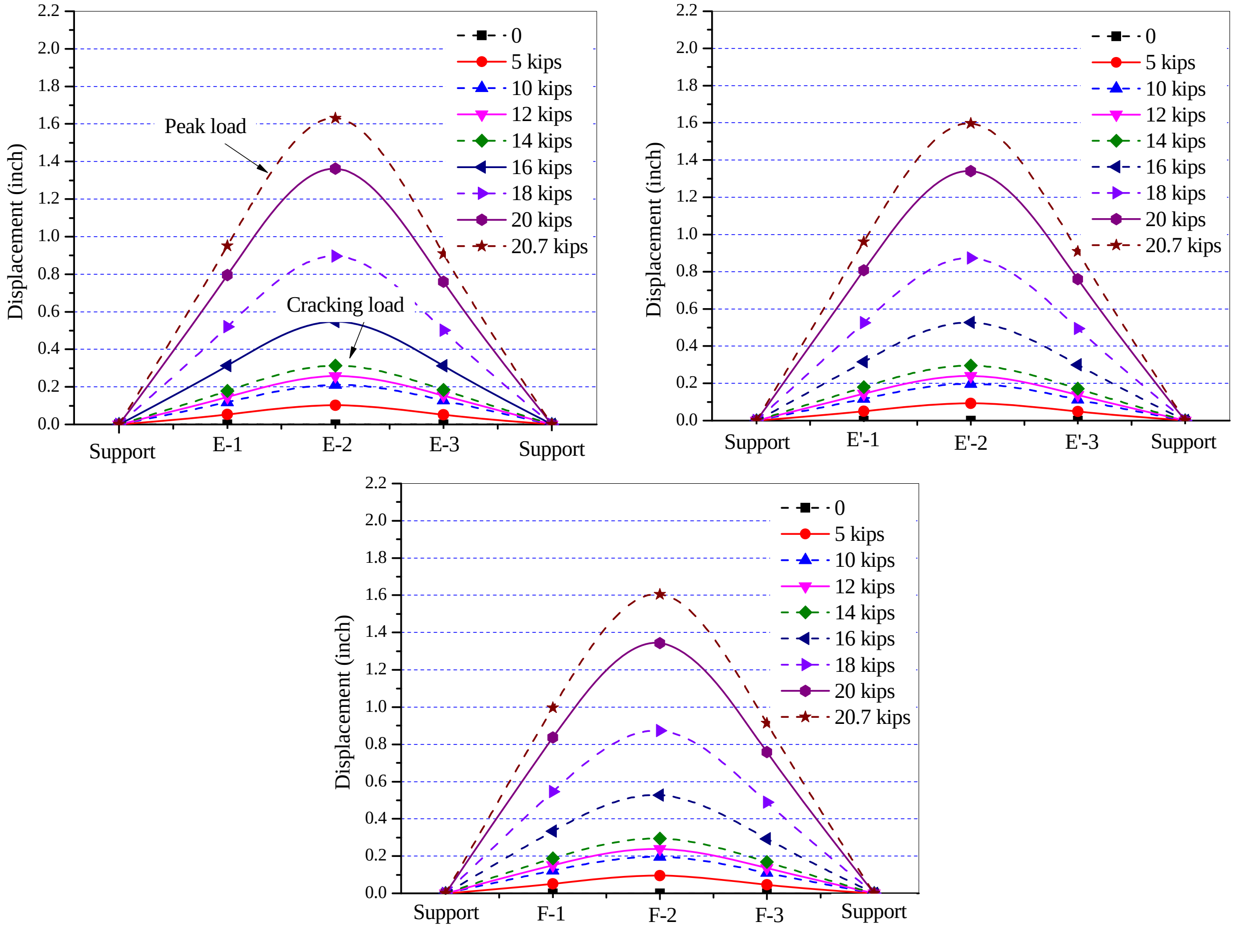

Figure C- 68 Panel ST-FRC-FL: Measured Displacement Along Panel Length

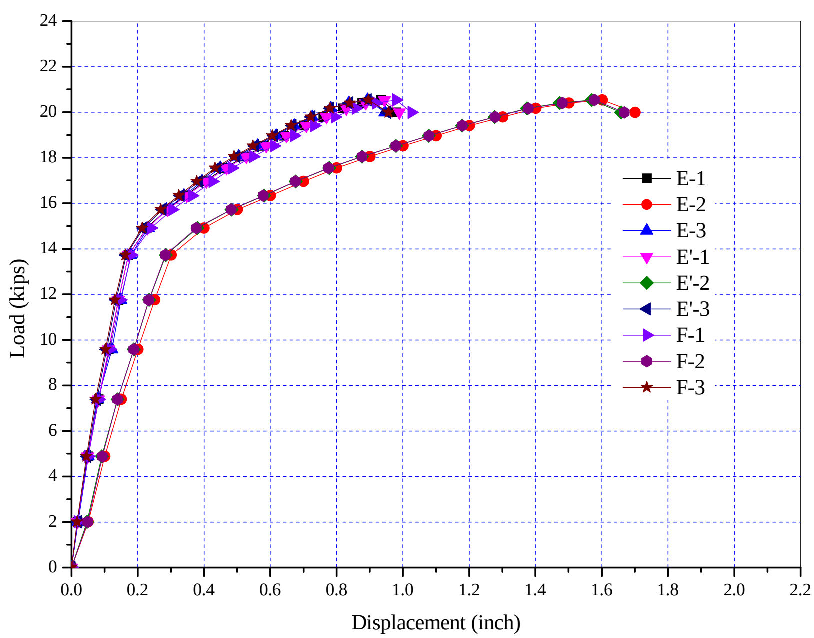

Figure C- 69 Panel ST-FRC-FL: Applied Load-Displacement Relationship

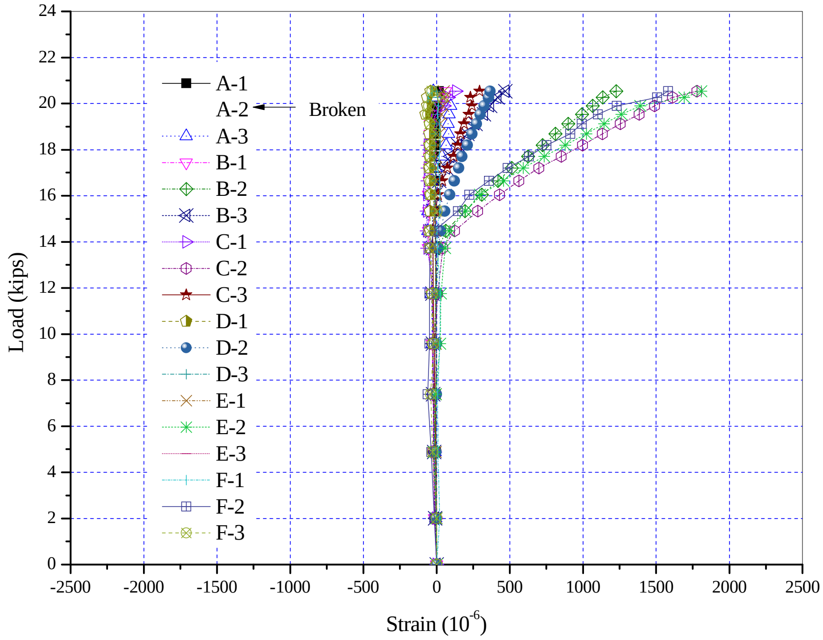

Figure C- 70 Panel ST-FRC-FL: Applied Load-Tendon Strain Relationship

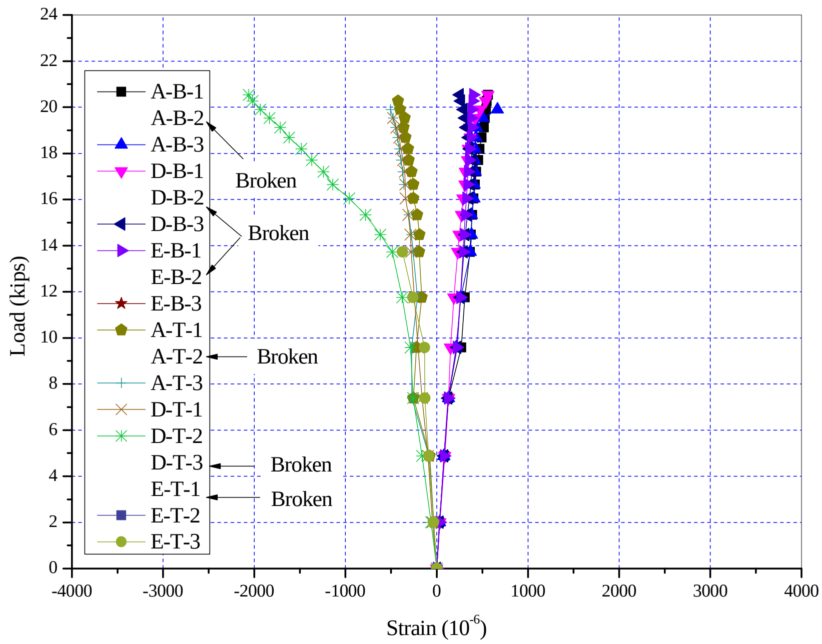

Figure C- 71 Panel ST-FRC-FL: Applied Load-Concrete Surface Strain Relationship

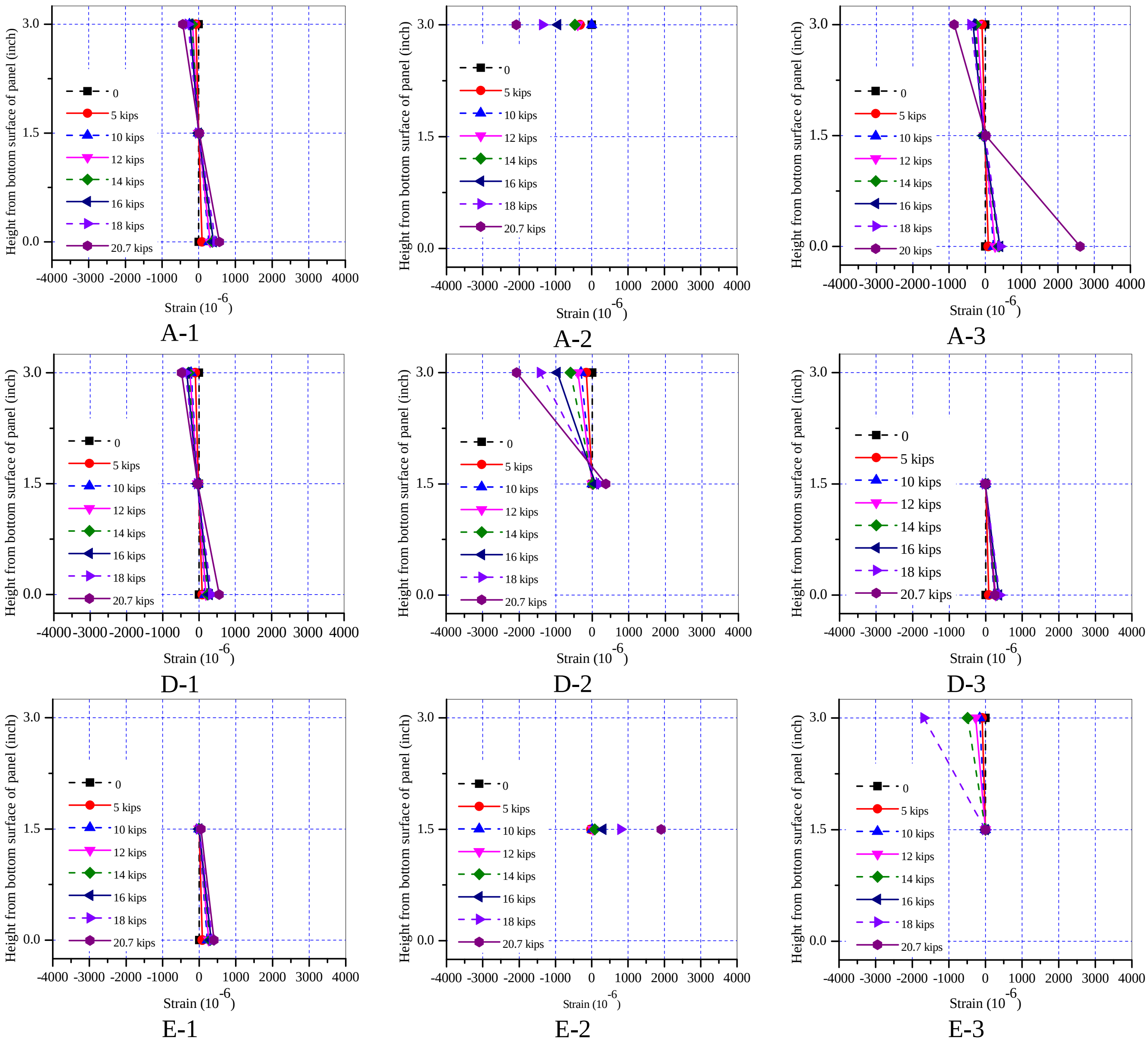

Figure C- 72 Panel ST-FRC-FL: Measured Strain Distribution, Post-Fatigue Quasi-Static Test

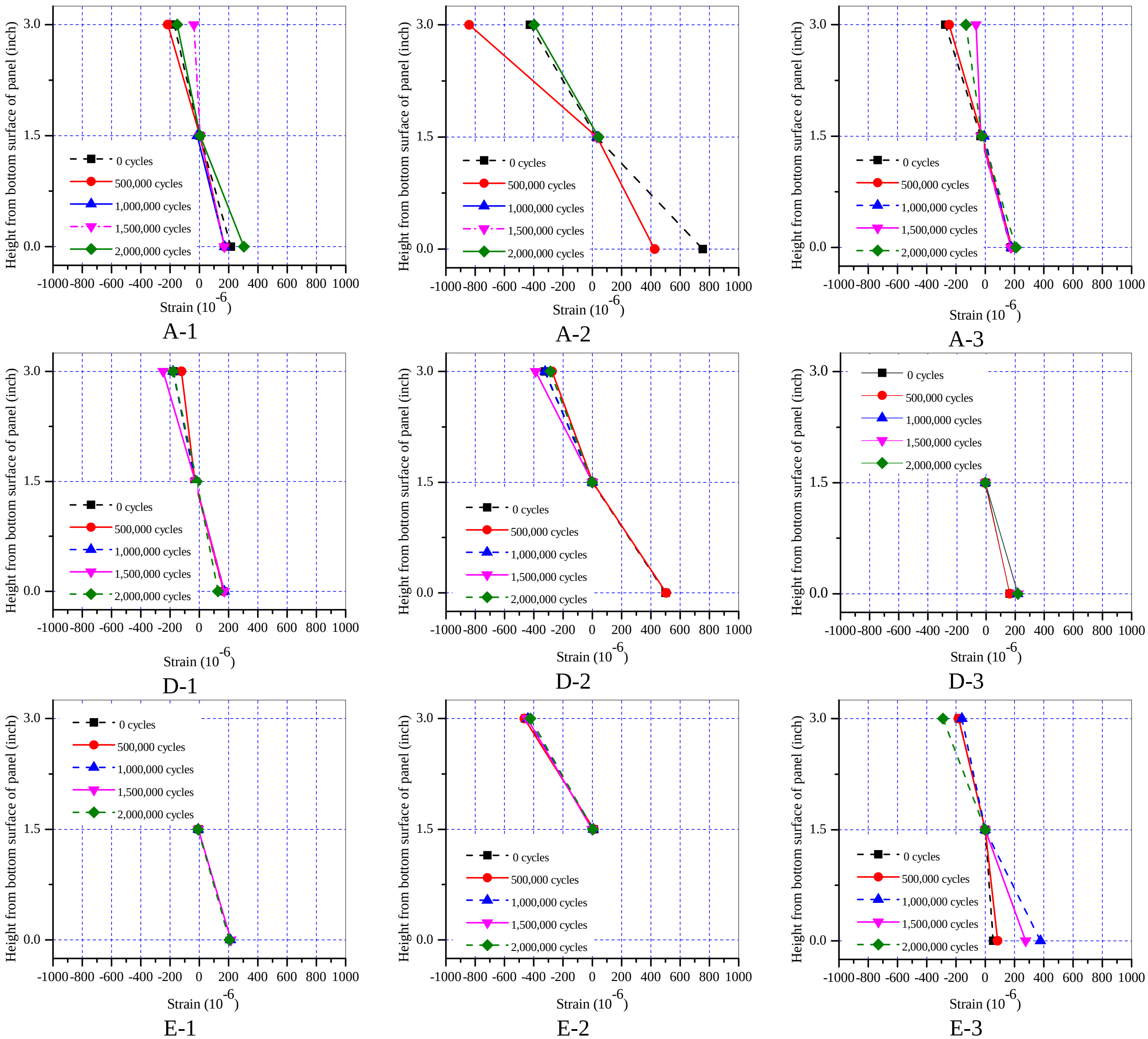

Figure C- 73 Panel ST-FRC-FL: Measured Strain Distribution at Various Cycles

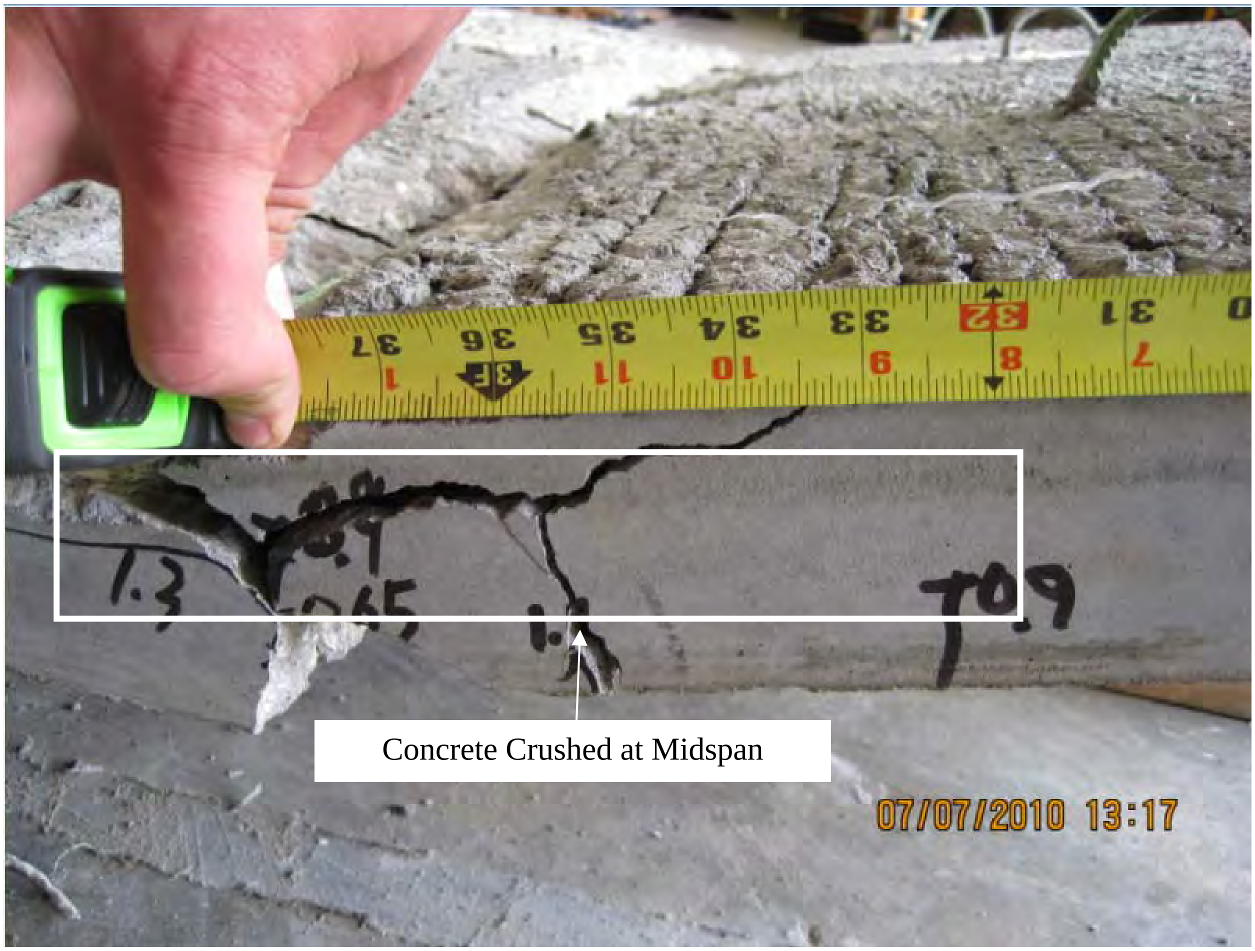

Figure C- 74 Flexural Failure at Midspan by Concrete Crushing of Panel ECST-NC-FL

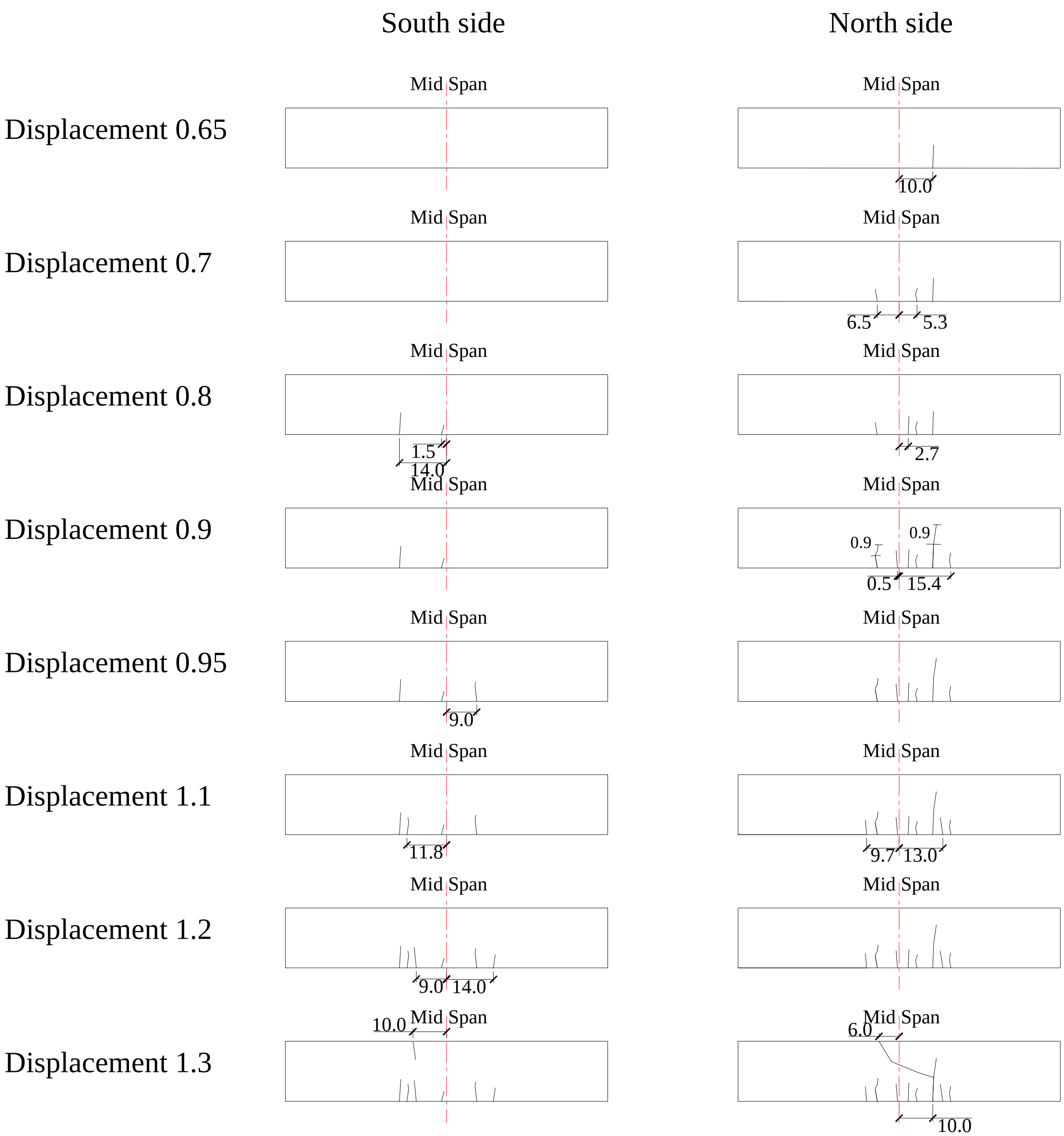

Figure C- 75 Panel ECST-NC-FL: Propagation of Cracking

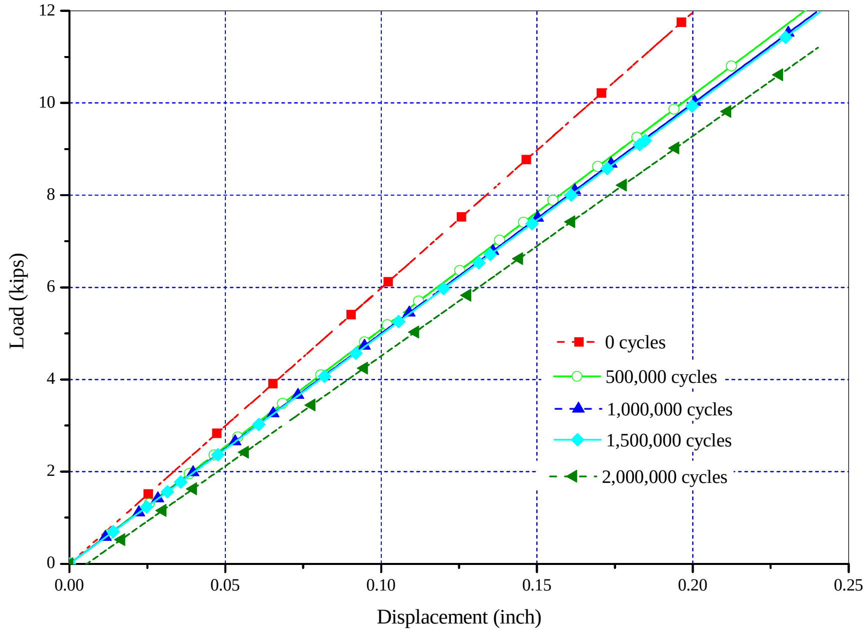

Figure C- 76 Panel ECST-NC-FL: Applied Load-Displacement Relationships of the Quasi-Static Load Tests

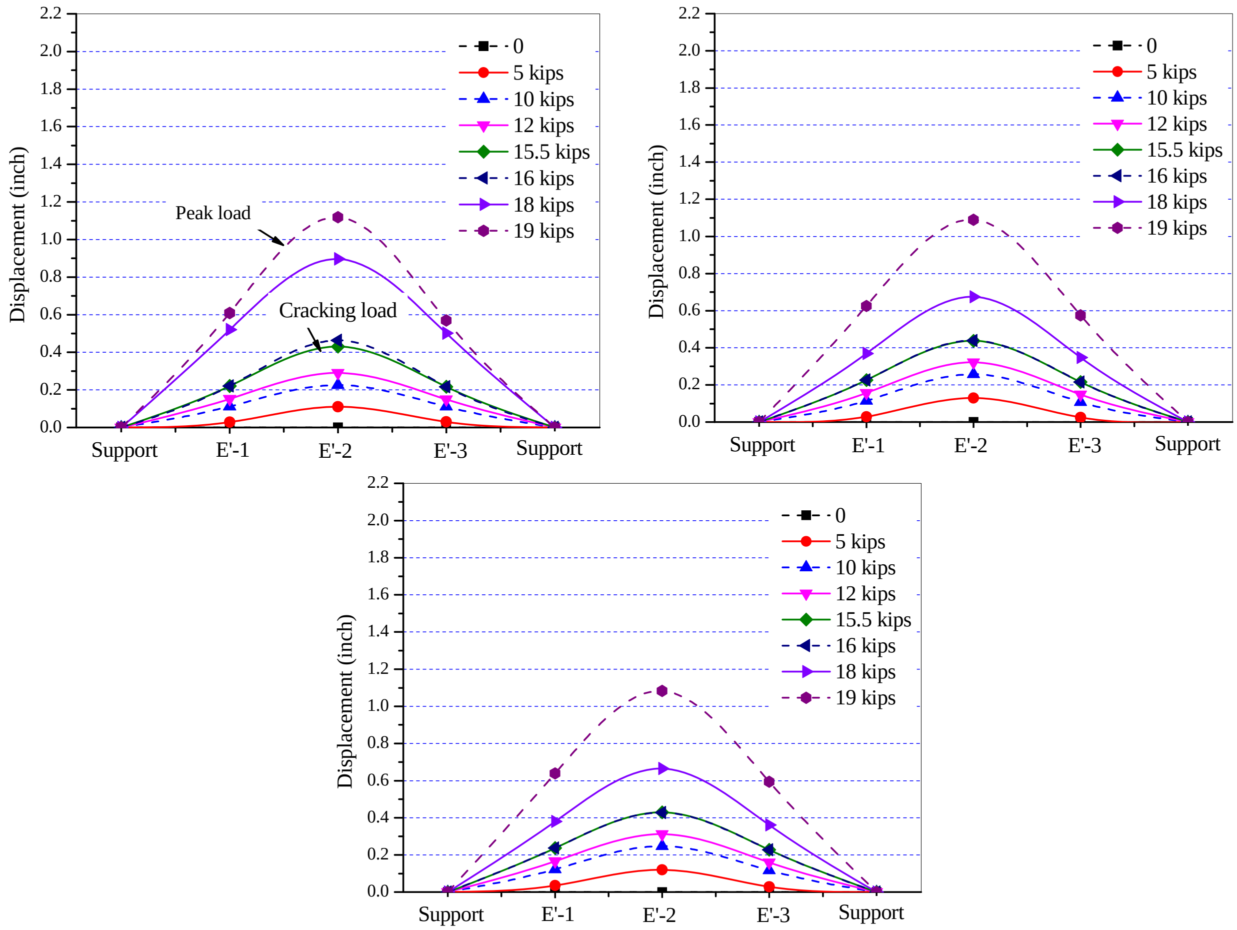

Figure C- 77 Panel ECST-NC-FL: Measured Displacement Along Panel Length

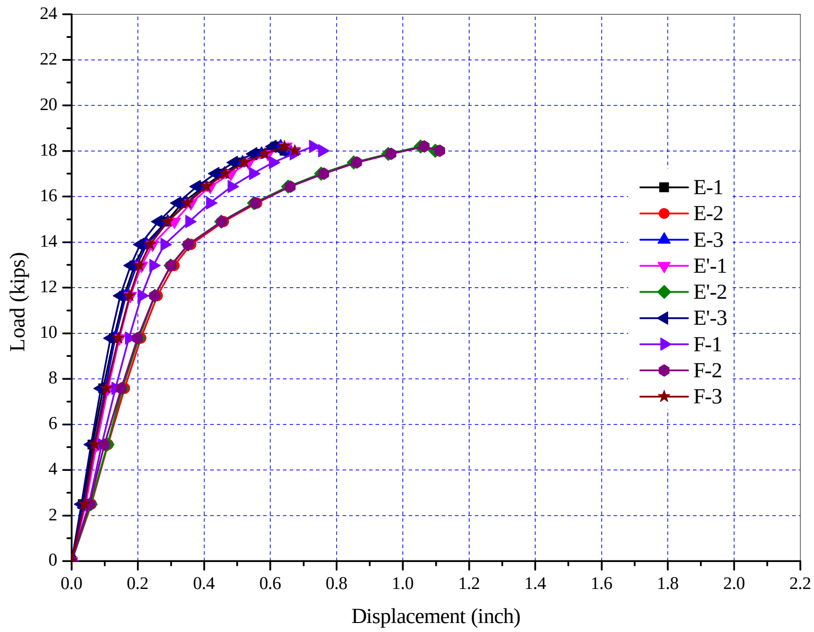

Figure C- 78 Panel ECST-NC-FL: Applied Load-Displacement Relationship

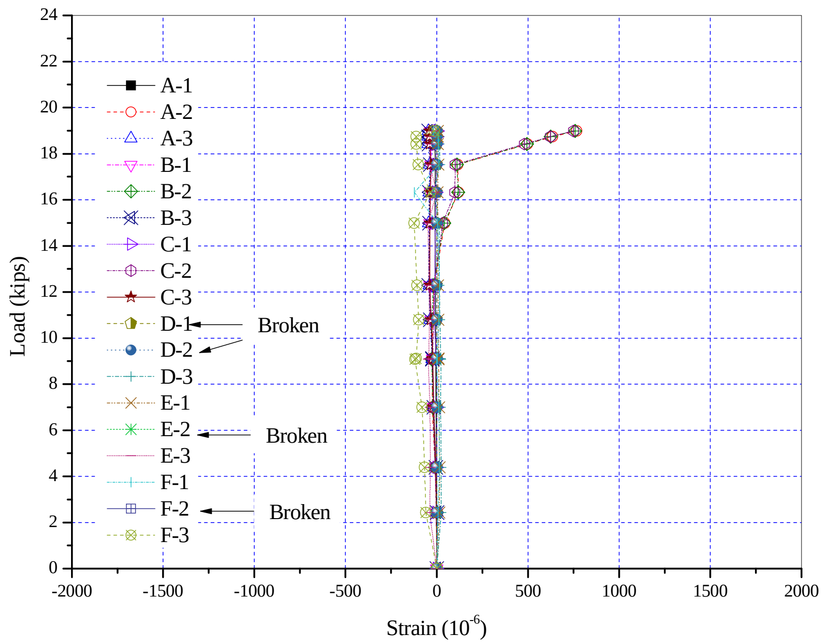

Figure C- 79 Panel ECST-NC-FL: Applied Load-Tendon Strain Relationship

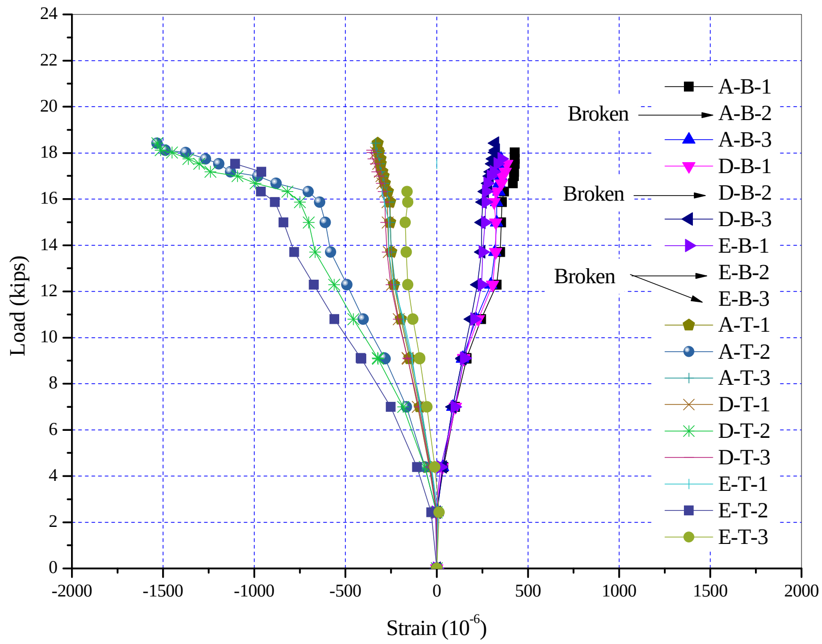

Figure C- 80 Panel ECST-NC-FL: Applied Load-Concrete Surface Strain Relationship

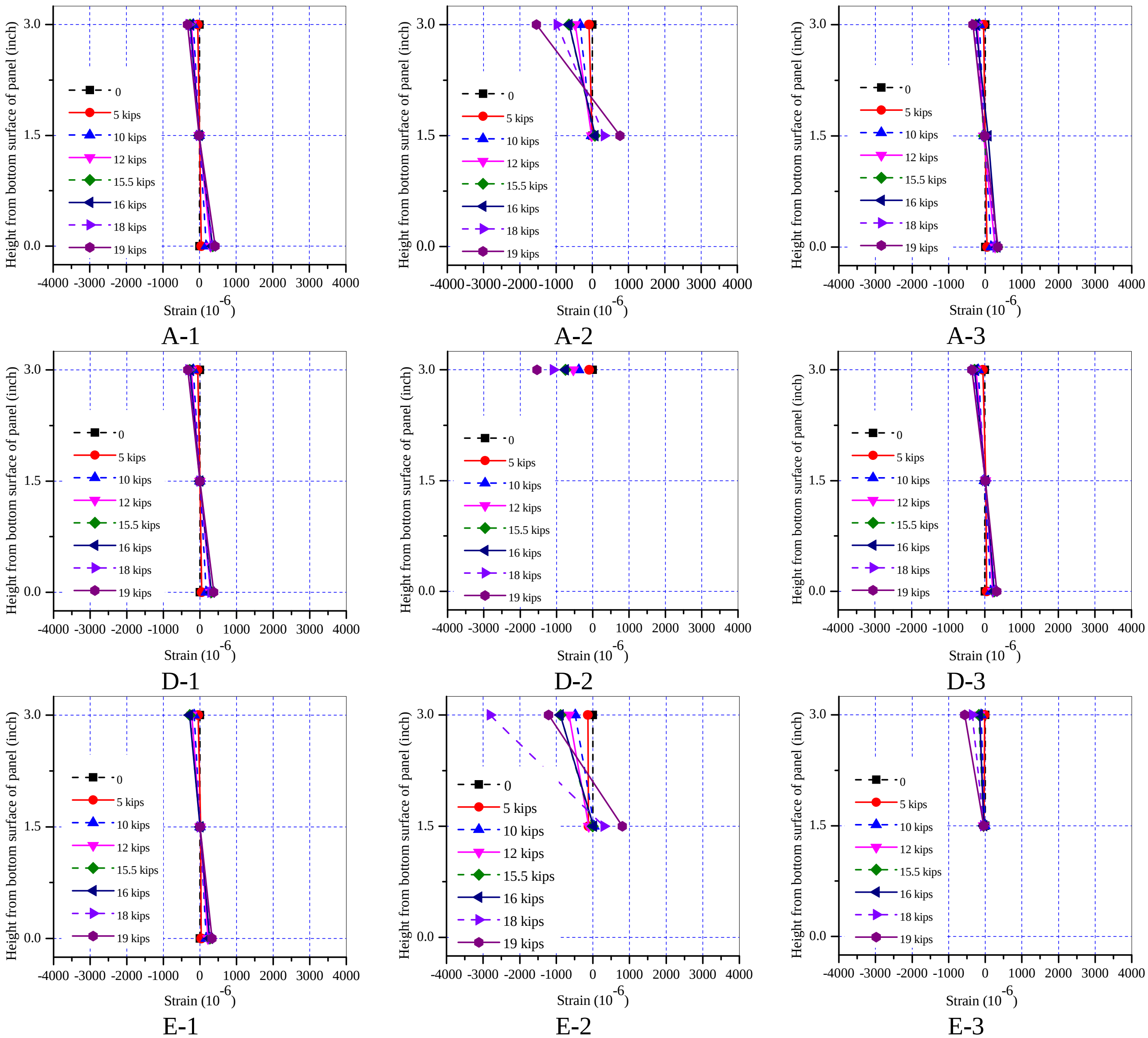

Figure C- 81 Panel ECST-NC-FL: Measured Strain Distribution, Post-Fatigue Quasi-Static Test

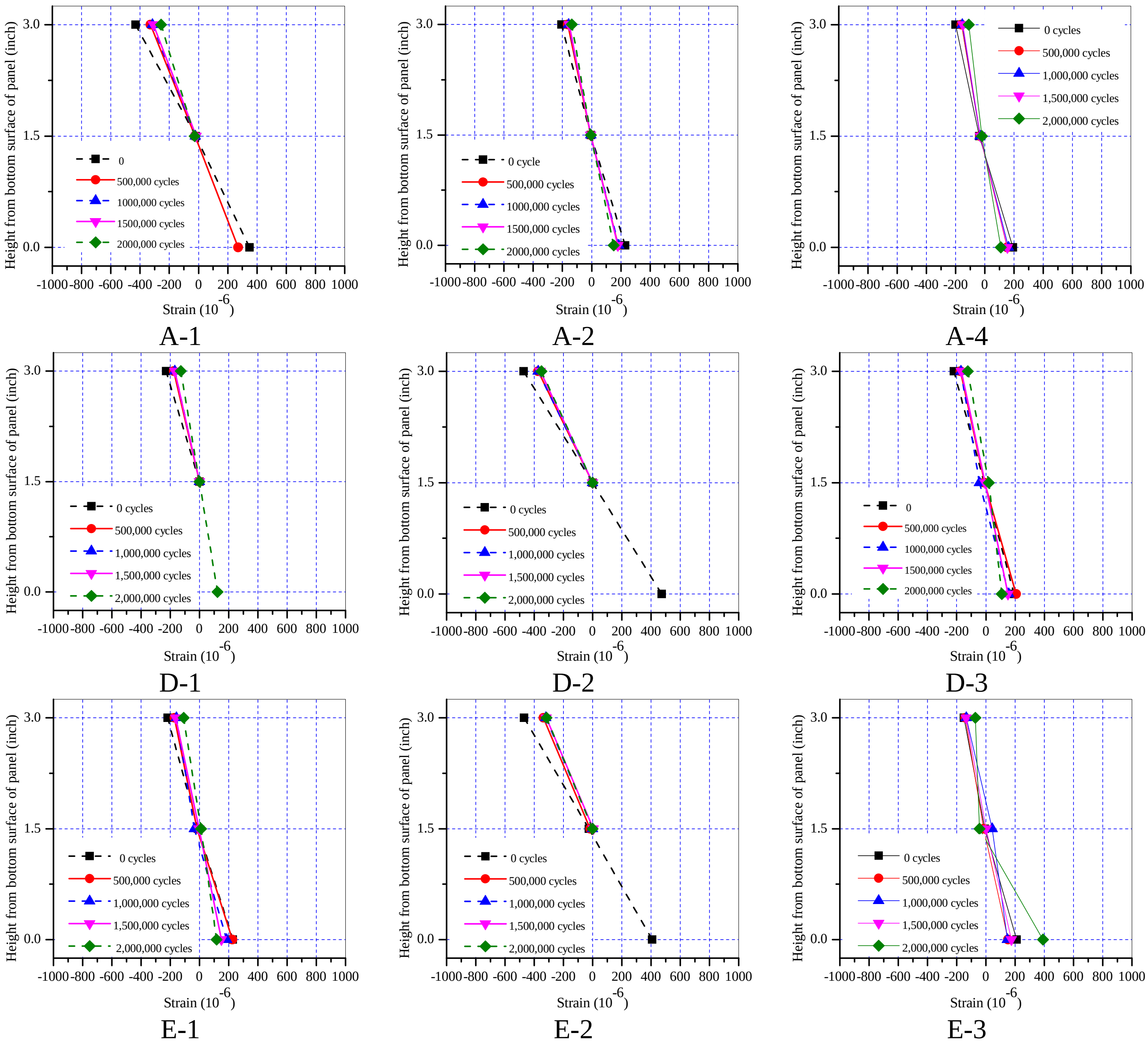

Figure C- 82 Panel ECST-NC-FL: Measured Strain Distribution at Various Cycles

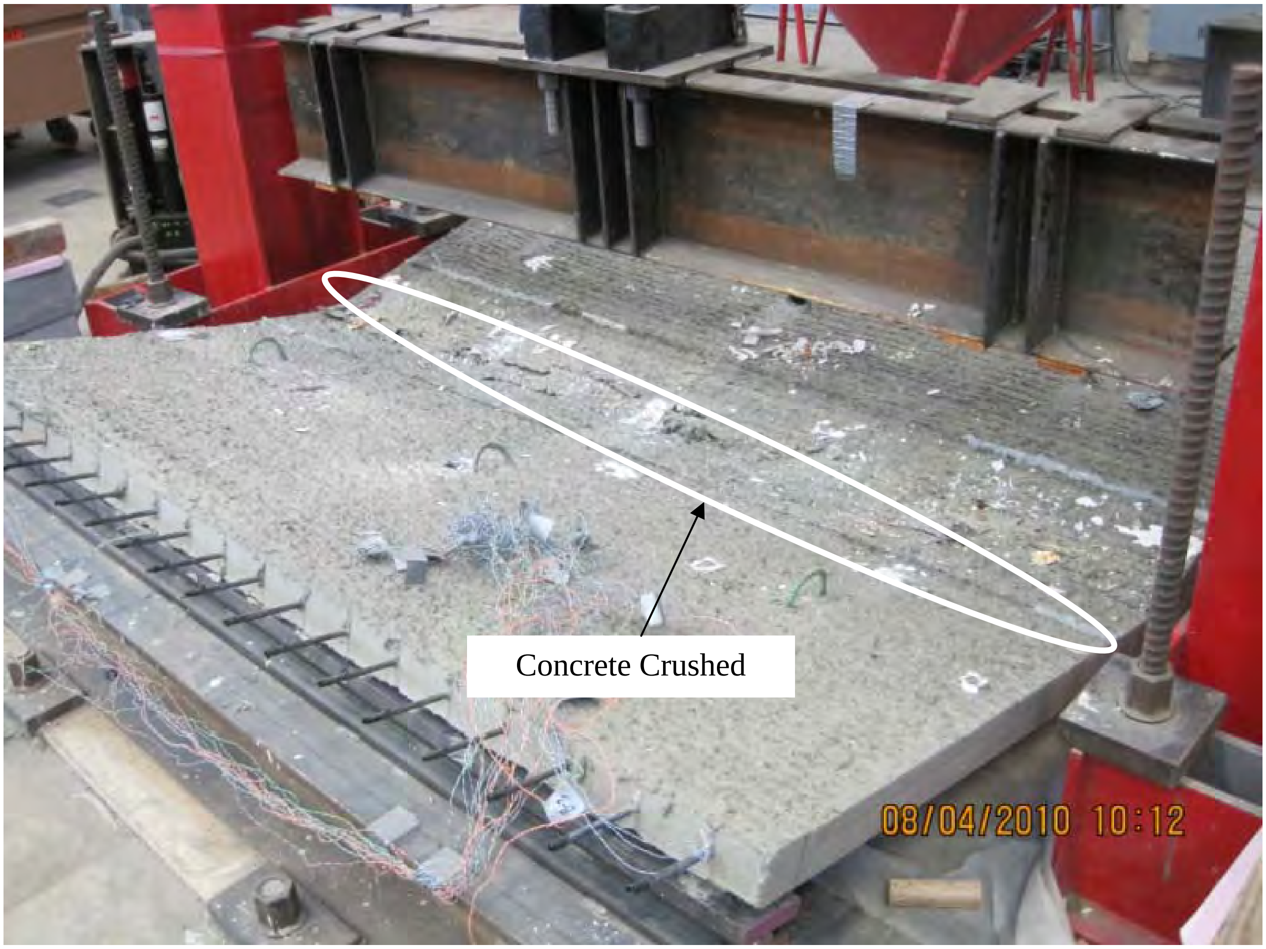

Figure C- 83 Flexural Failure at Midspan by Concrete Crushing of Panel ECST-FRC-FL

Figure C- 84 Panel ECST-FRC-FL: Propagation of Cracking

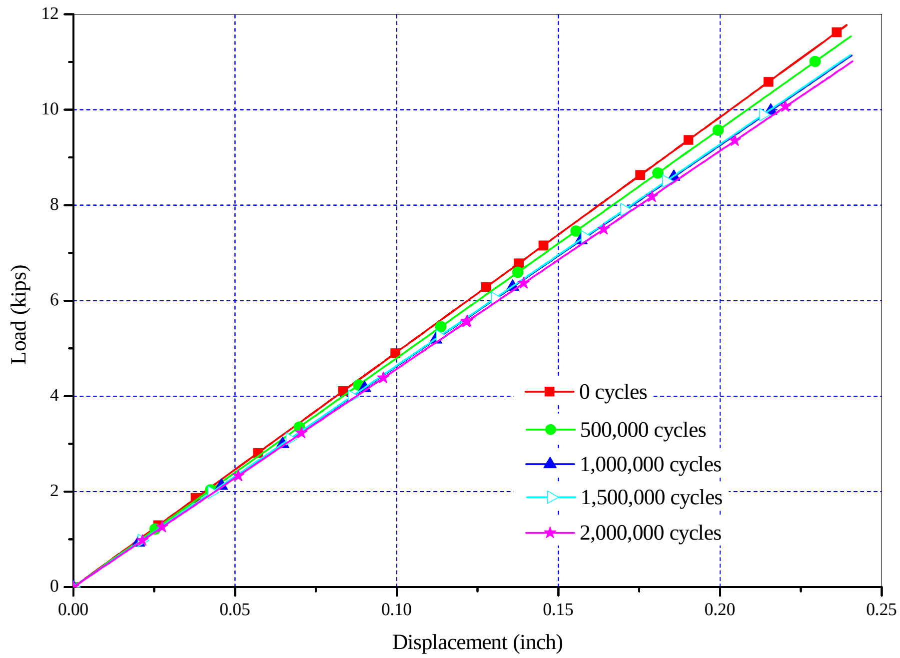

Figure C- 85 Panel ECST-FRC-FL: Applied Load-Displacement Relationships of the Quasi-Static Load Tests

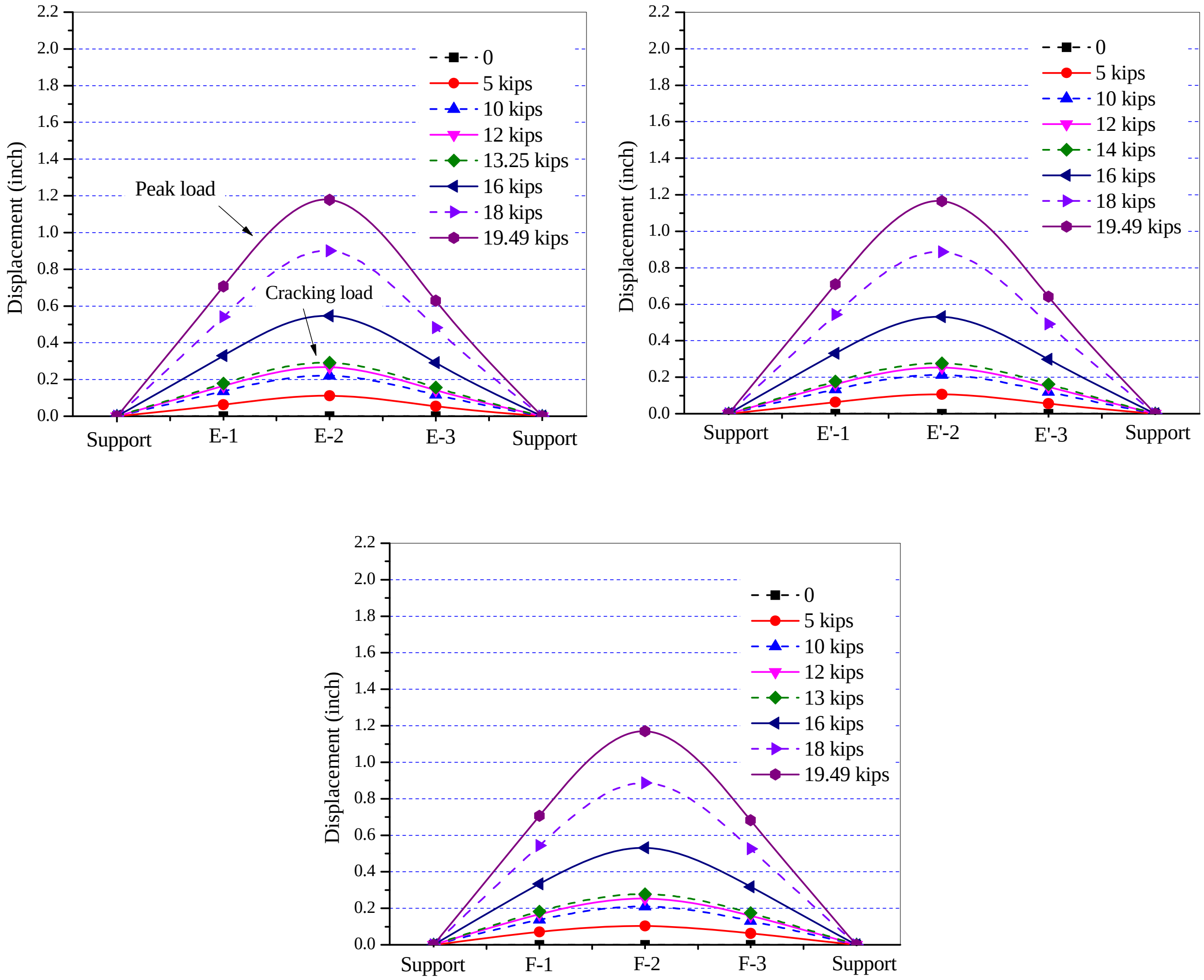

Figure C- 86 Panel ECST-FRC-FL: Measured Displacement Along Panel Length

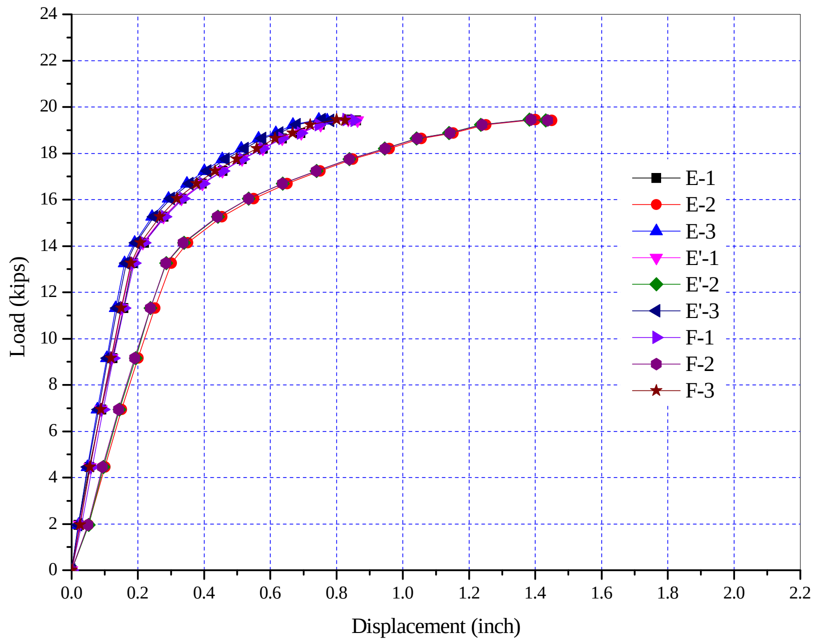

Figure C- 87 Panel ECST-FRC-FL: Applied Load-Displacement Relationship

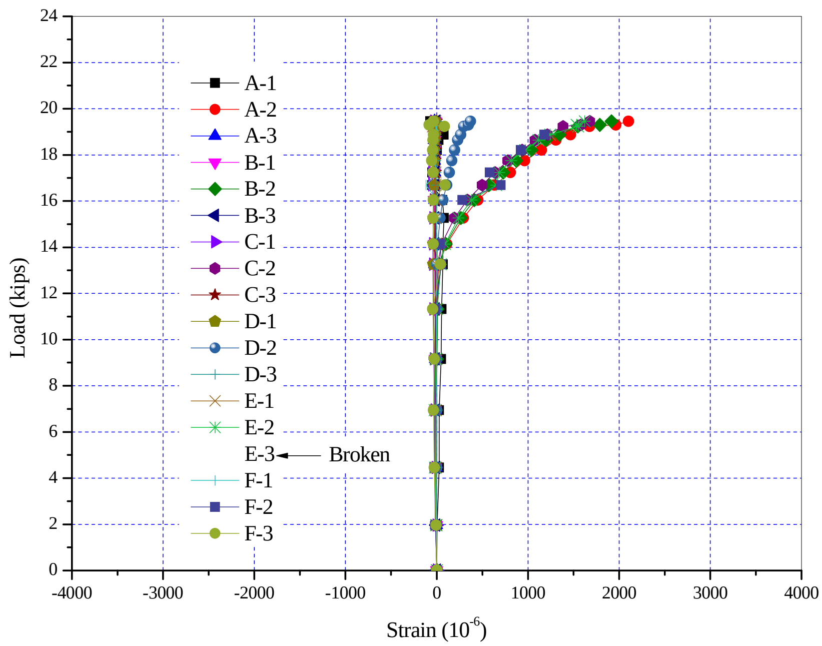

Figure C- 88 Panel ECST-FRC-FL: Applied Load-Tendon Strain Relationship

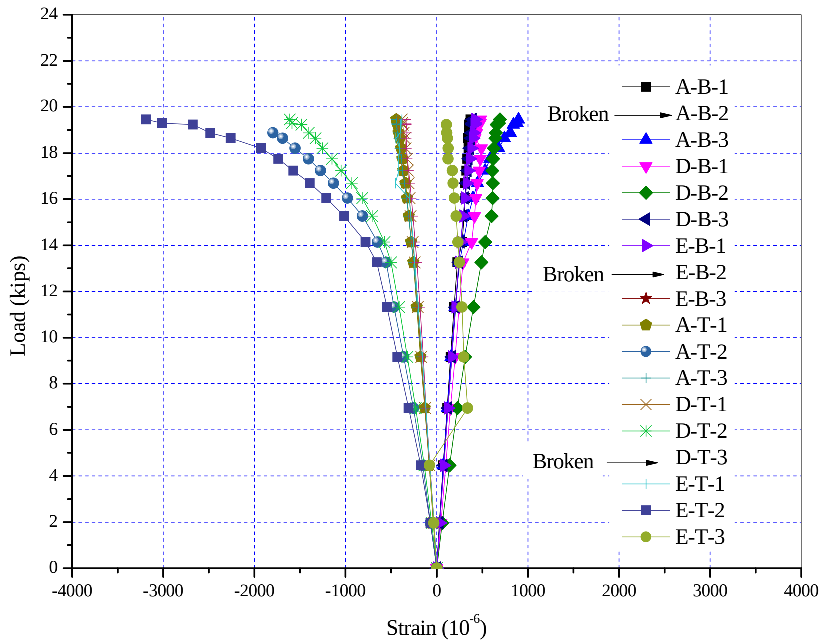

Figure C- 89 Panel ECST-FRC-FL: Applied Load-Concrete Surface Strain Relationship

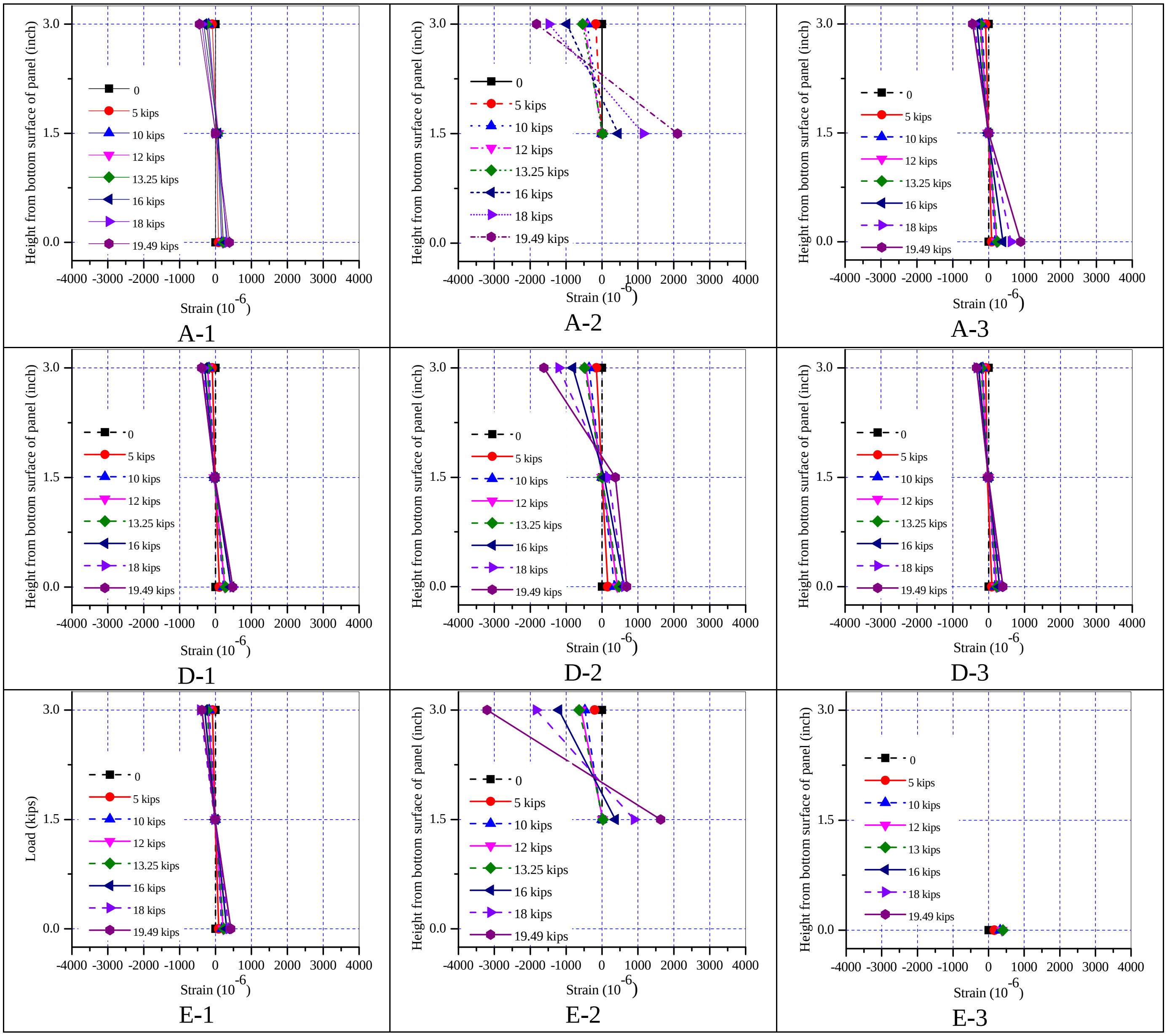

Figure C- 90 Panel ECST-FRC-FL: Measured Strain Distribution, Post-Fatigue Quasi-Static Test

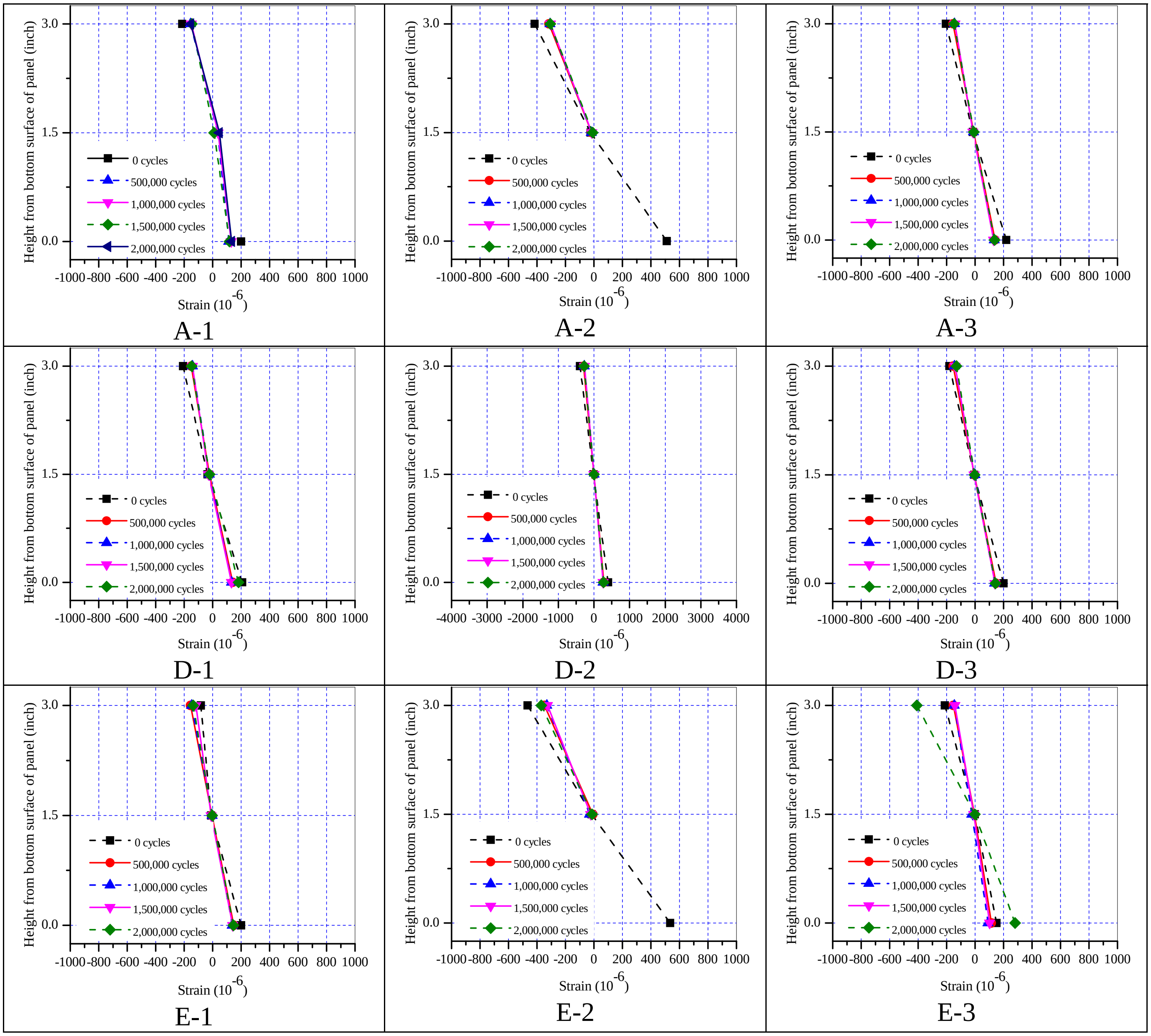

Figure C- 91 Panel ECST-FRC-FL: Measured Strain Distribution at Various Cycles

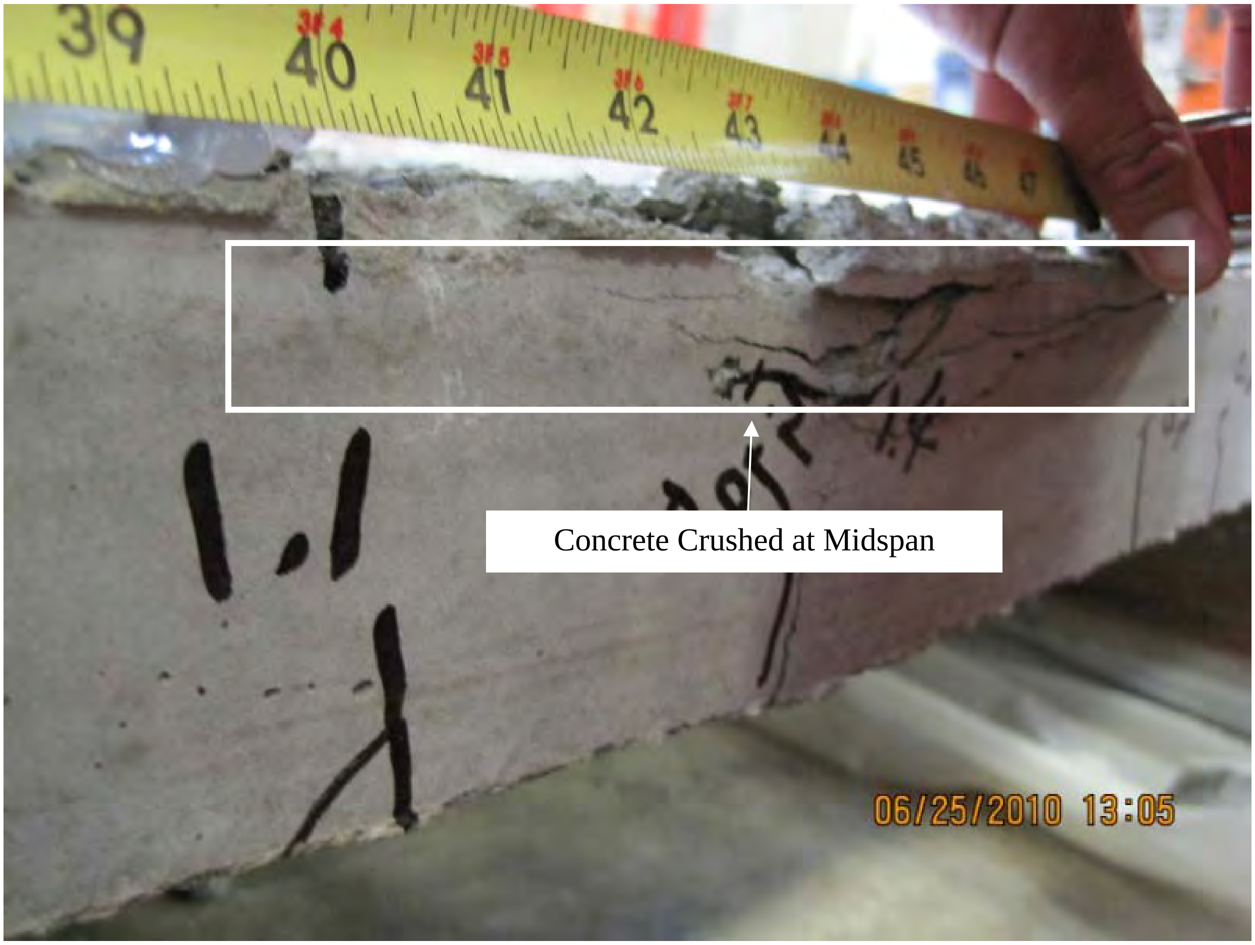

Figure C- 92 Flexural Failure at Midspan by Concrete Crushing of Panel CFRPT-NC-FL

Figure C- 93 Panel CFRPT-NC-FL: Propagation of Cracking

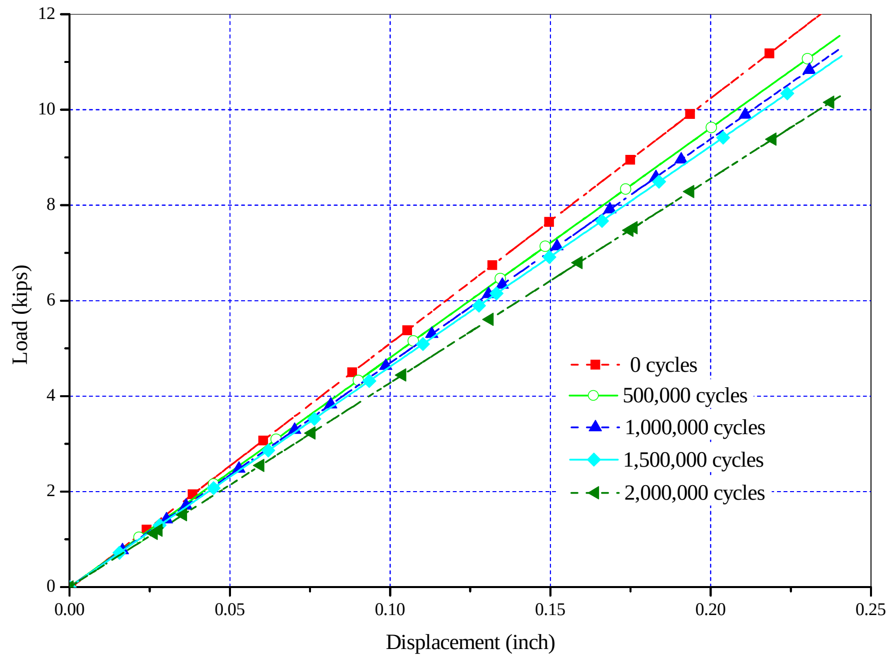

Figure C- 94 Panel CFRPT-NC-FL: Applied Load-Displacement Relationships of the Quasi-Static Load Tests

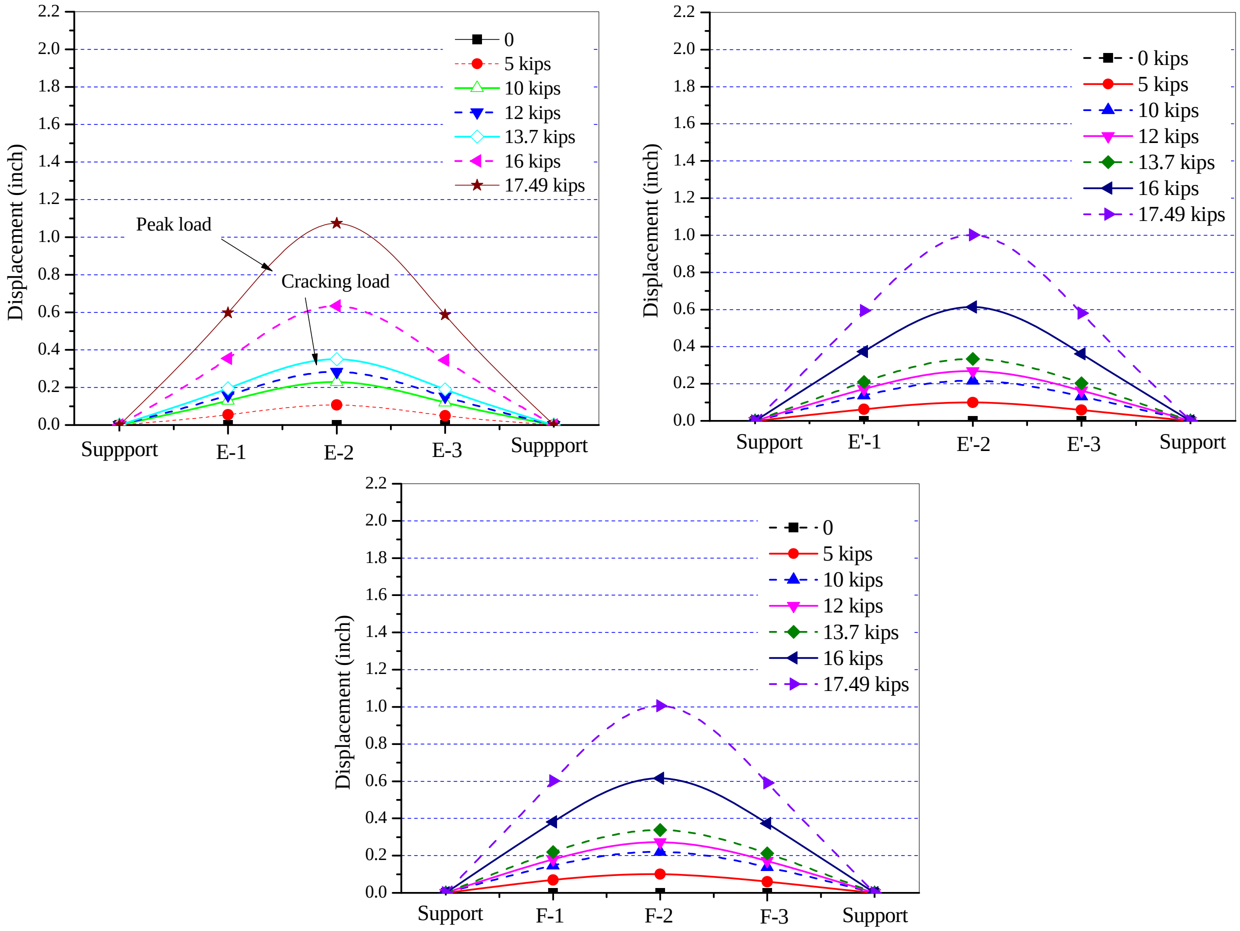

Figure C- 95 Panel CFRPT-NC-FL: Measured Displacement Along Panel Length

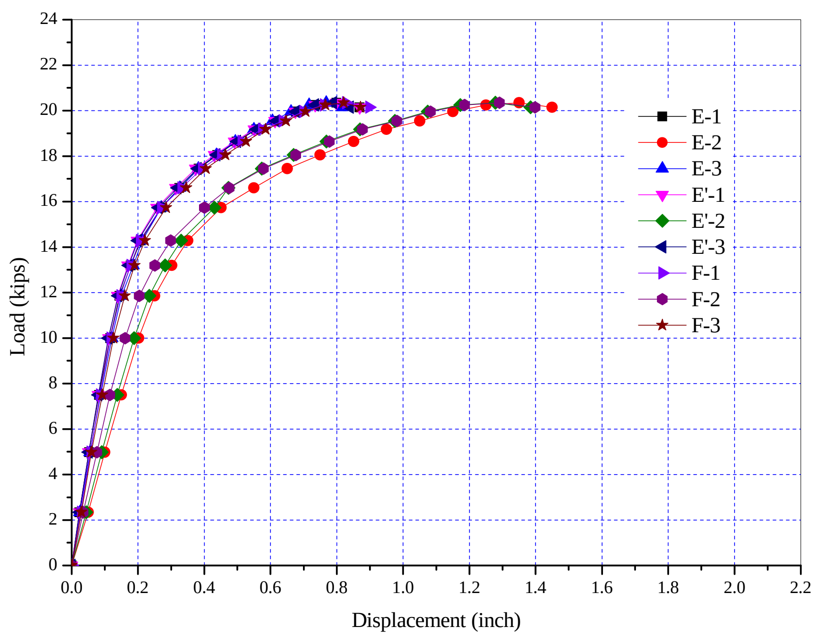

Figure C- 96 Panel CFRPT-NC-FL: Applied Load-Displacement Relationship

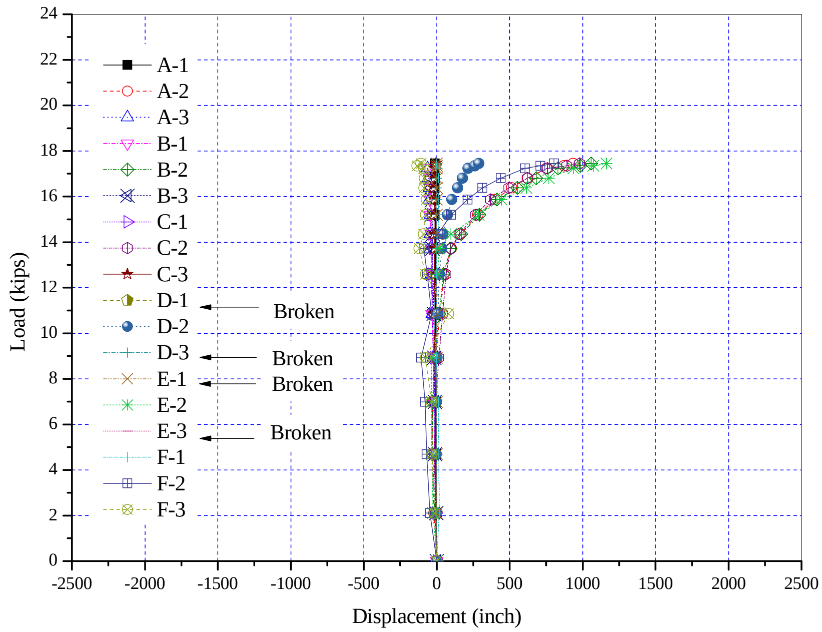

Figure C- 97 Panel CFRPT-NC-FL: Applied Load-Tendon Strain Relationship

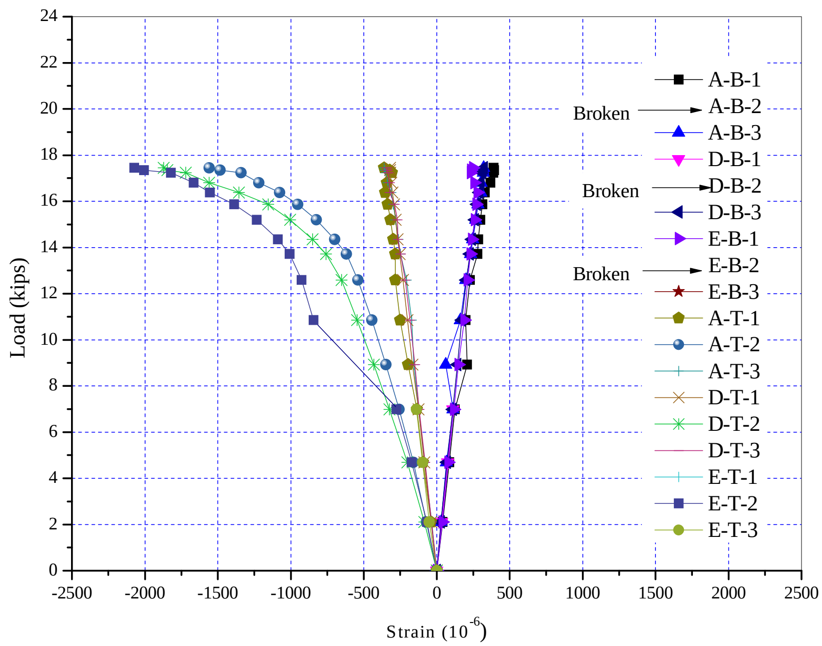

Figure C- 98 Panel CFRPT-NC-FL: Applied Load-Concrete Surface Strain Relationship

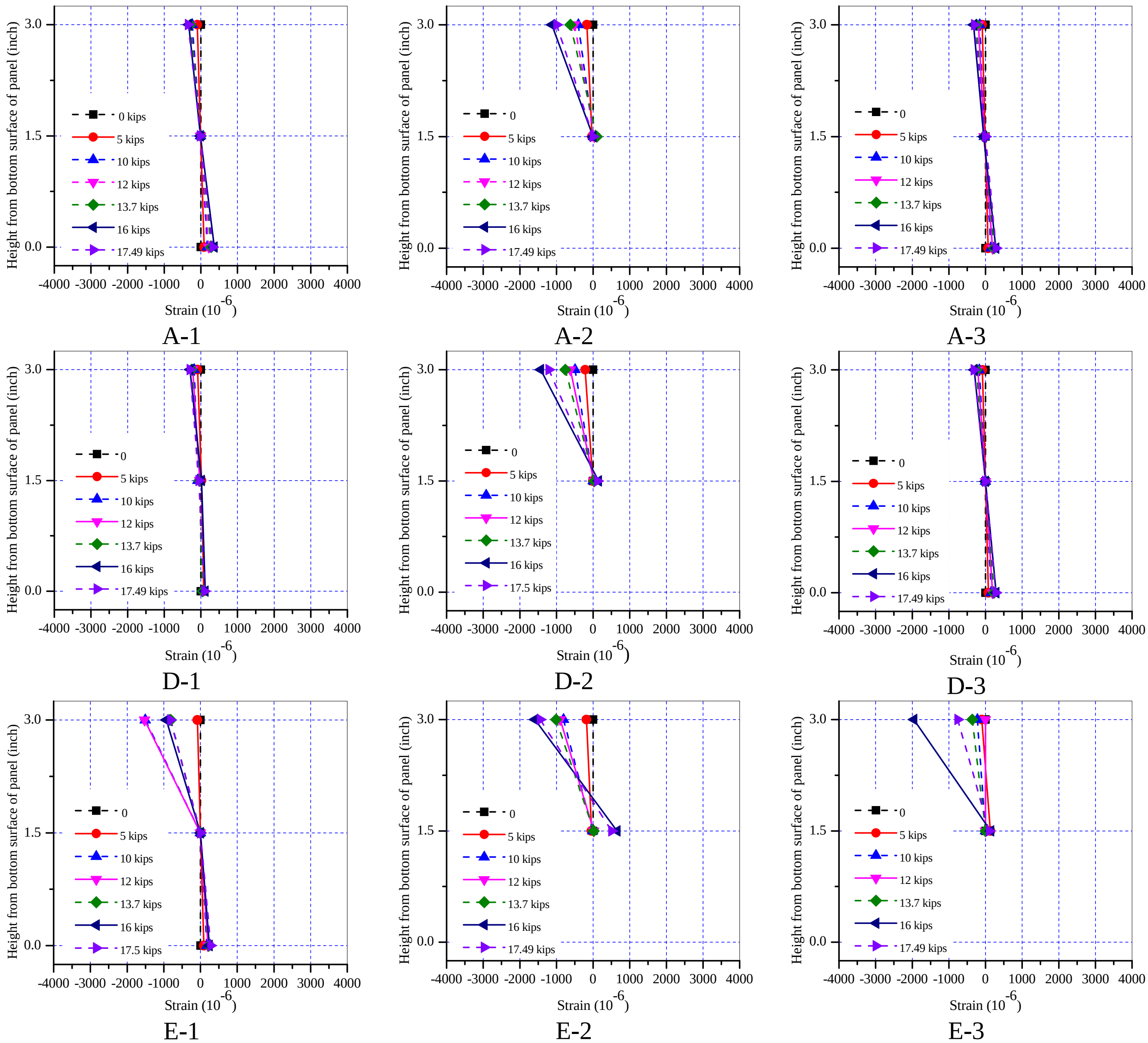

Figure C- 99 Panel CFRPT-NC-FL: Measured Strain Distribution, Post-Fatigue Quasi-Static Test

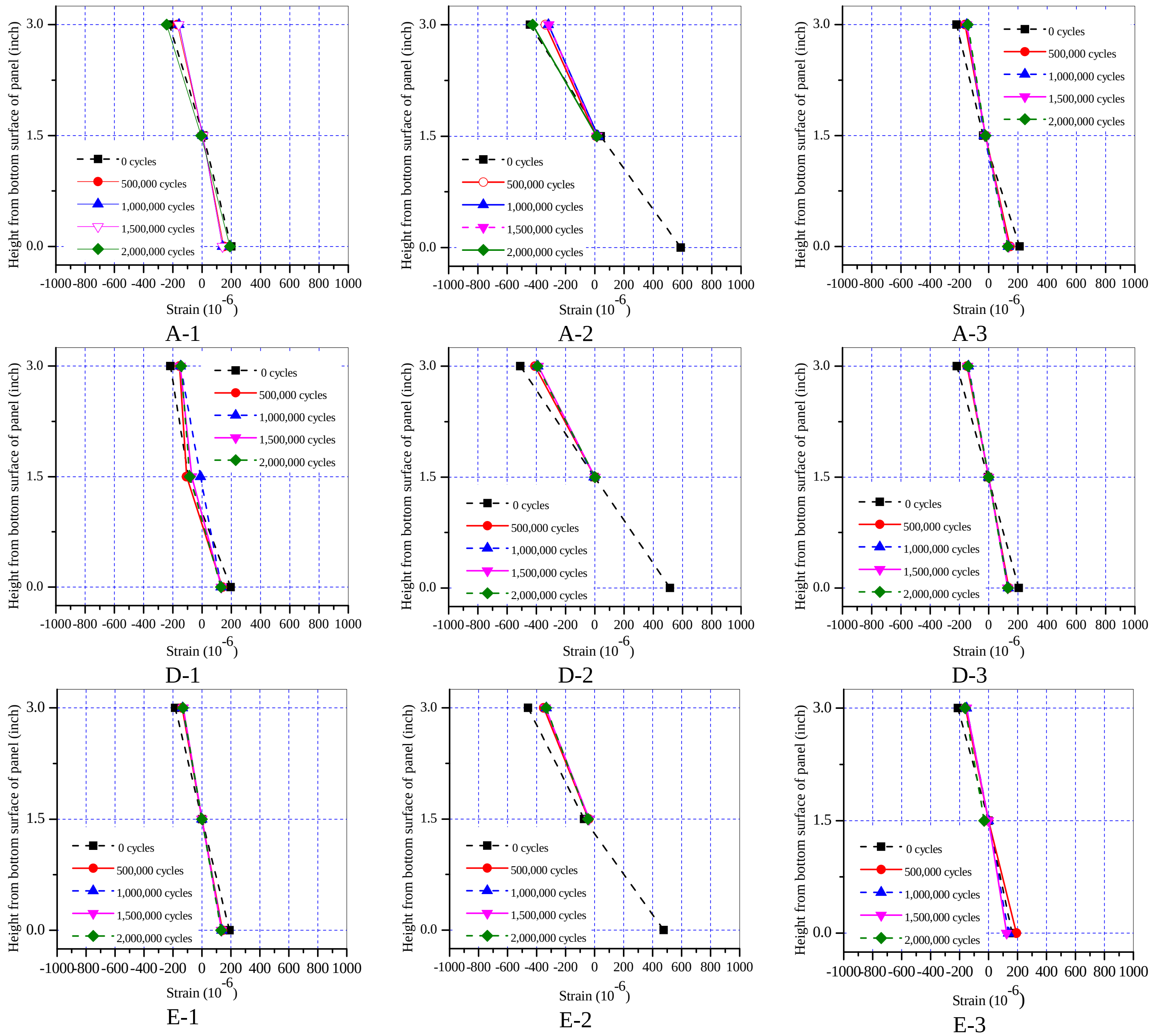

Figure C- 100 Panel CFRPT-NC-FL: Measured Strain Distribution at Various Cycles

Figure C- 101 Flexural Failure at Midspan by Concrete Crushing of Panel CFRPT-FRC-FL

Figure C- 102 Panel CFRPT-FRC-FL: Propagation of Cracking

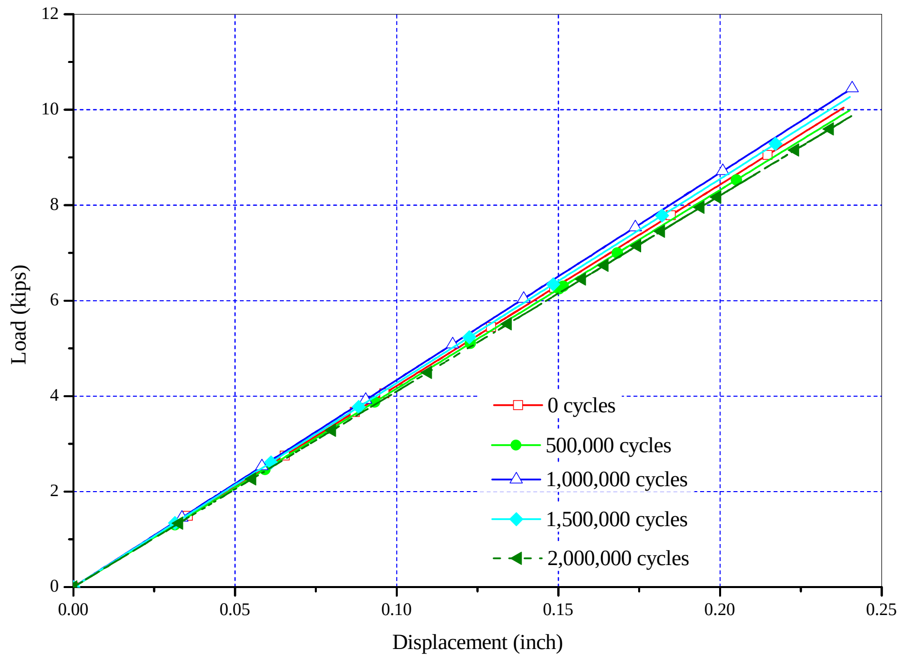

Figure C- 103 Panel CFRPT-FRC-FL: Applied Load-Displacement Relationships of the Quasi-Static Load Tests

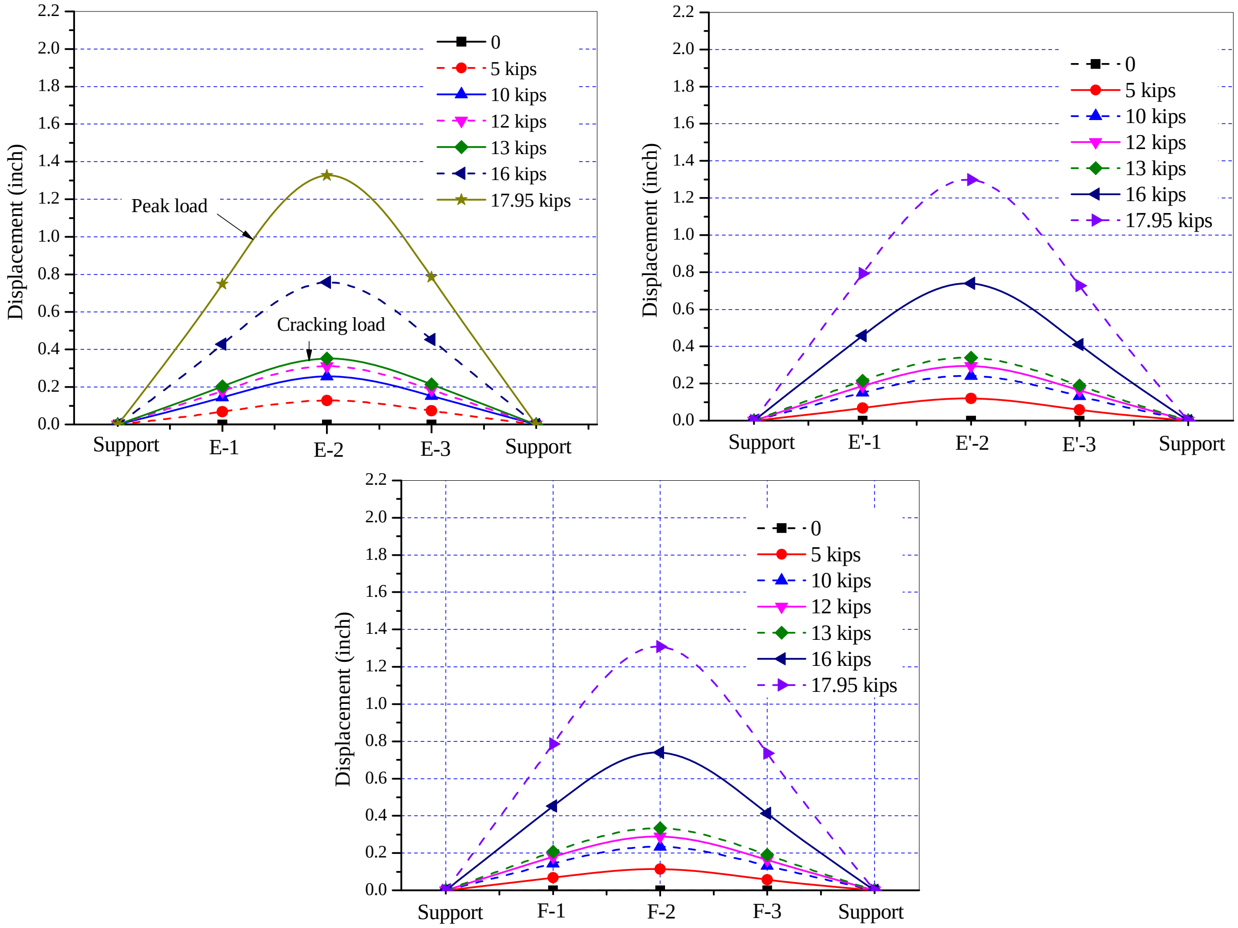

Figure C- 104 Panel CFRPT-FRC-FL: Measured Displacement Along Panel Length

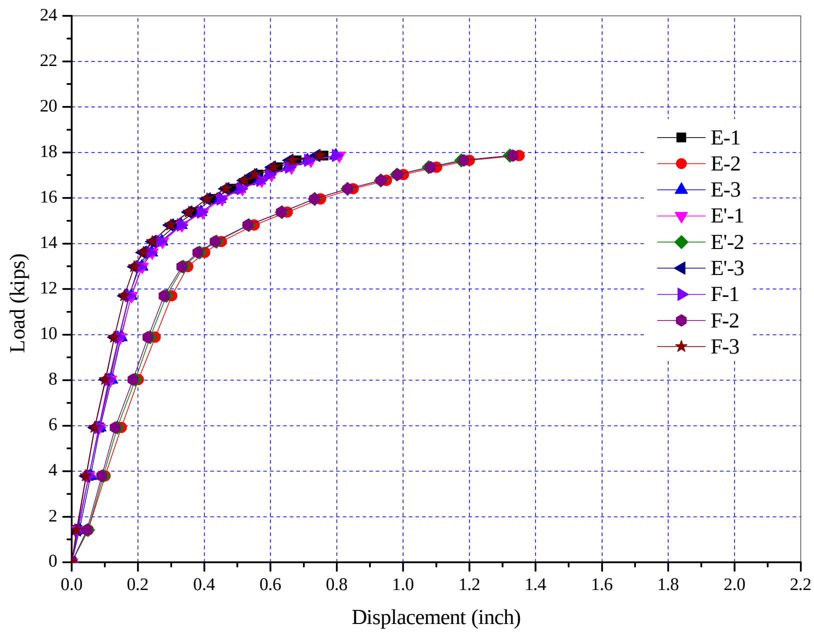

Figure C- 105 Panel CFRPT-FRC-FL: Applied load-displacement relationship

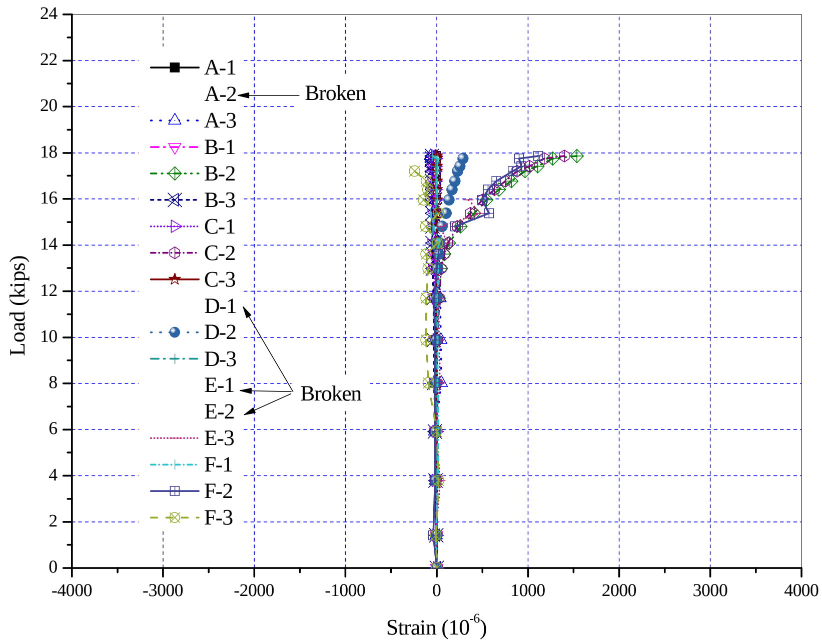

Figure C- 106 Panel CFRPT-FRC-FL: Applied Load-Tendon Strain Relationship

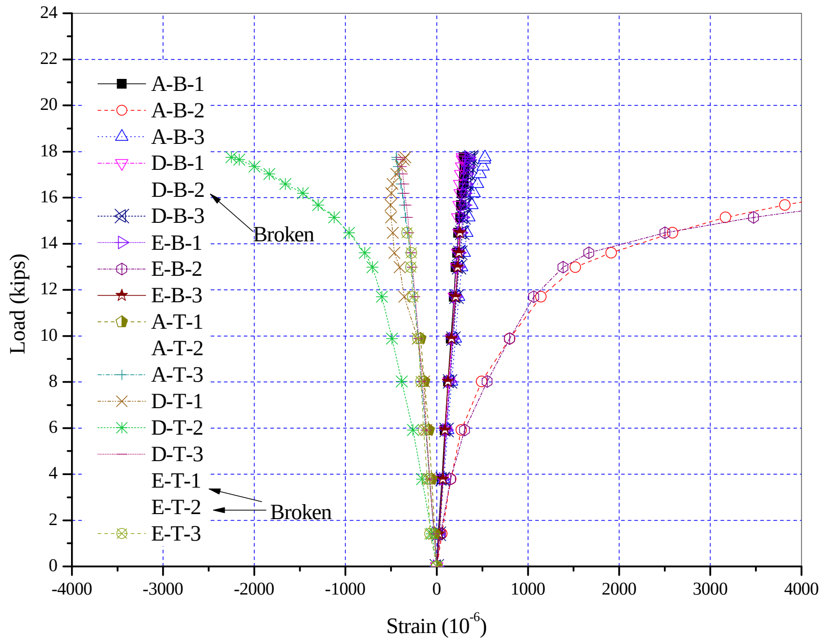

Figure C- 107 Panel CFRPT-FRC-FL: Applied Load-Concrete Surface Strain Relationship

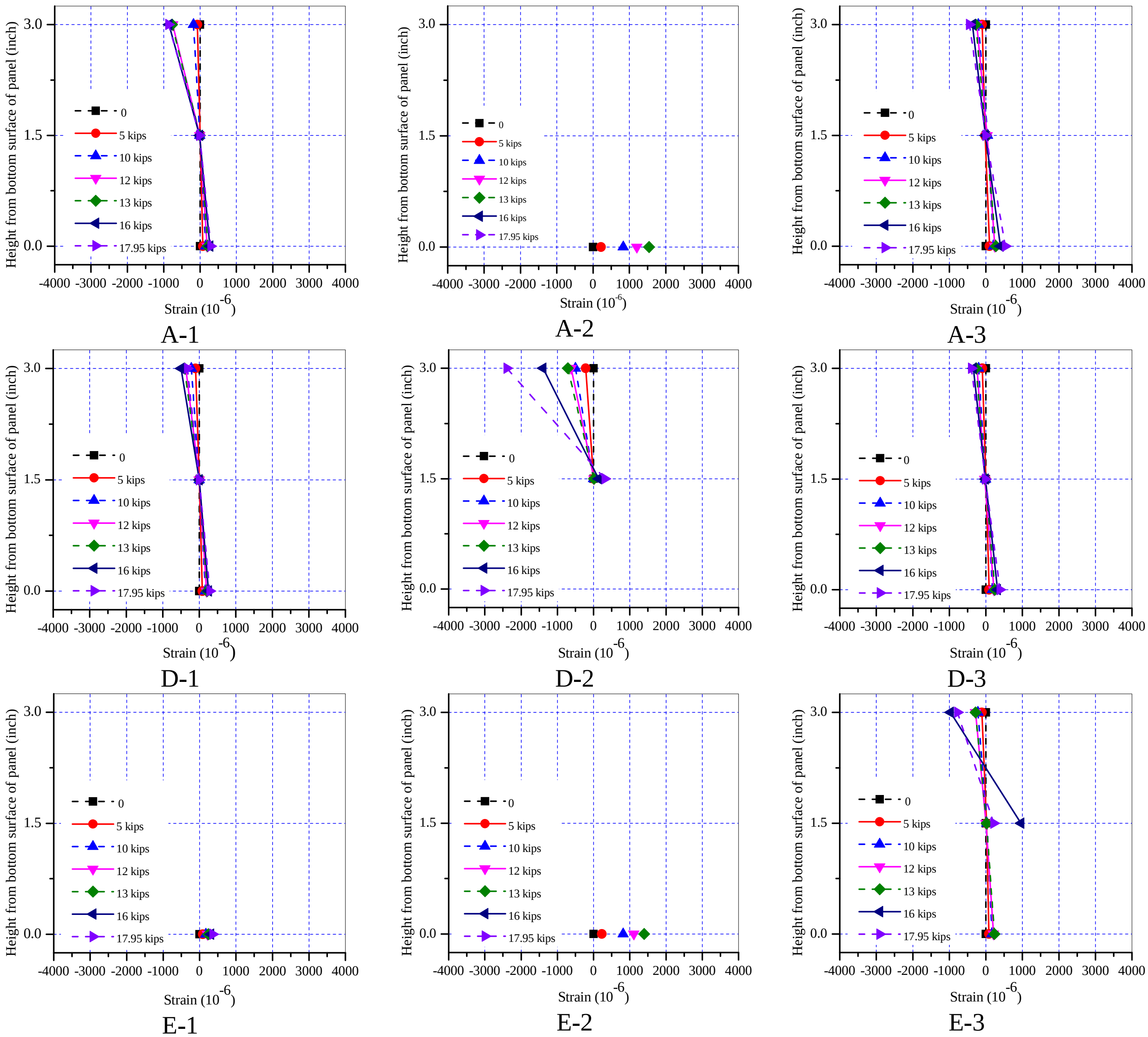

Figure C- 108 Panel CFRPT-FRC-FL: Measured Strain Distribution, Post-Fatigue Quasi-Static Test

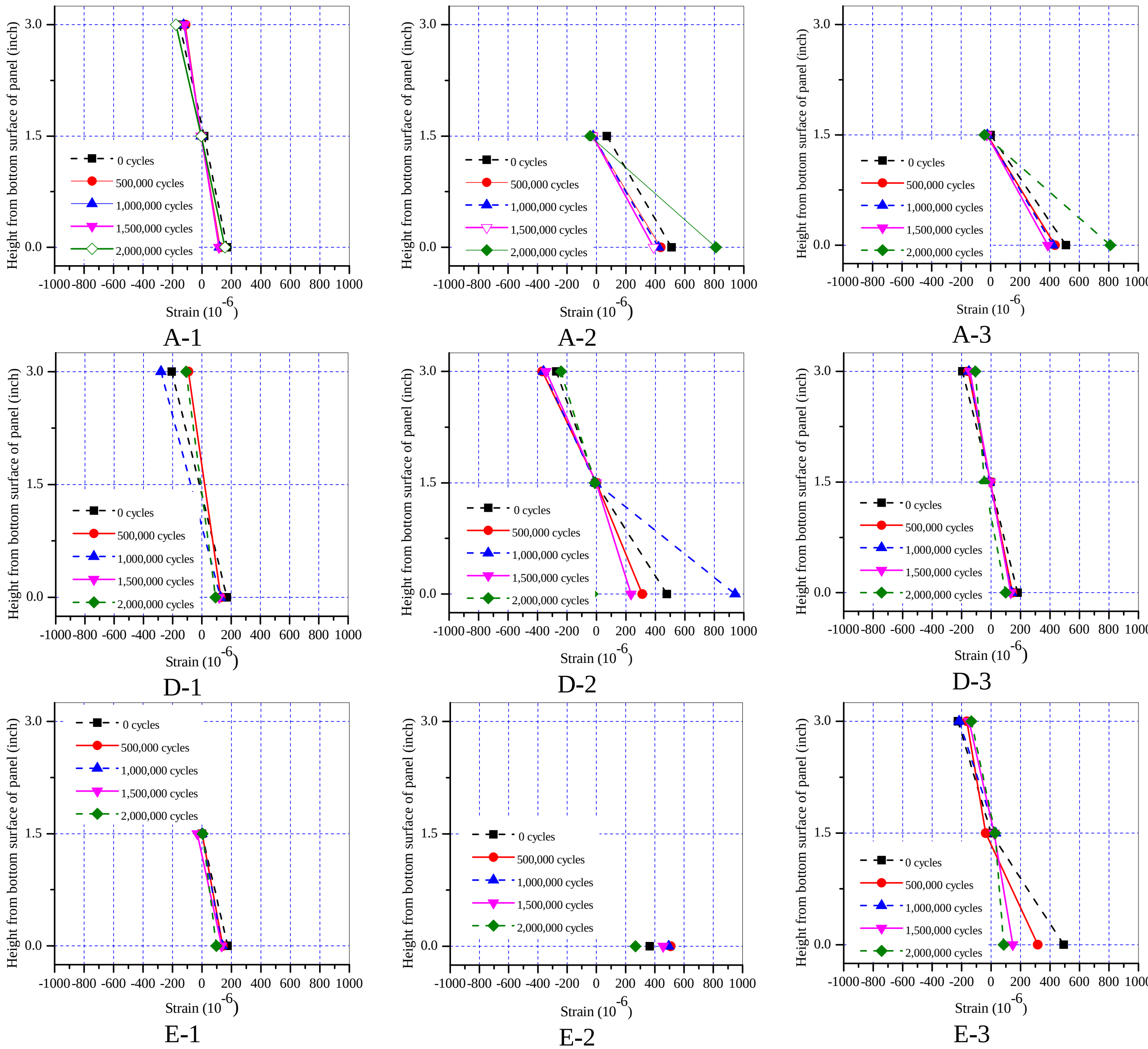

Figure C- 109 Panel CFRPT-FRC-FL: Measured Strain Distribution at Various Cycles

NaCl content (% of cement weight)	Name of specimens	Normal concrete No. of specimens	FRC* No. of specimens	Concrete with CI** No. of specimens	Specimen longitudinal sections	Specimen cross sections
0 %	SP1	3	3	3	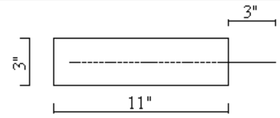	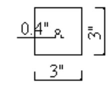
	SP2	3	3	3	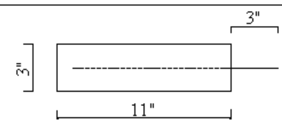	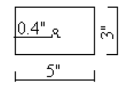
	SP3	3	3	3	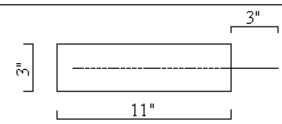	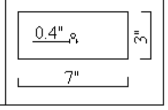
Total number of each concrete type		9	9	9		

* FRC: Fiber Reinforced Concrete
**CI: Corrosion Inhibitor

Figure C- 110 Corrosion Initiation Test Specimen Dimensions

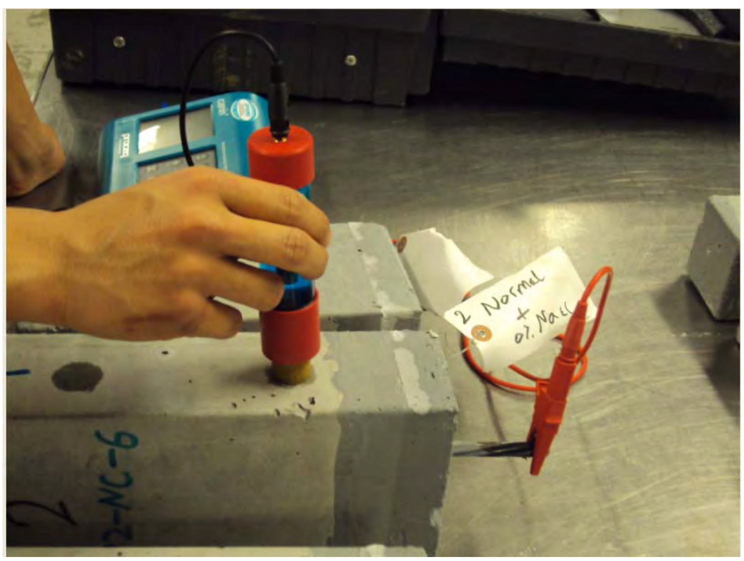

Figure C- 111 Half-cell Potential Measurements

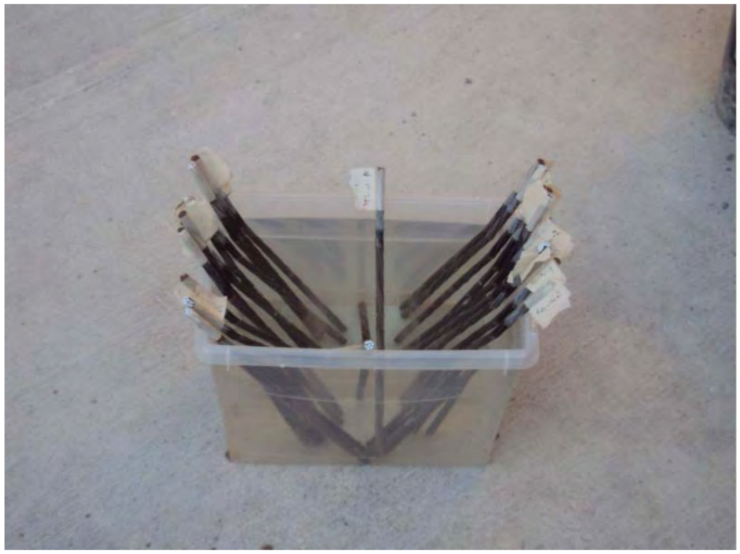

Figure C- 112 Steel Tendons Immersed in Muriatic Acid Solution

NaCl content (% of cement weight)	Name of specimens	Normal concrete No. of specimens	FRC* No. of specimens	Concrete with CI** No. of specimens	Specimen longitudinal sections	Specimen cross sections
3%	SP1	2	2	2	3" 3" 11"	0.4" 3" 3"
	SP2	2	2	2	3" 3" 11"	0.4" 3" 5"
	SP3	2	2	2	3" 3" 11"	0.4" 3" 7"
Total number of each concrete type		6	6	6		

* FRC: Fiber Reinforced Concrete
**CI: Corrosion Inhibitor

Figure C- 113 Accelerated Corrosion Test Specimen Dimensions

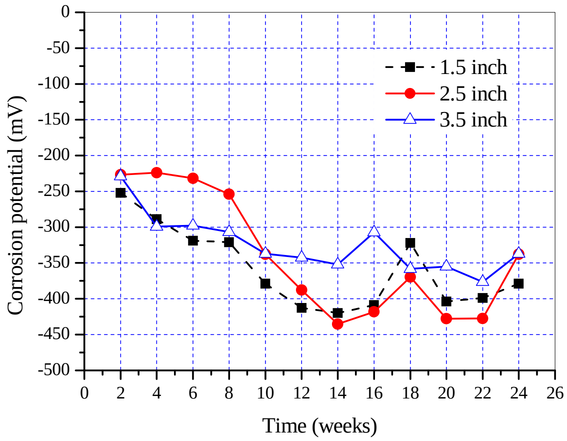

Normal concrete

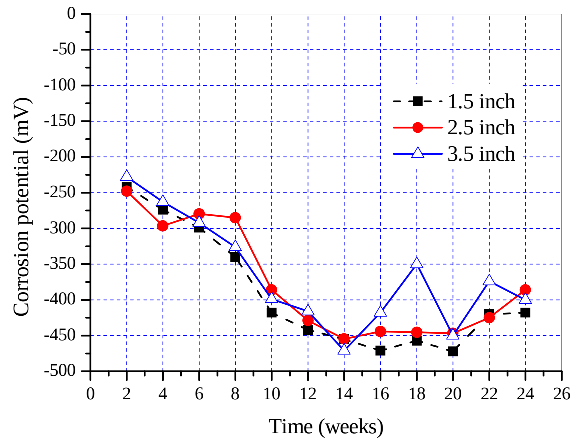

Concrete with corrosion inhibitors

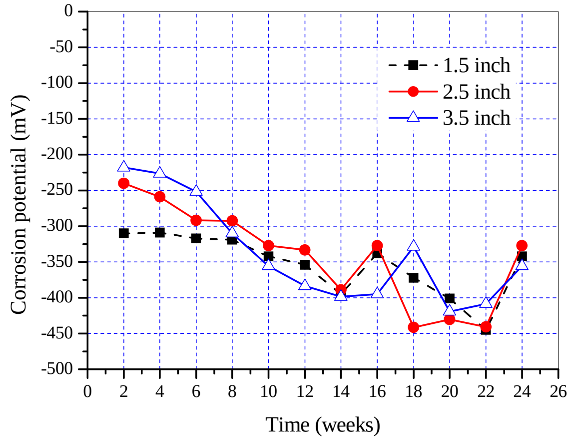

Concrete with fibers

Figure C- 114 Corrosion Potential - Time Relationship for Specimens with Same Concrete Type

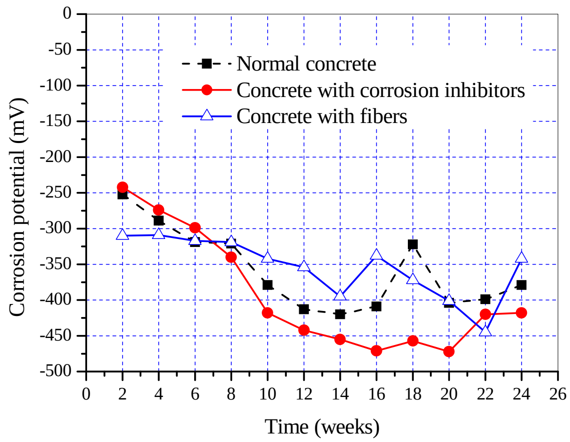

1.5 in. edge distance

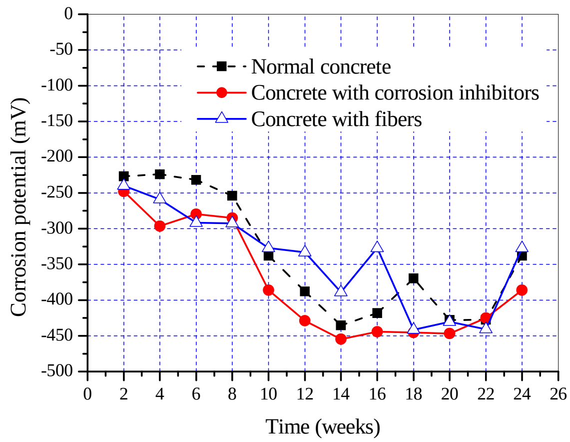

2.5 in. edge distance

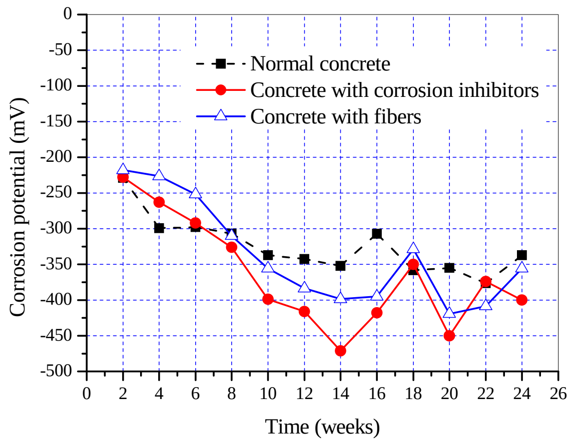

3.5 in. edge distance

Figure C- 115 Corrosion Potential - Time Relationship for Specimens with Same Edge Distance

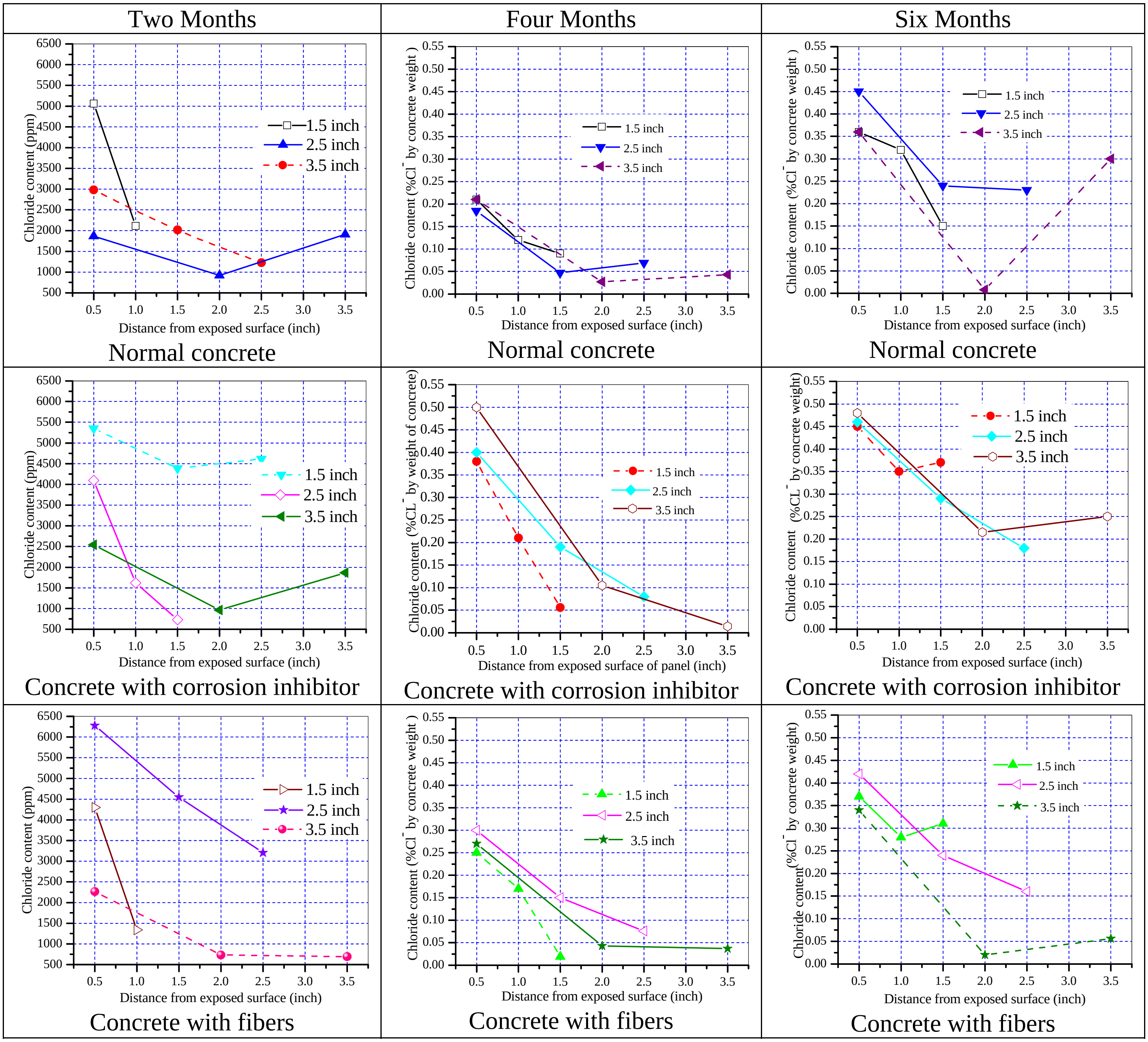

Figure C- 116 Chloride Content Profiles for Specimens with Same Concrete Type

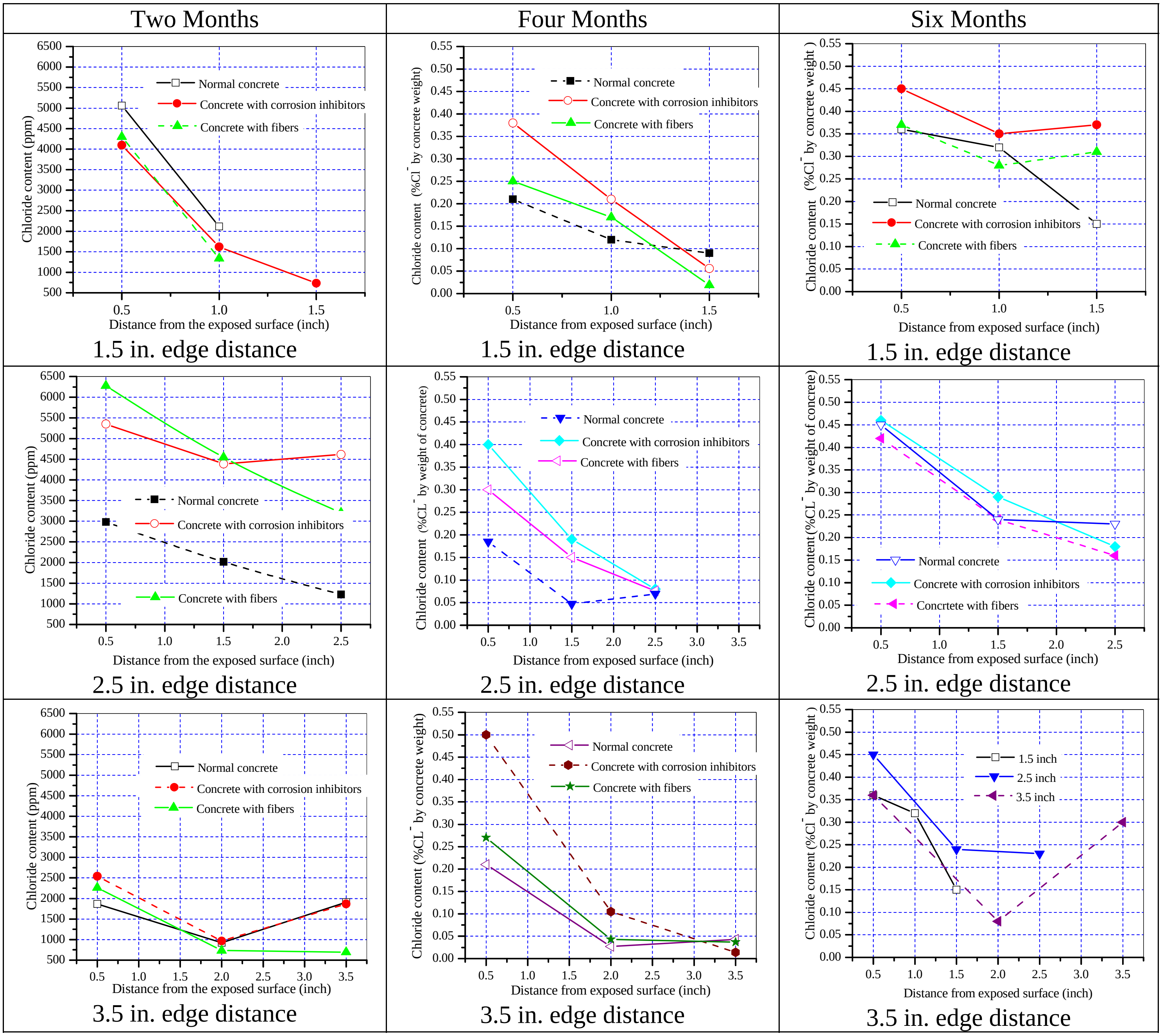

Figure C- 117 Chloride Content Profiles for Specimens with Same Edge Distance

REFERENCES

ASTM A370, 2010. "Standard Test Methods and Definitions for Mechanical Testing of Steel Products," ASTM, West Conshohocken, PA, 47 pp.

ASTM A416, 2010. "Standard Specification for Steel Strand, Uncoated Seven-Wire for Prestressed Concrete," ASTM, West Conshohocken, PA, 5 pp.

ASTM A882, 2010. "Standard Specification for Filled Epoxy-Coated Seven-Wire Prestressing Steel Strand," ASTM, West Conshohocken, PA, 5 pp.

ASTM C1116, 2010. "Standard Specification for Fiber-Reinforced Concrete," ASTM, West Conshohocken, PA, 7 pp.

ASTM C1218, 1999, "Standard Test Method for Water-Soluble Chloride in Mortar and Concrete," ASTM, ASTM, West Conshohocken, PA, 3 pp.

ASTM C150, 2009. "Standard Specification for Portland Cement," ASTM, West Conshohocken, PA, 10 pp.

ASTM C260, 2008. "Standard Specification for Air-Entraining Admixtures for Concrete," ASTM, West Conshohocken, PA, 3 pp.

ASTM C293, 2008. "Standard Test Method for Flexural Strength of Concrete (Using Simple Beam With Center-Point Loading)," ASTM, West Conshohocken, PA, 3 pp.

ASTM C33, 2008. "Standard Specification for Concrete Aggregates," ASTM, West Conshohocken, PA, 11 pp.

ASTM C494, 2010. "Standard Specification for Chemical Admixtures for Concrete," ASTM, West Conshohocken, PA, 10 pp.

ASTM C876, 1991, "Standard Test Method for Half-Cell Potentials of Uncoated Reinforcing Steel in Concrete," ASTM, West Conshohocken, PA, 6 pp.

ASTM G1, 2003, "Standard Practice for Preparing, Cleaning, and Evaluating Corrosion Test Specimens," ASTM, West Conshohocken, PA, 9 pp.

Missouri Department of Transportation (MoDOT), 2004, "2004 Missouri Standard Specification Book for Highway Construction," Missouri Department of Transportation,Jefferson city, MO.

APPENDIX D

NUMERICAL ANALYSES OF SIP PANEL SYSTEMS

TABLE OF CONTENTS

LIST OF FIGURES

D.1 Introduction

This appendix provides supplemental information and detailed results of the FE simulations summarized in Chapter 6.

D.2 Simulation of SIP Panel Spalling

D.2.1 2D FE simulation of reinforcement arrangement effects on corrosion process

Two main FE models were developed according to different locations of the U1 bar as shown in Figure D-1 . Case I represents a critical configuration of reinforcement arrangement that can occur, while Case II represents a typical reinforcement arrangement. Based on these models, side cover was varied from 1.5 in. to 4 in. in both FE models. Crack patterns and Von Mises stress variations for all simulated FE models are presented in this section to compare the effects of the parameters considered.

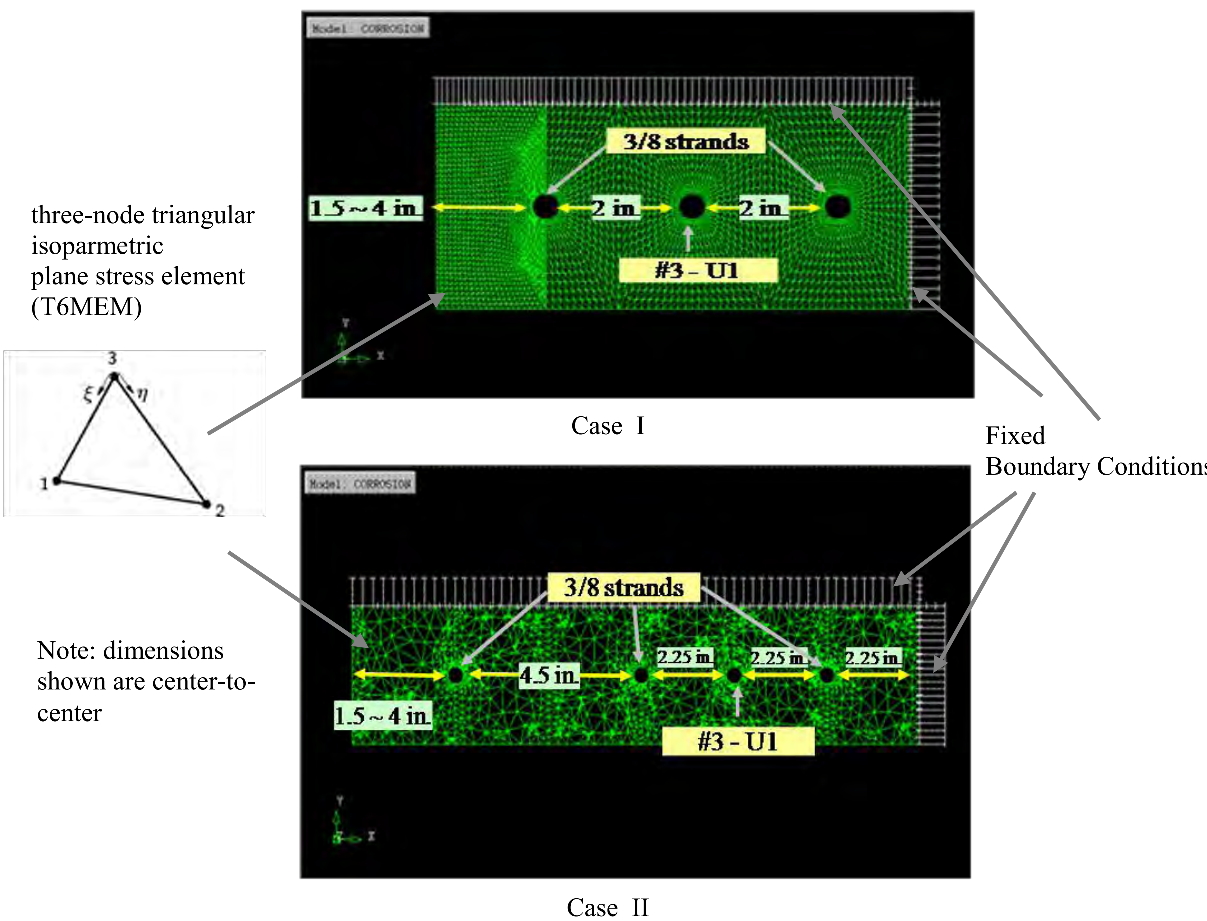

Figure D-1 Two-Dimensional FE Models for Corrosion Process

D.2.1.1 Case I FE analysis results

Crack patterns and corresponding Von Mises stress variations of Case I FE analyses are illustrated from Figure D-2 to Figure D-6. Each figure represents a different side cover, and results are presented with respect to incrementally increasing internal pressures.

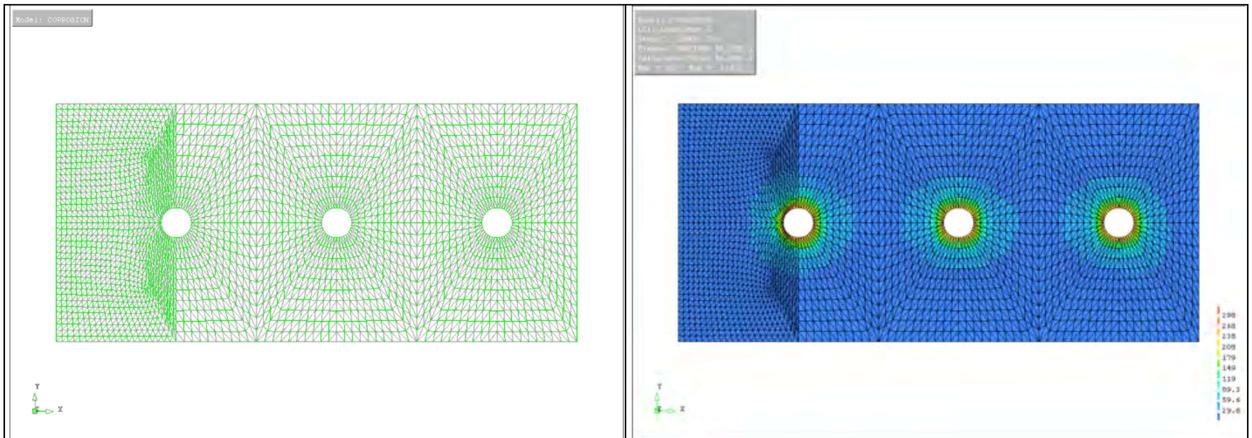

p_{int} = 200 psi

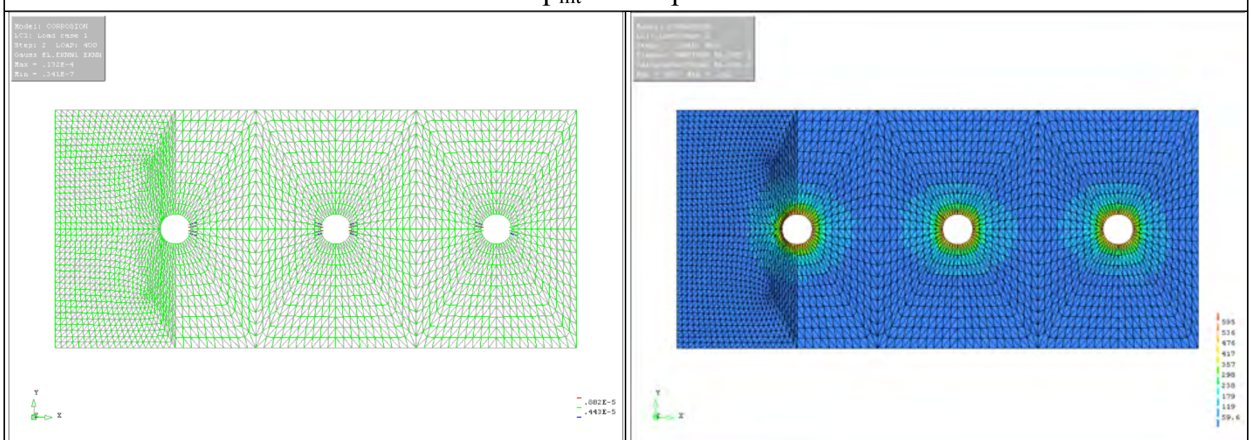

p_{int} = 400 psi

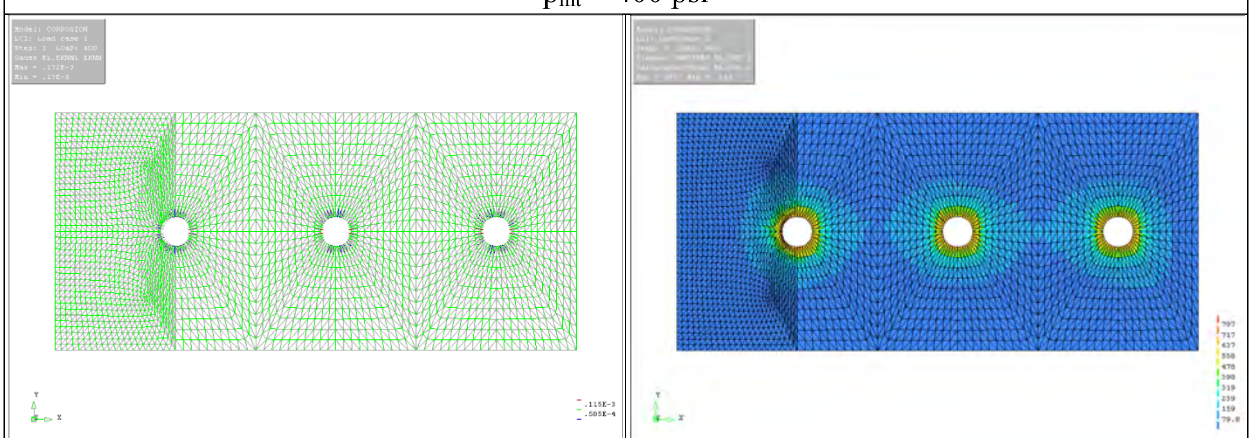

p_{int} = 600 psi

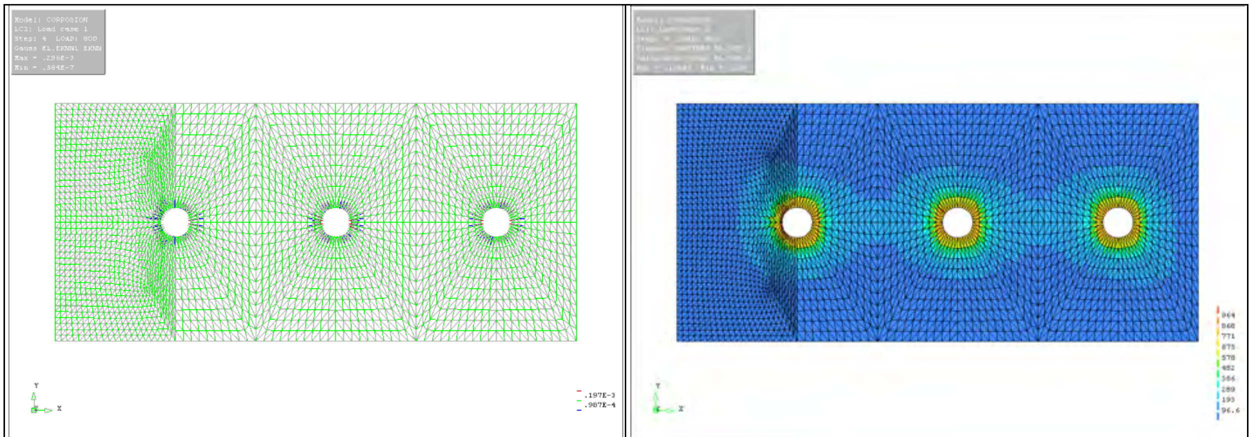

p_{int} = 800 psi

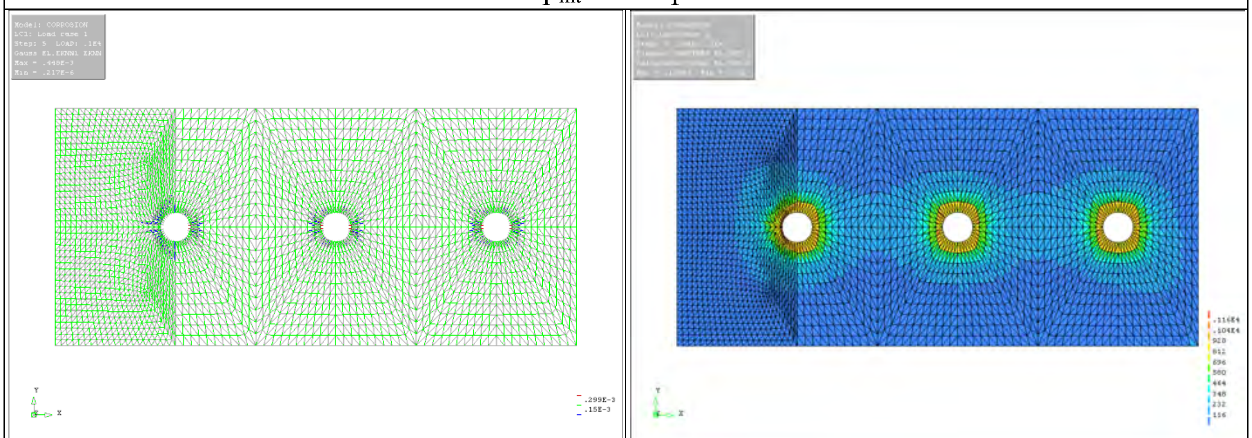

p_{int} = 1,000 psi

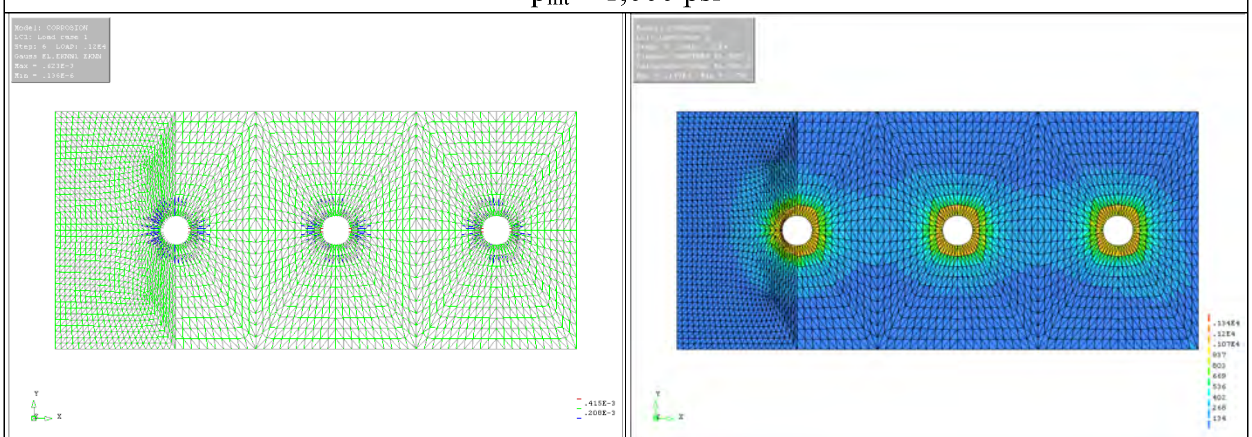

p_{int} = 1,200 psi

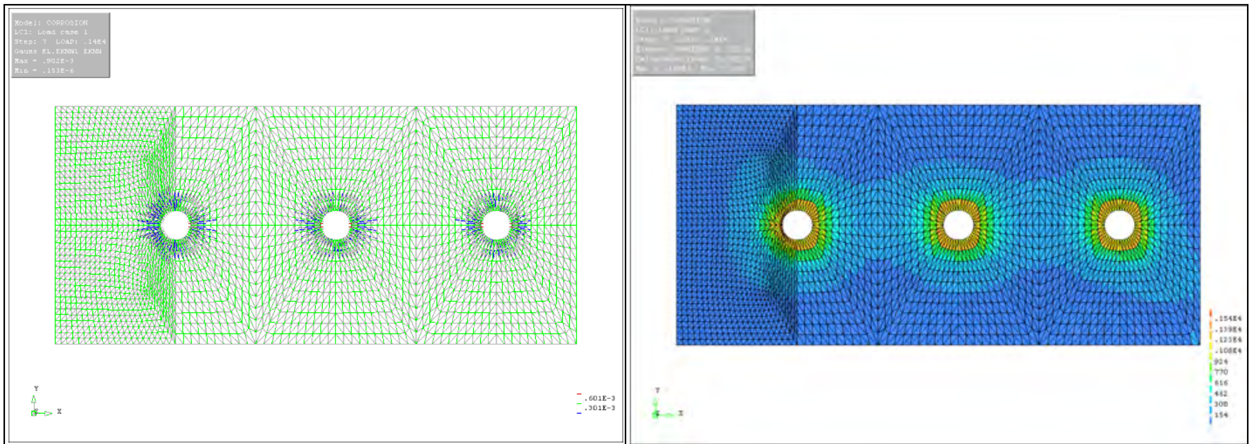

p_{int} = 1,400 psi

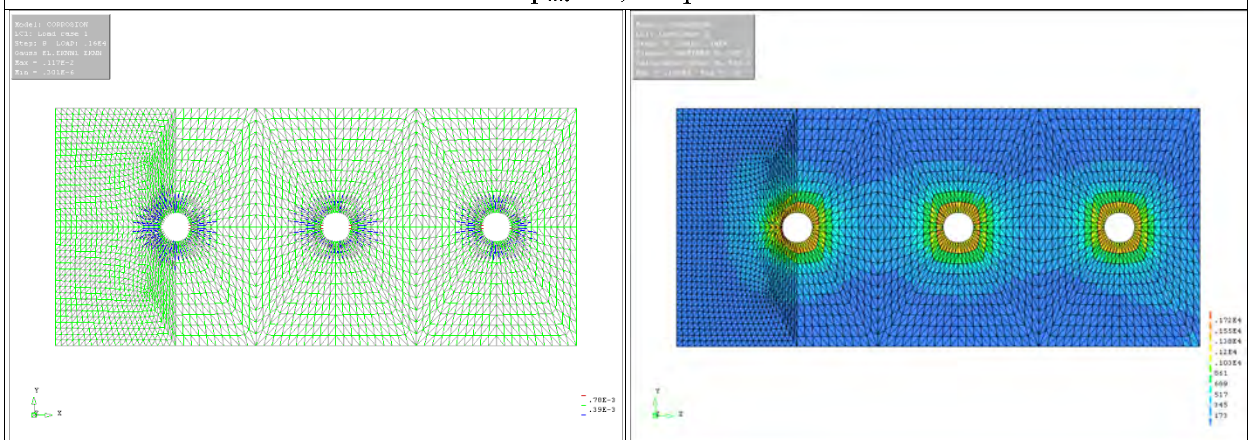

p_{int} = 1,600 psi

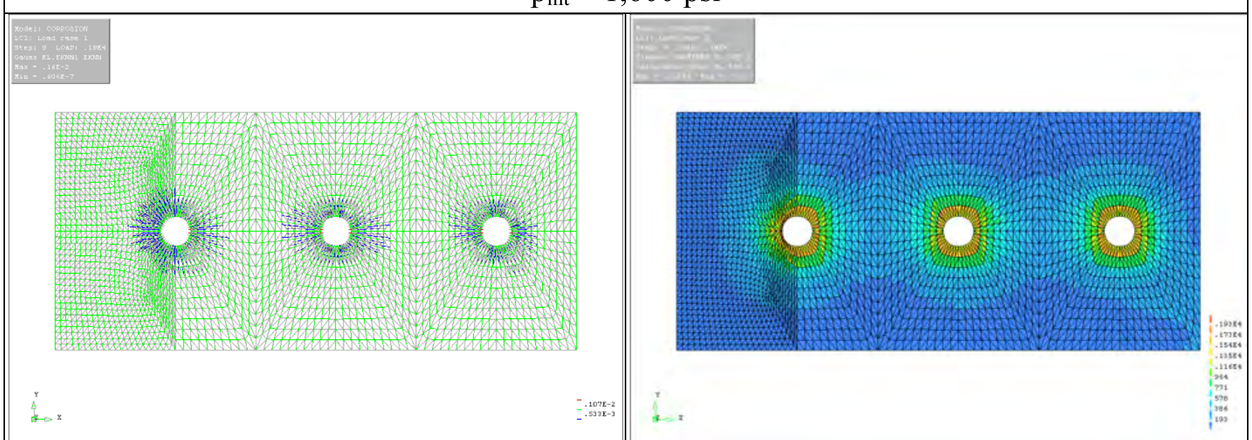

p_{int} = 1,800 psi

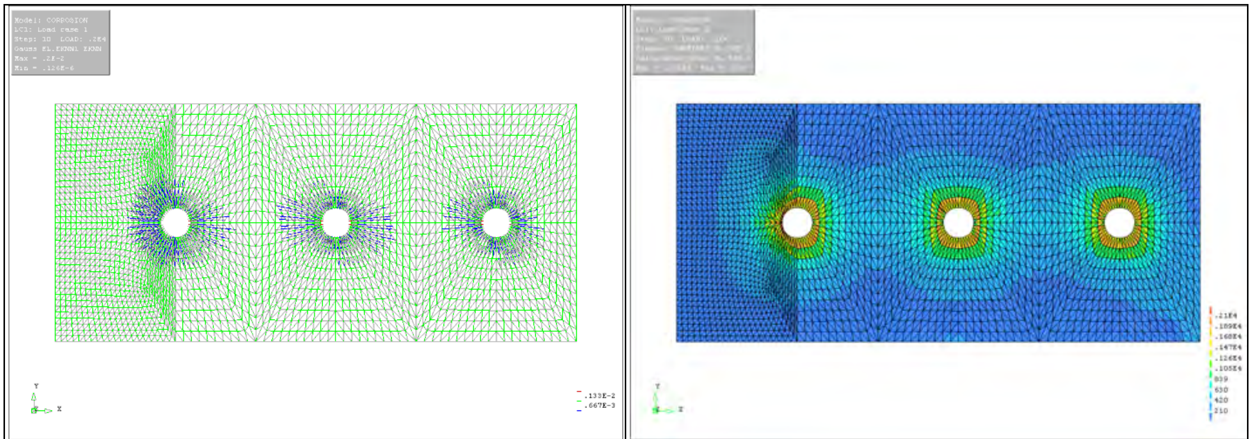

p_{int} = 2,000 psi

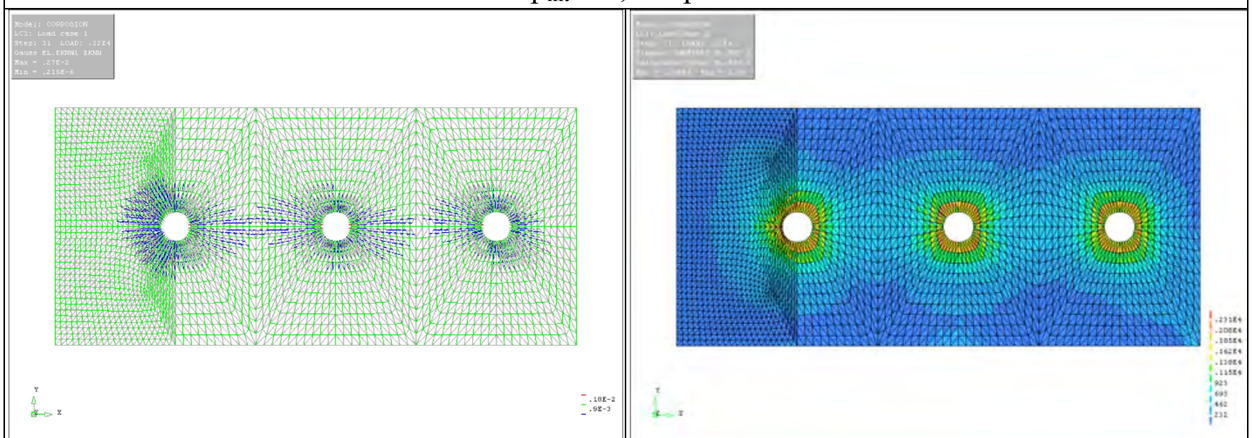

p_{int} = 2,200 psi

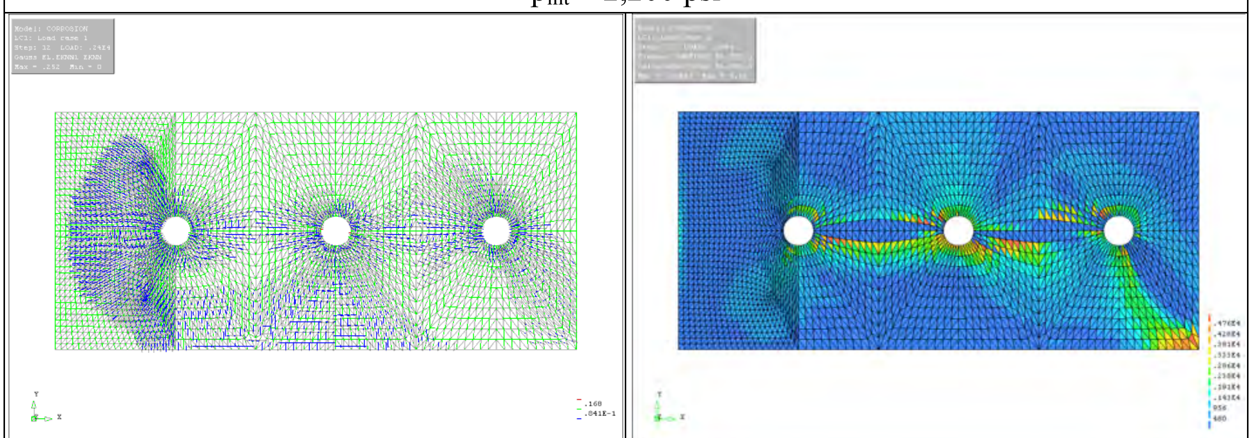

p_{int} = 2,400 psi

Figure D-2 Crack Patterns & Von Mises Stress Variations of Case I FE Model (Cover = 1.5 in.)

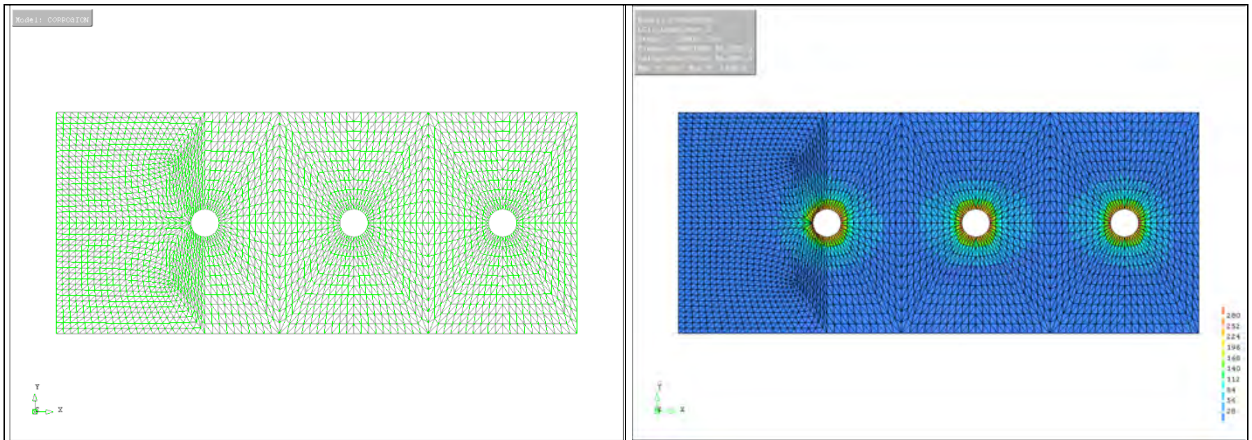

p_{int} = 200 psi

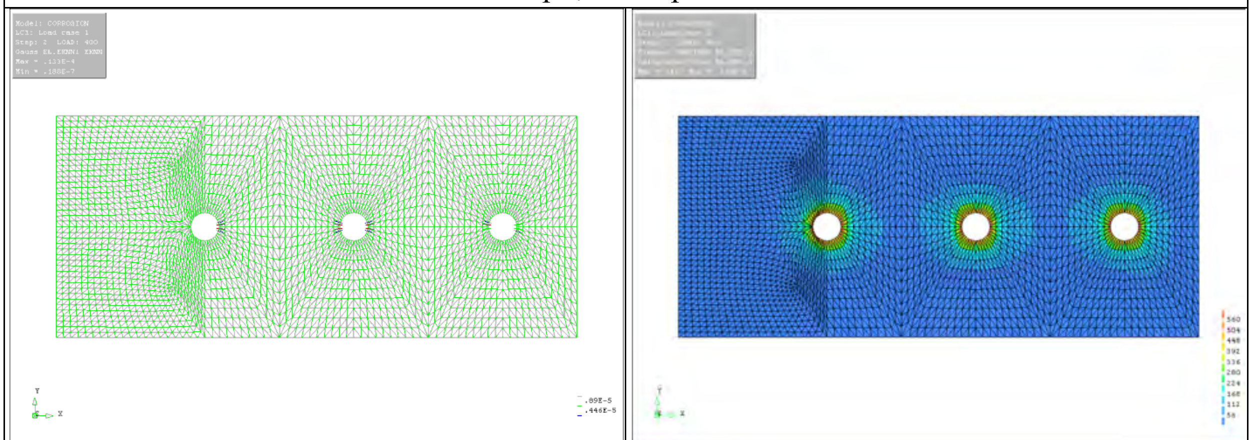

p_{int} = 400 psi

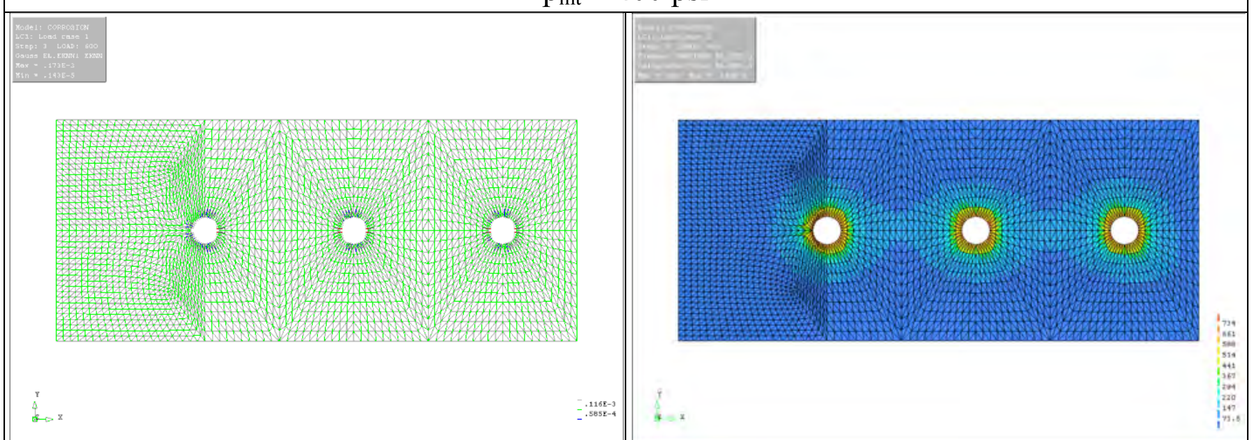

p_{int} = 600 psi

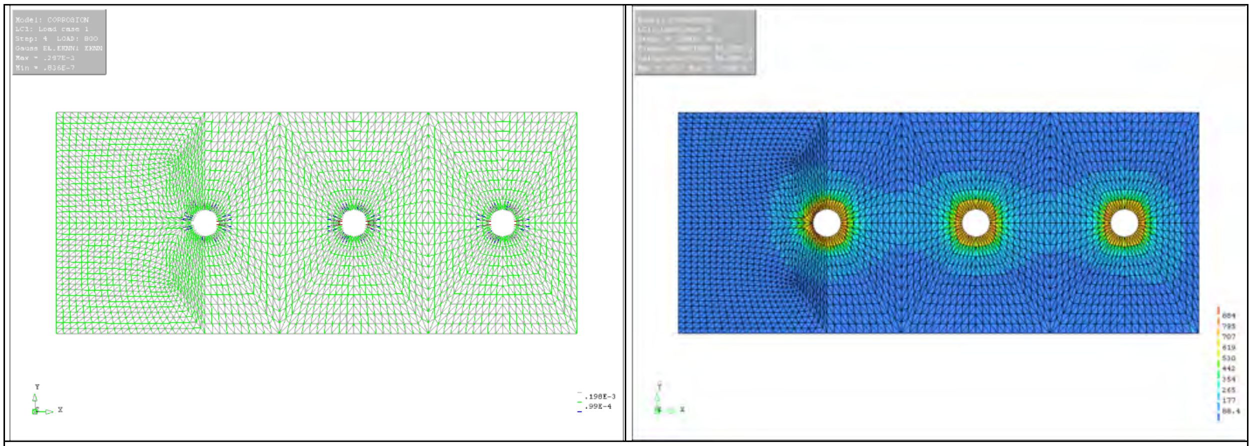

p_{int} = 800 psi

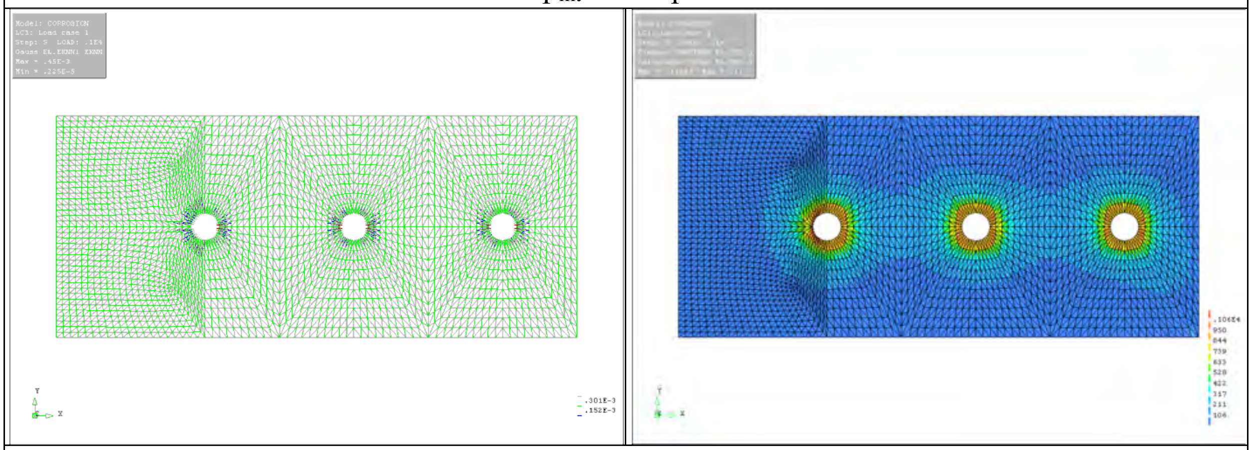

p_{int} = 1,000 psi

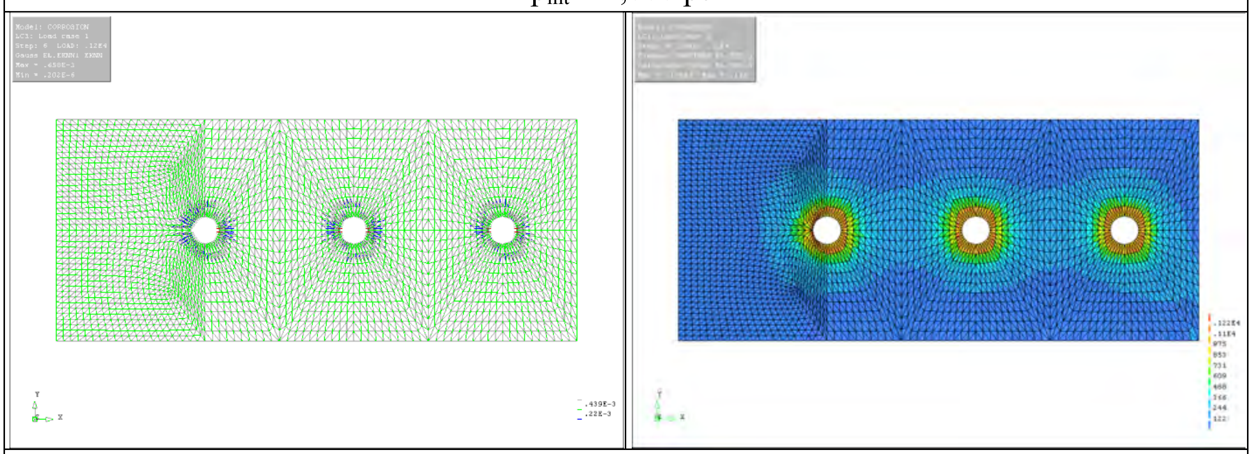

p_{int} = 1,200 psi

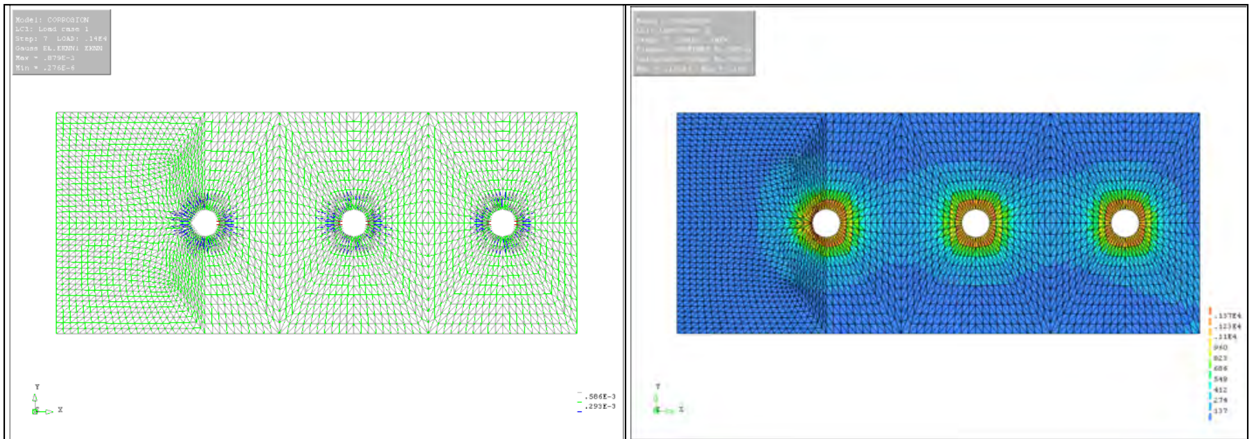

p_{int} = 1,400 psi

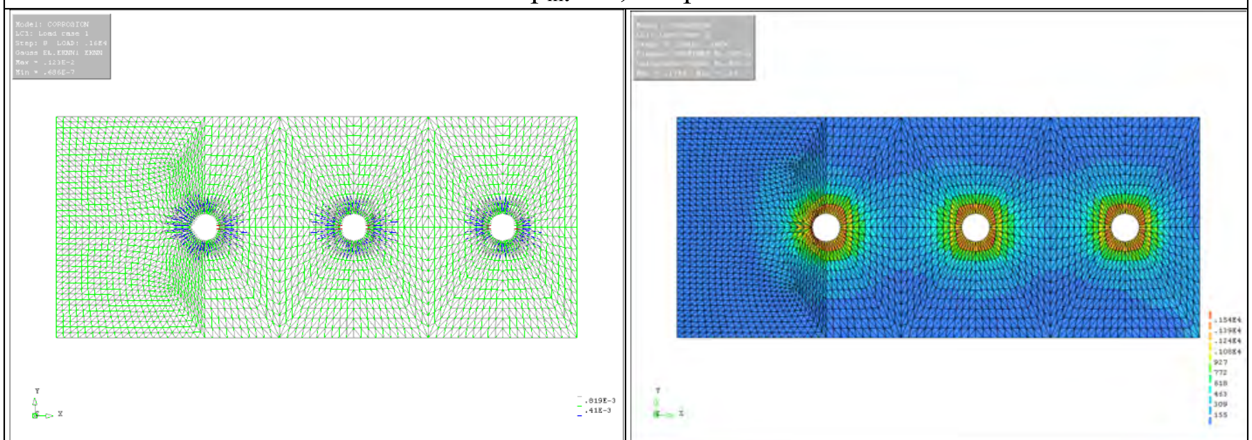

p_{int} = 1,600 psi

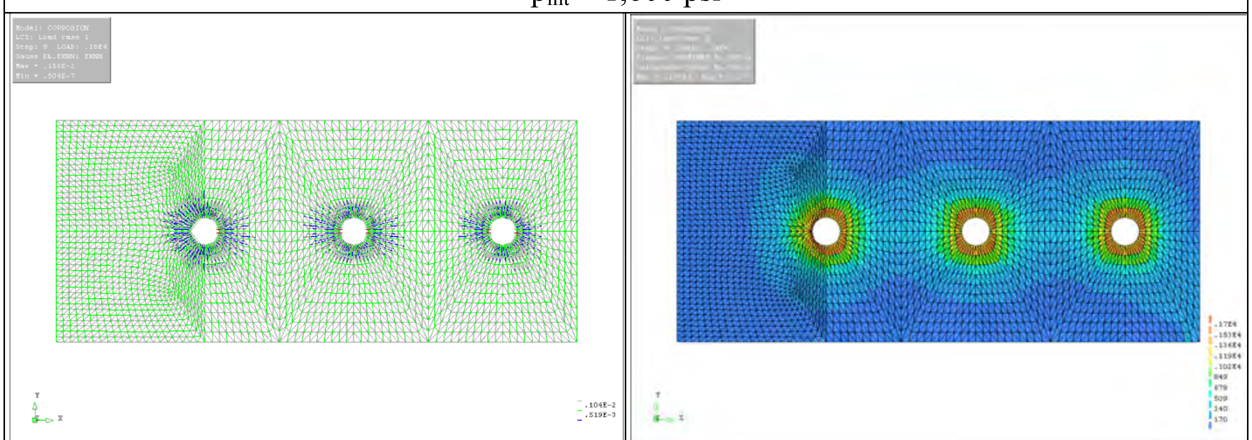

p_{int} = 1,800 psi

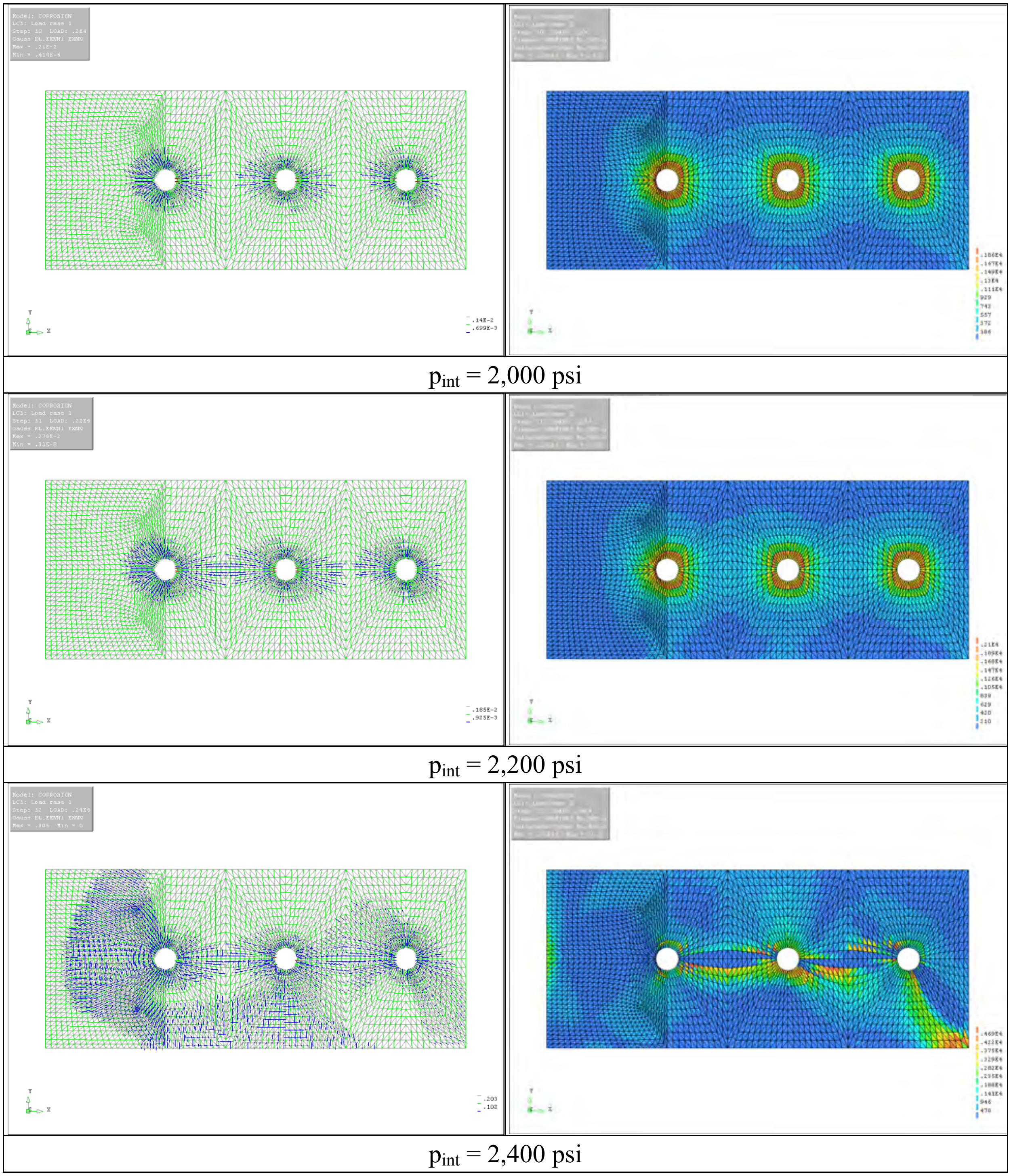

Figure D-3 Crack Patterns & Von Mises Stress Variations of Case I FE Model (Cover = 2.0 in.)

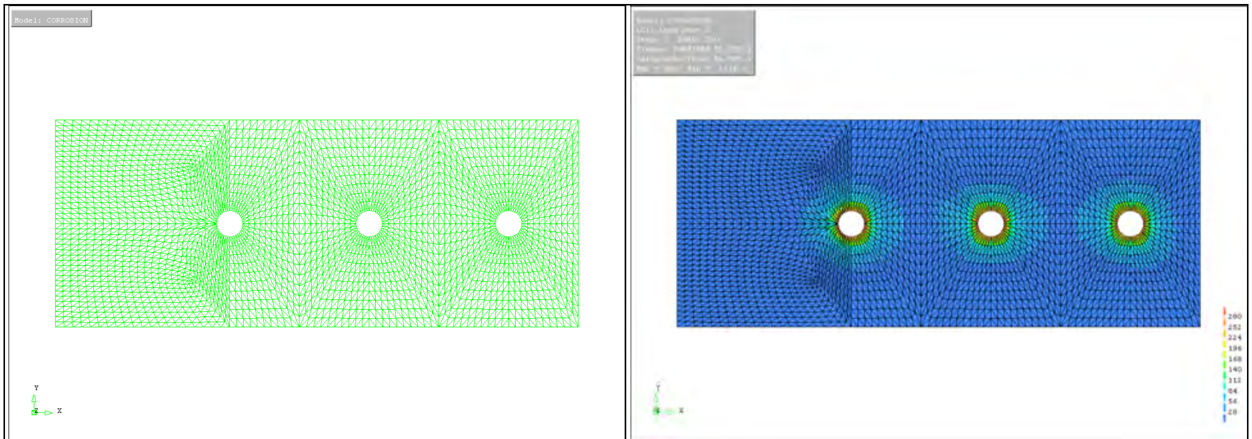

p_{int} = 200 psi

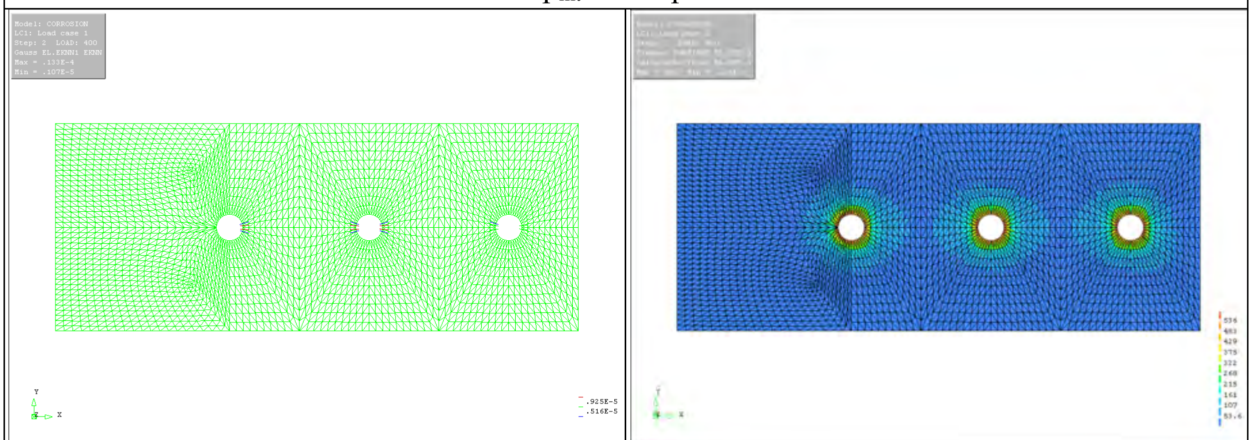

p_{int} = 400 psi

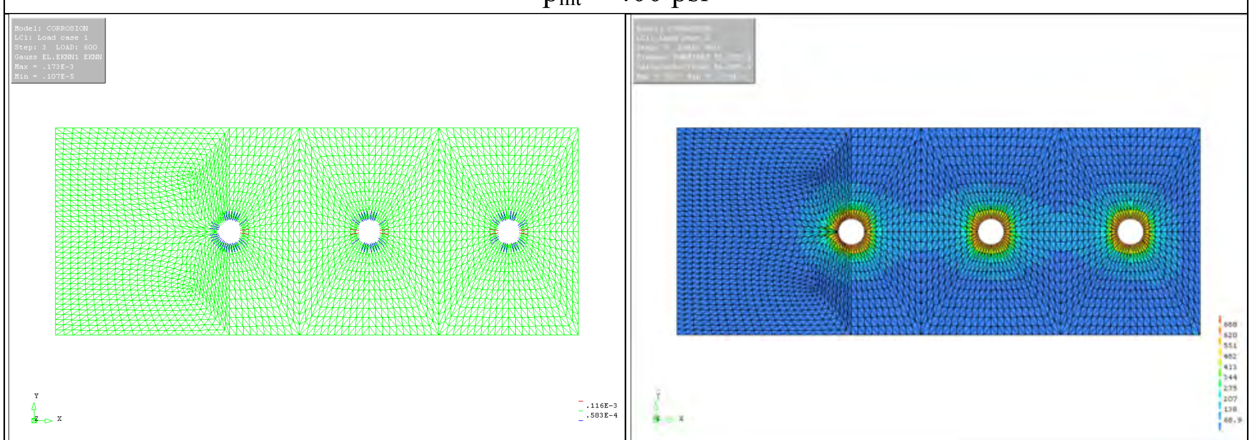

p_{int} = 600 psi

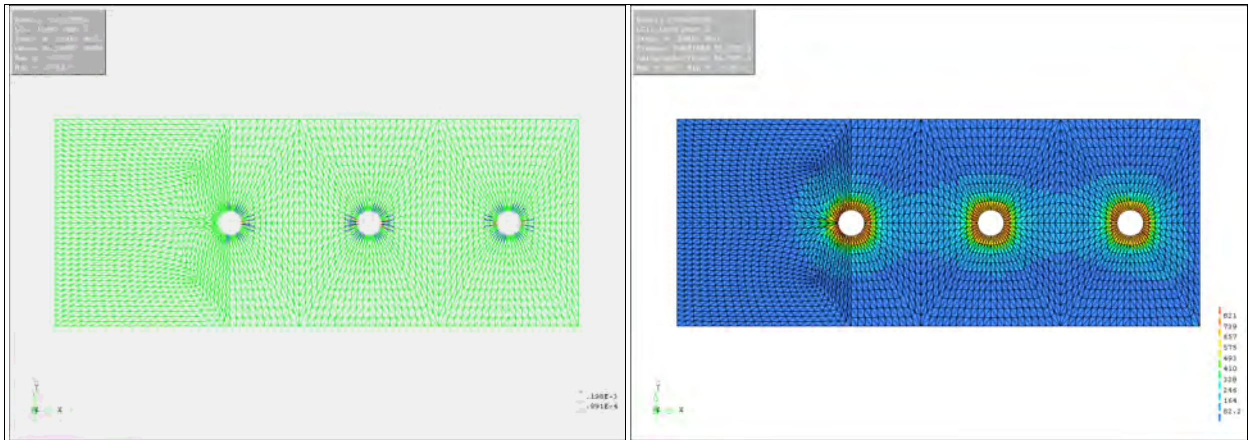

p_{int} = 800 psi

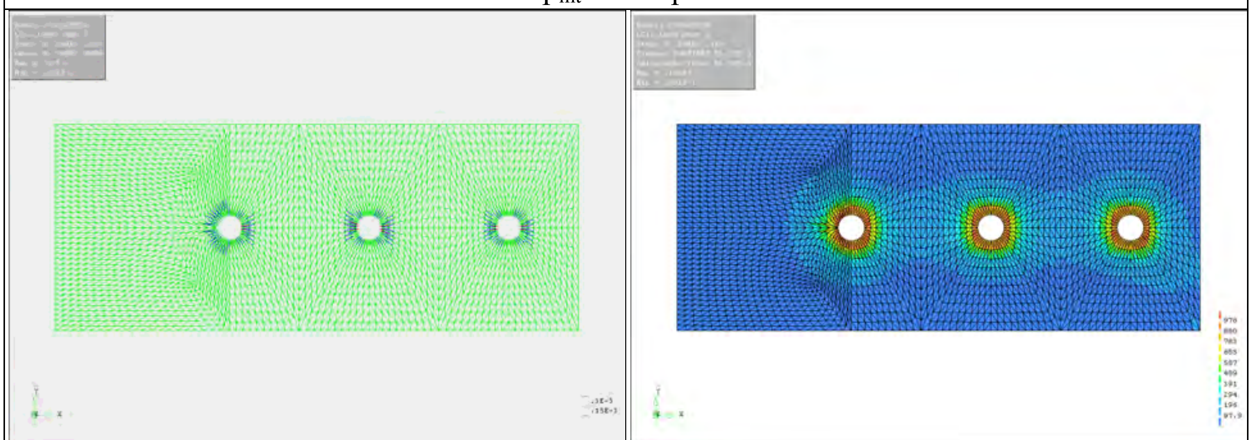

p_{int} = 1,000 psi

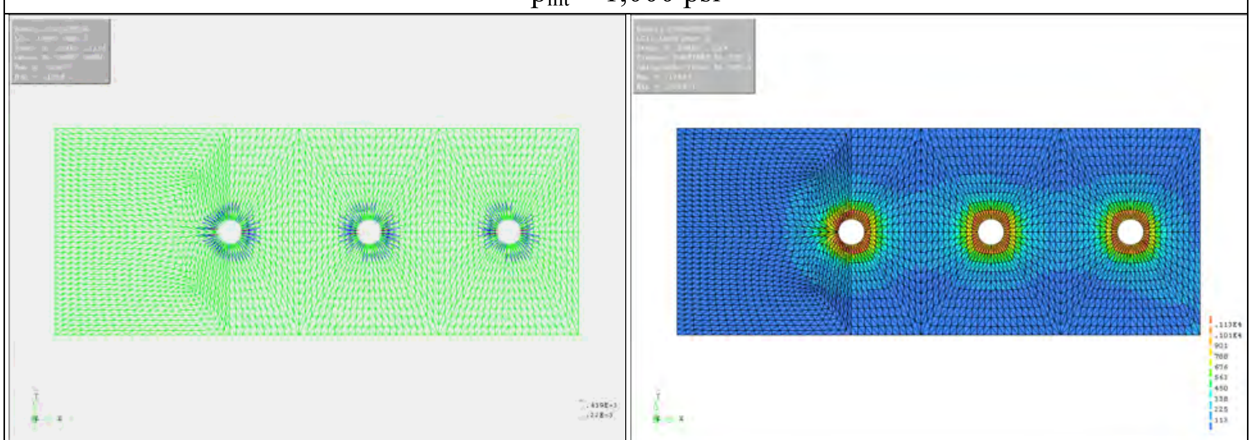

p_{int} = 1,200 psi

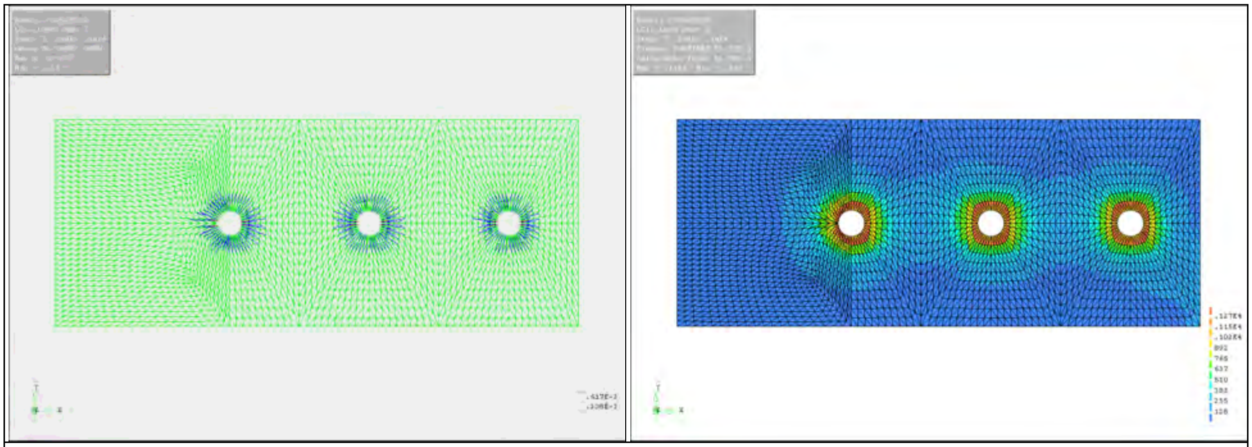

p_{int} = 1,400 psi

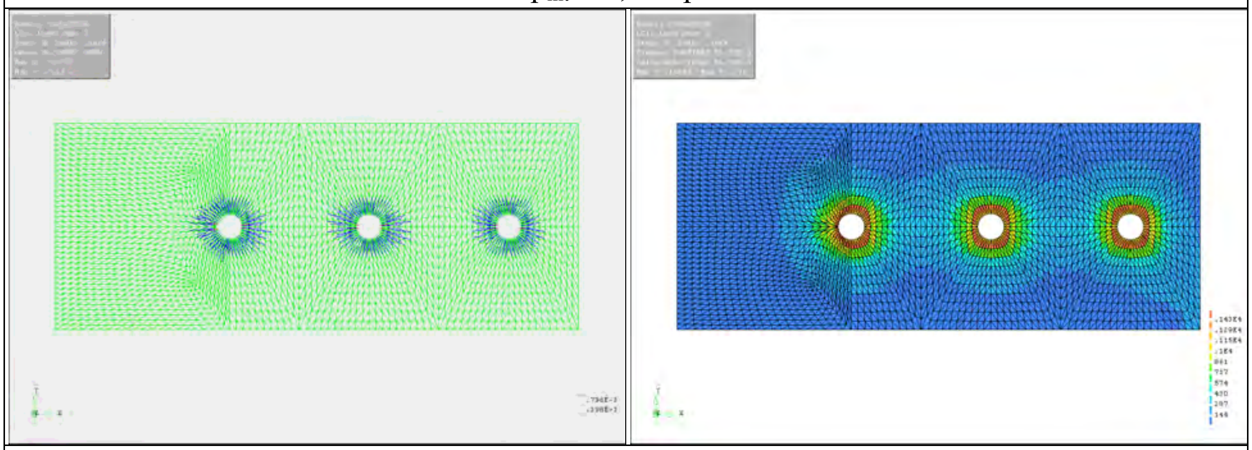

p_{int} = 1,600 psi

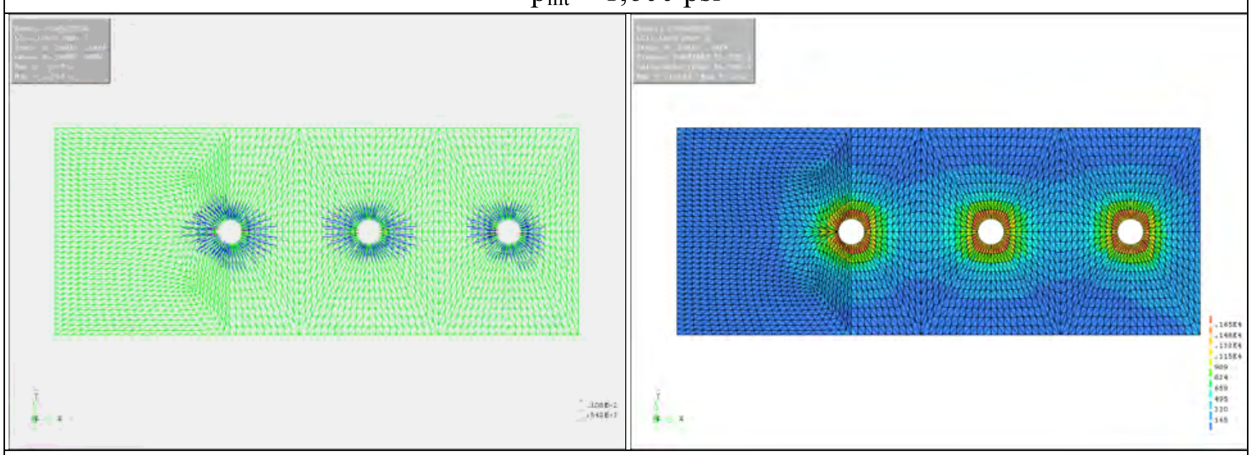

p_{int} = 1,800 psi

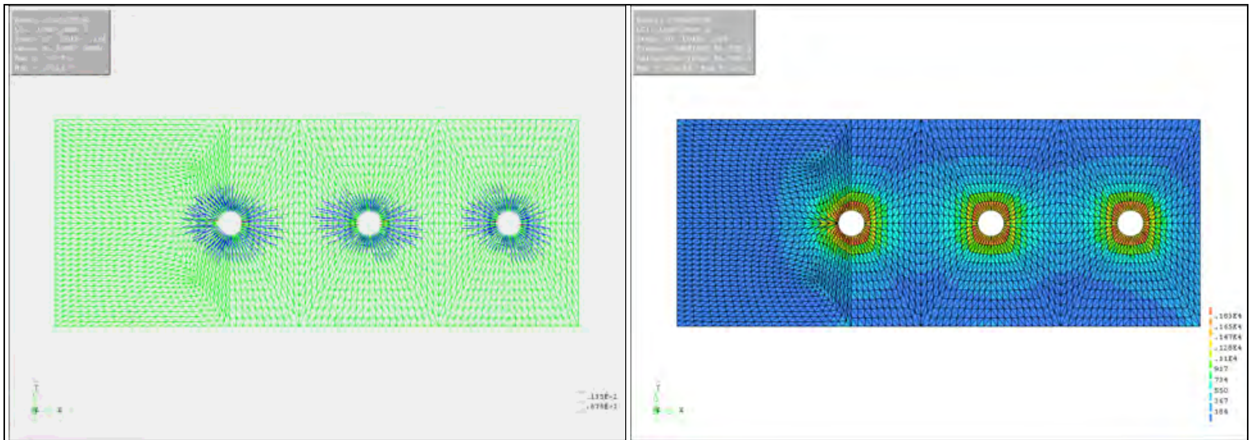

p_{int} = 2,000 psi

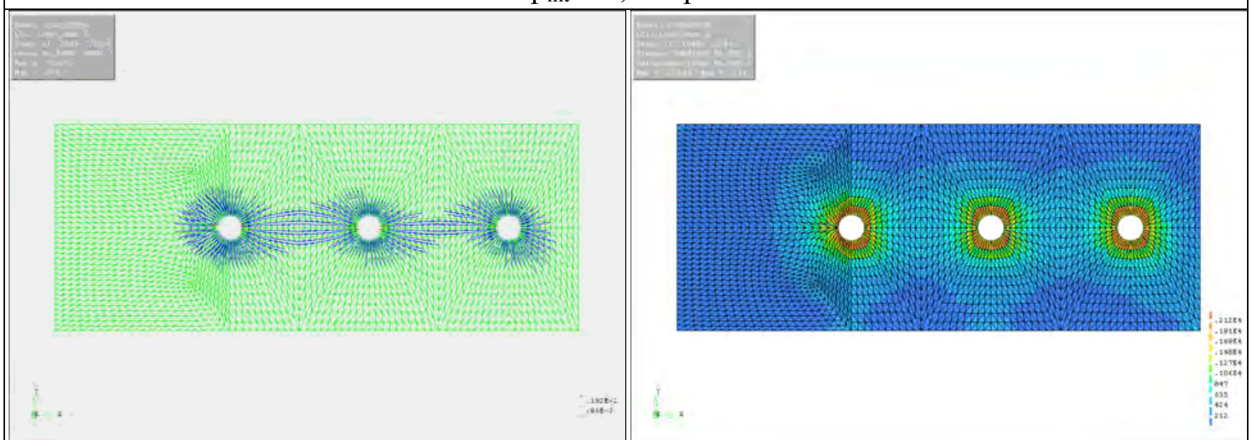

p_{int} = 2,200 psi

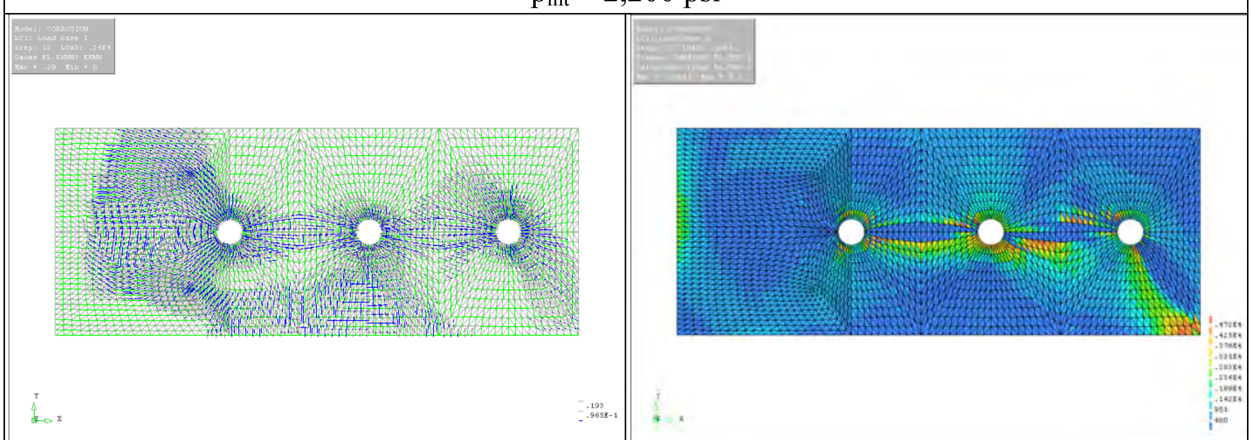

p_{int} = 2,400 psi

Figure D-4 Crack Patterns & Von Mises Stress Variations of Case I FE Model (Cover = 2.5 in.)

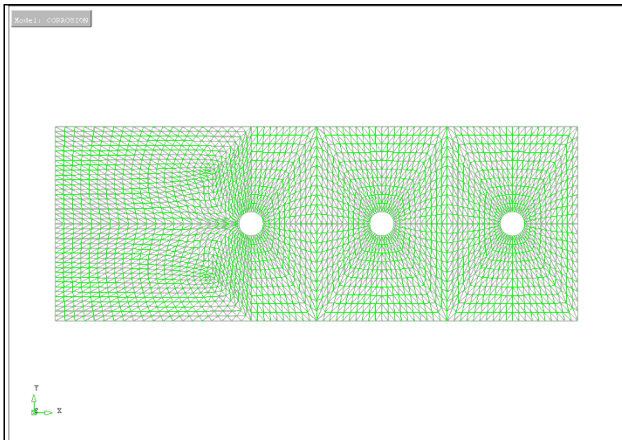
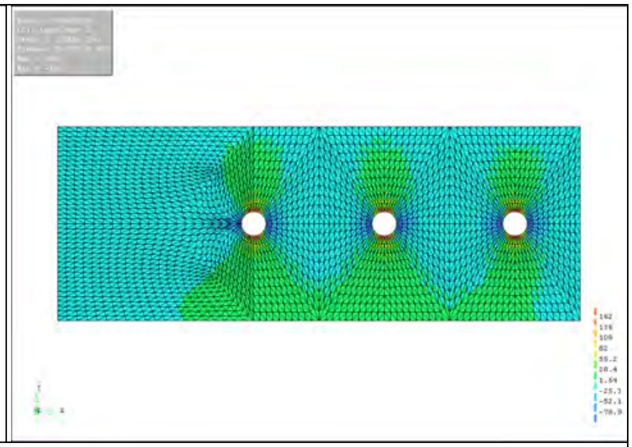

p_{int} = 200 psi

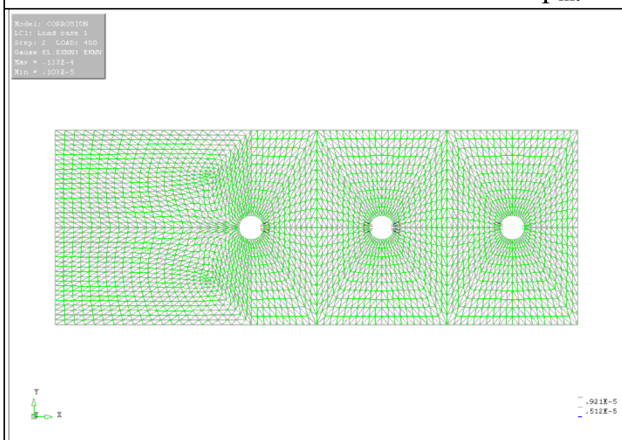
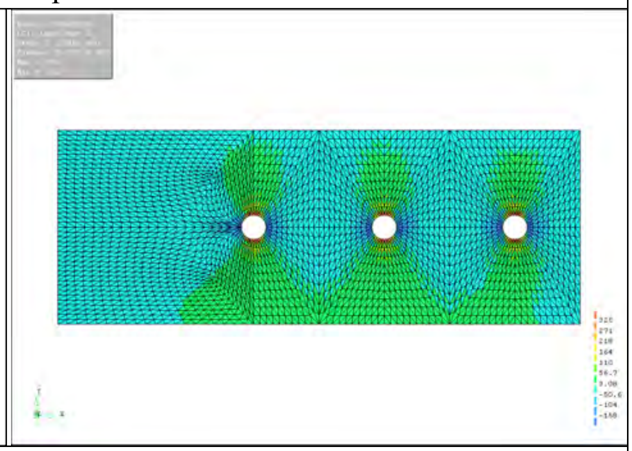

p_{int} = 400 psi

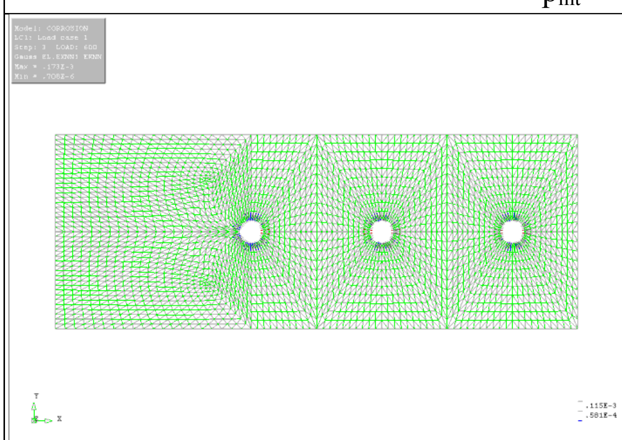
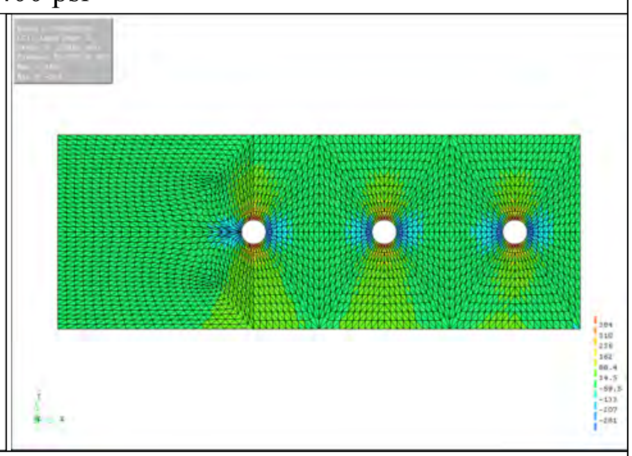

p_{int} = 600 psi

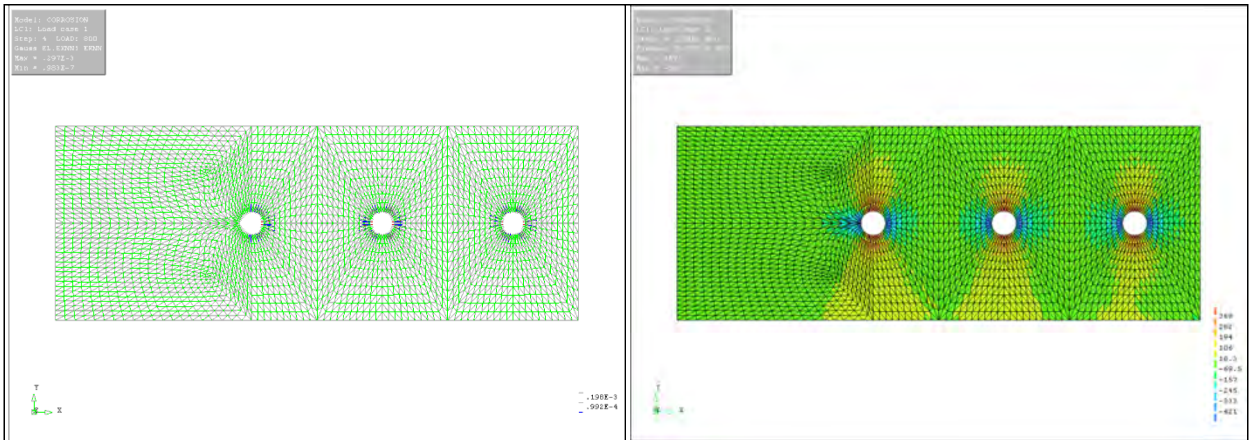

p_{int} = 800 psi

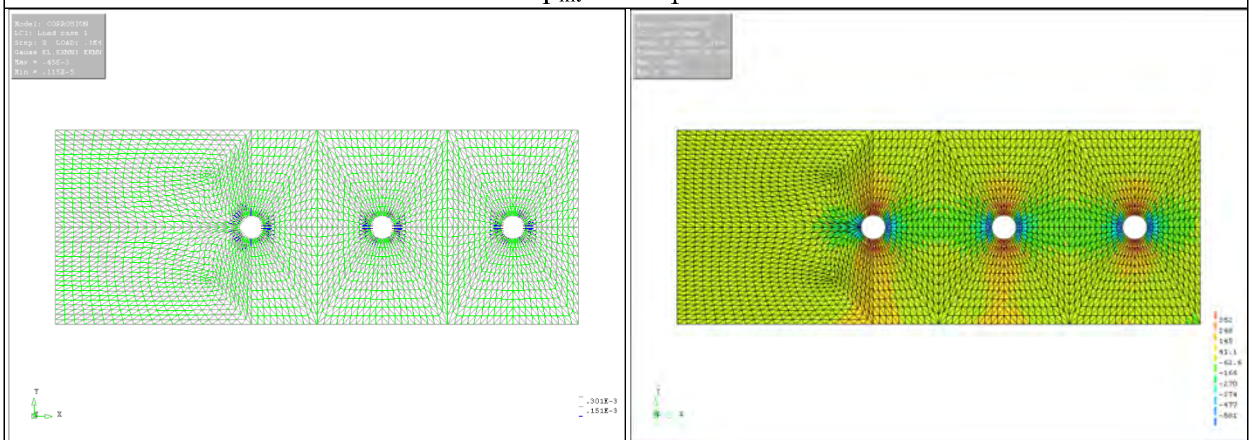

p_{int} = 1,000 psi

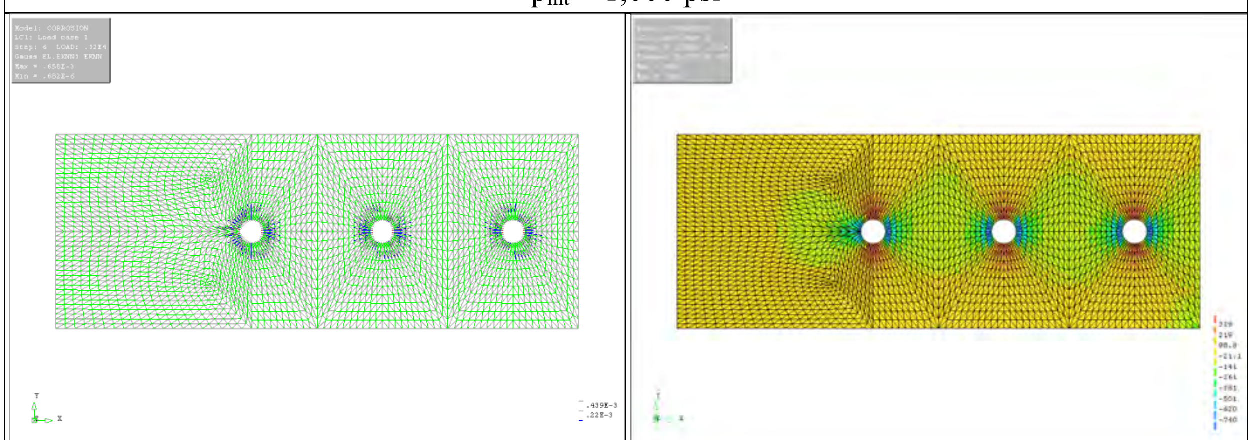

p_{int} = 1,200 psi

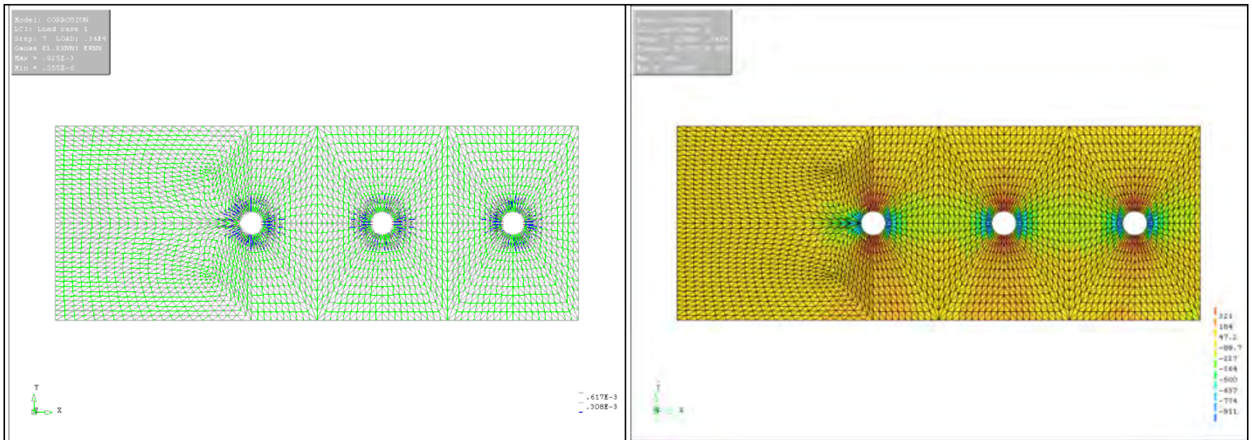

p_{int} = 1,400 psi

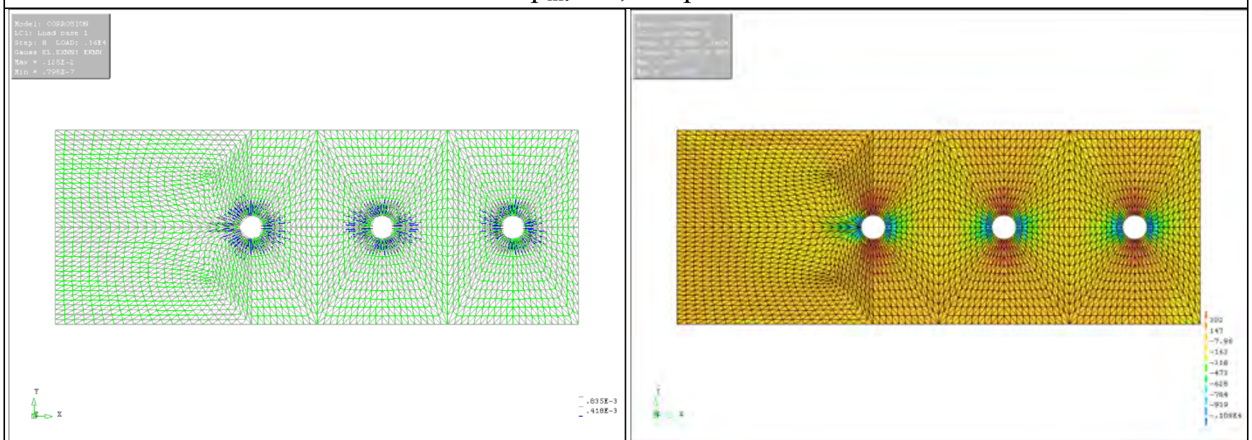

p_{int} = 1,600 psi

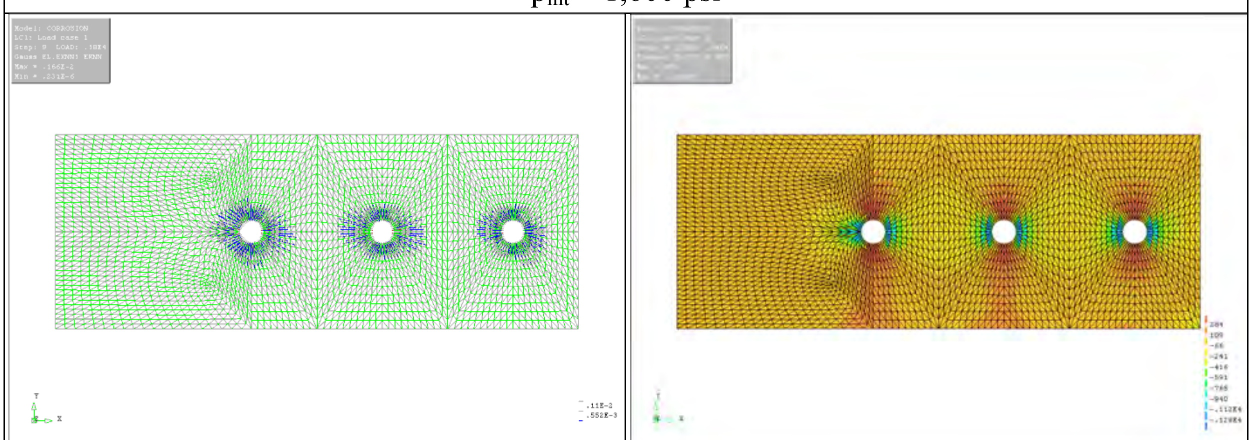

p_{int} = 1,800 psi

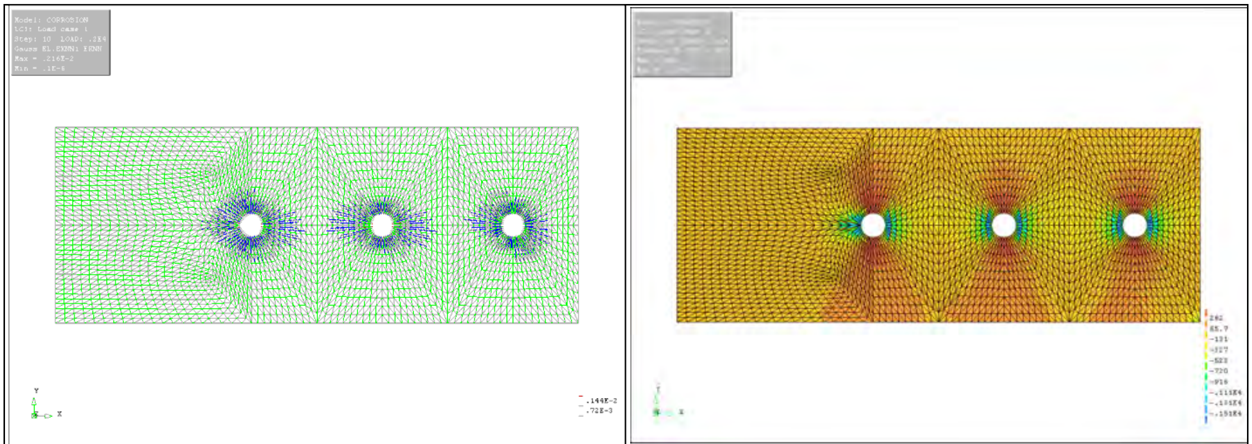

p_{int} = 2,000 psi

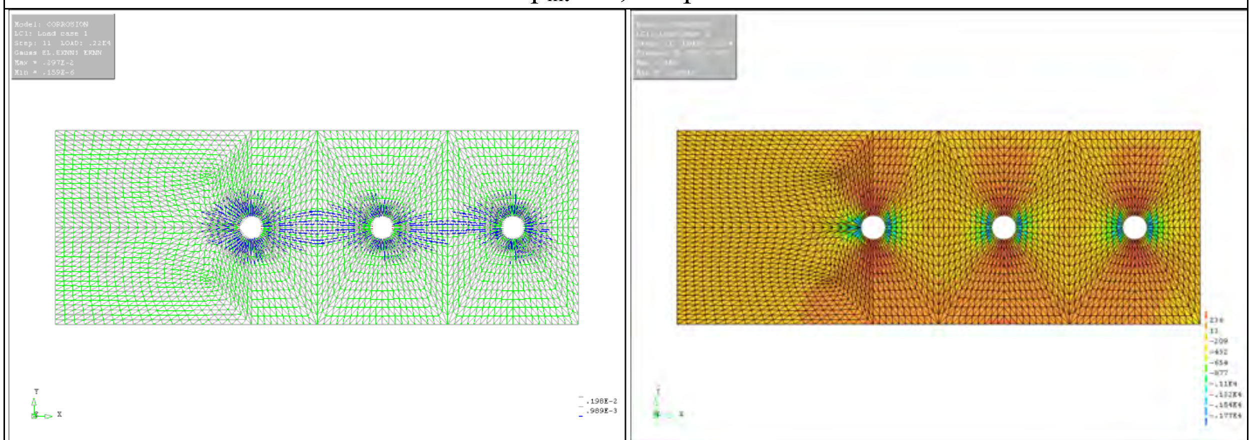

p_{int} = 2,200 psi

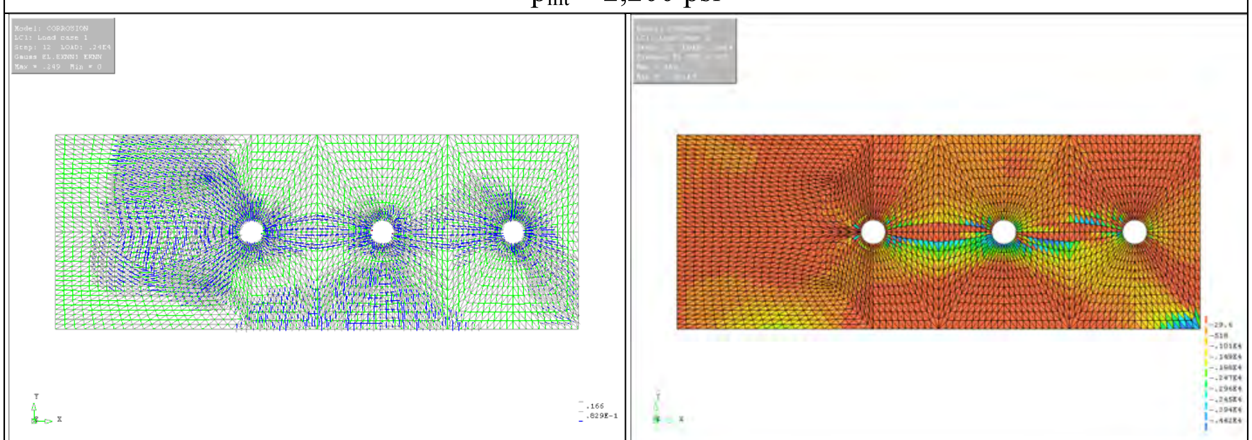

p_{int} = 2,400 psi

Figure D-5 Crack Patterns & Von Mises Stress Variations of Case I FE Model (Cover = 3.0 in.)

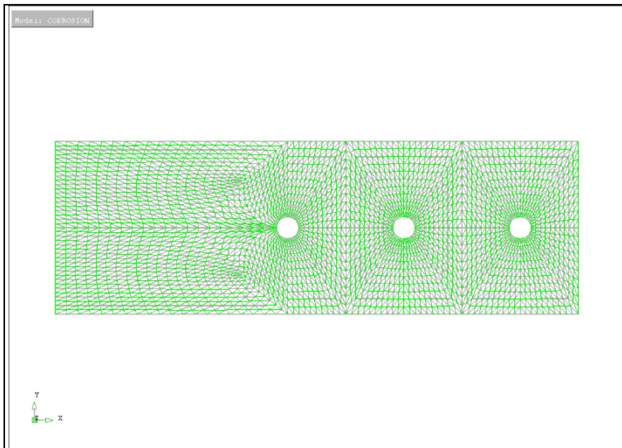
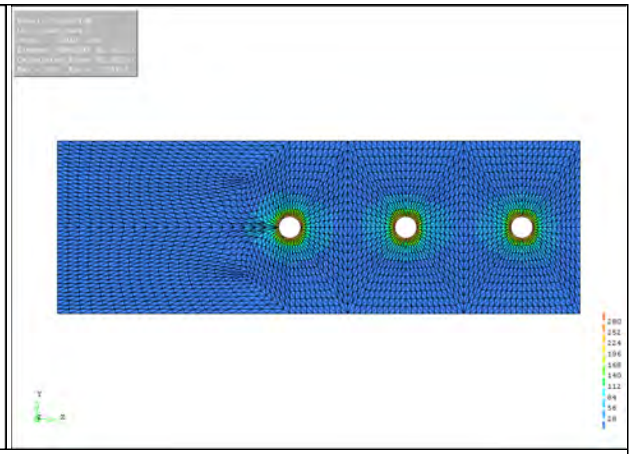

p_{int} = 200 psi

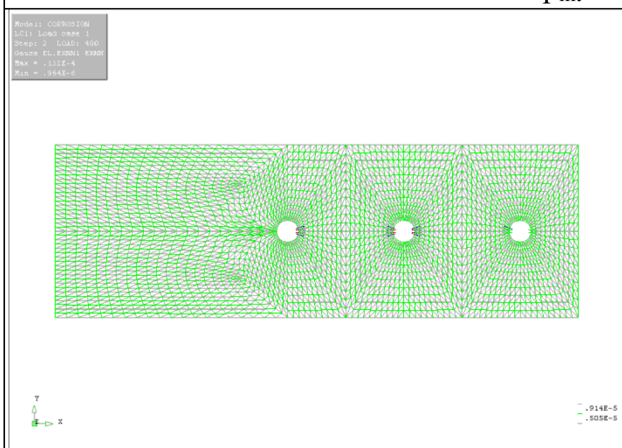
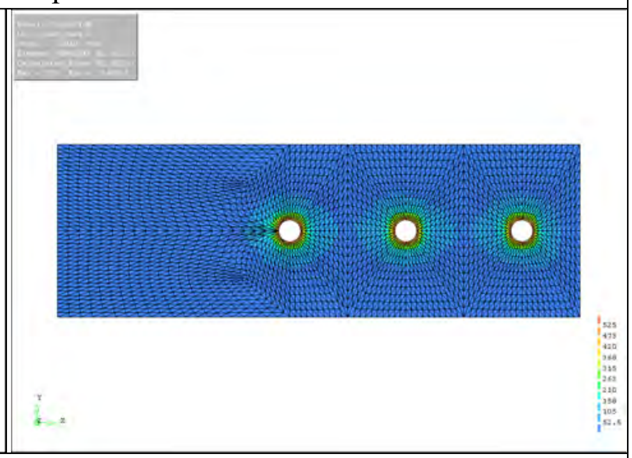

p_{int} = 400 psi

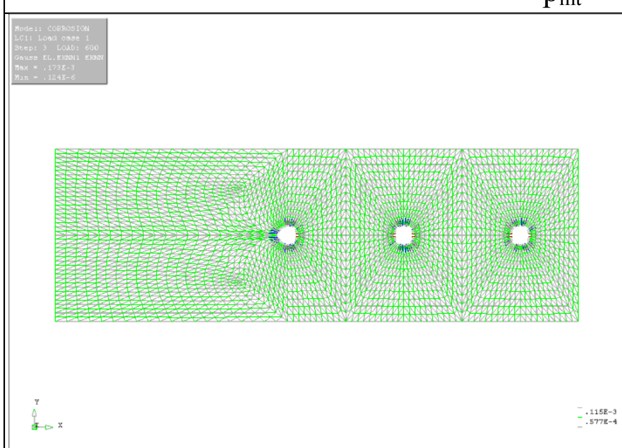
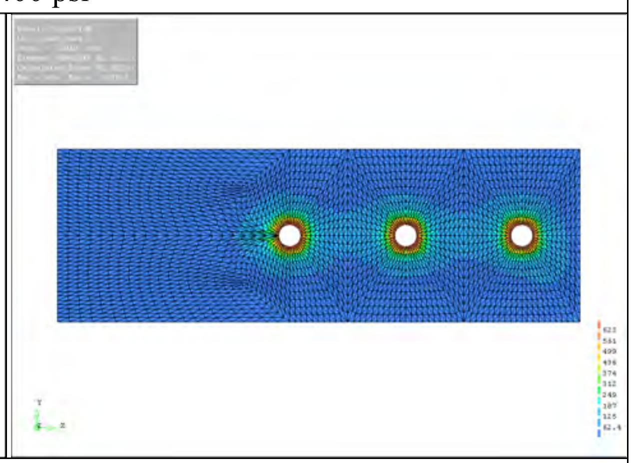

p_{int} = 600 psi

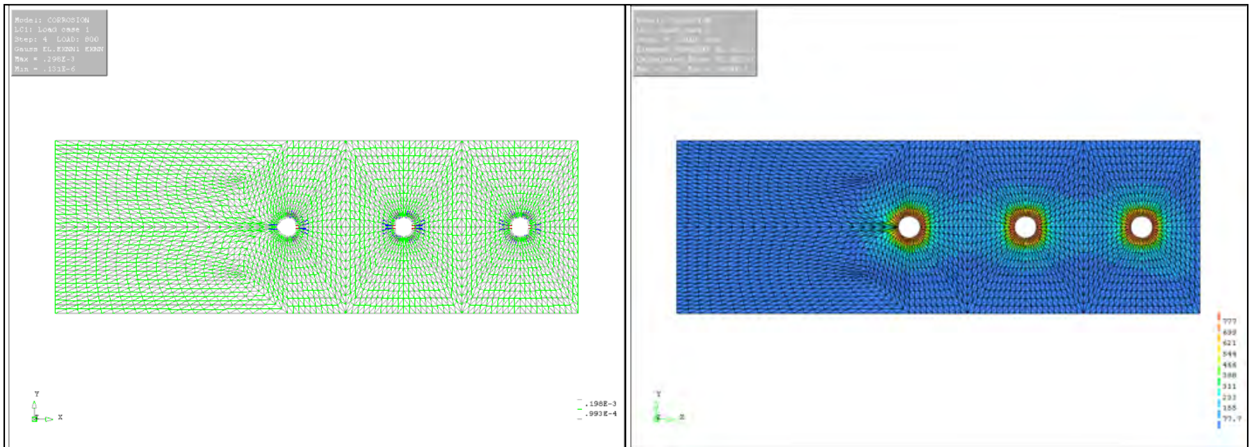

p_{int} = 800 psi

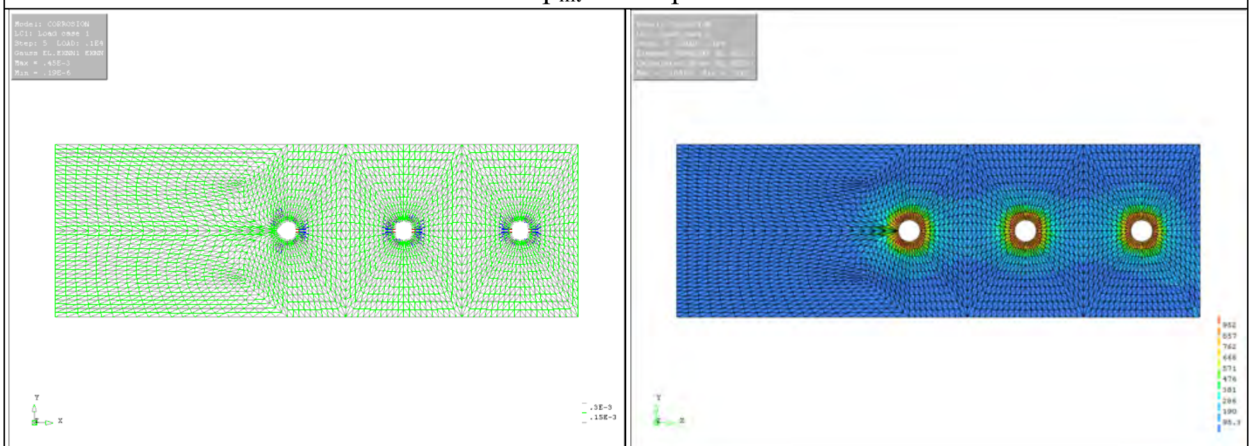

p_{int} = 1,000 psi

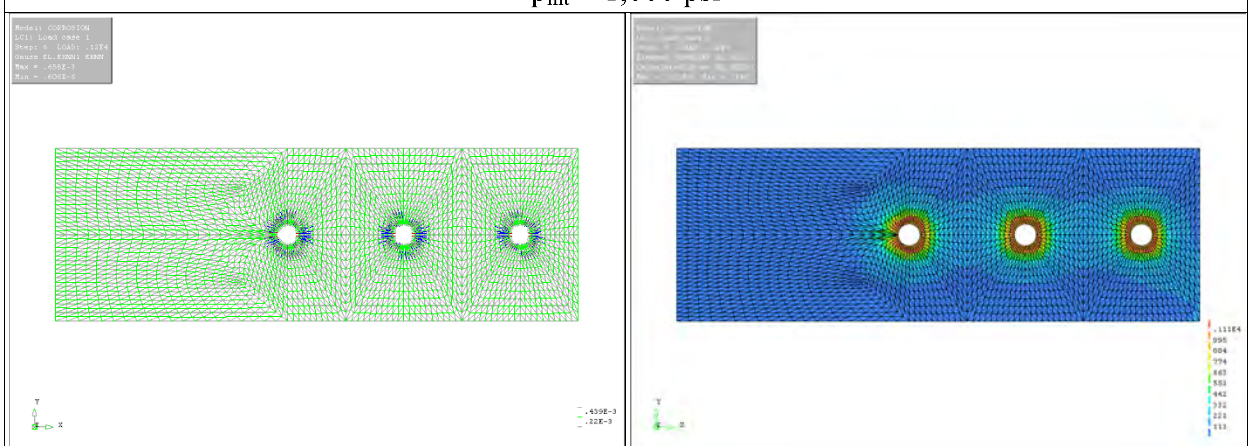

p_{int} = 1,200 psi

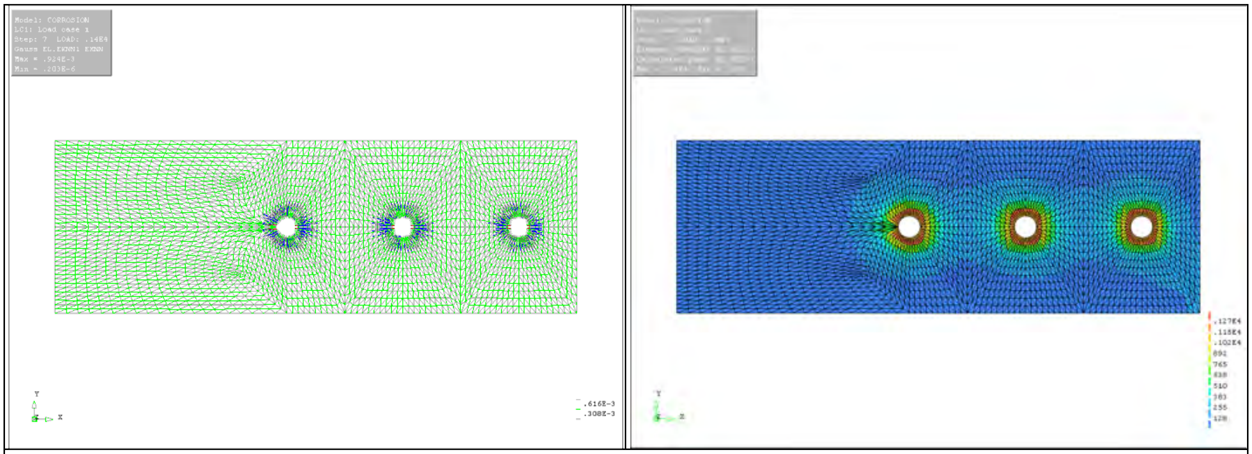

p_{int} = 1,400 psi

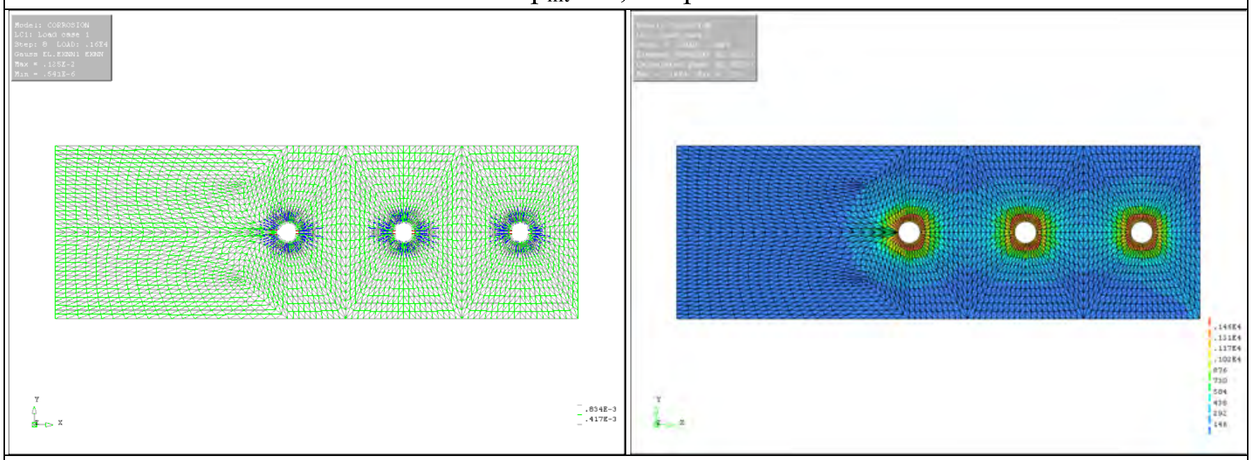

p_{int} = 1,600 psi

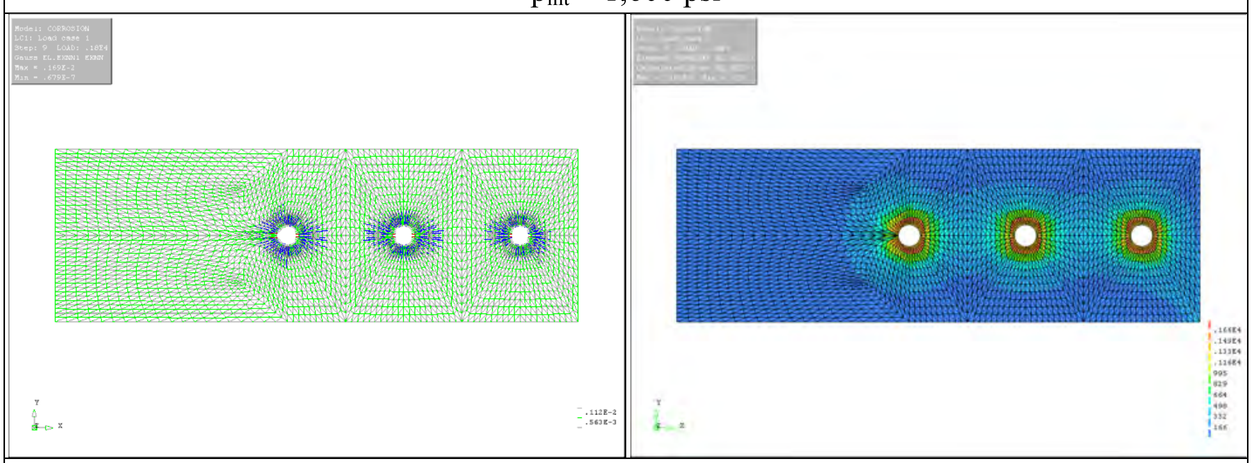

p_{int} = 1,800 psi

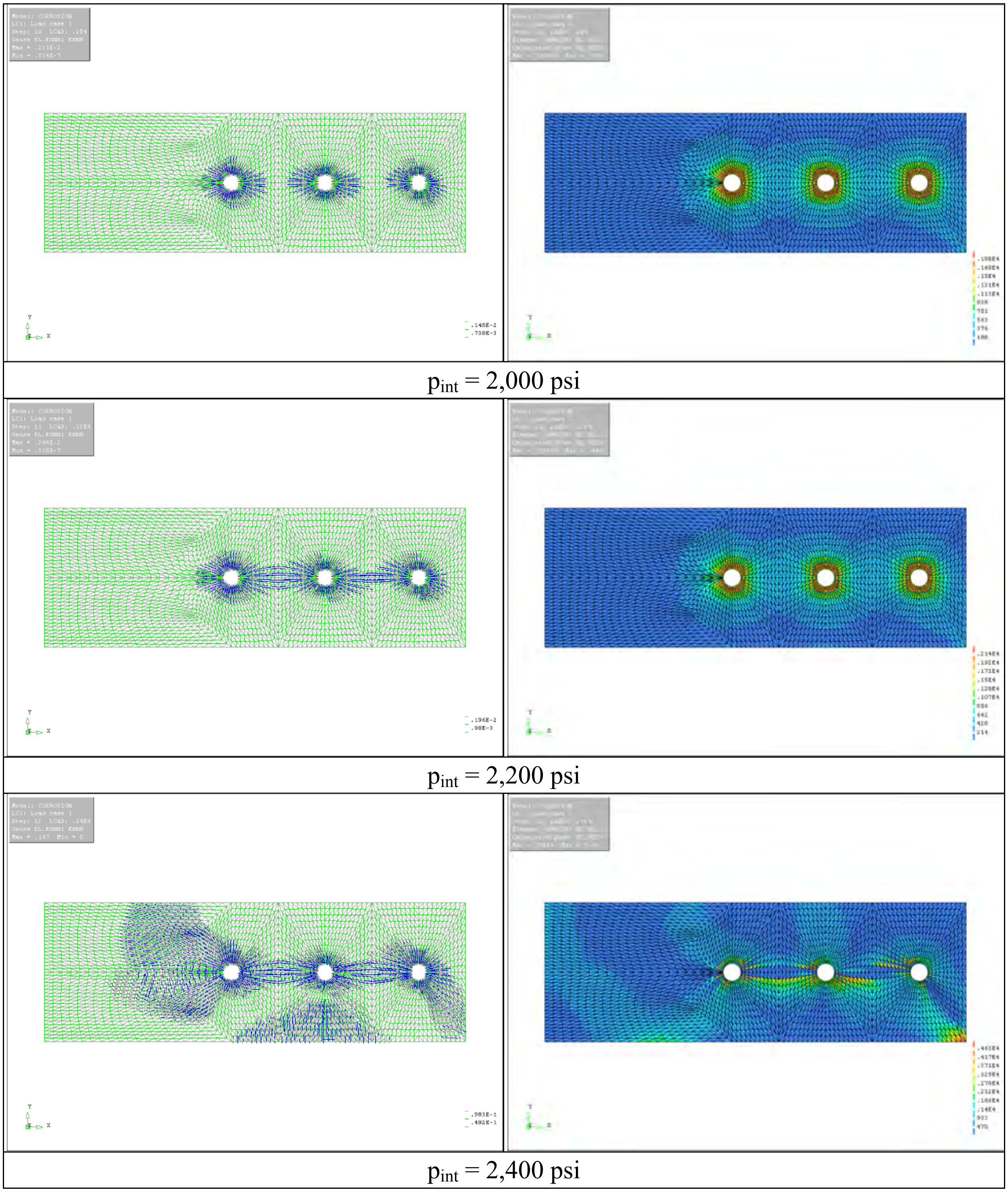

Figure D-6 Crack Patterns & Von Mises Stress Variations of Case I FE Model (Cover = 4.0 in.)

D.2.1.2 Case II FE analysis results

Crack patterns and corresponding Von Mises stress variations of Case II FE analyses are illustrated from Figure D-7 to Figure D-11. Each figure represents a different side cover, and results are presented with respect to incrementally increasing internal pressures.

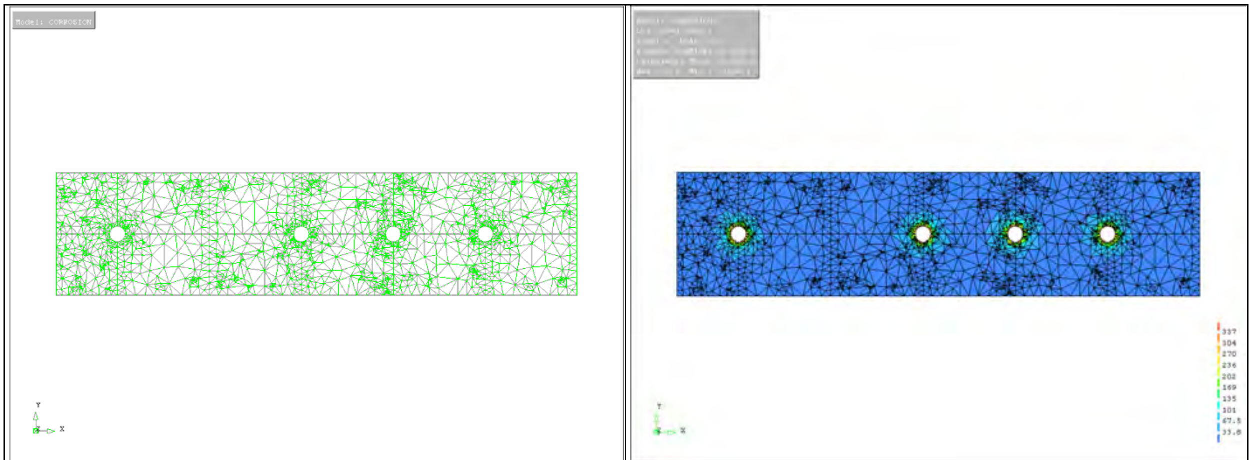

p_{int} = 200 psi

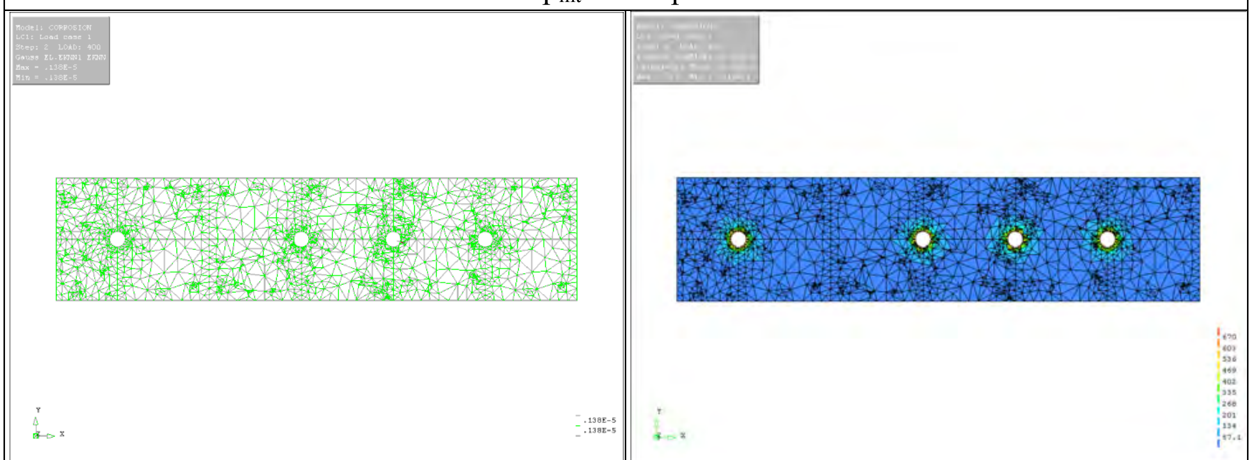

p_{int} = 400 psi

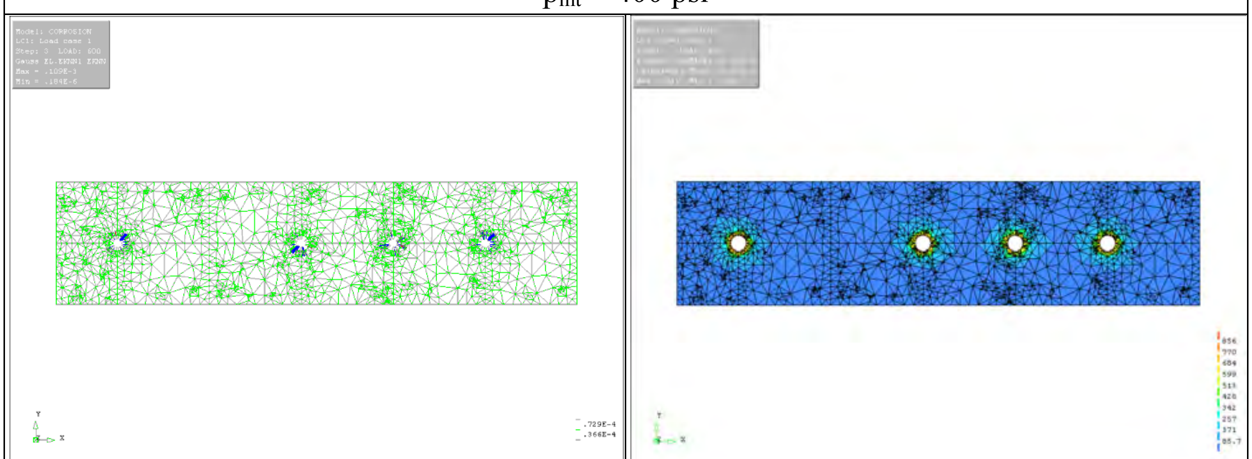

p_{int} = 600 psi

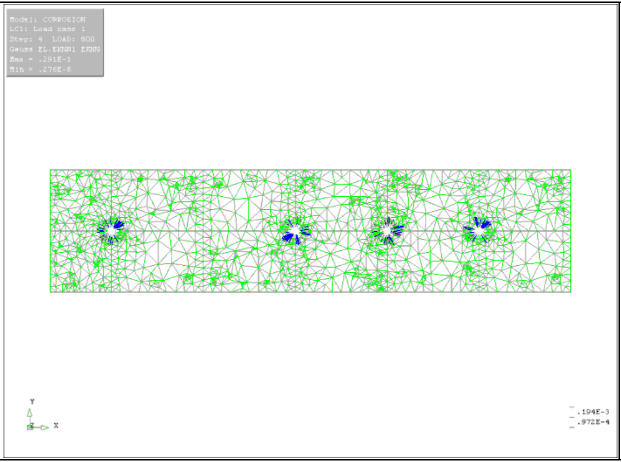
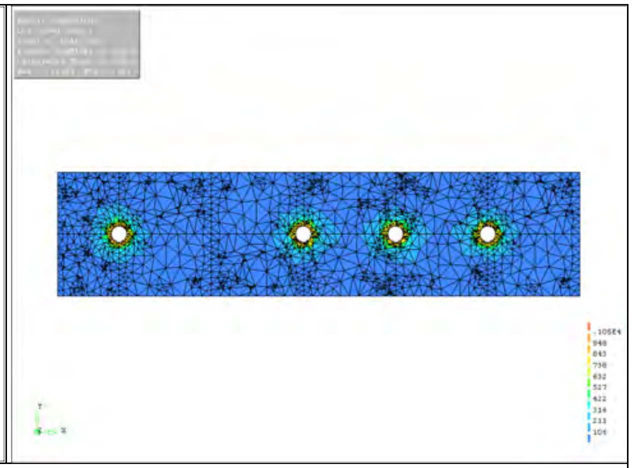

p_{int} = 800 psi

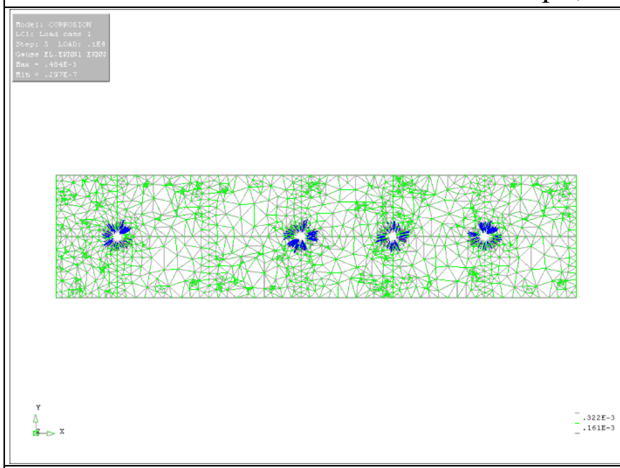
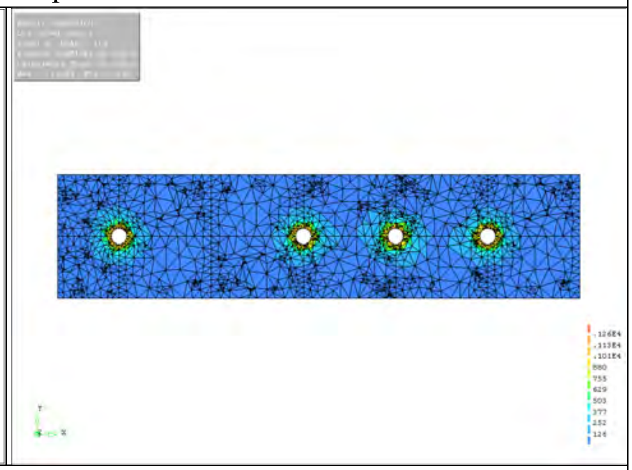

p_{int} = 1,000 psi

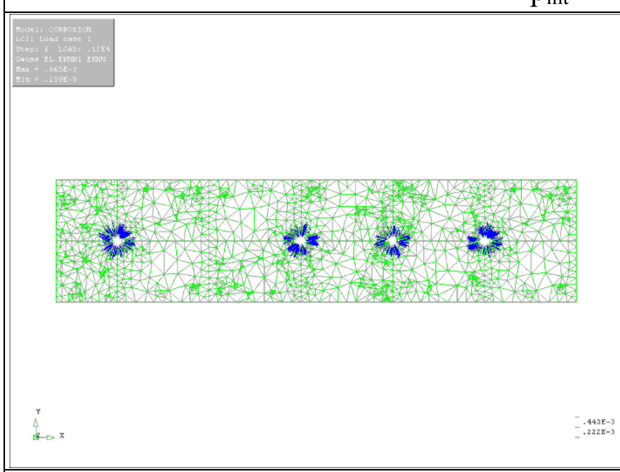
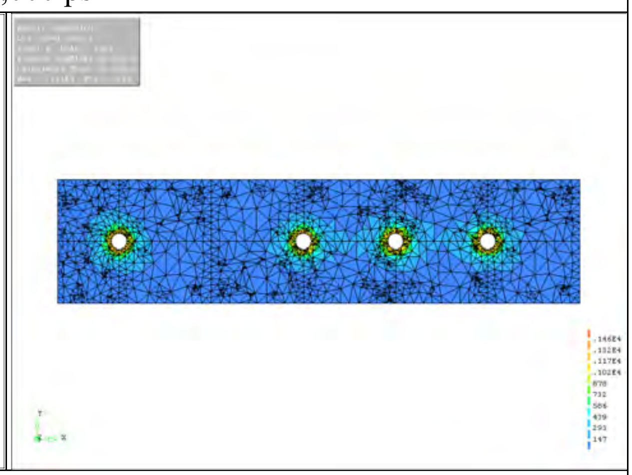

p_{int} = 1,200 psi

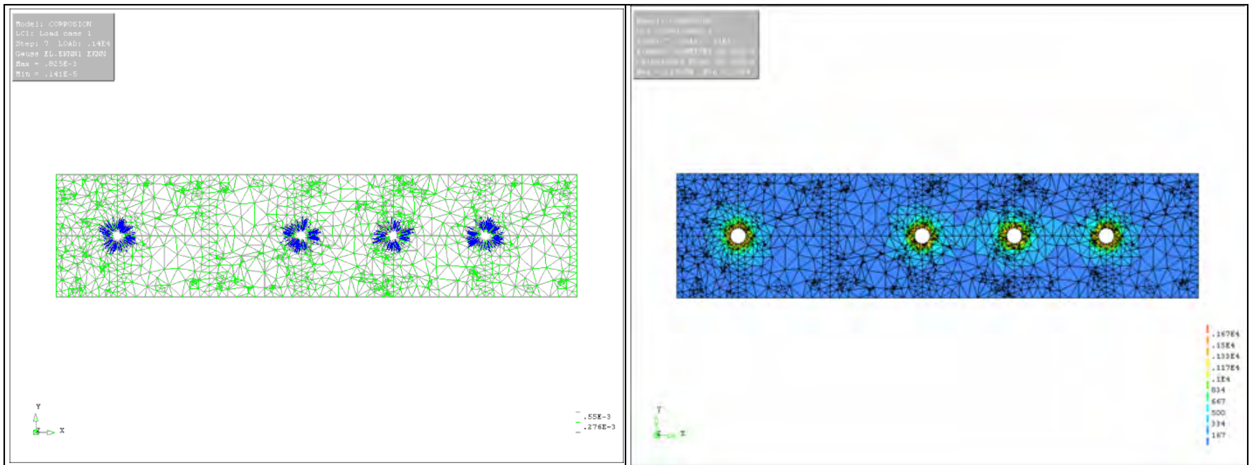

p_{int} = 1,400 psi

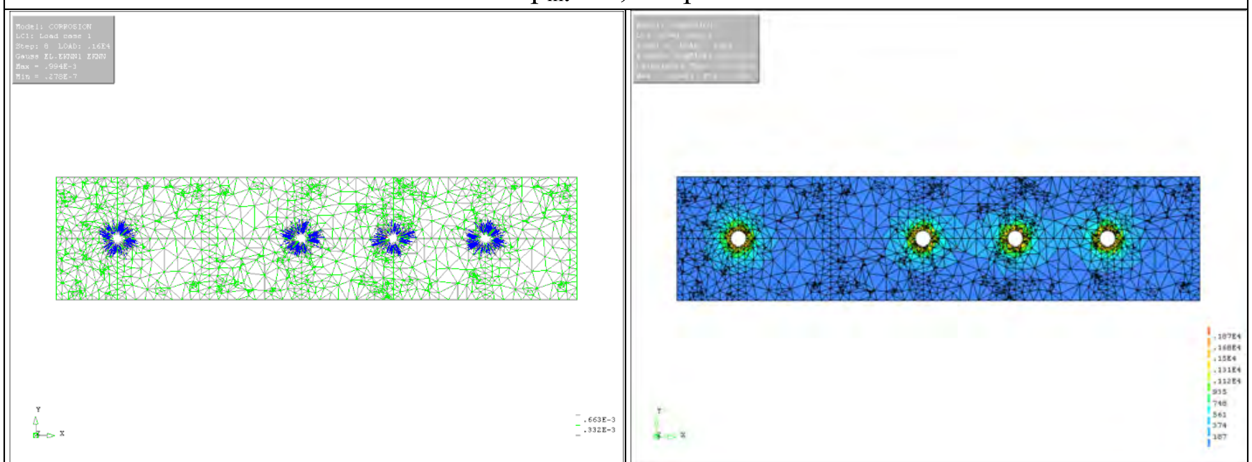

p_{int} = 1,600 psi

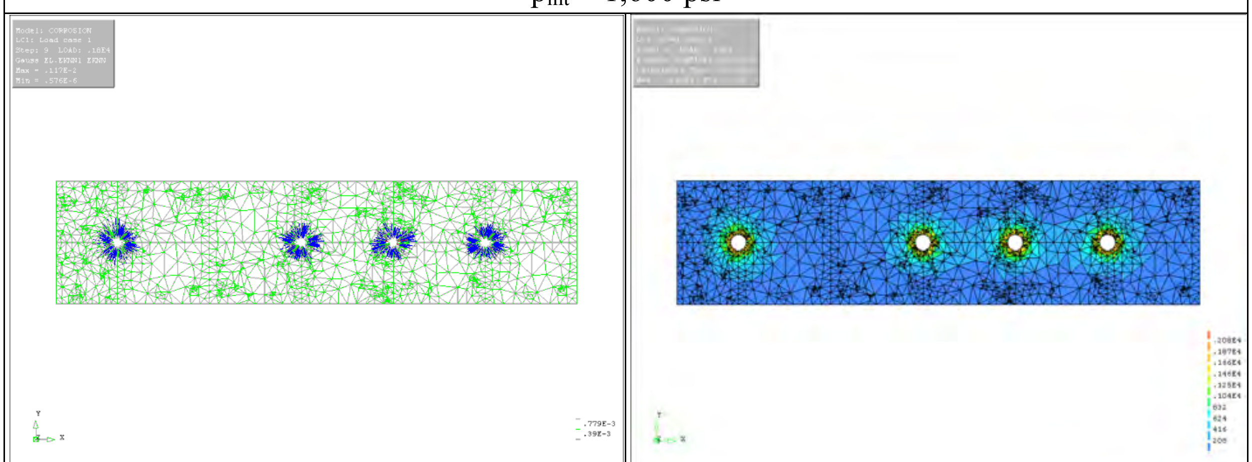

p_{int} = 1,800 psi

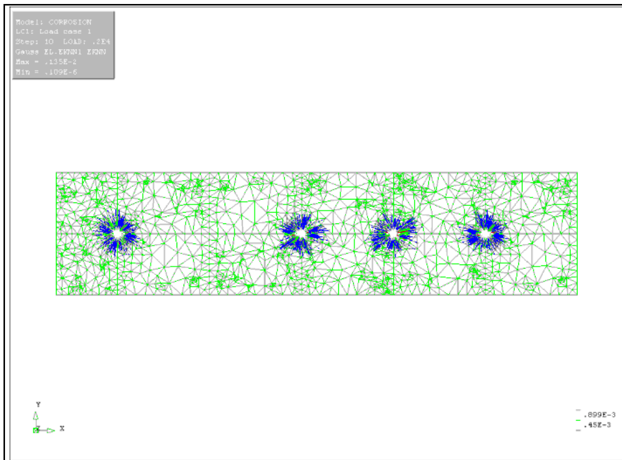
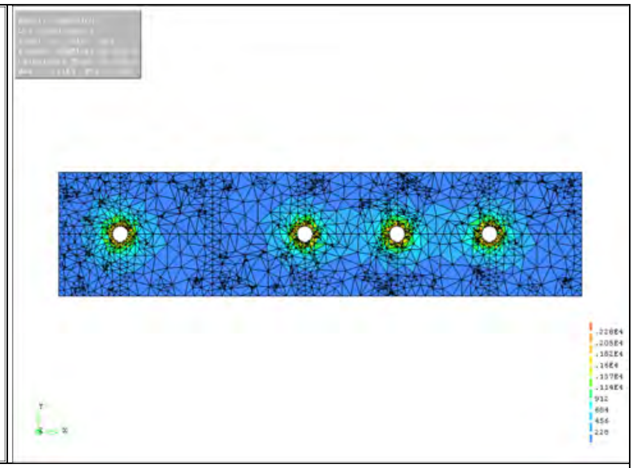

p_{int} = 2,000 psi

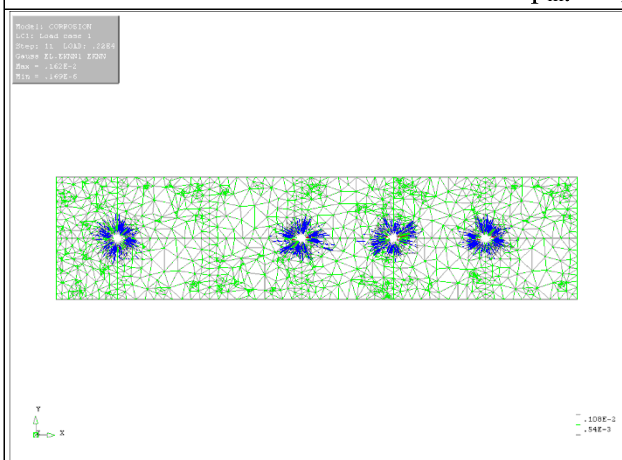
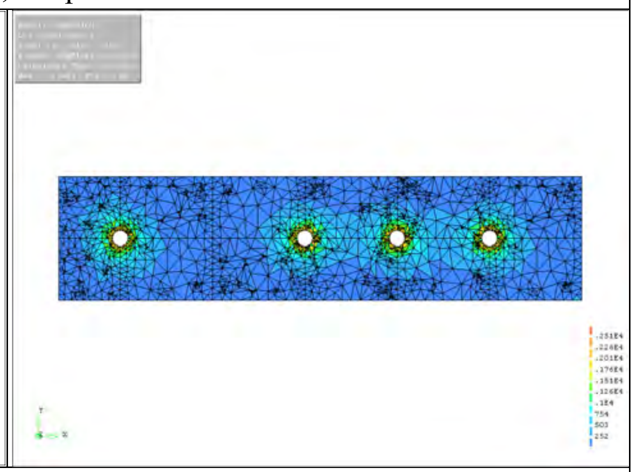

p_{int} = 2,200 psi

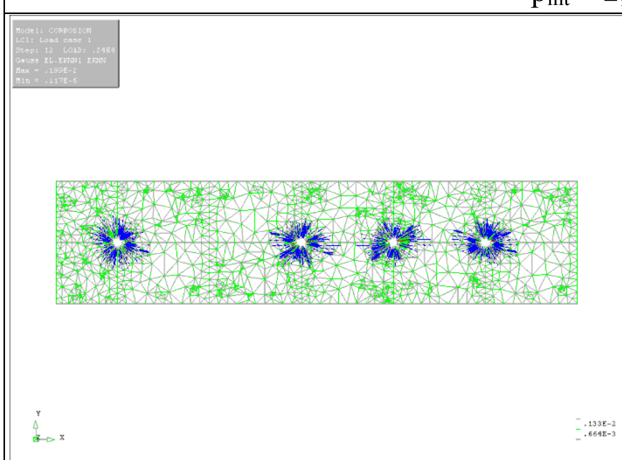
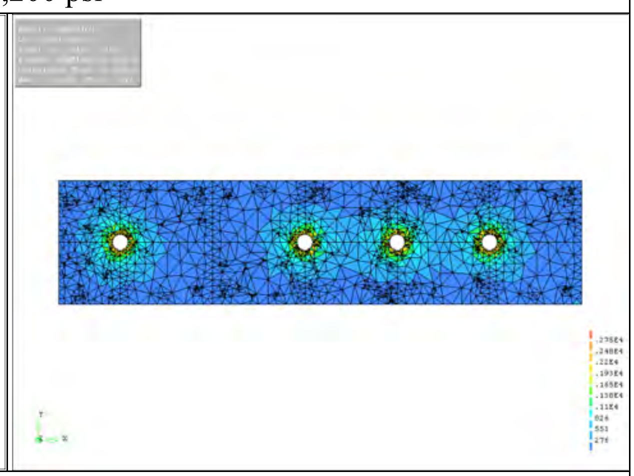

p_{int} = 2,400 psi

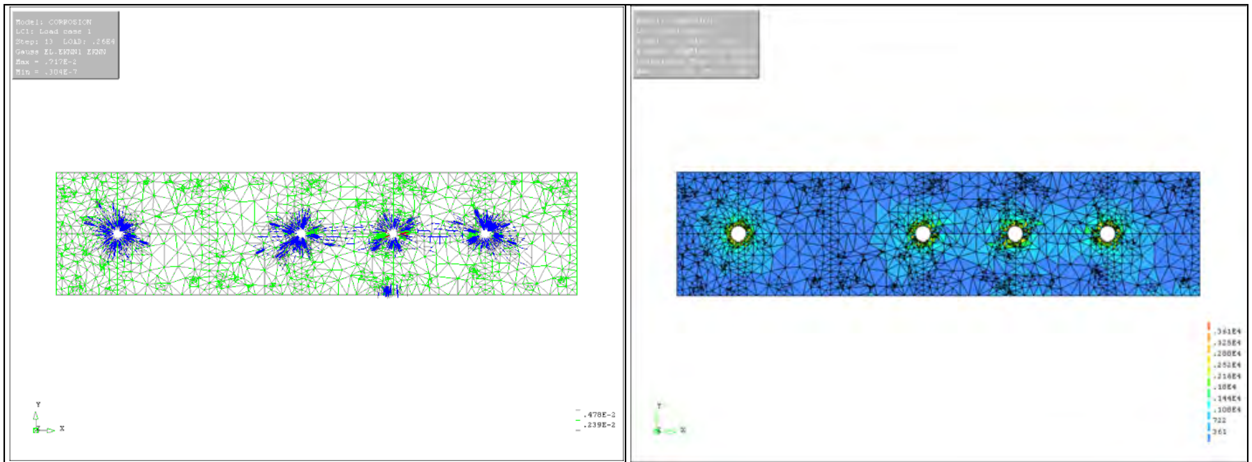

p_{int} = 2,600 psi

Figure D-7 Crack Patterns & Von Mises Stress Variations of Case II FE Model (Cover = 1.5 in.)

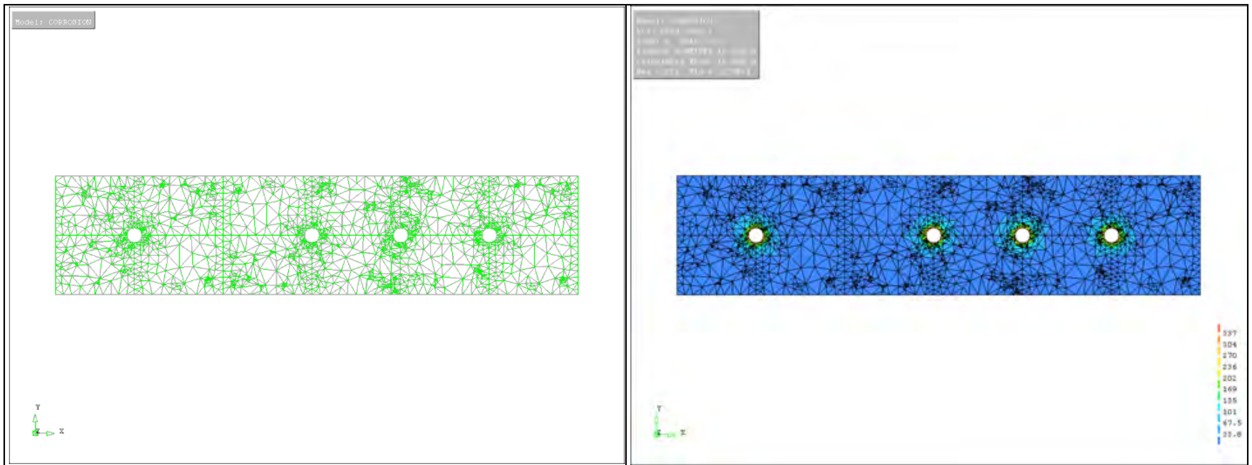

p_{int} = 200 psi

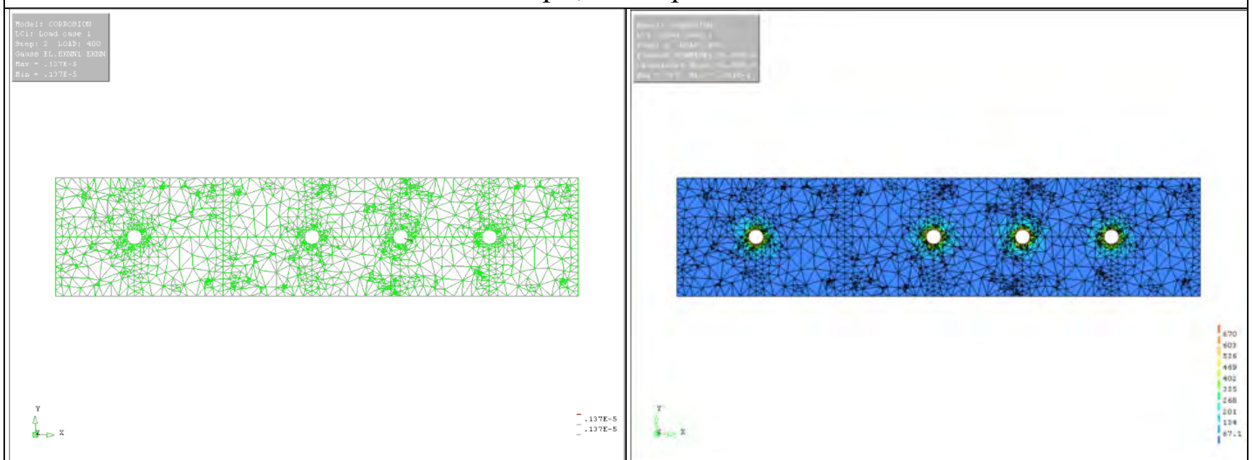

p_{int} = 400 psi

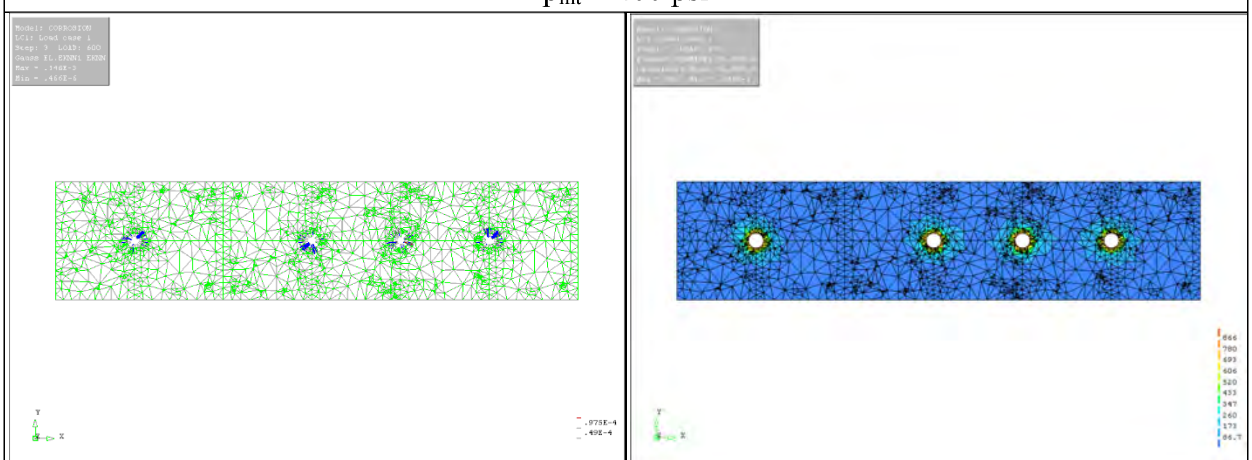

p_{int} = 600 psi

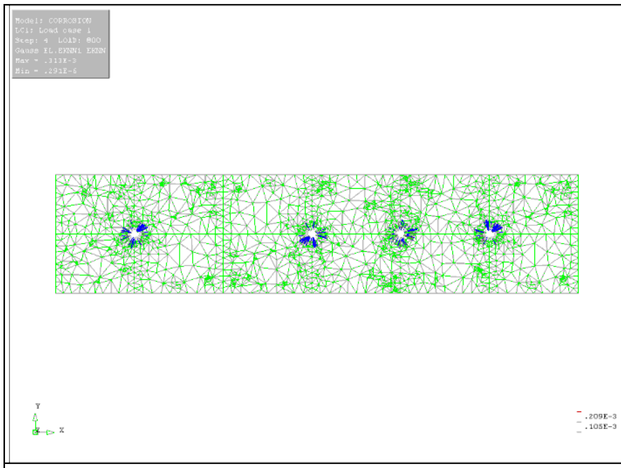
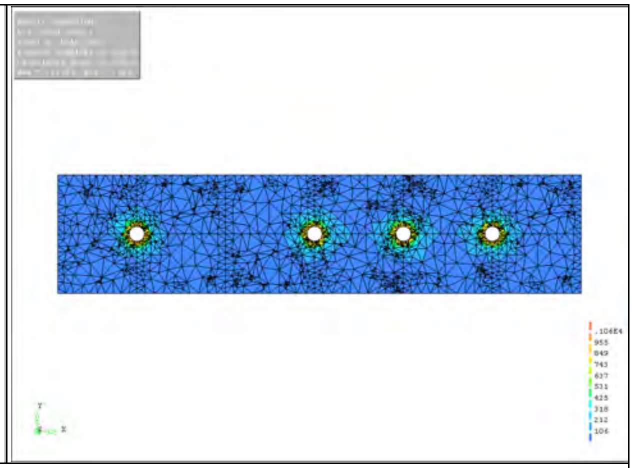

p_{int} = 800 psi

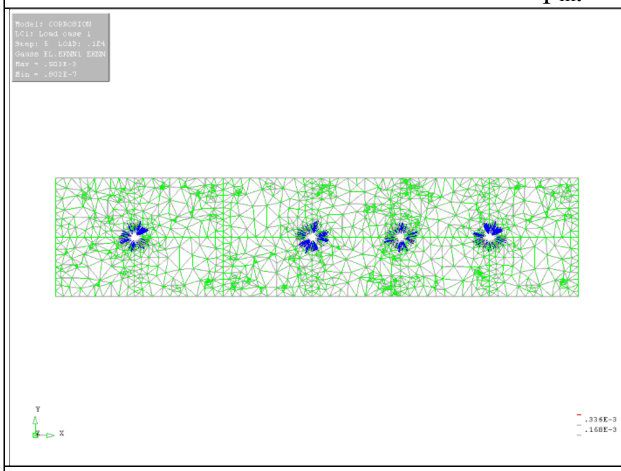
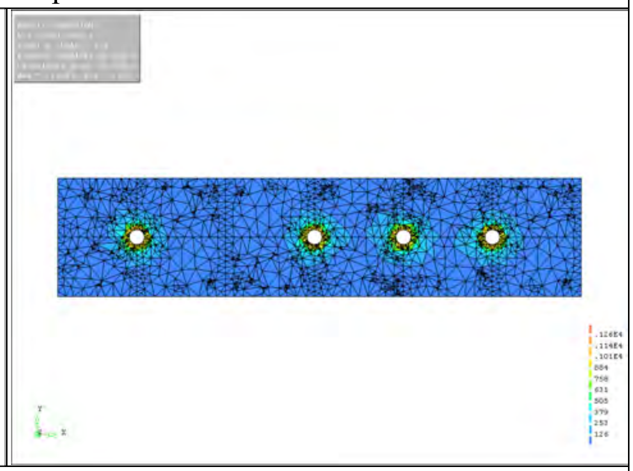

p_{int} = 1,000 psi

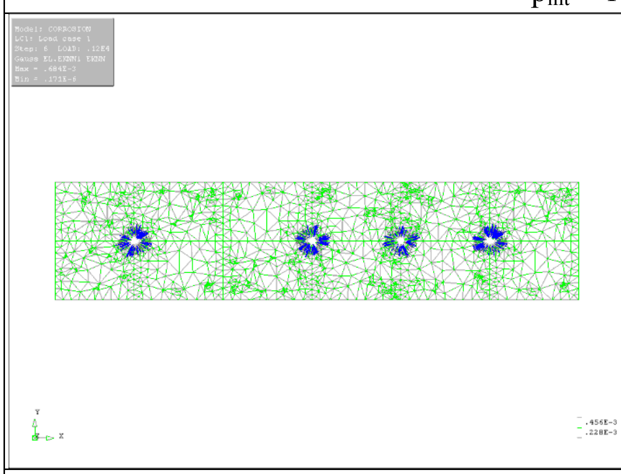
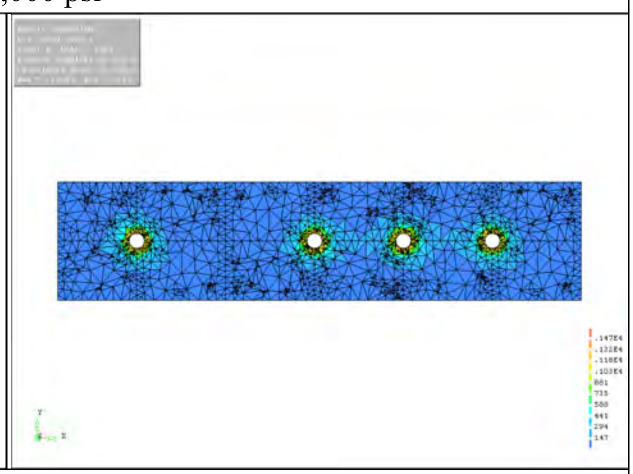

p_{int} = 1,200 psi

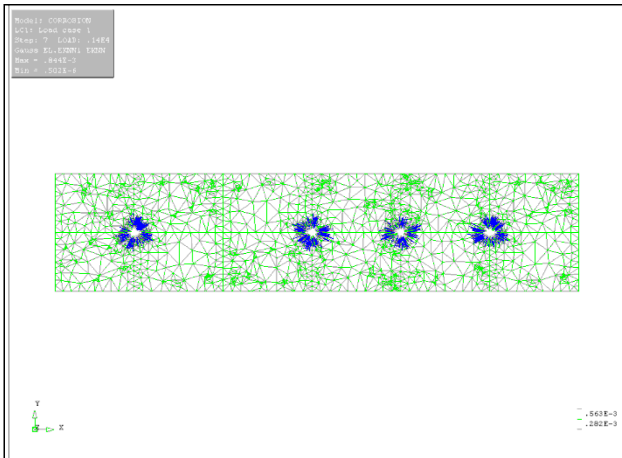
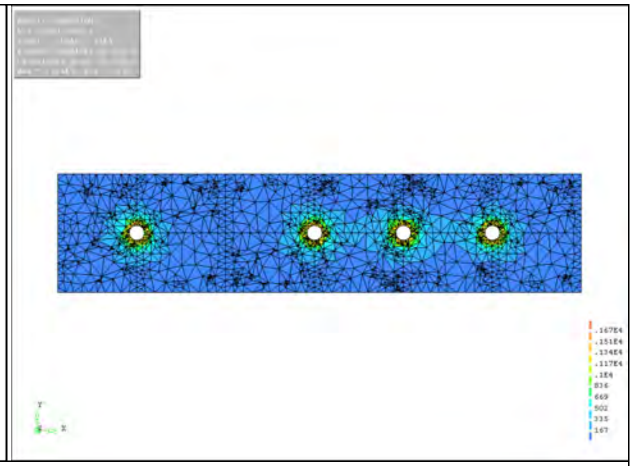

p_{int} = 1,400 psi

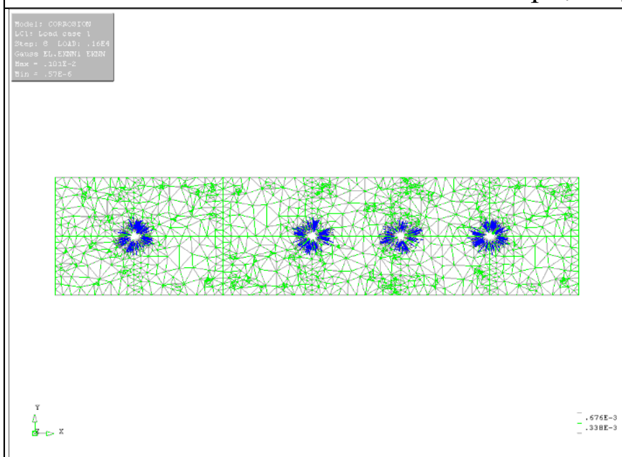
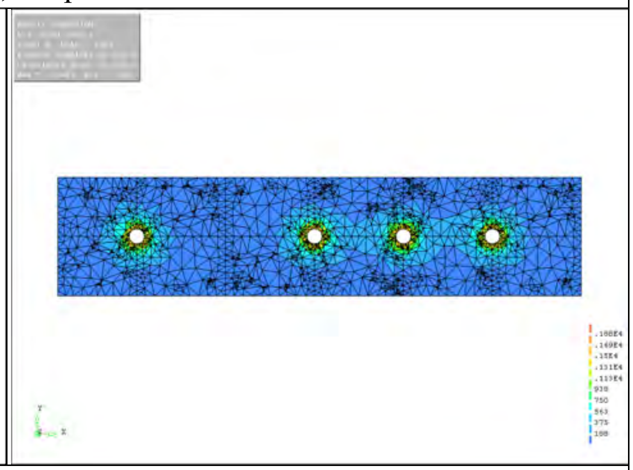

p_{int} = 1,600 psi

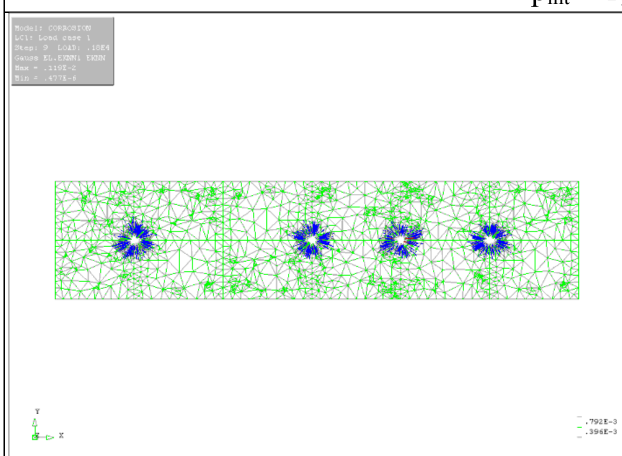
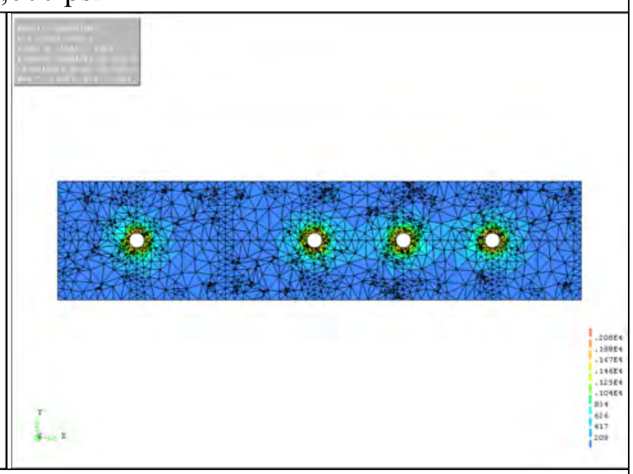

p_{int} = 1,800 psi

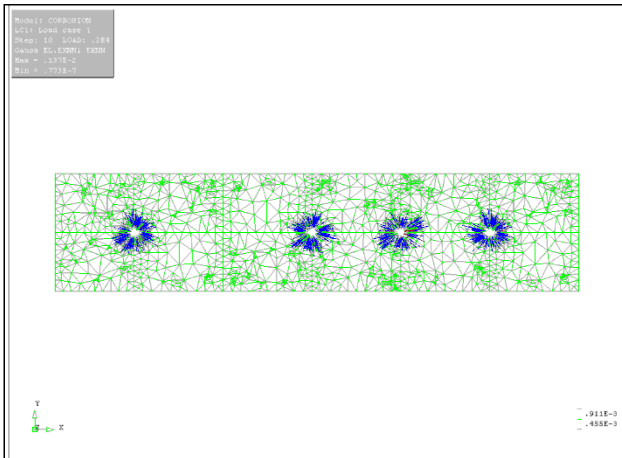

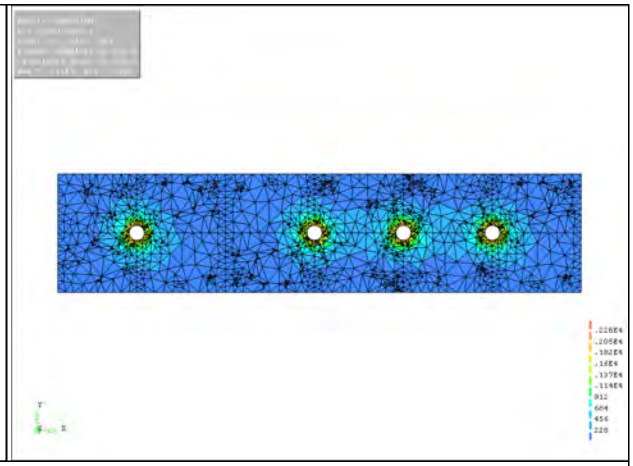

p_{int} = 2,000 psi

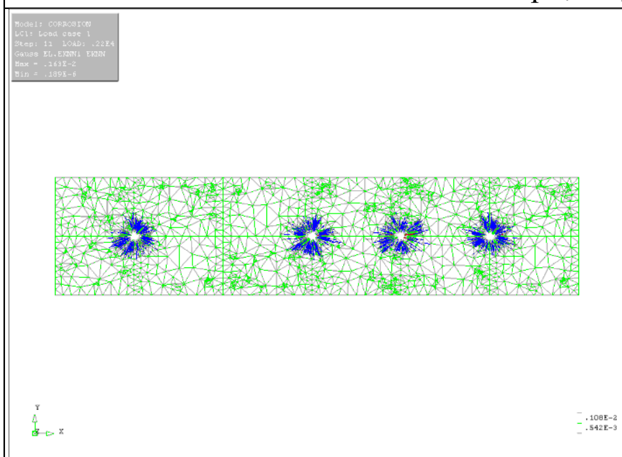

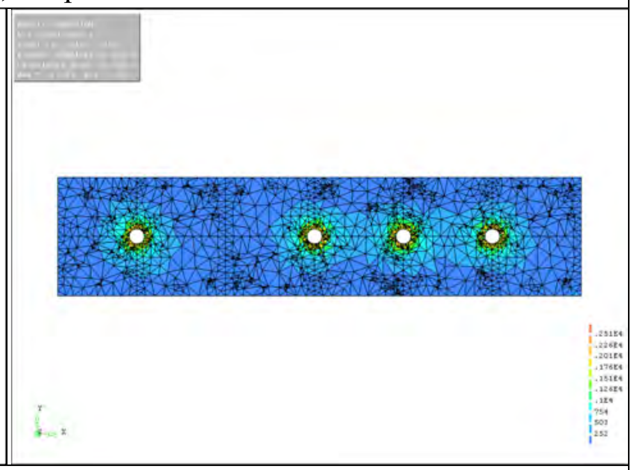

p_{int} = 2,200 psi

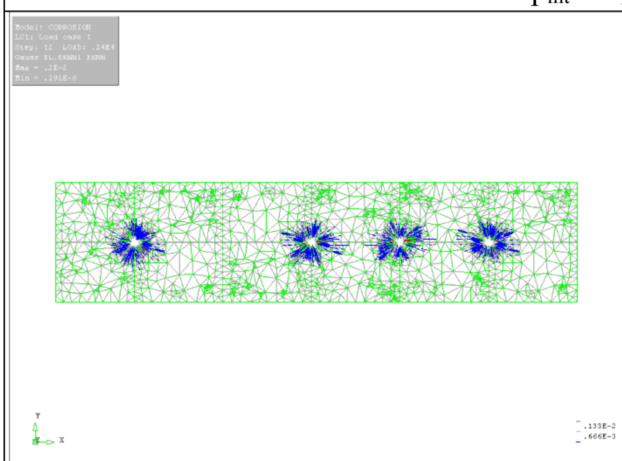

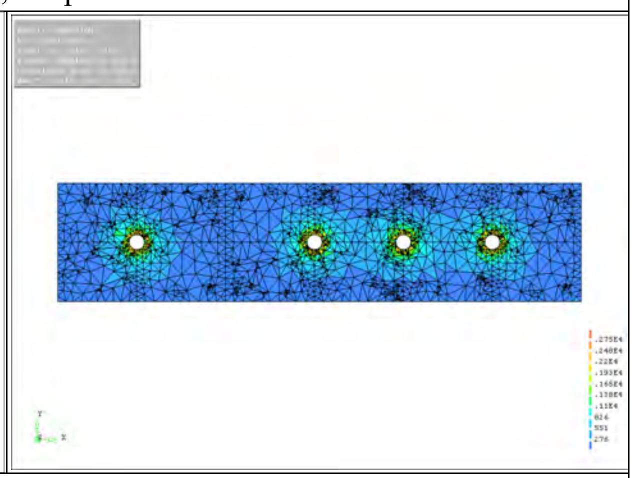

p_{int} = 2,400 psi

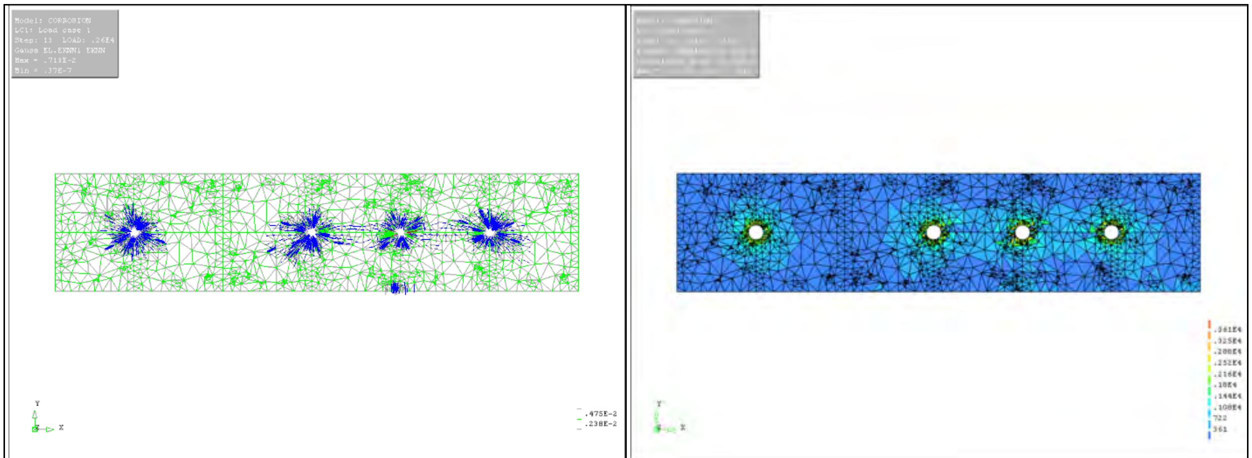

p_{int} = 2,600 psi

Figure D-8 Crack Patterns & Von Mises Stress Variations of Case II FE Model (Cover = 2.0 in.)

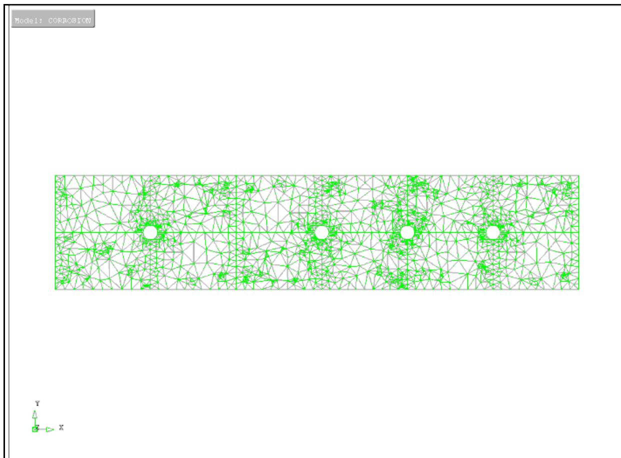
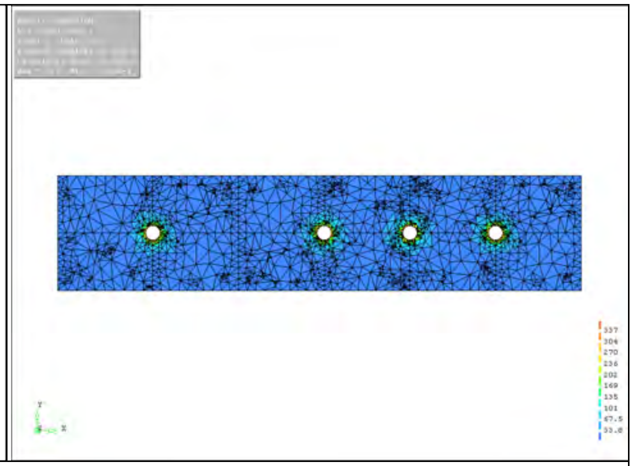

p_{int} = 200 psi

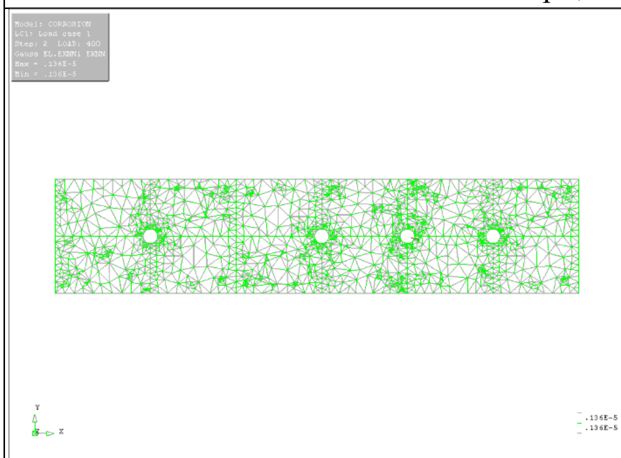
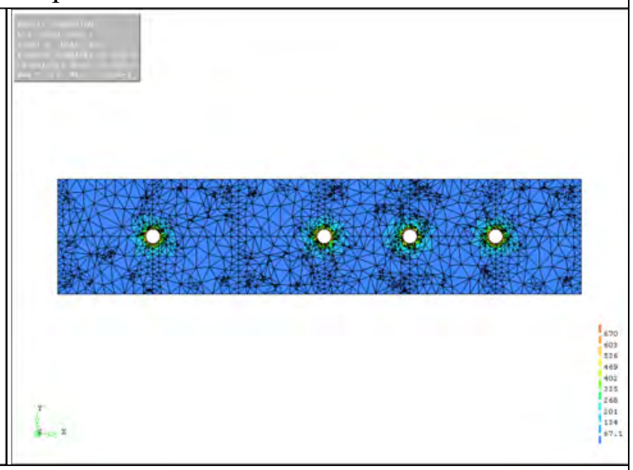

p_{int} = 400 psi

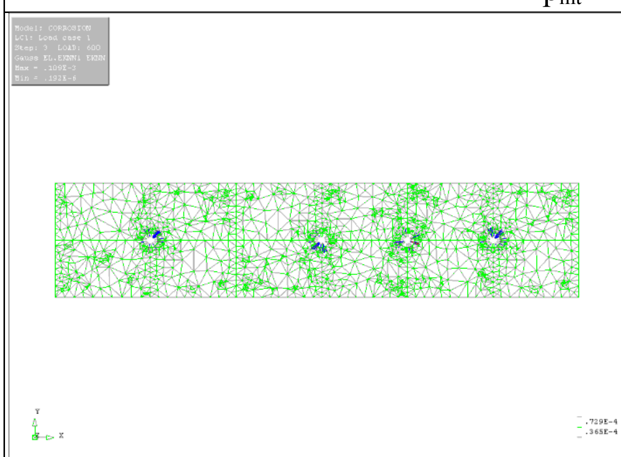
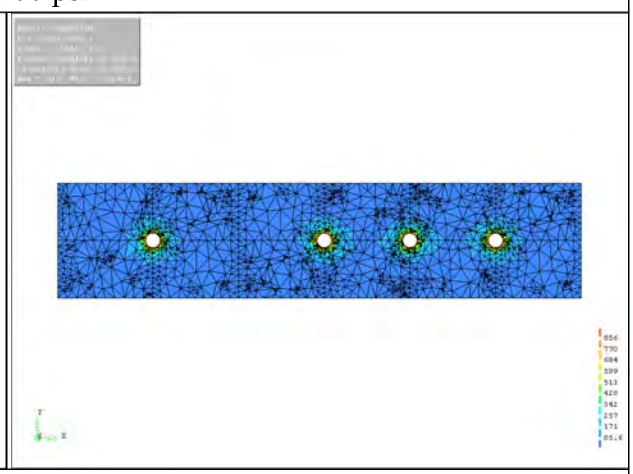

p_{int} = 600 psi

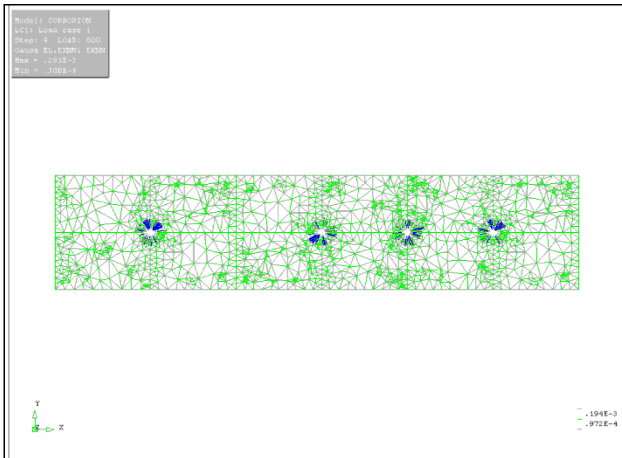
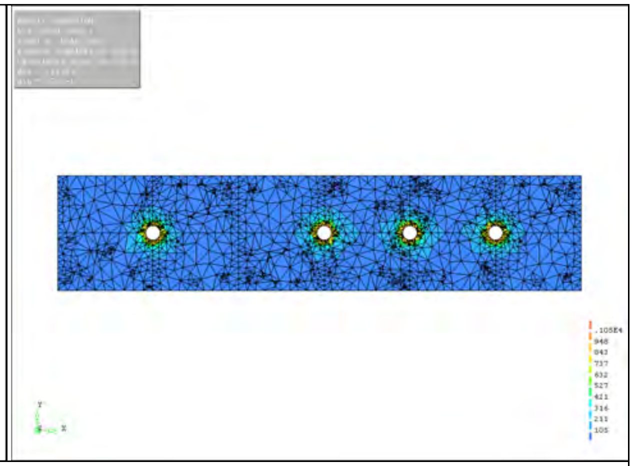

p_{int} = 800 psi

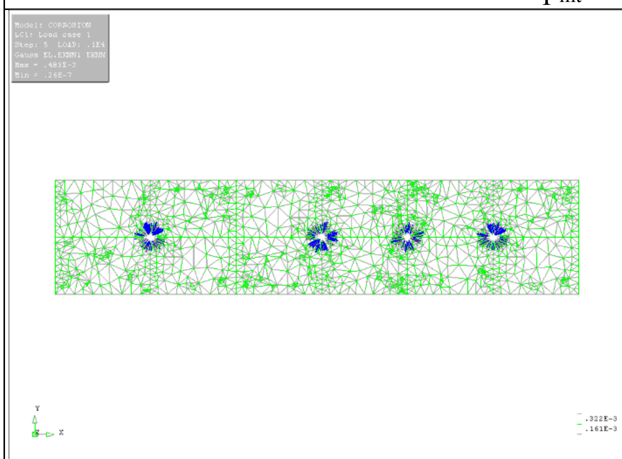
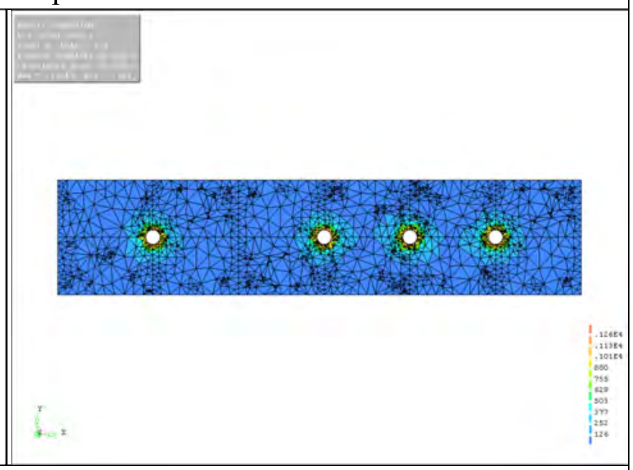

p_{int} = 1,000 psi

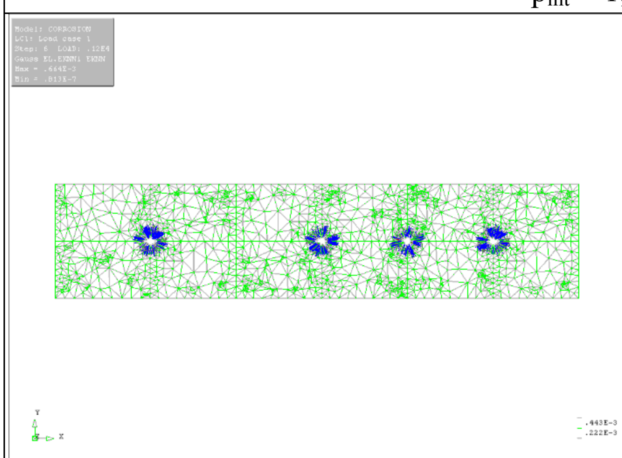
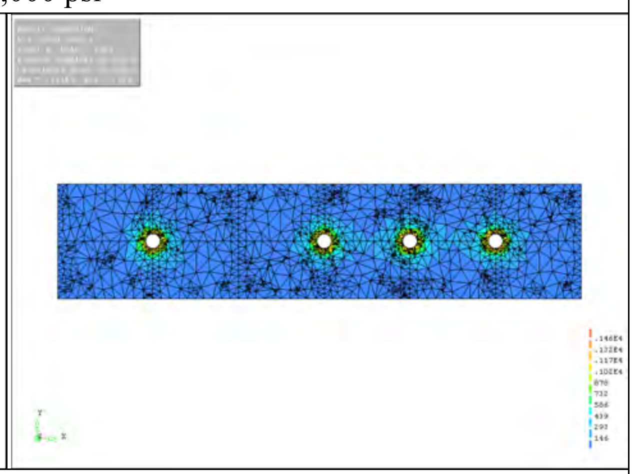

p_{int} = 1,200 psi

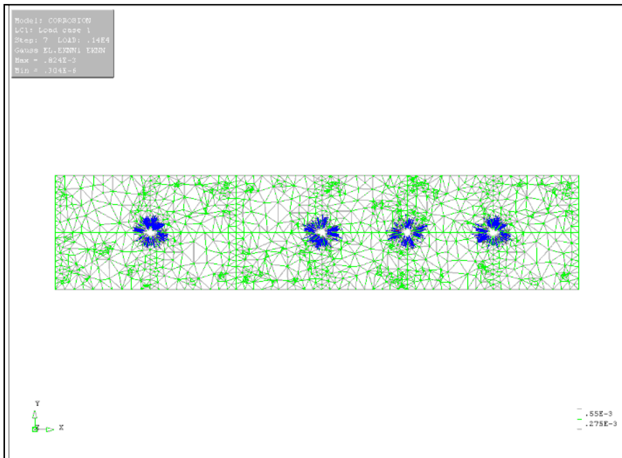

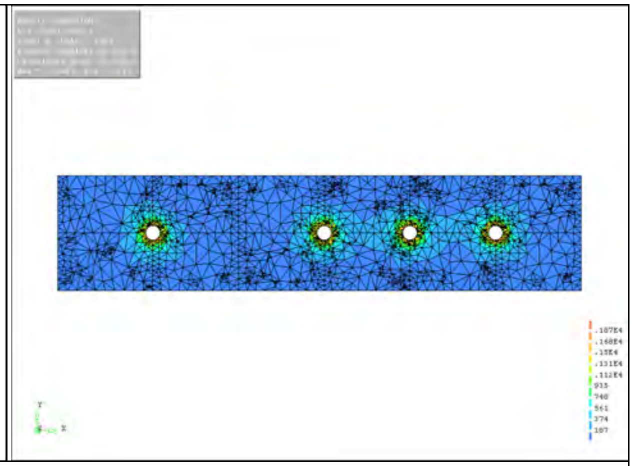

p_{int} = 1,400 psi

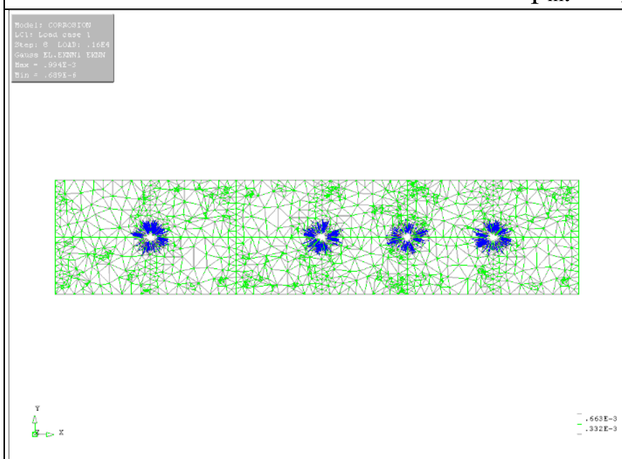

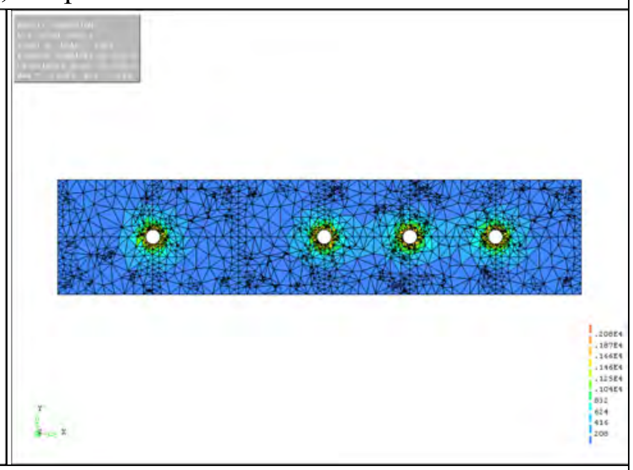

p_{int} = 1,600 psi

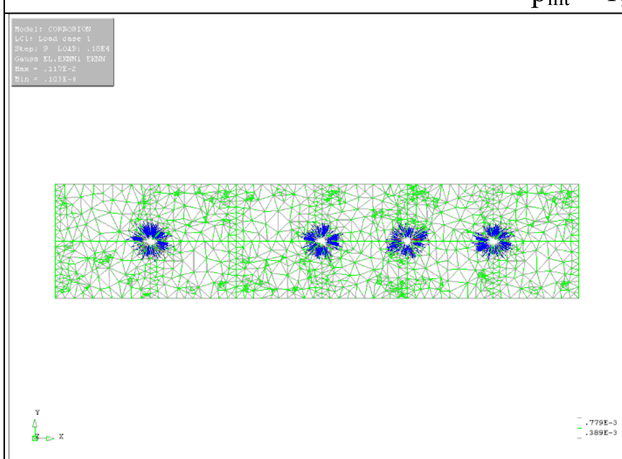

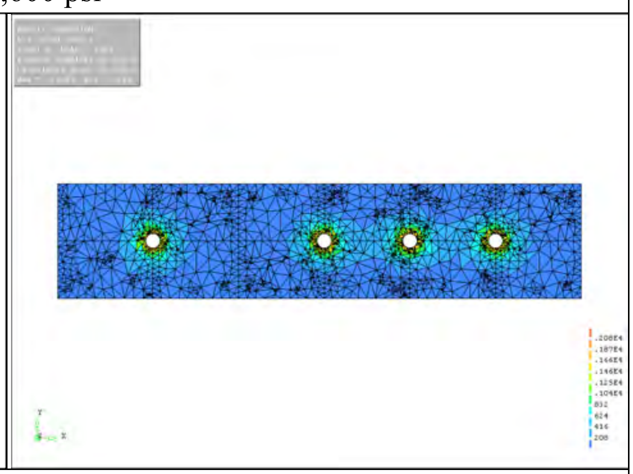

p_{int} = 1,800 psi

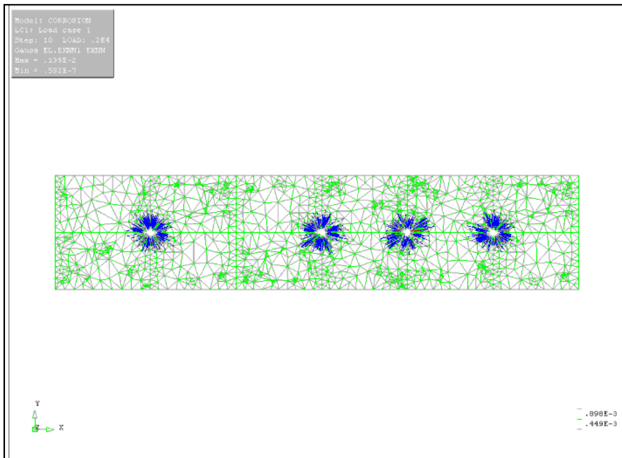
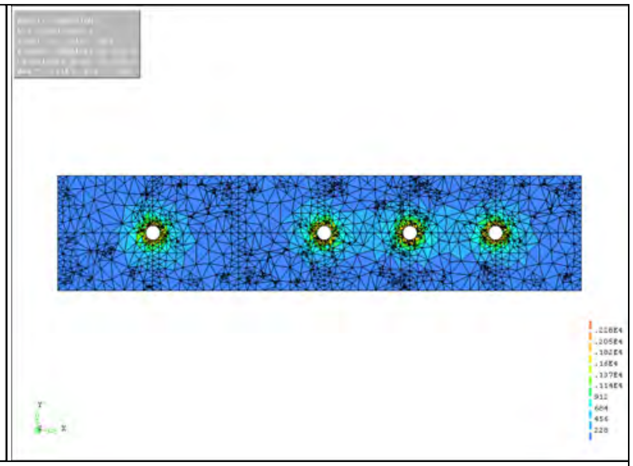

p_{int} = 2,000 psi

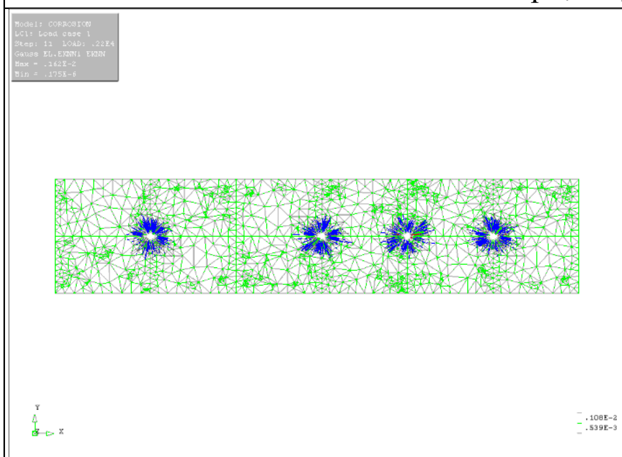
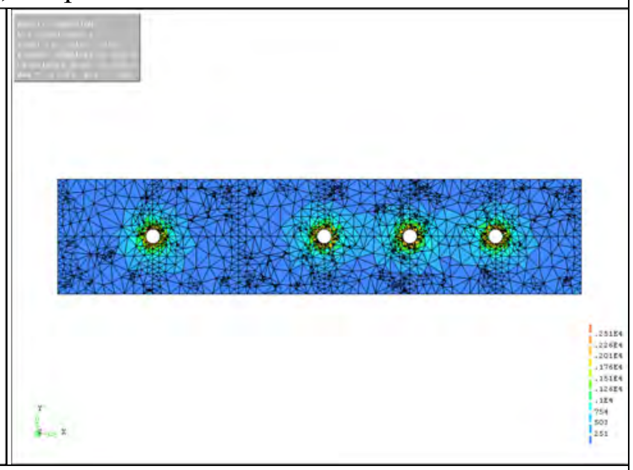

p_{int} = 2,200 psi

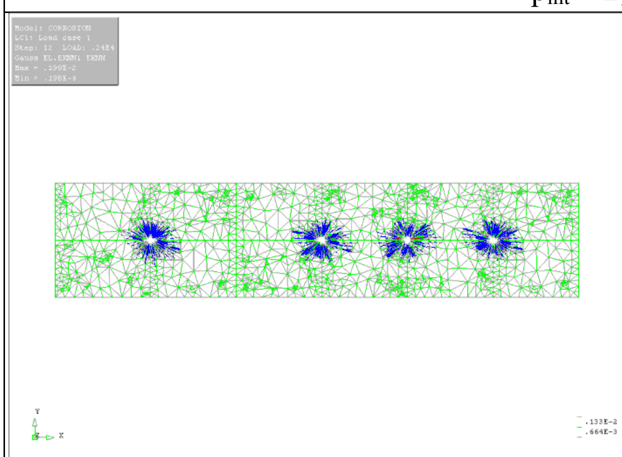
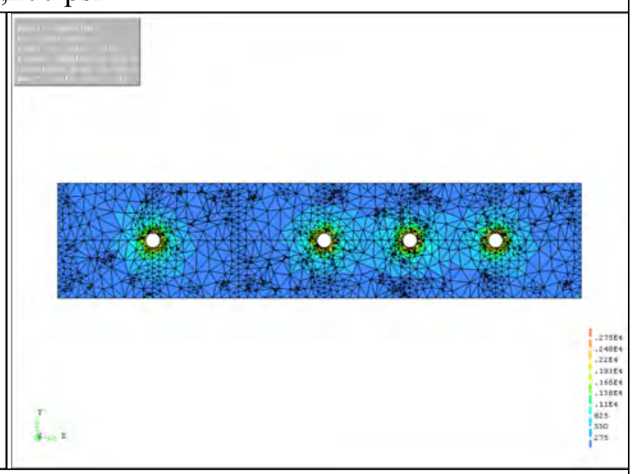

p_{int} = 2,400 psi

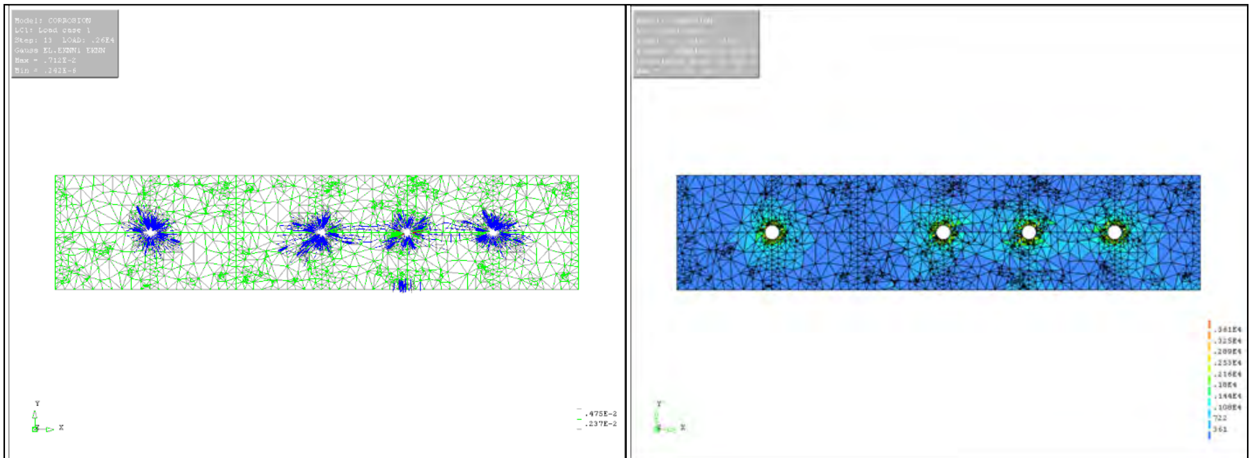

p_{int} = 2,600 psi

Figure D-9 Crack Patterns & Von Mises Stress Variations of Case II FE Model (Cover = 2.5 in.)

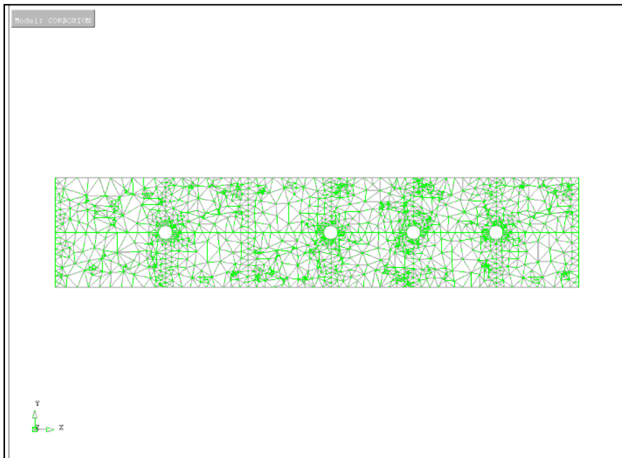
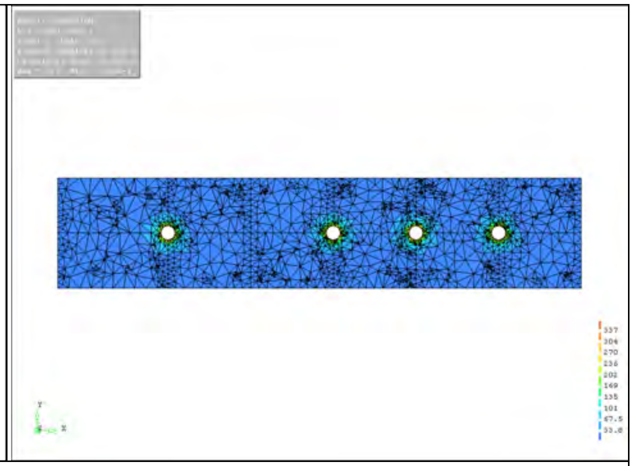

p_{int} = 200 psi

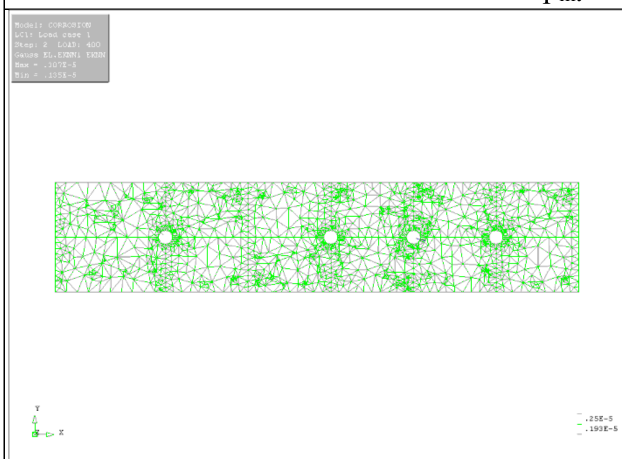
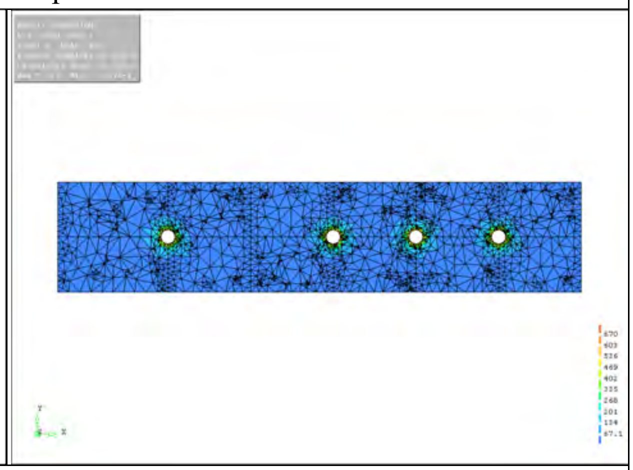

p_{int} = 400 psi

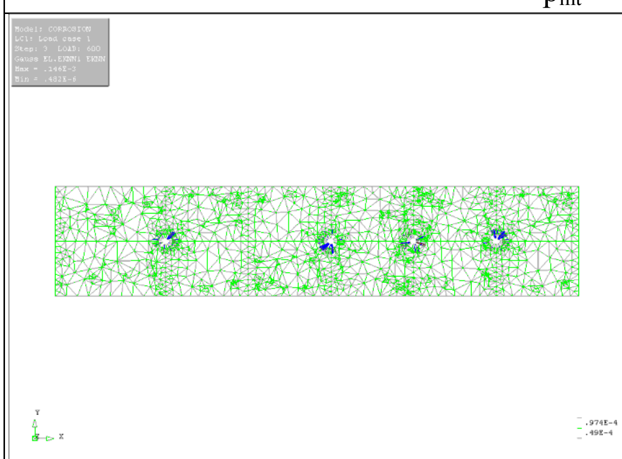
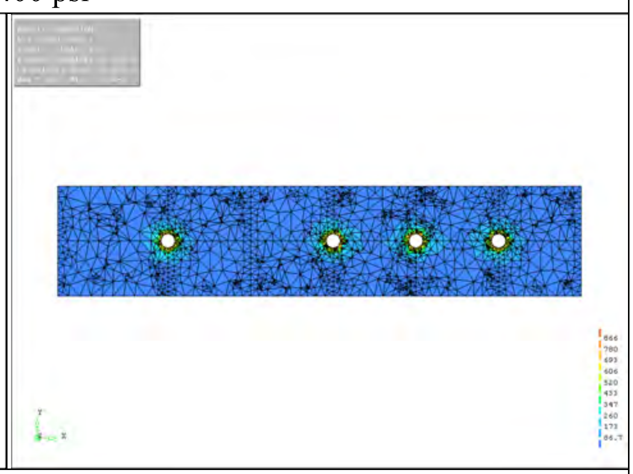

p_{int} = 600 psi

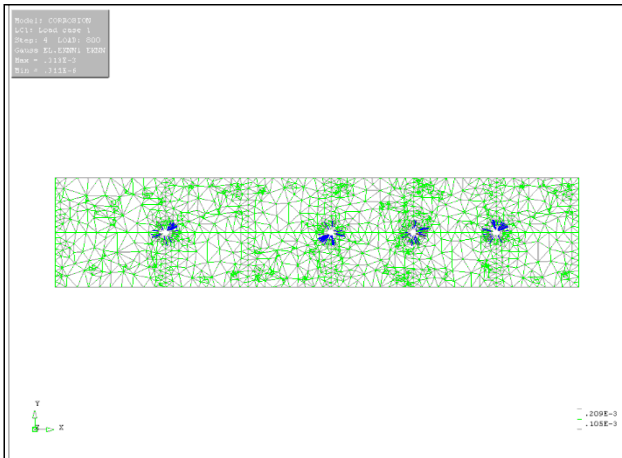
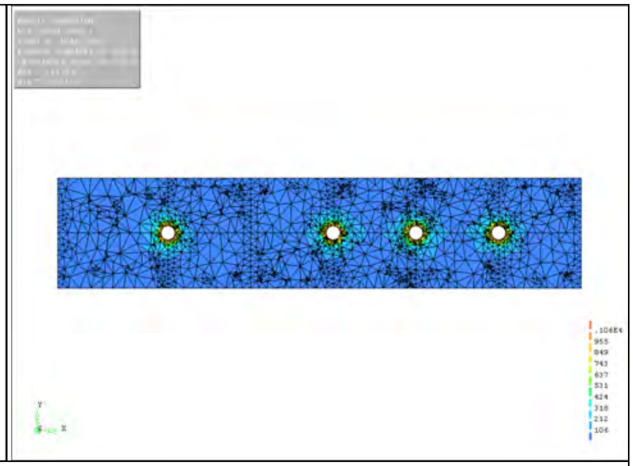

p_{int} = 800 psi

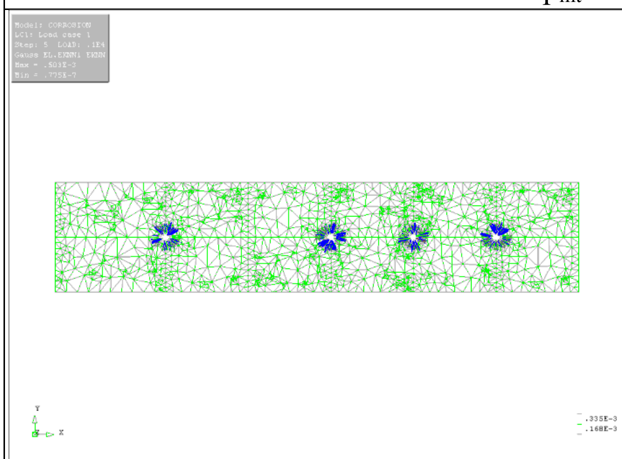
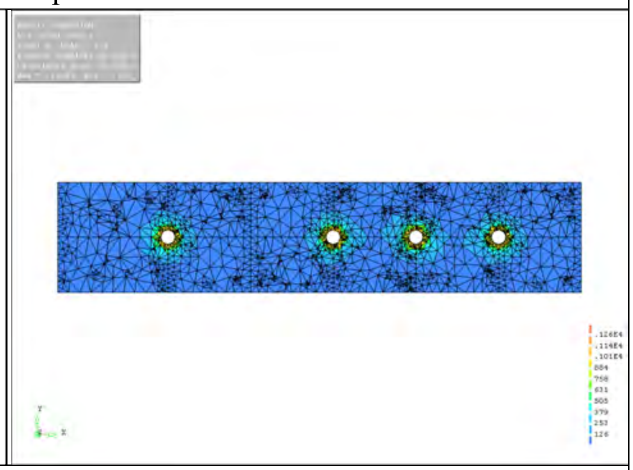

p_{int} = 1,000 psi

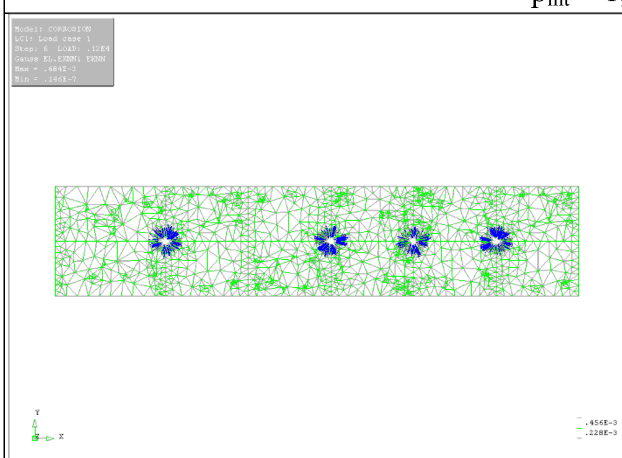
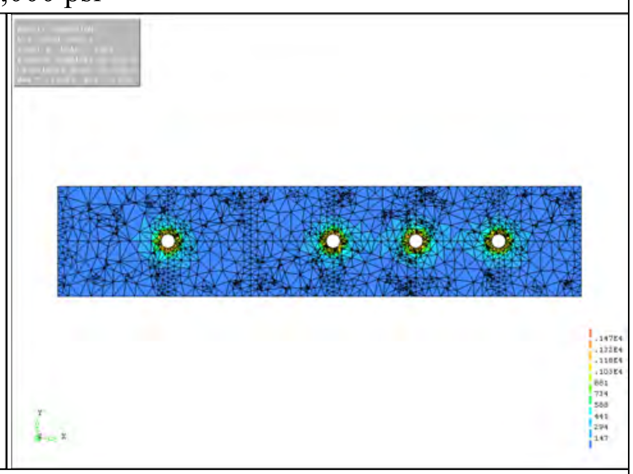

p_{int} = 1,200 psi

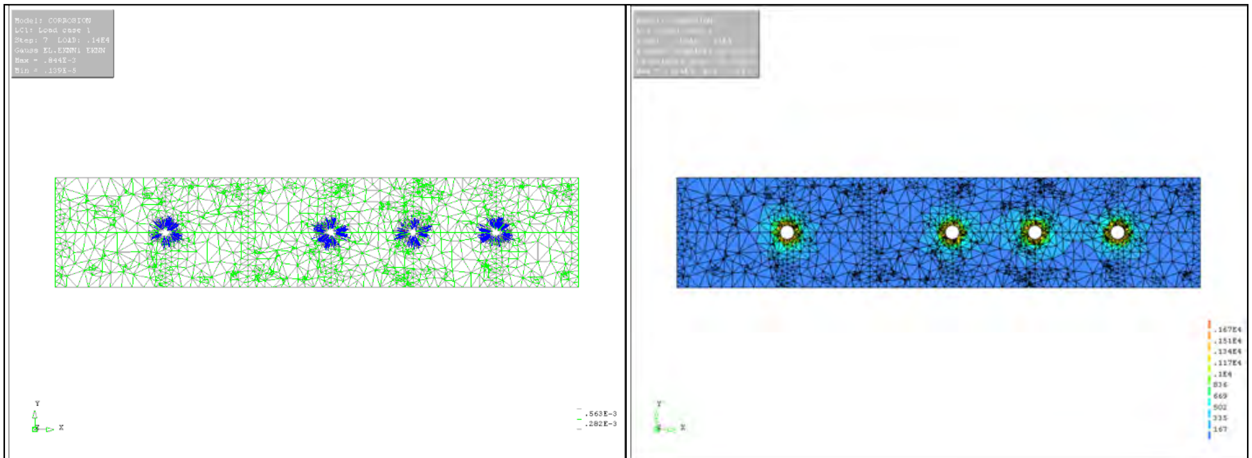

p_{int} = 1,400 psi

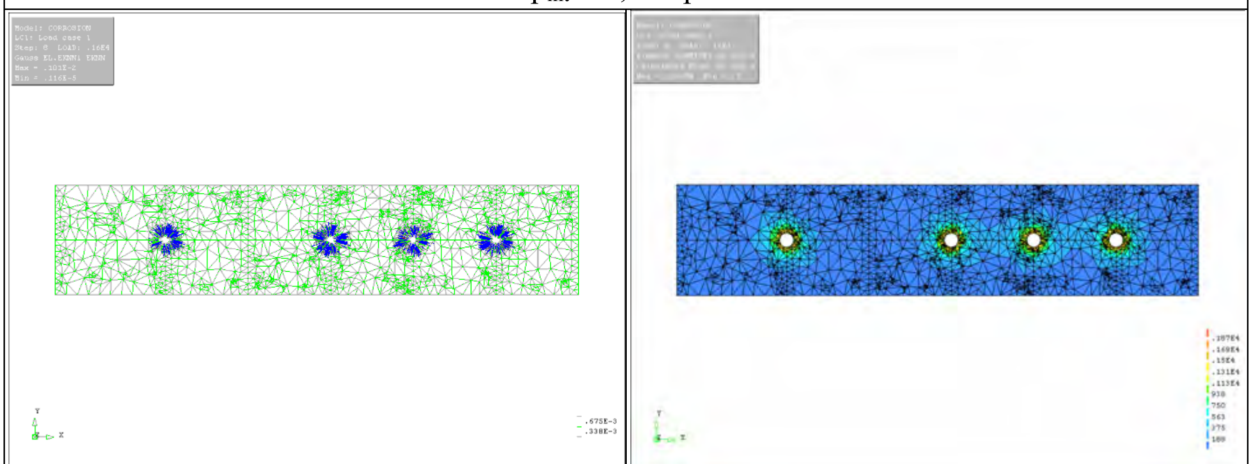

p_{int} = 1,600 psi

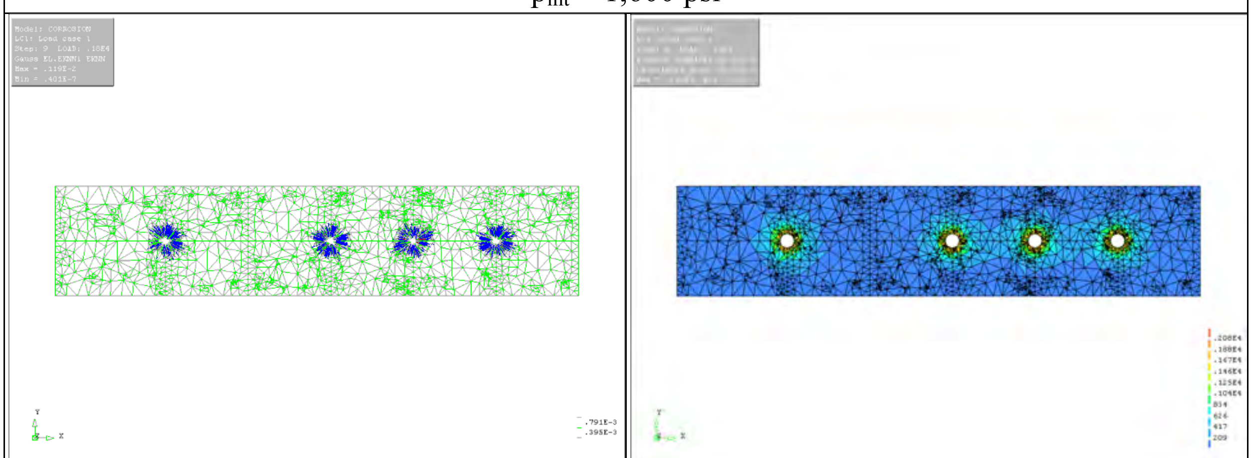

p_{int} = 1,800 psi

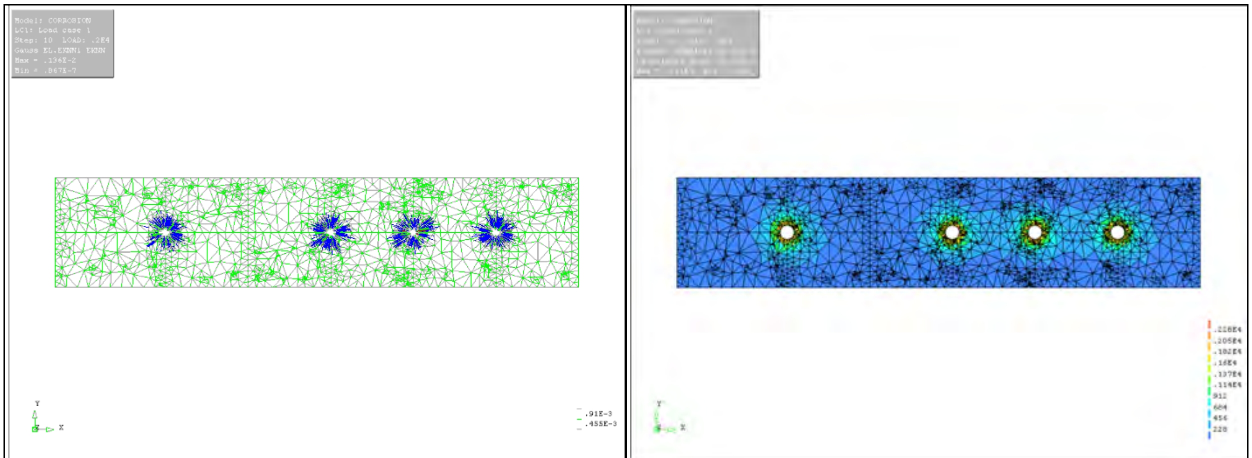

p_{int} = 2,000 psi

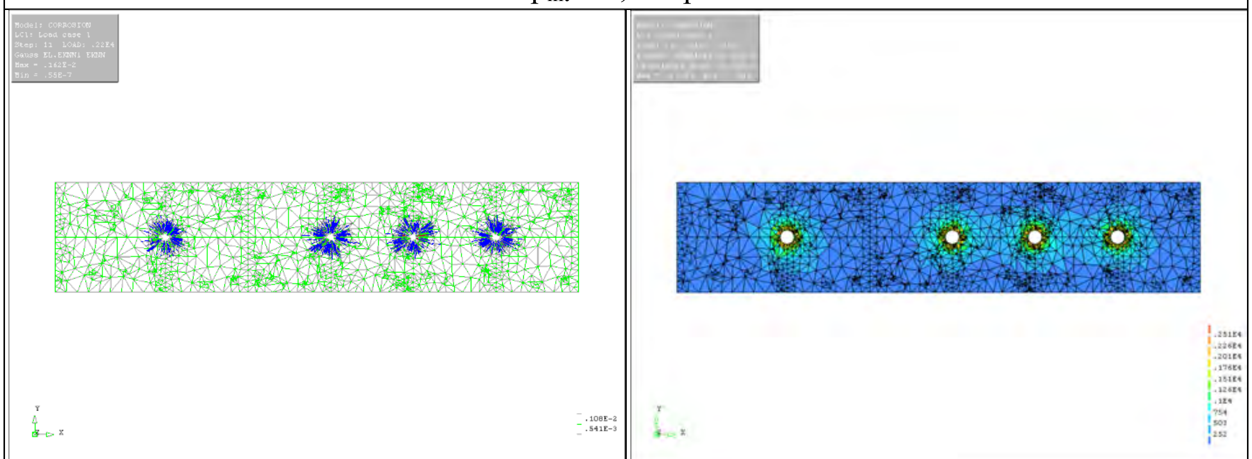

p_{int} = 2,200 psi

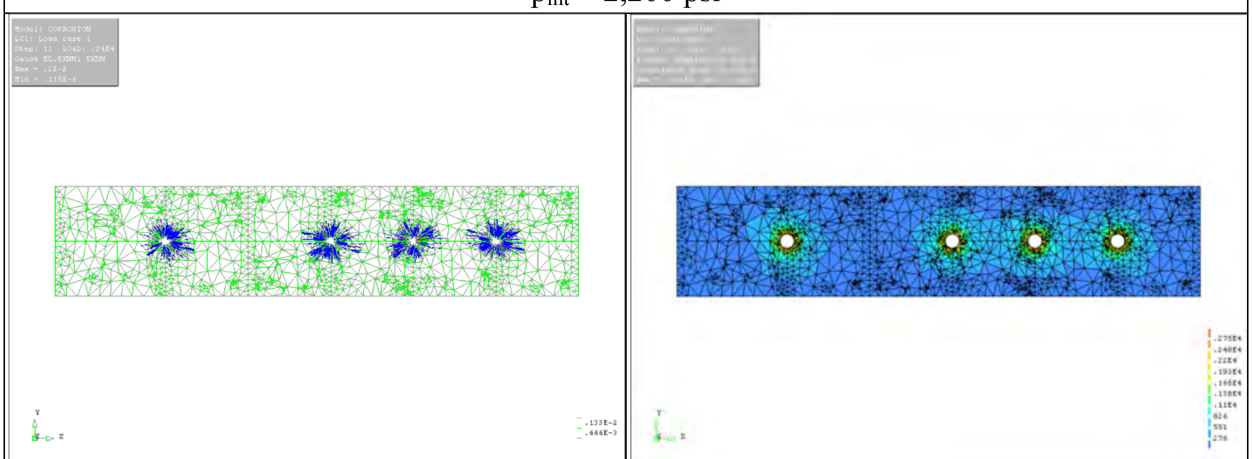

p_{int} = 2,400 psi

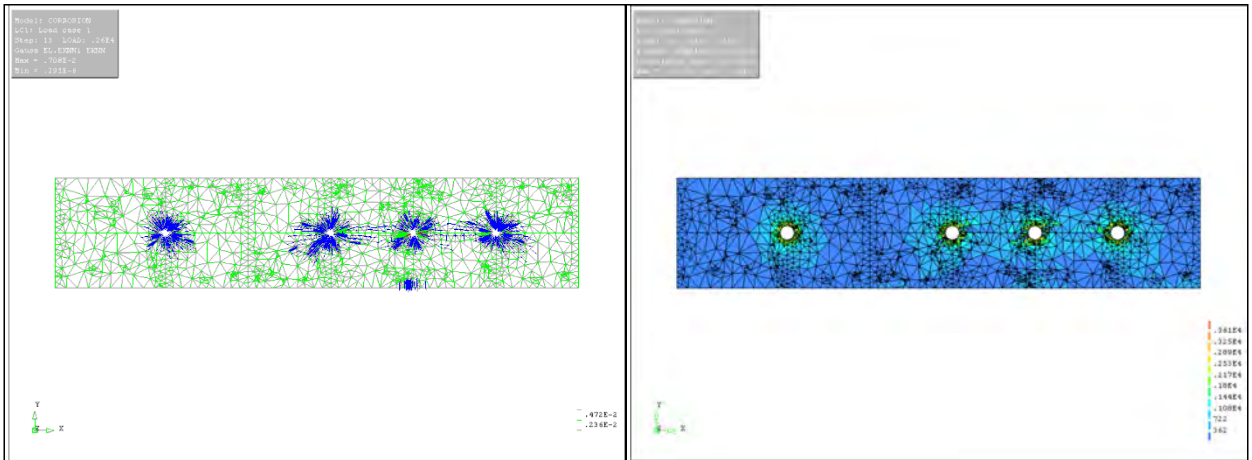

p_{int} = 2,600 psi

Figure D-10 Crack Patterns & Von Mises Stress Variations of Case II FE Model (Cover = 3.0 in.)

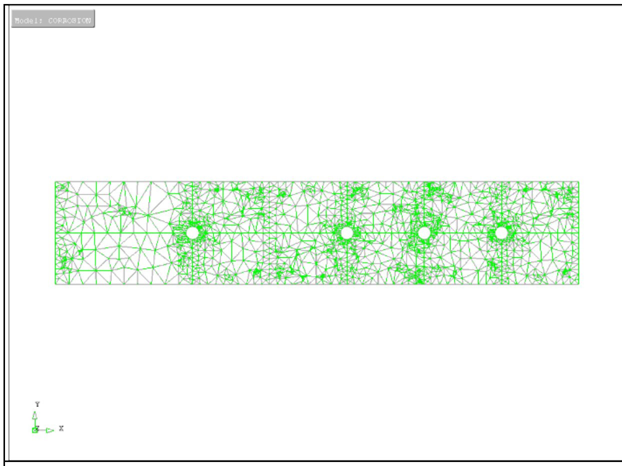

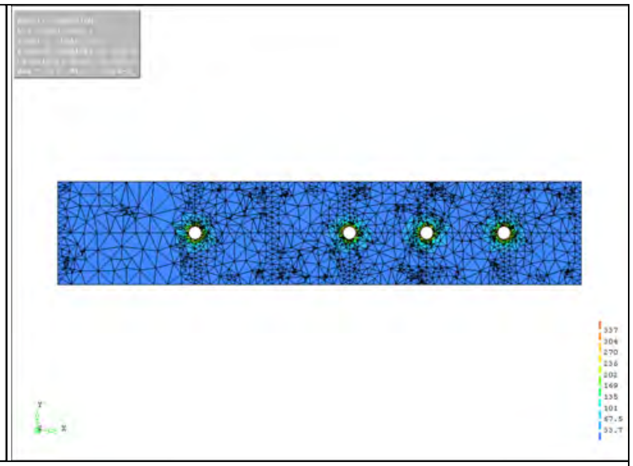

p_{int} = 200 psi

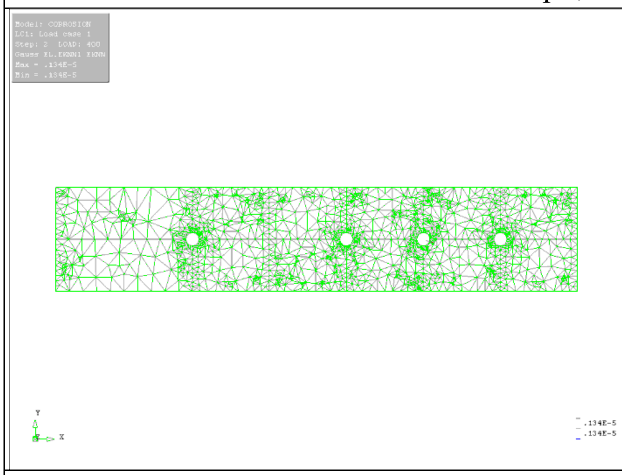

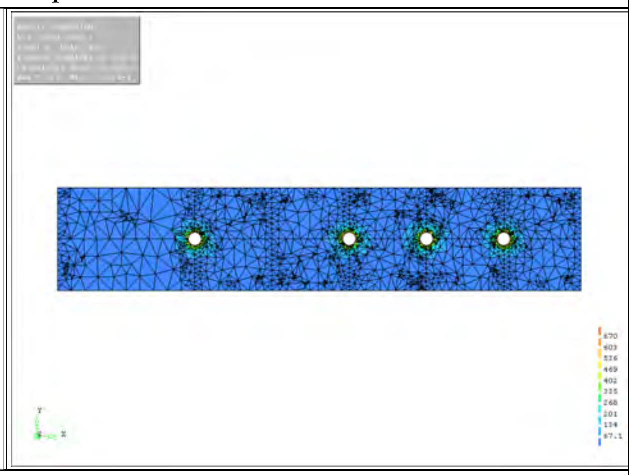

p_{int} = 400 psi

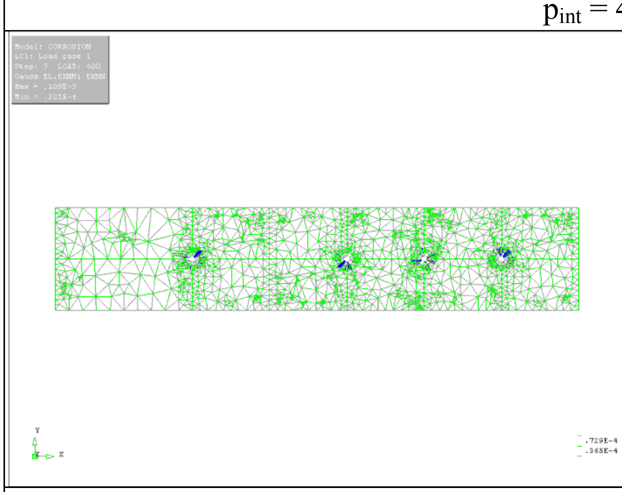

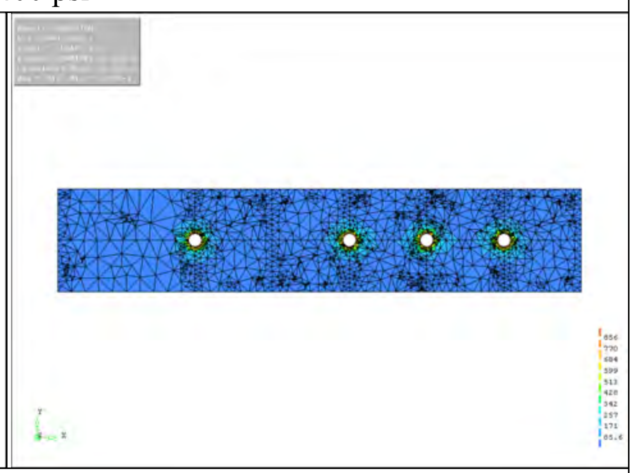

p_{int} = 600 psi

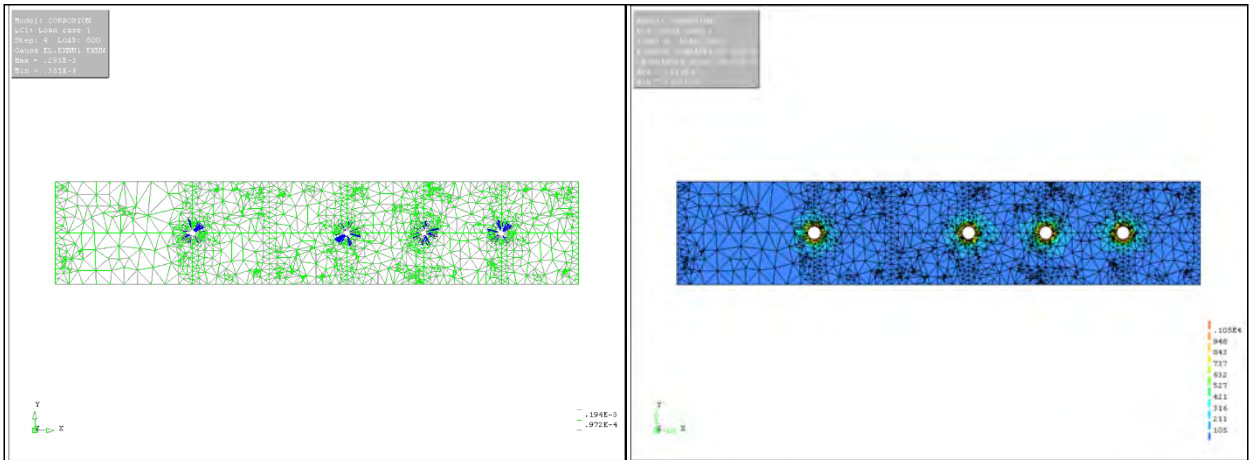

p_{int} = 800 psi

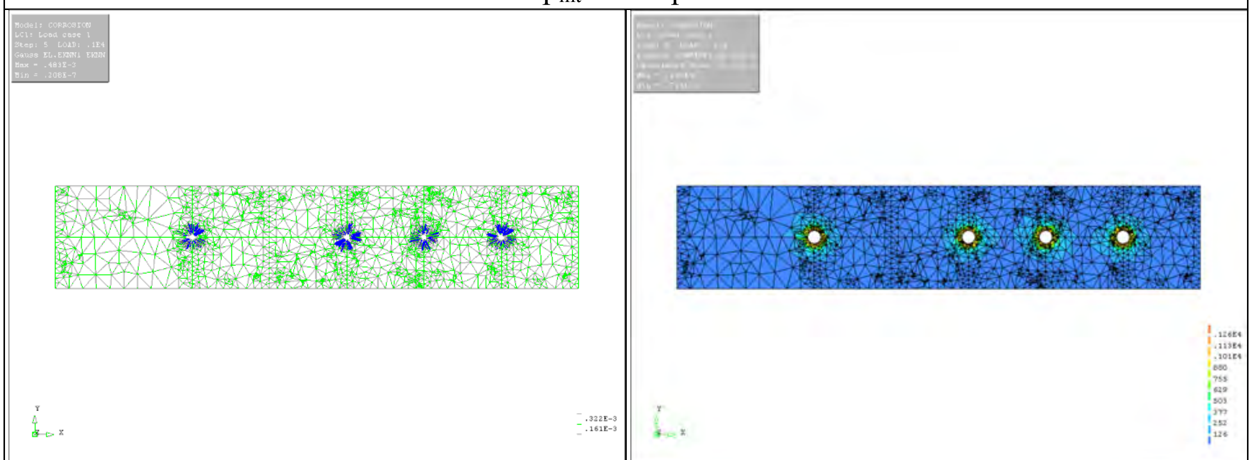

p_{int} = 1,000 psi

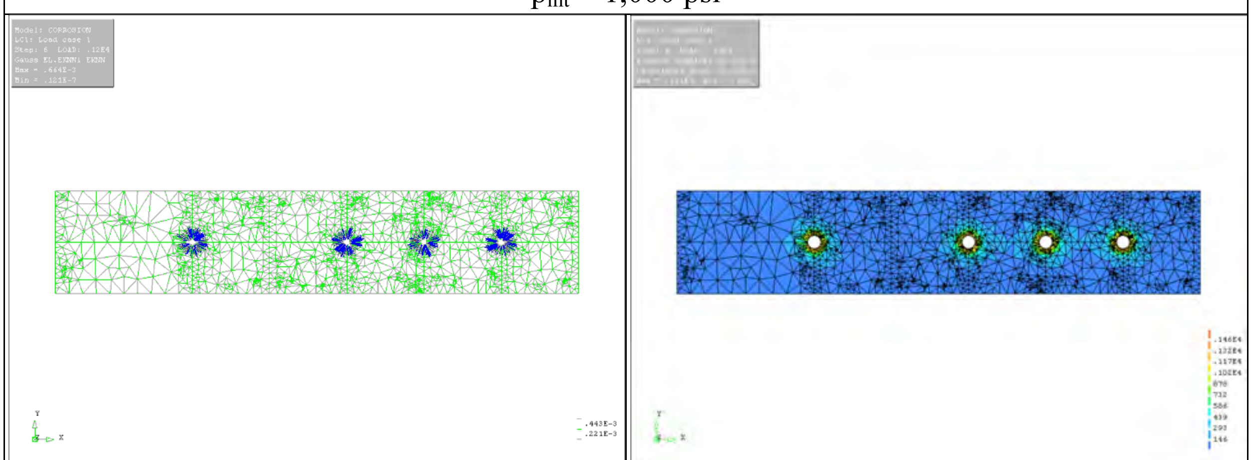

p_{int} = 1,200 psi

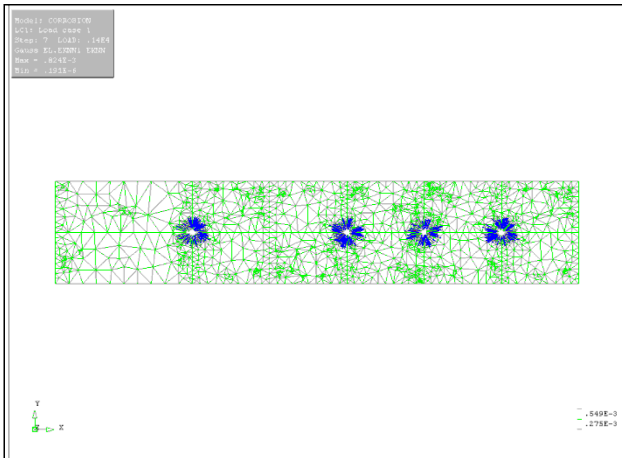
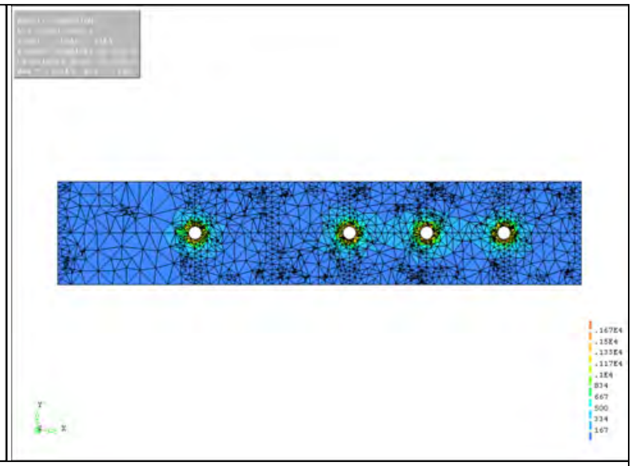

p_{int} = 1,400 psi

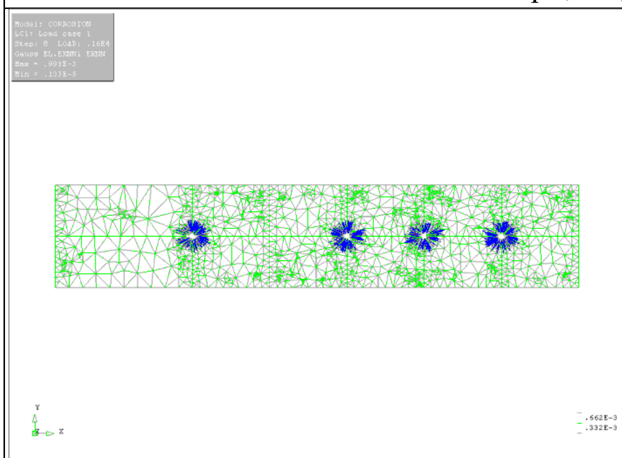
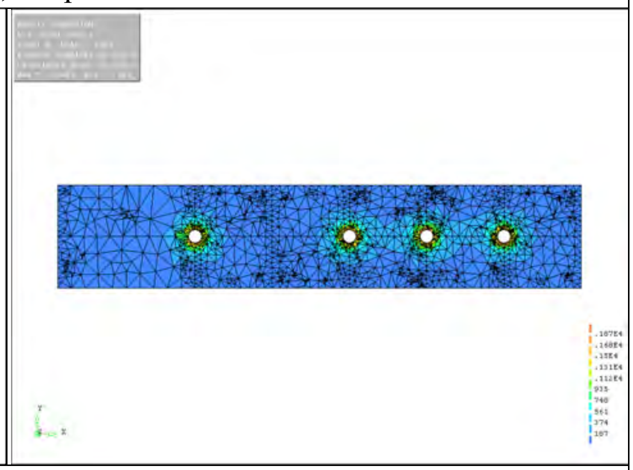

p_{int} = 1,600 psi

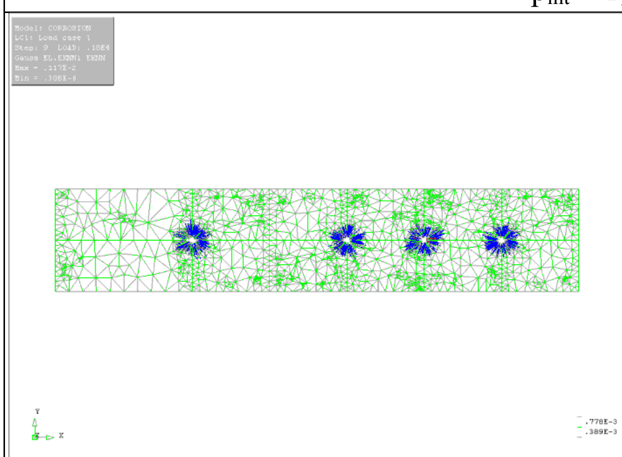
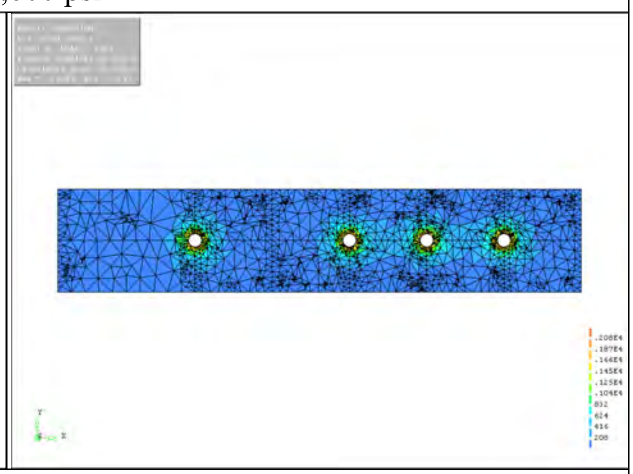

p_{int} = 1,800 psi

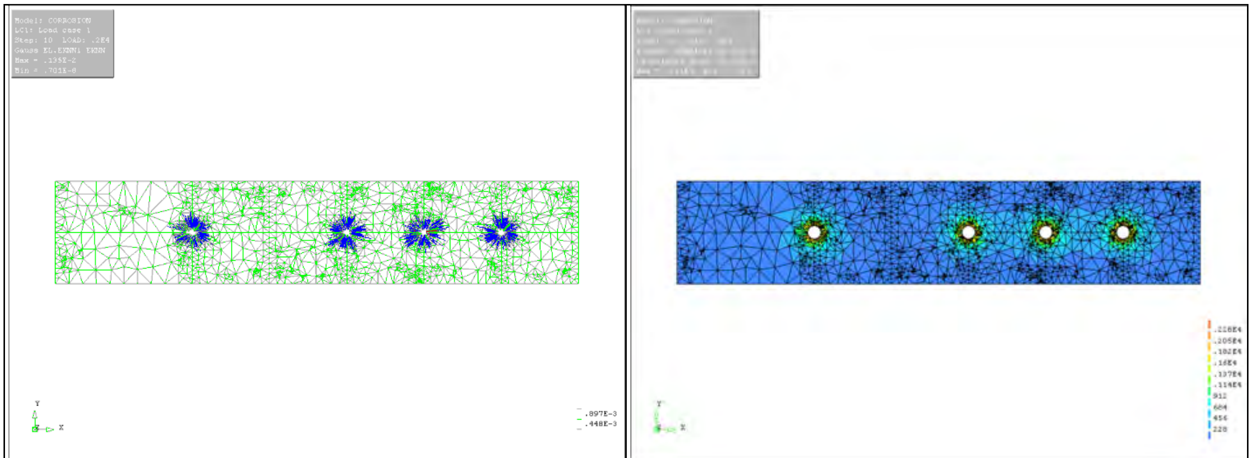

p_{int} = 2,000 psi

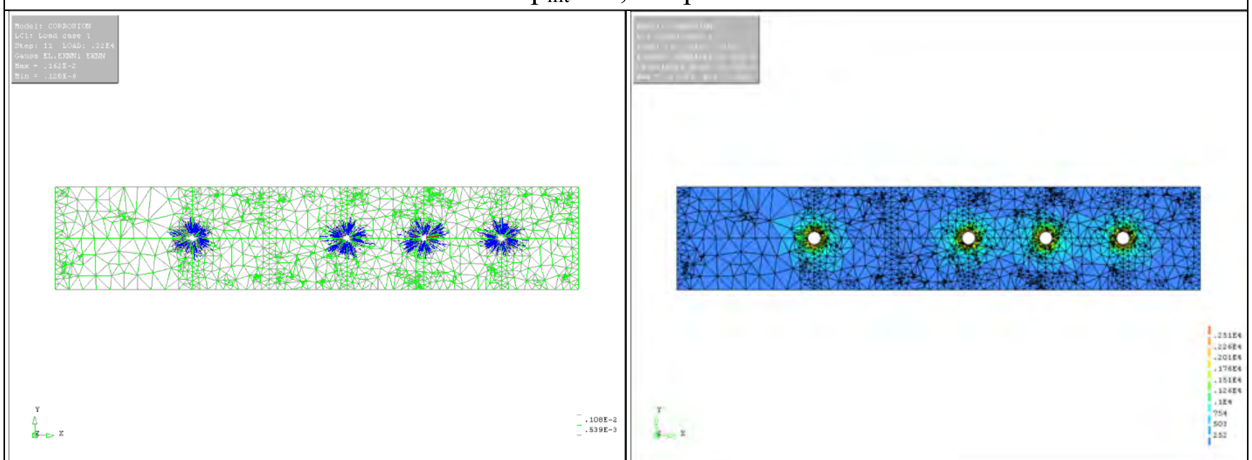

p_{int} = 2,200 psi

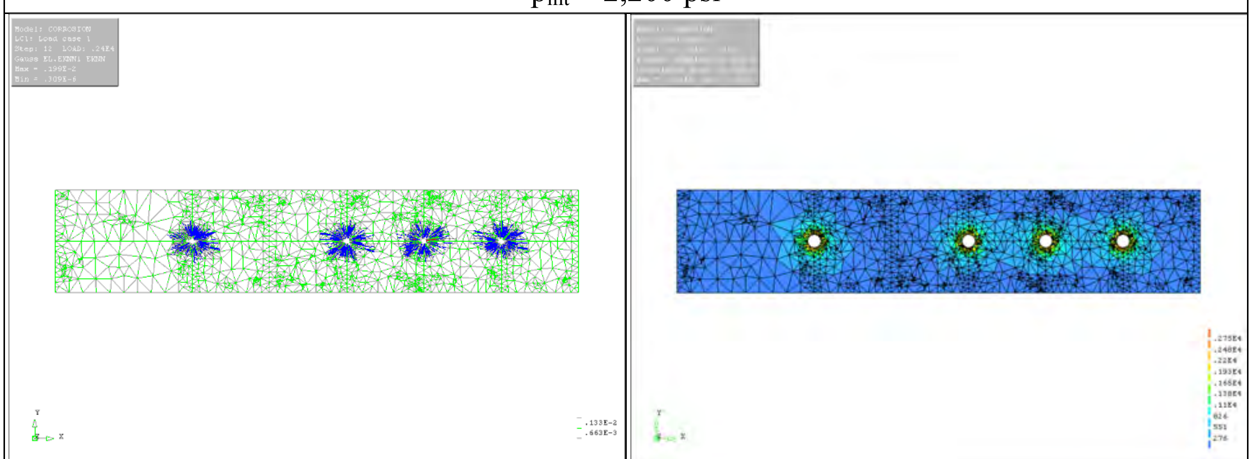

p_{int} = 2,400 psi

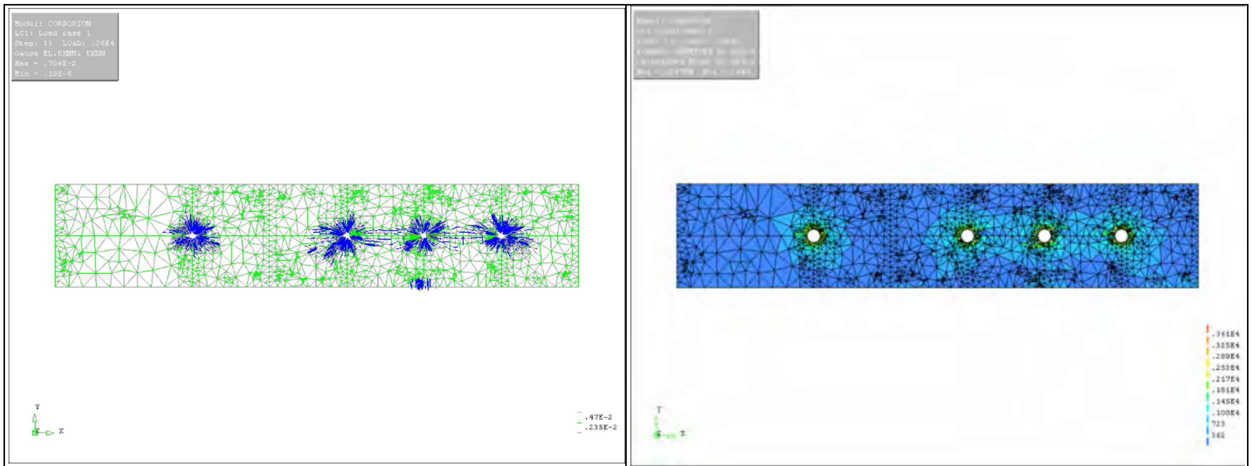

p_{int} = 2,600 psi

Figure D-11 Crack Patterns & Von Mises Stress Variations of Case II FE Model (Cover = 4.0 in.)

D.2.2 2D FE simulation of butting effects

This section presents detailed results of FE analysis performed to model the effects of panel butting. FE simulation was conducted on the Case II FE model in the corrosion analysis with varying configurations of boundary conditions and loading conditions as shown in Figure D-12. Based on results of the Case II FE analysis, 50% of the ultimate internal pressure, 1,300 psi, was applied at each reinforcement location to simulate a small amount of corrosion. Then, impact load induced by butting of the adjacent panel was modeled by incrementally increasing pressure, 200 psi, of varying area on the panel joint side of the panel to account for varying misalignment of the panels. To simulate this sequential loading effect, phased analysis was conducted. Crack patterns and Von Mises stress variations are illustrated from Figure D-13 to Figure D-17 with respect to the parameters considered.

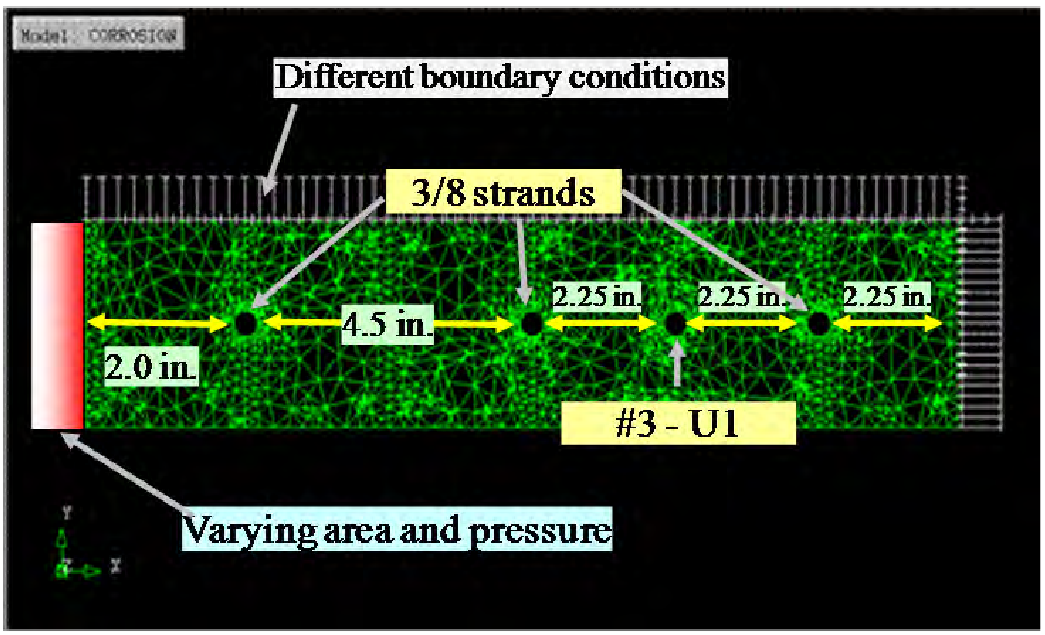

Figure D-12 2D FE Butting Model

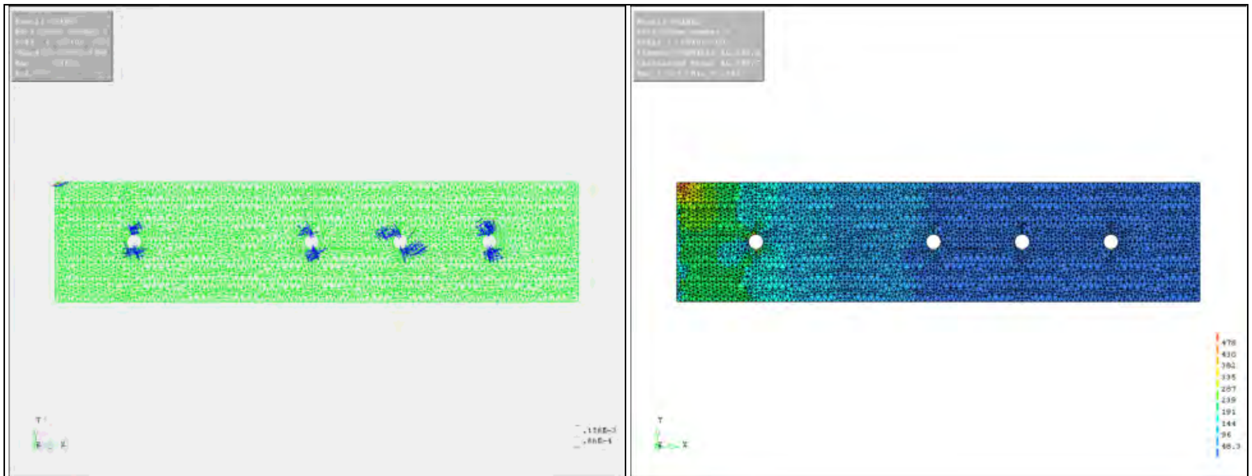

p_{impact} = 200 psi

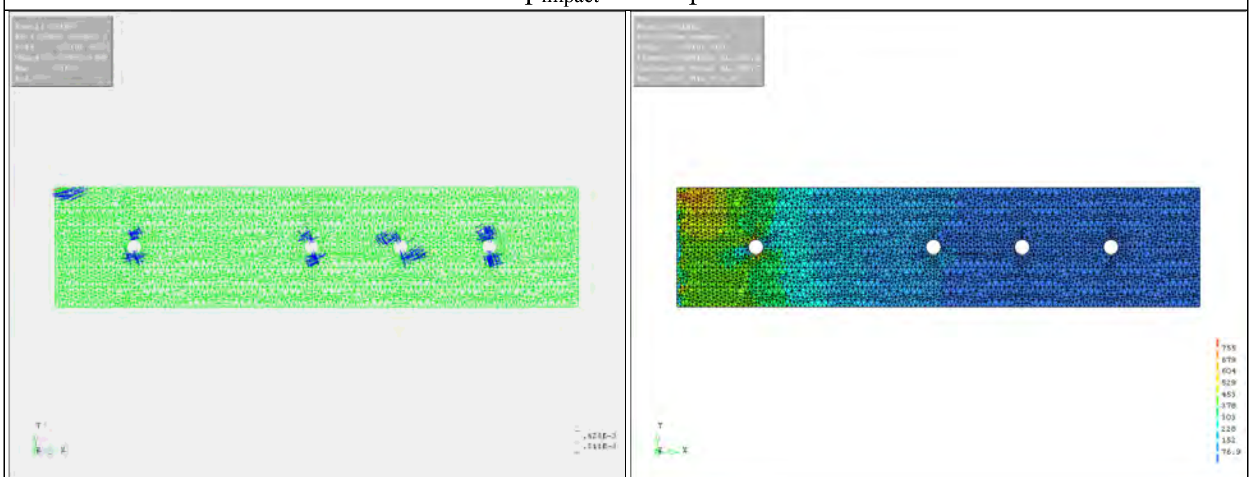

p_{impact} = 400 psi

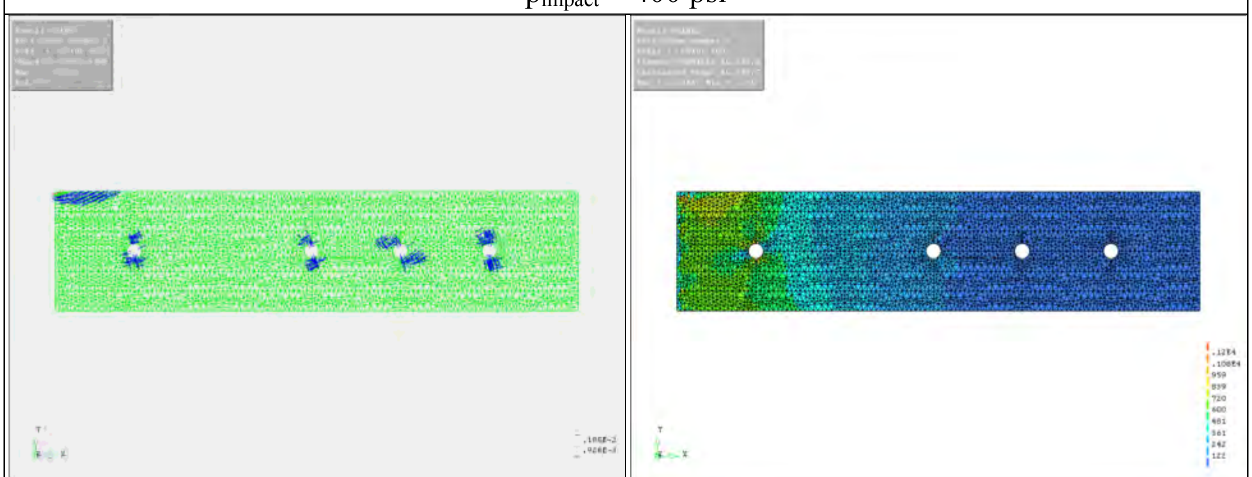

p_{impact} = 600 psi

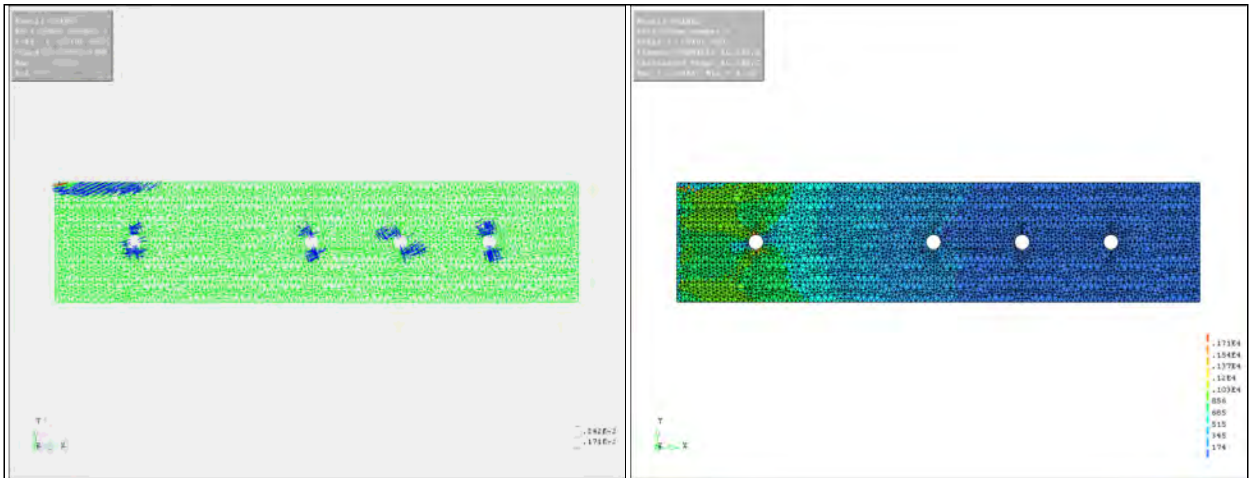

p_{impact} = 800 psi

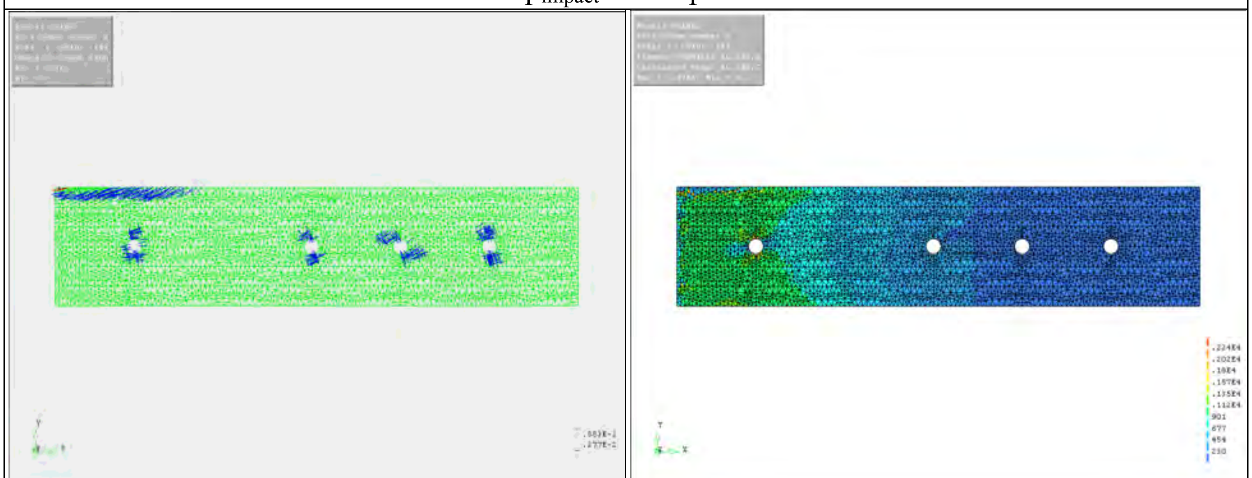

p_{impact} = 1,000 psi

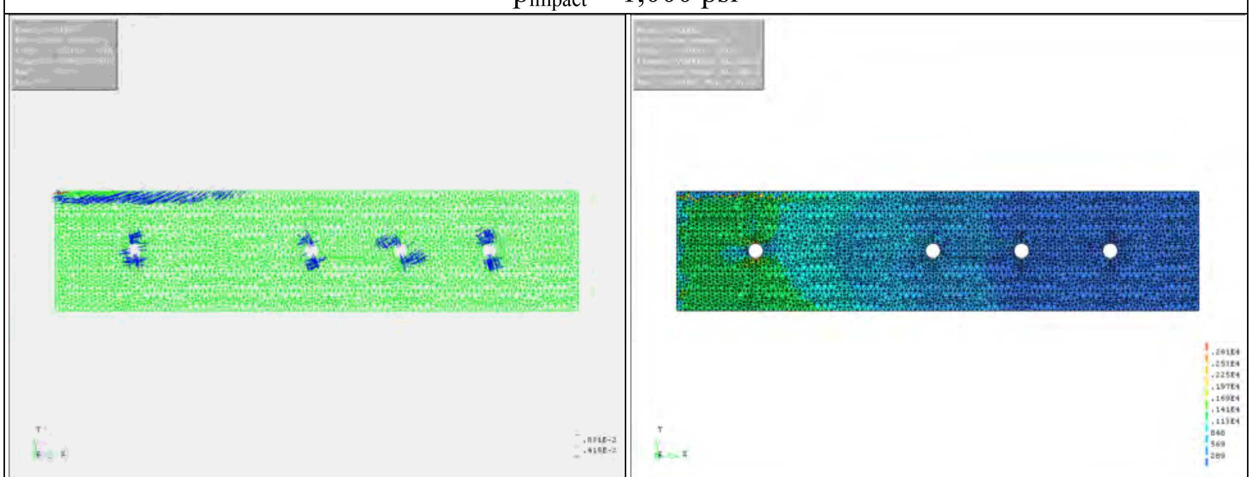

p_{impact} = 1,200 psi

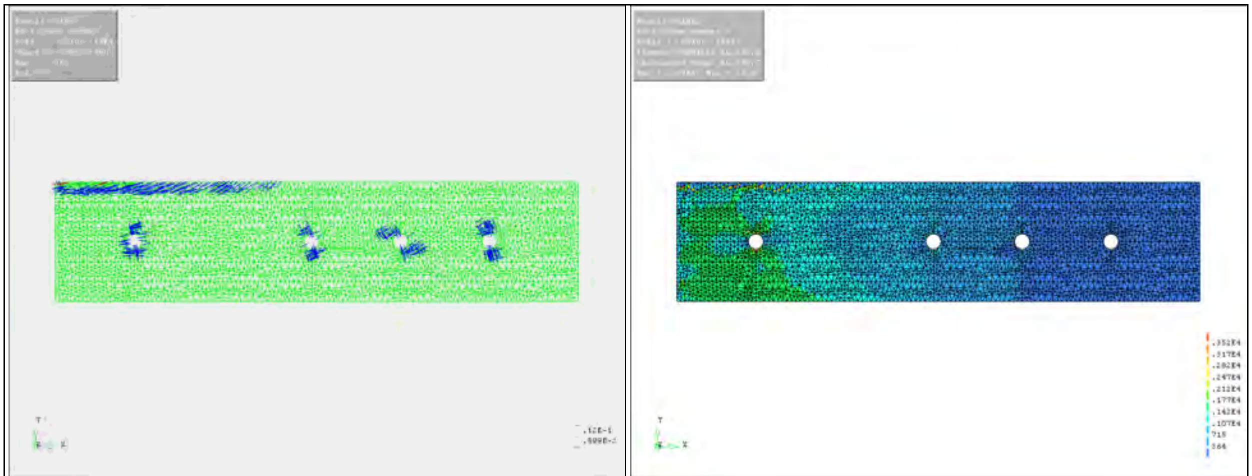

p_{impact} = 1,400 psi

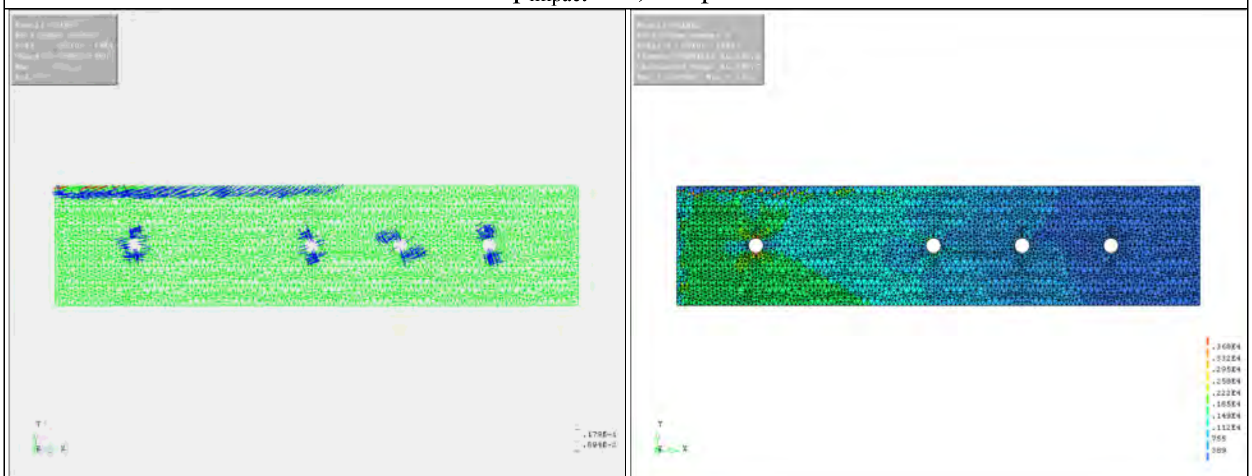

p_{impact} = 1,600 psi

Figure D-13 Crack Patterns & Von Mises Stress Variations of FE Model
(Full Compression + Fixed Boundary Condition)

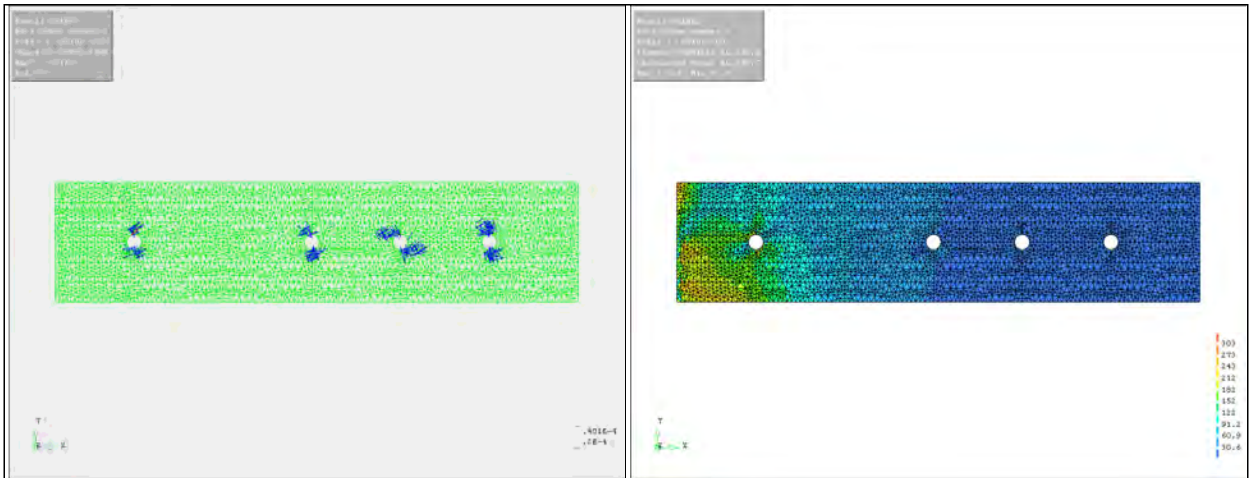

p_{impact} = 200 psi

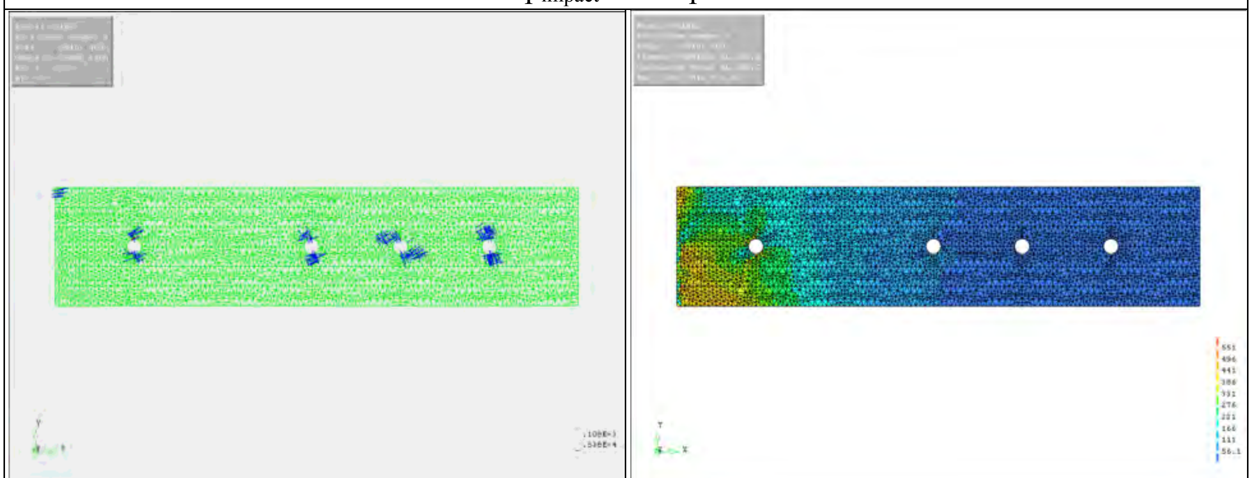

p_{impact} = 400 psi

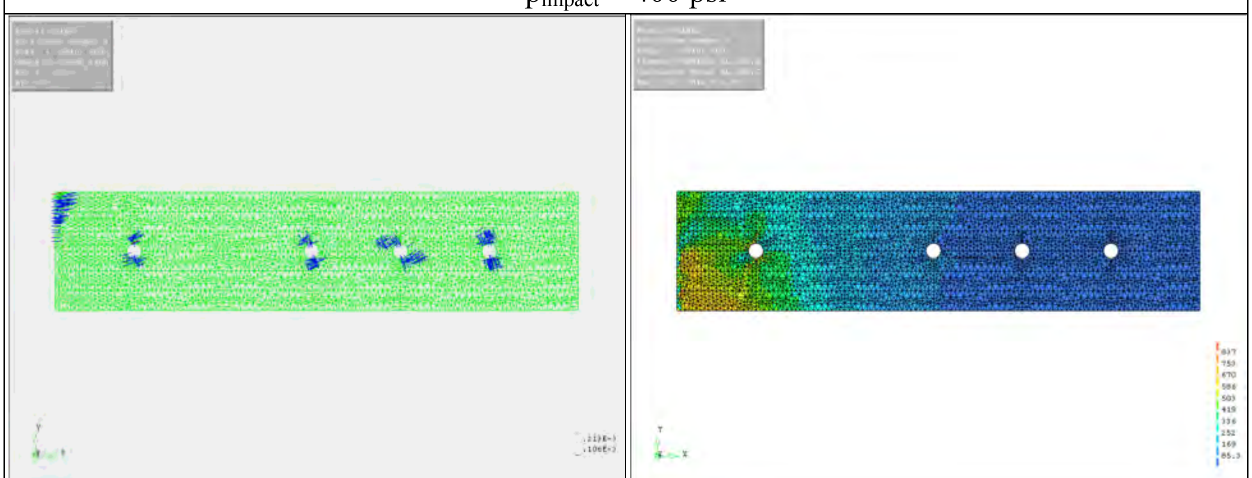

p_{impact} = 600 psi

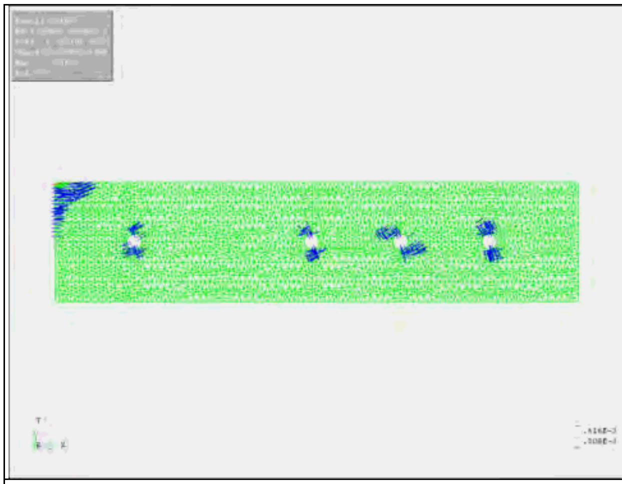
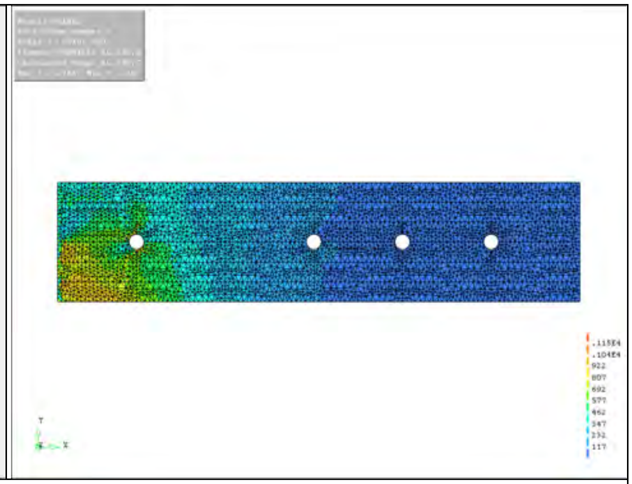

p_{impact} = 800 psi

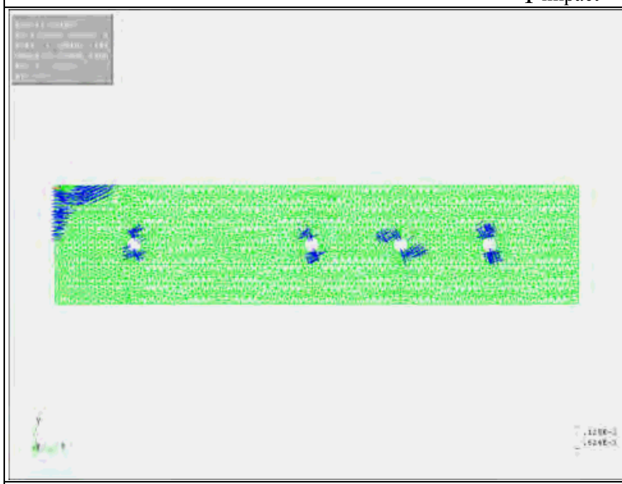
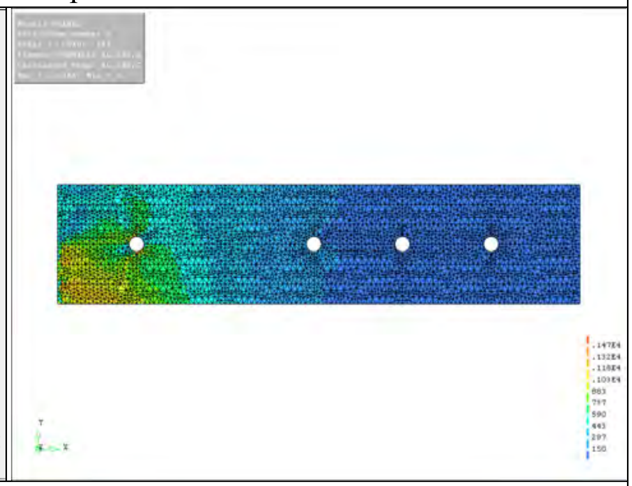

p_{impact} = 1,000 psi

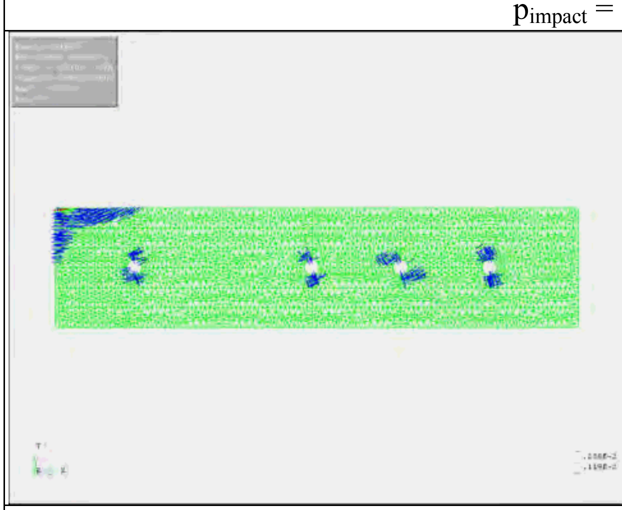
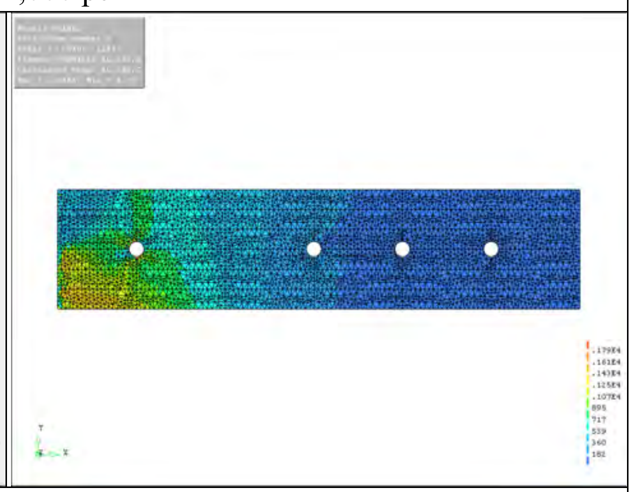

p_{impact} = 1,200 psi

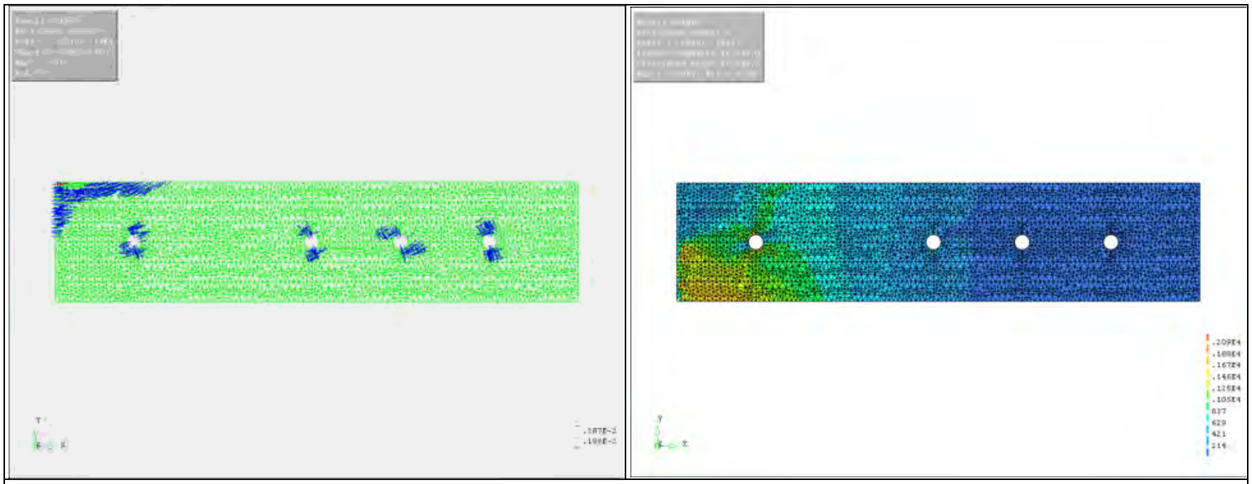

p_{impact} = 1,400 psi

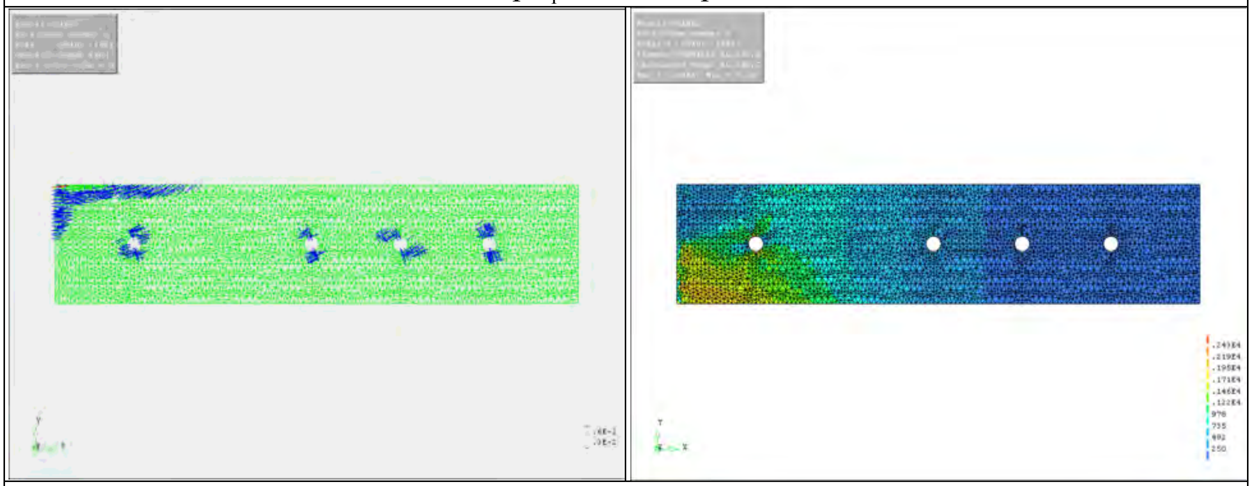

p_{impact} = 1,600 psi

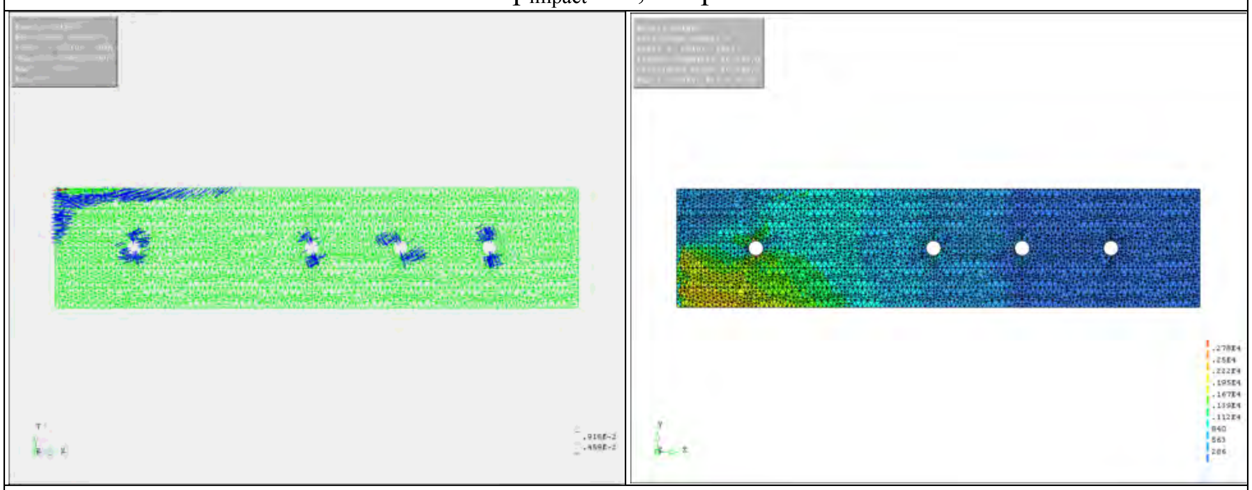

p_{impact} = 2,000 psi

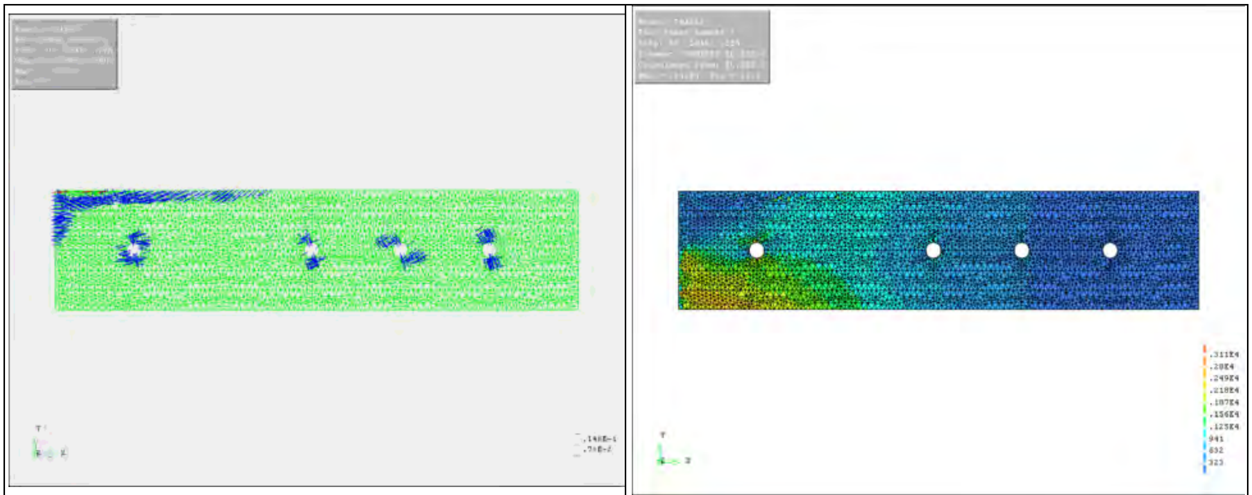

p_{impact} = 2,200 psi

Figure D-14 Crack Patterns & Von Mises Stress Variations of FE Model
(Half Compression + Fixed Boundary Condition)

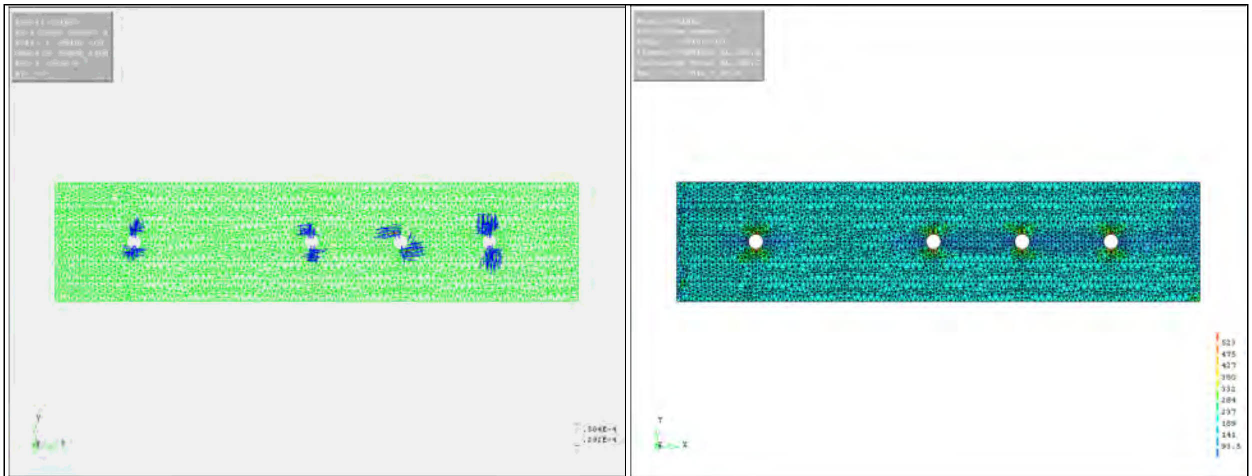

p_{impact} = 200 psi

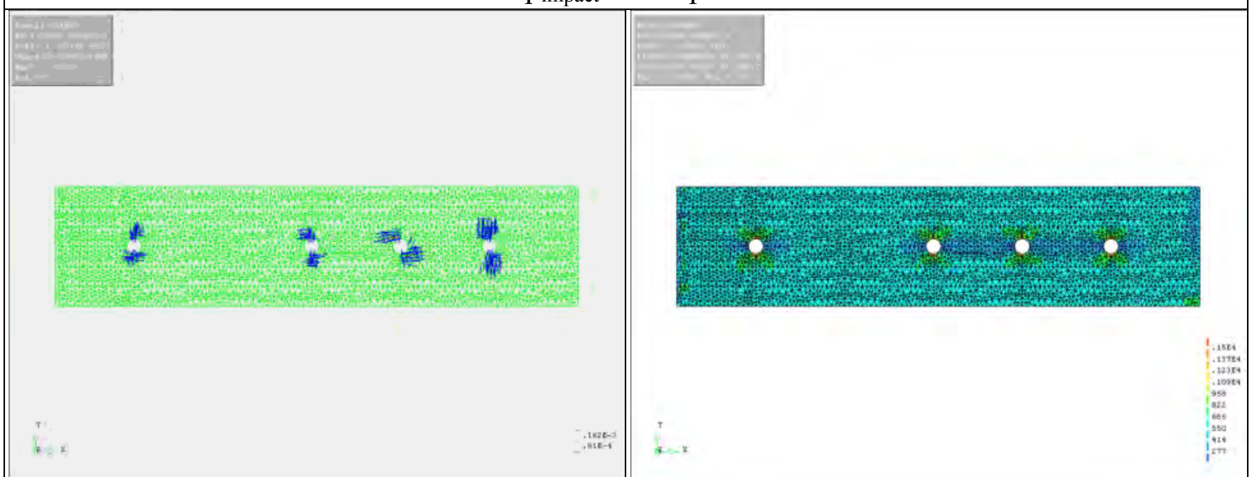

p_{impact} = 600 psi

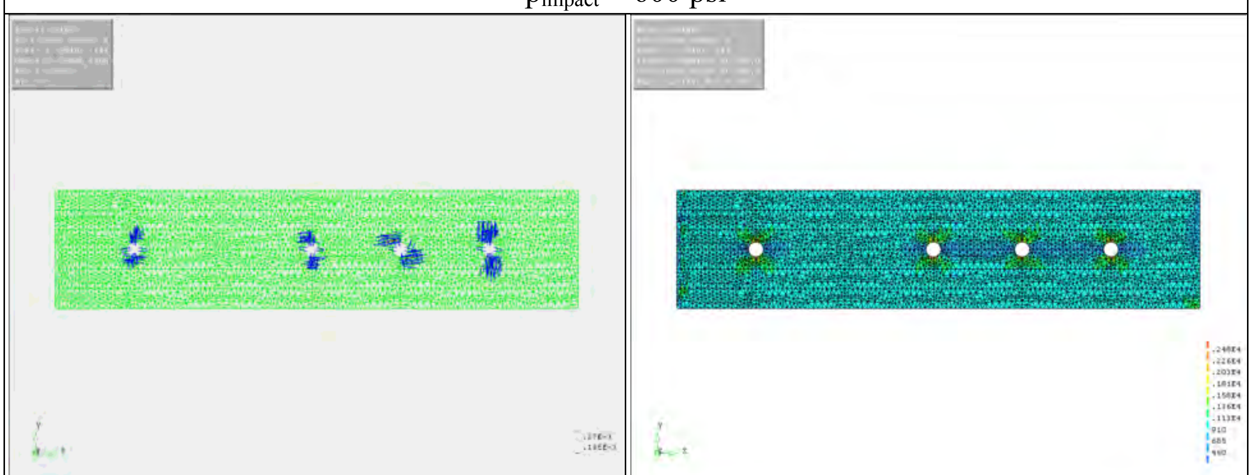

p_{impact} = 1,000 psi

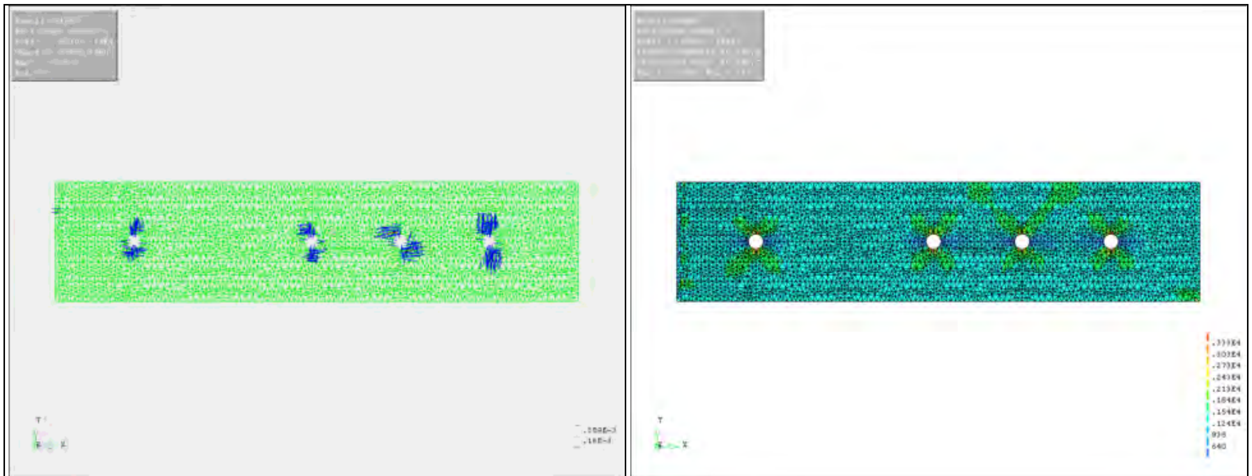

p_{impact} = 1,400 psi

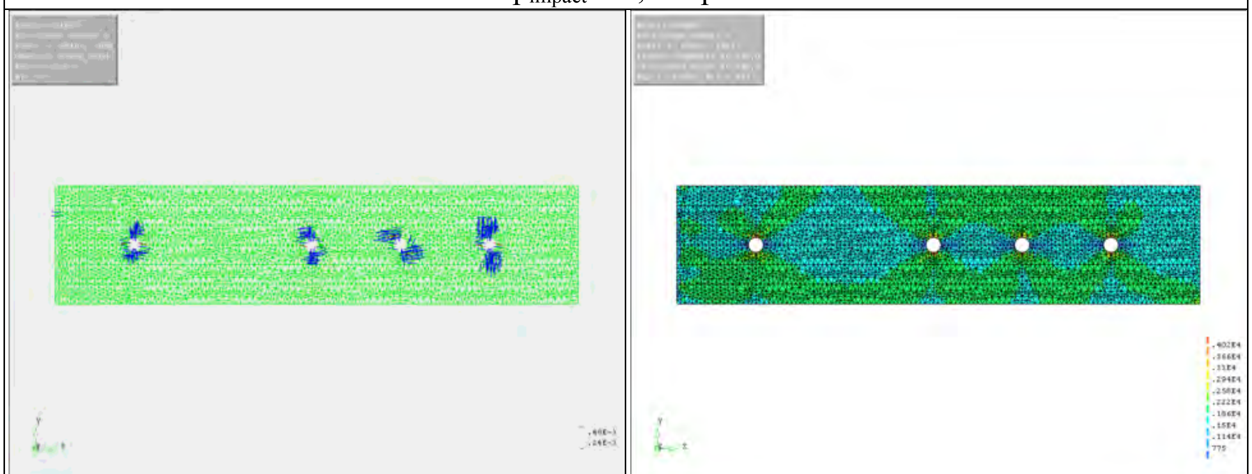

p_{impact} = 1,800 psi

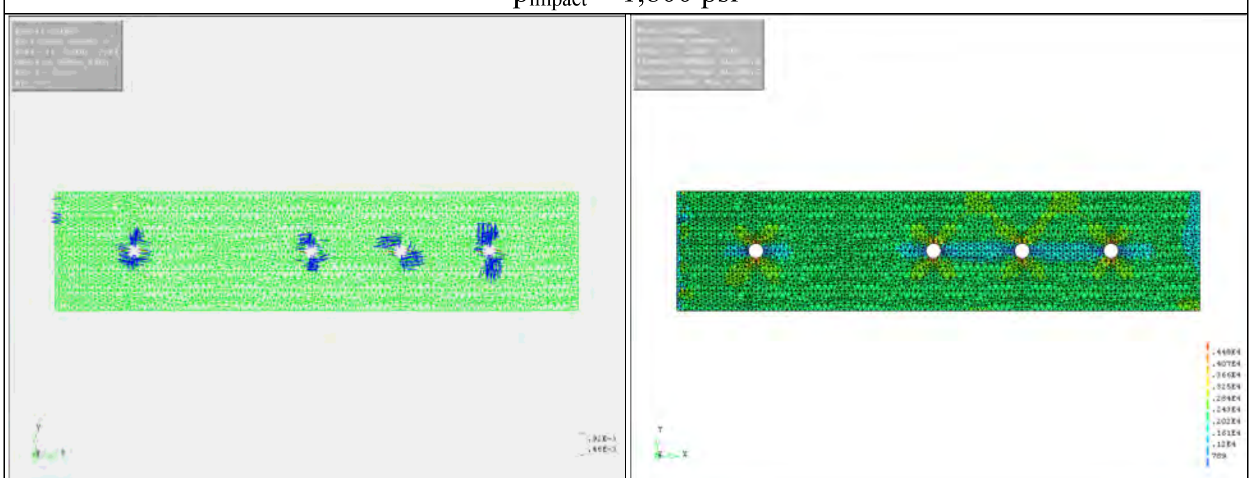

p_{impact} = 2,200 psi

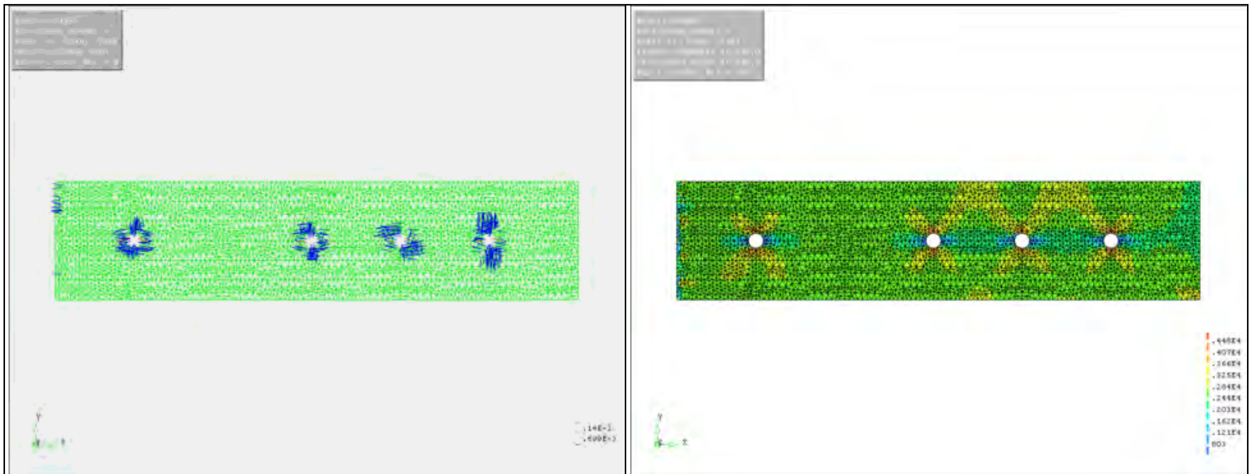

p_{impact} = 2,600 psi

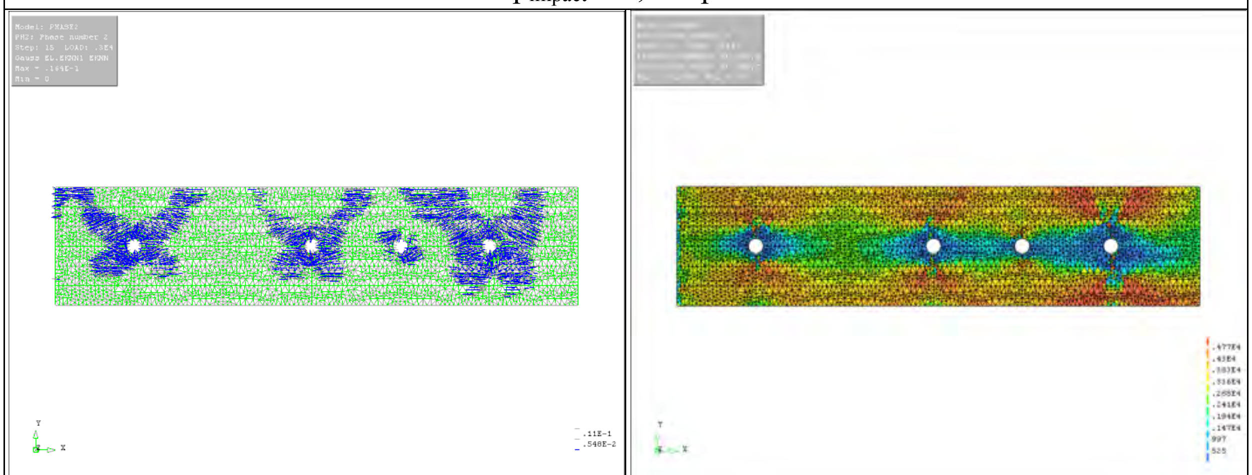

p_{impact} = 3,000 psi

Figure D-15 Crack Patterns & Von Mises Stress Variations of FE Model
(Full Compression + Released Boundary Condition)

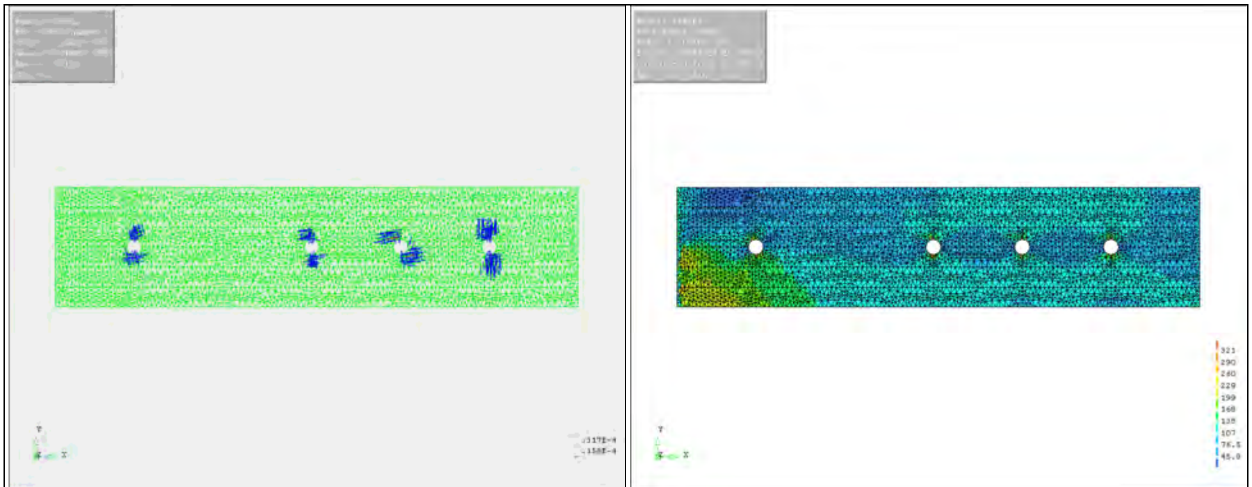

p_{impact} = 200 psi

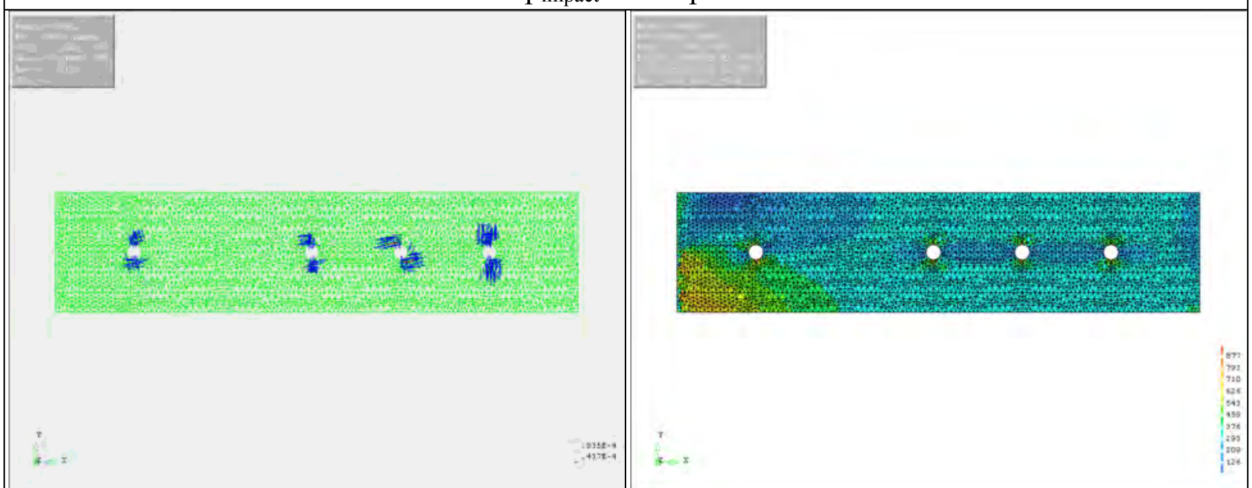

p_{impact} = 600 psi

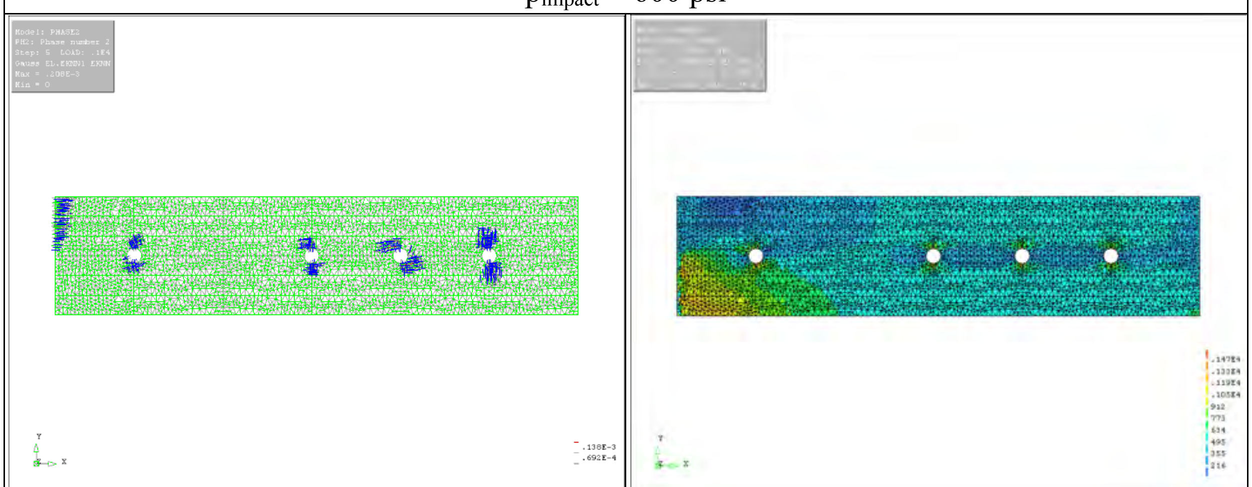

p_{impact} = 1,000 psi

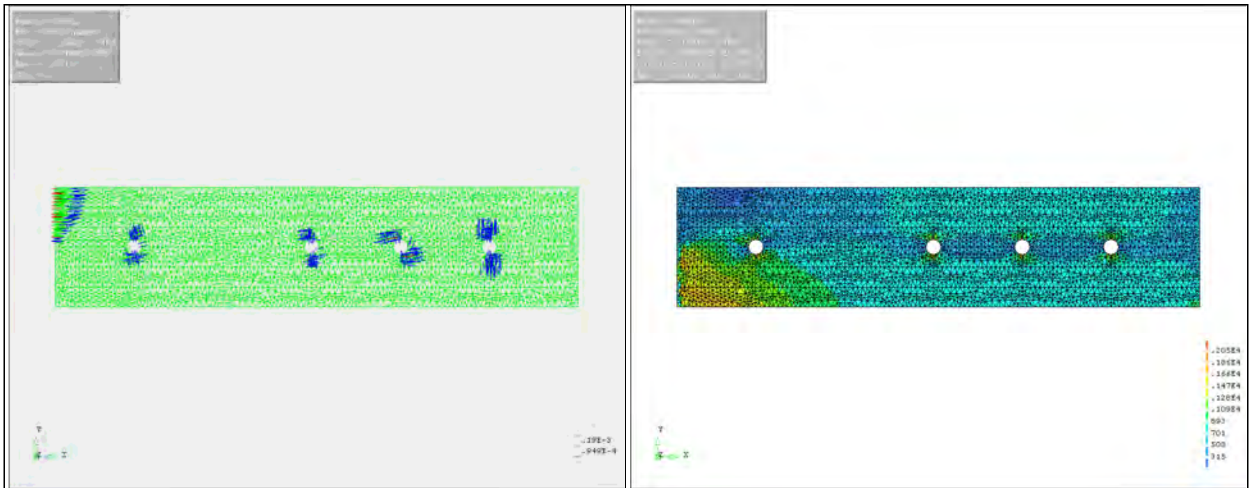

p_{impact} = 1,400 psi

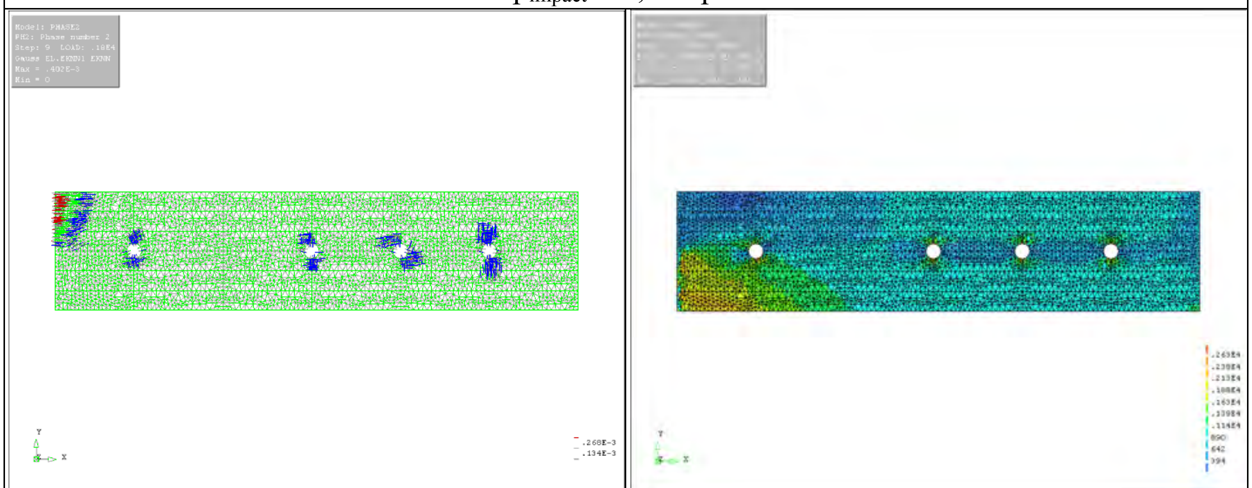

p_{impact} = 1,800 psi

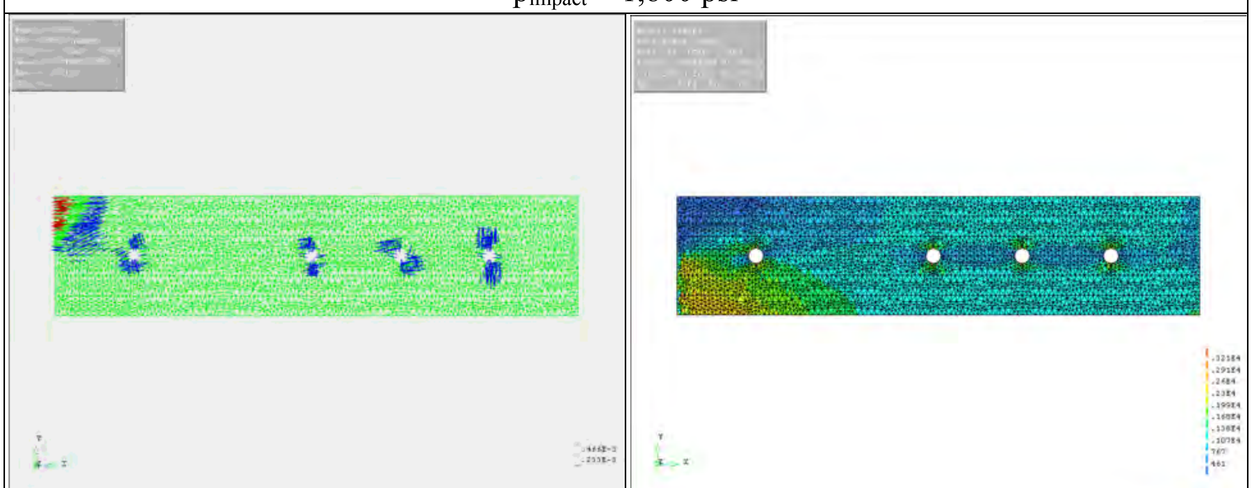

p_{impact} = 2,200 psi

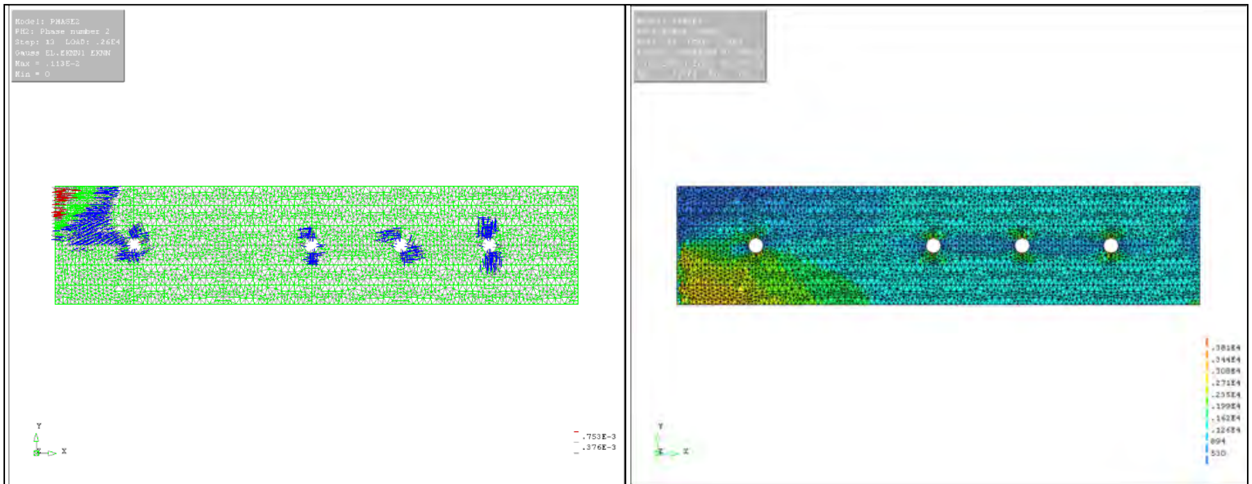

p_{impact} = 2,600 psi

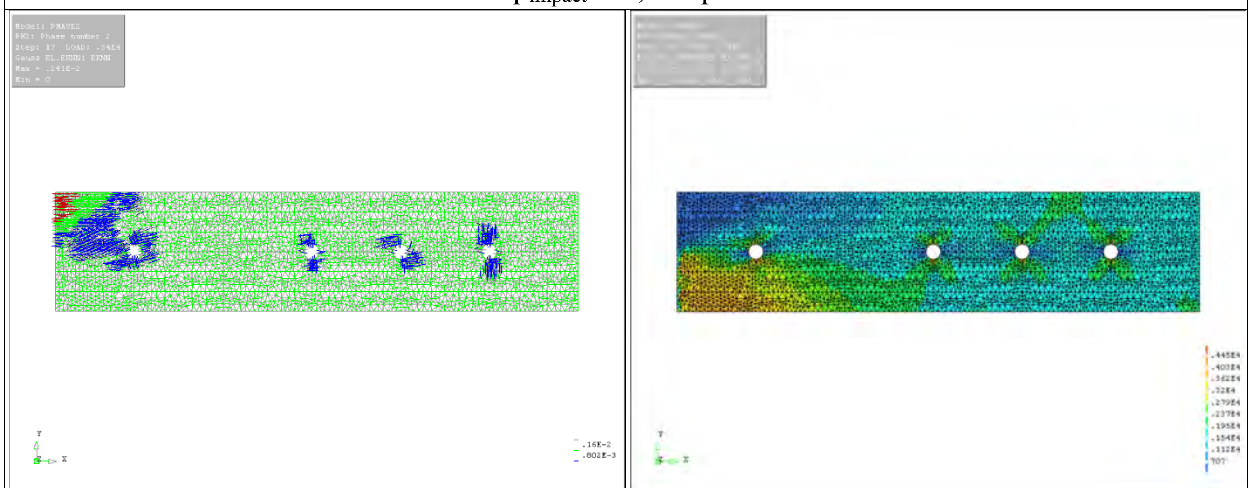

p_{impact} = 3,000 psi

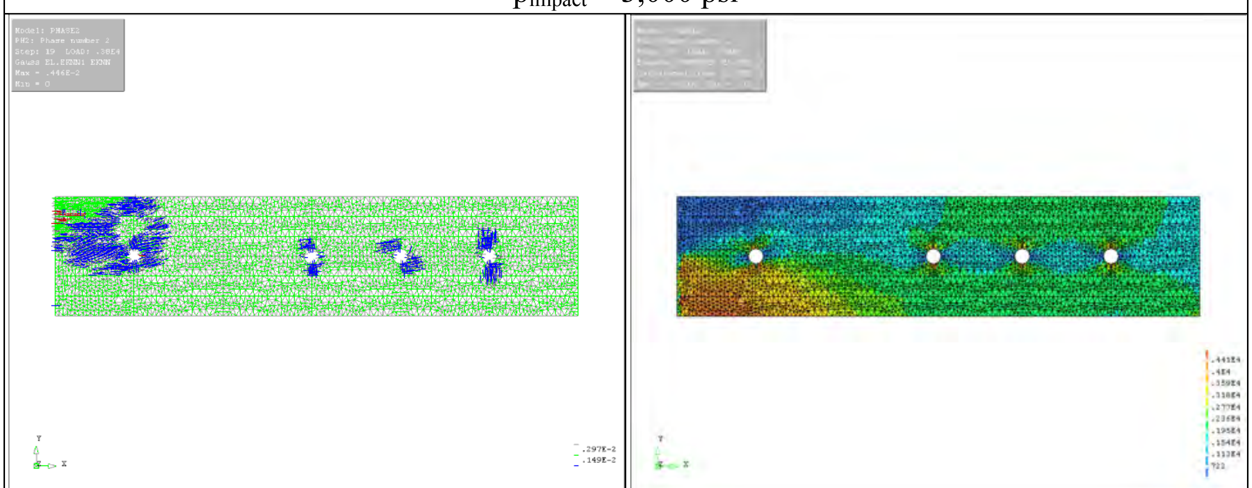

p_{impact} = 3,400 psi

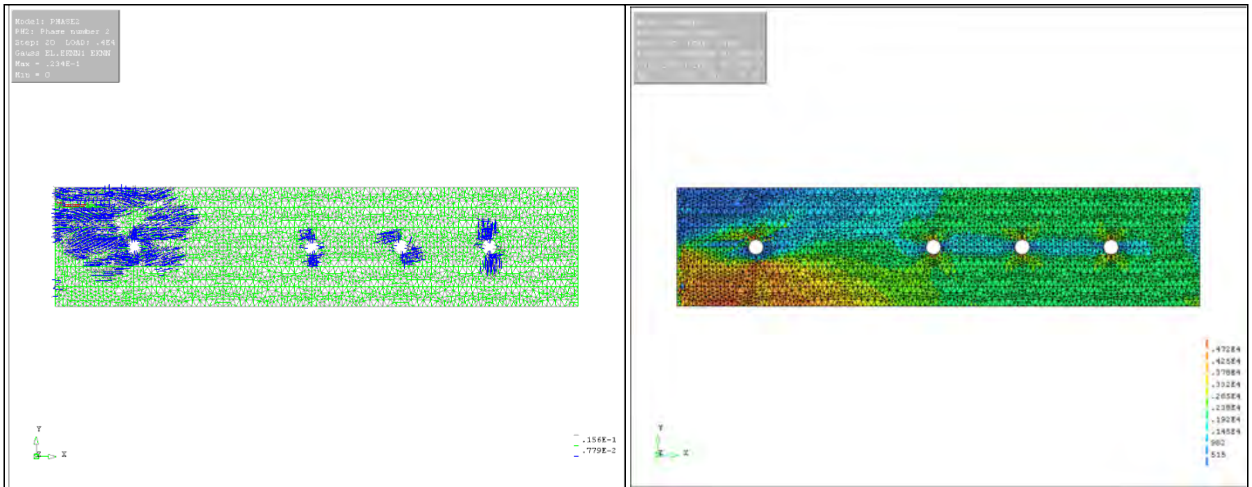

p_{impact} = 3,600 psi

Figure D-16 Crack Patterns & Von Mises Stress Variations of FE Model
(Half Compression + Released Boundary Condition)

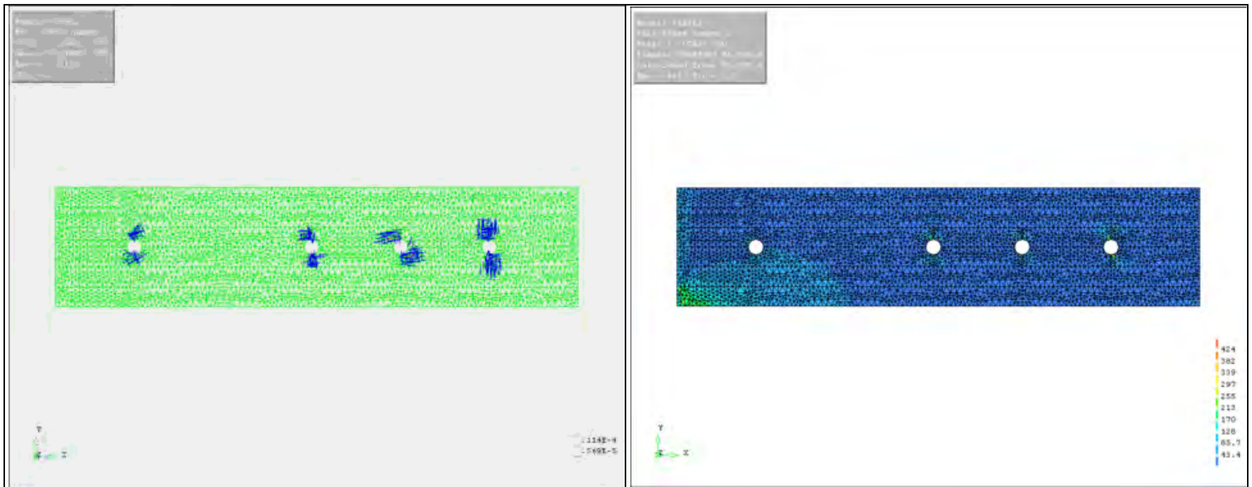

p_{impact} = 200 psi

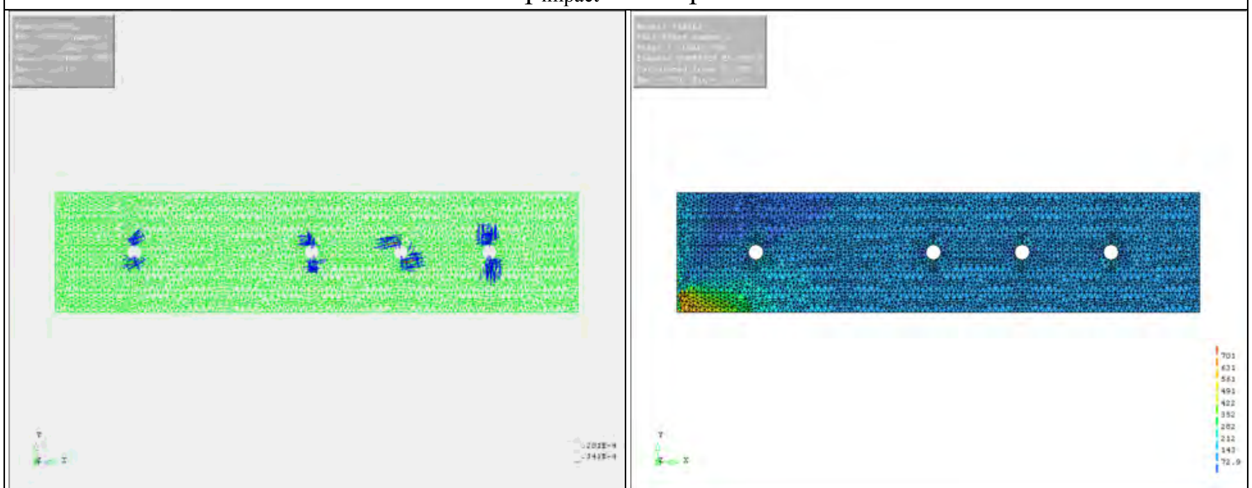

p_{impact} = 600 psi

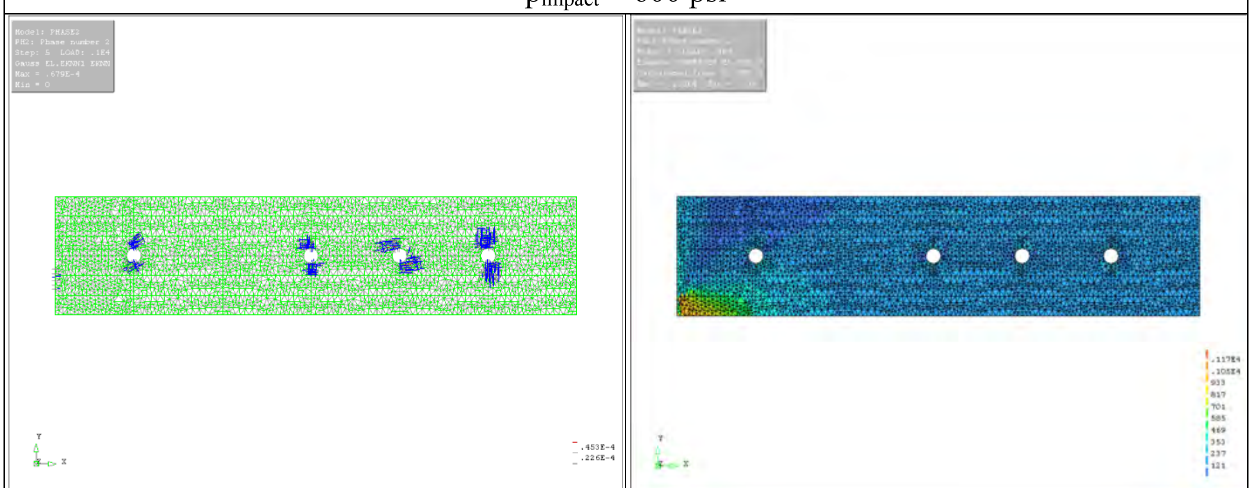

p_{impact} = 1,000 psi

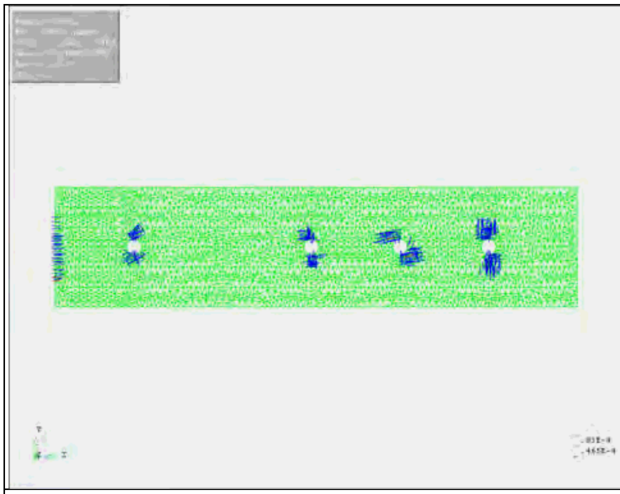

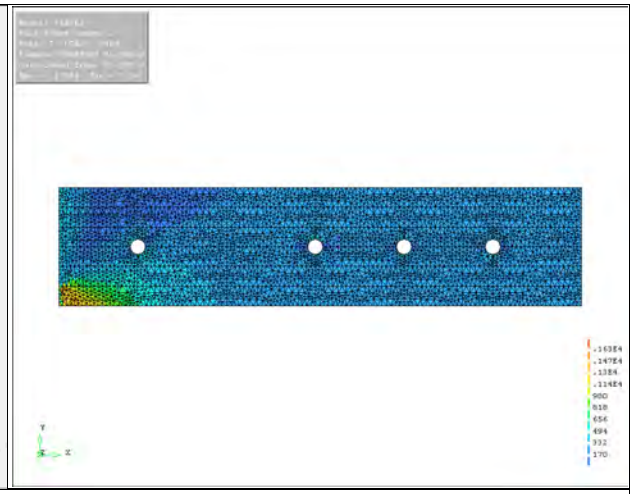

p_{impact} = 1,400 psi

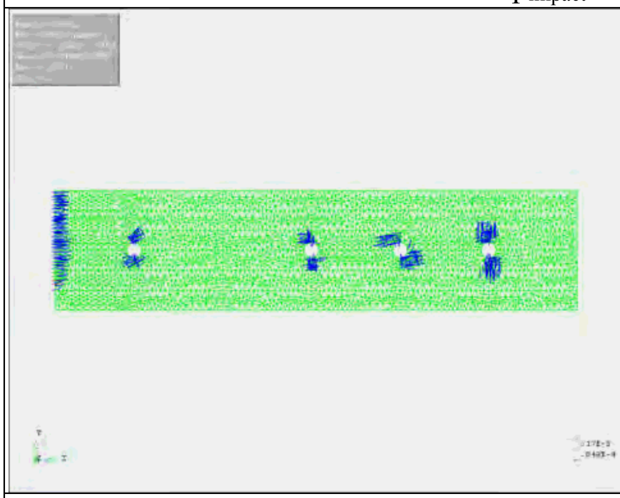

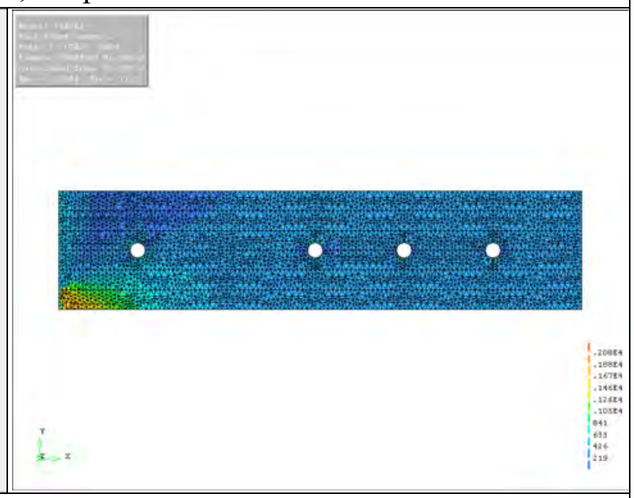

p_{impact} = 1,800 psi

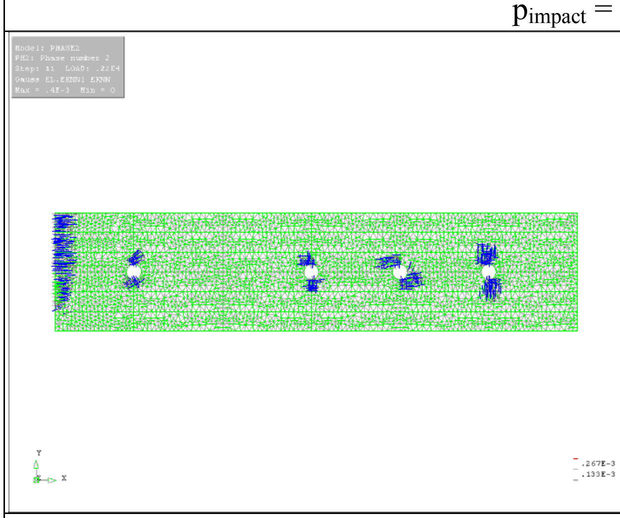

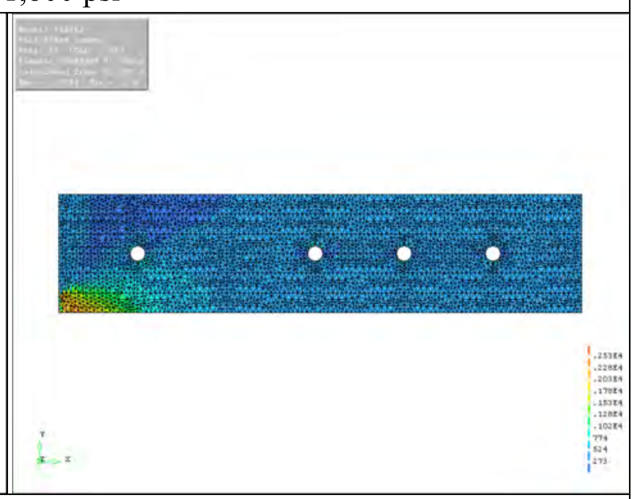

p_{impact} = 2,200 psi

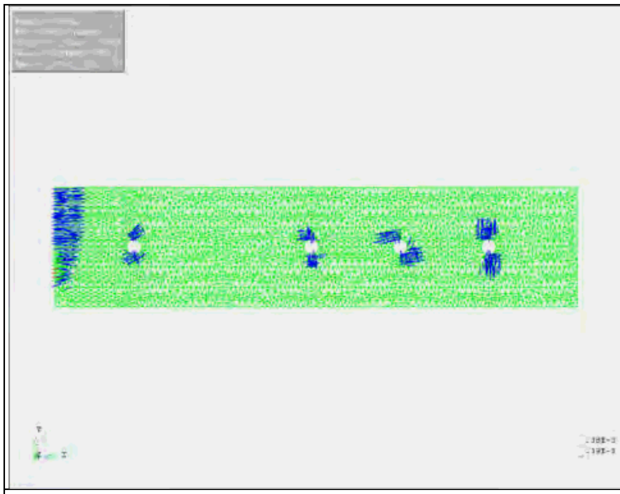
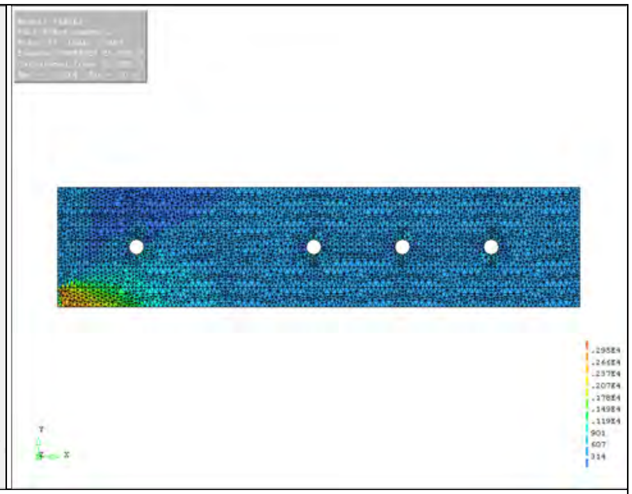

$p_{impact} = 2{,}600$ psi

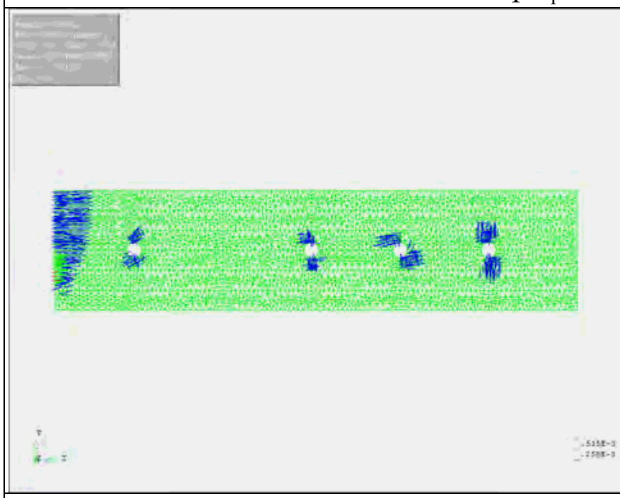
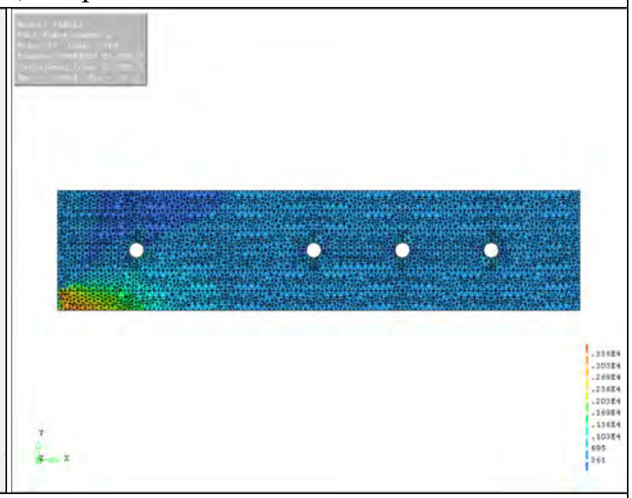

$p_{impact} = 3{,}000$ psi

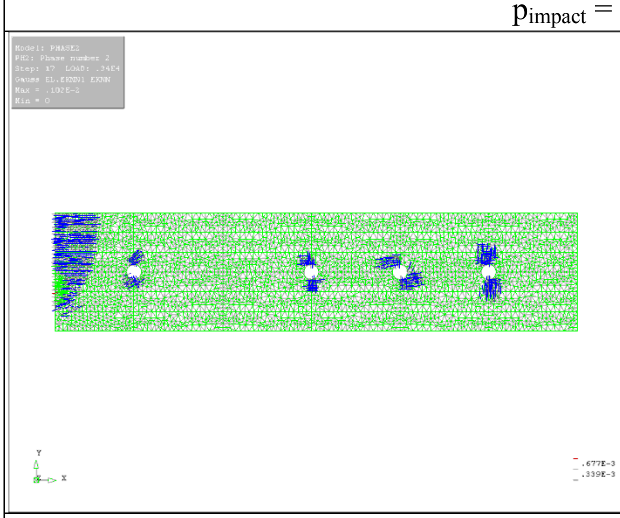
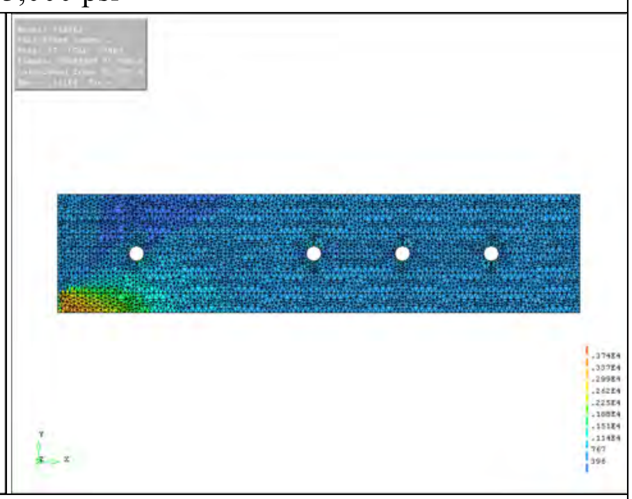

$p_{impact} = 3{,}400$ psi

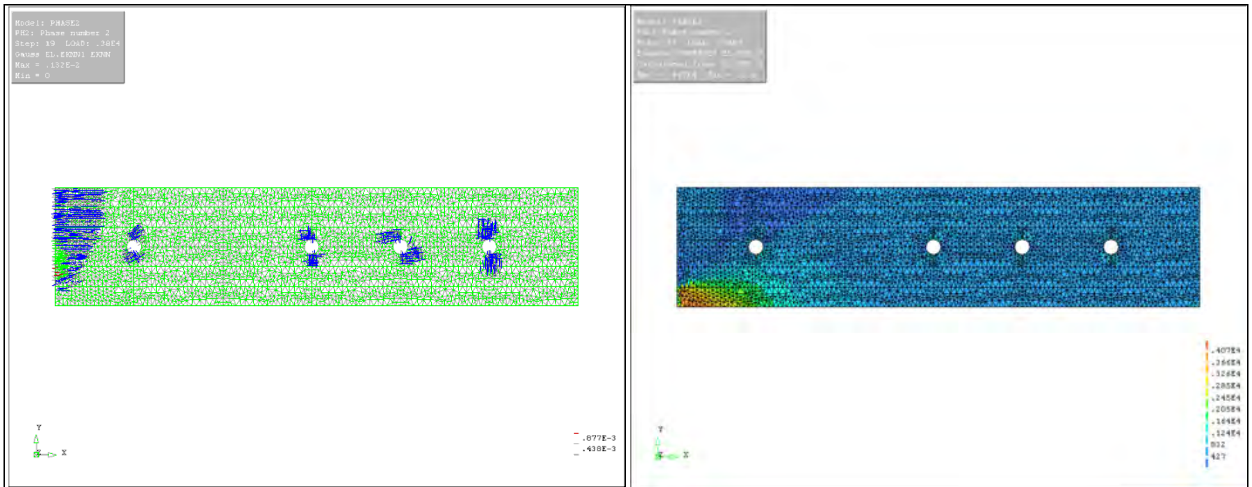

p_{impact} = 3,800 psi

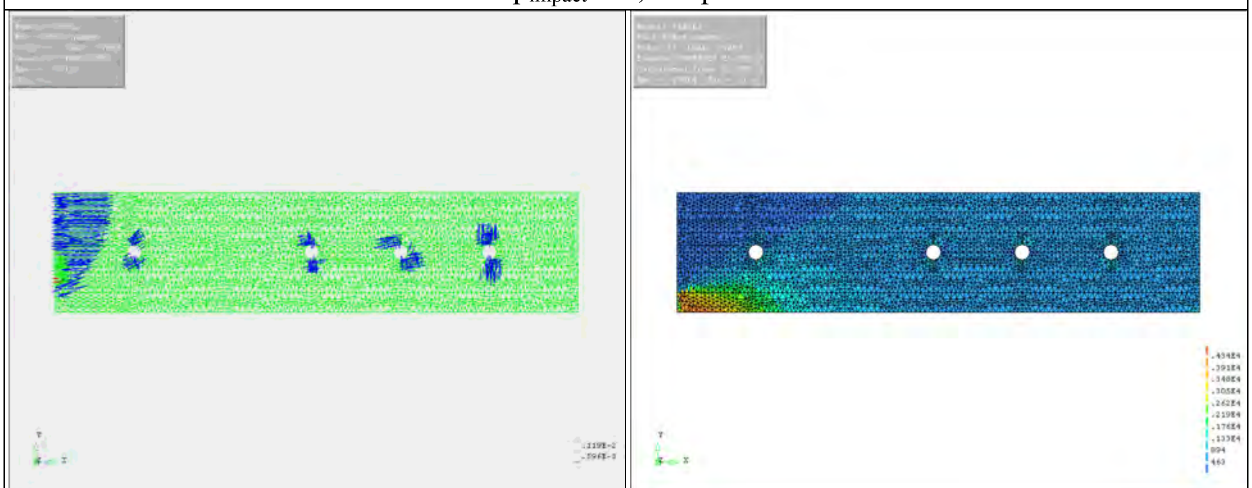

p_{impact} = 4,200 psi

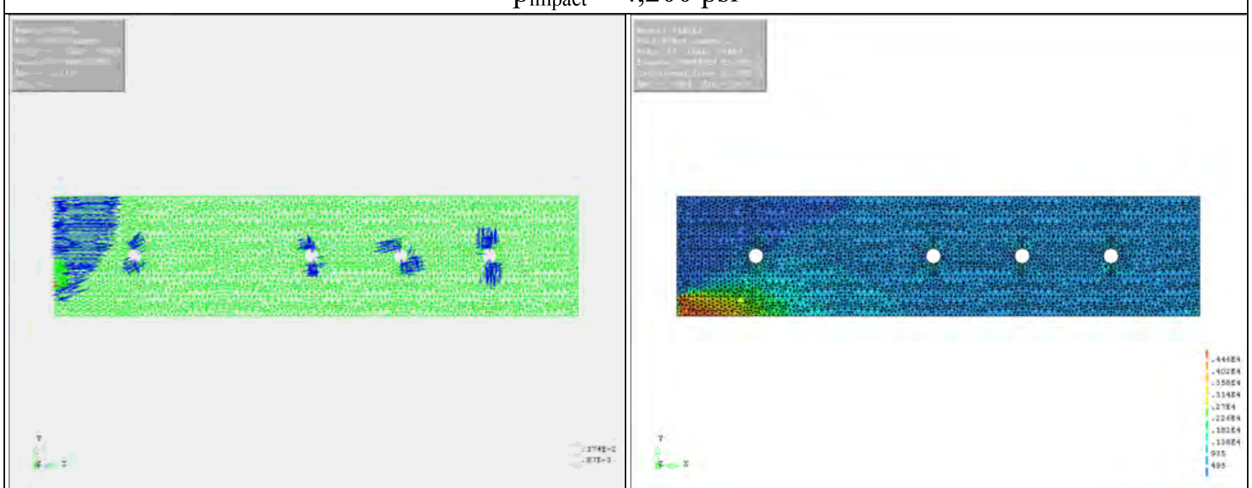

p_{impact} = 4,600 psi

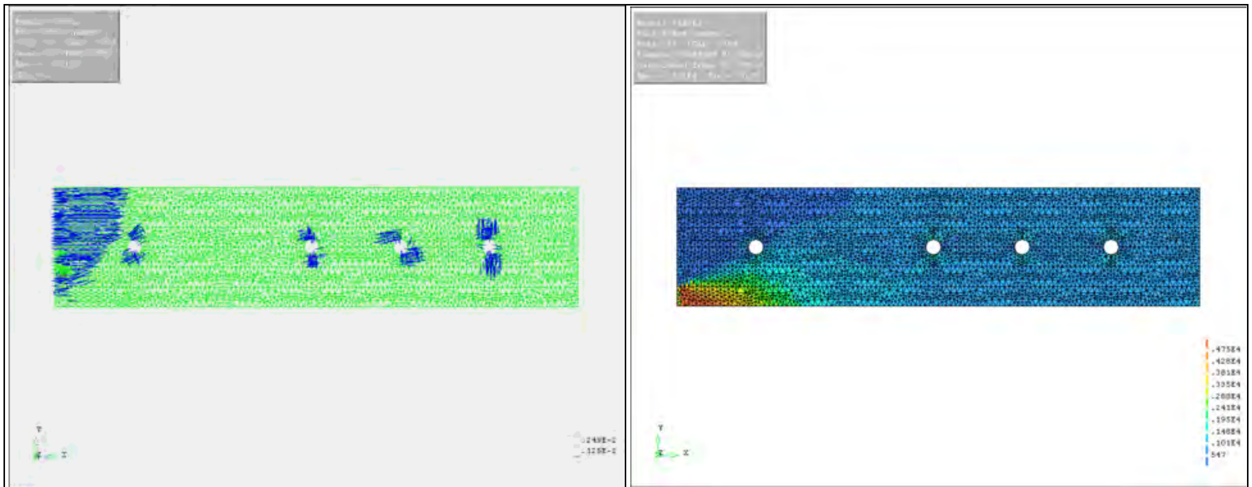

p_{impact} = 5,000 psi

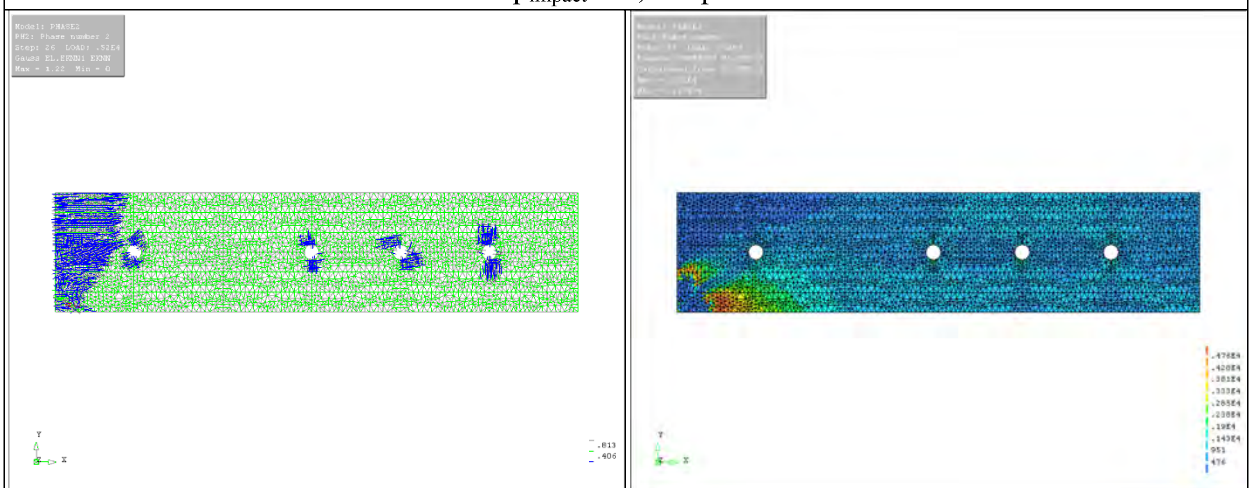

p_{impact} = 5,200 psi

Figure D-17 Crack Patterns & Von Mises Stress Variations of FE Model
(Edge Compression + Released Boundary Condition)

D.3 SIMULATION OF PROPOSED UNIT PANEL BEHAVIOR

This section presents direct comparison between analytical and experimental results with respect to load-displacement relationships. Measured displacements from the Chapter 5 unit panel static load experiments are compared with FE results in Figure D-19 to Figure D-22. Figure D-18 shows the locations of measured displacements for reference.

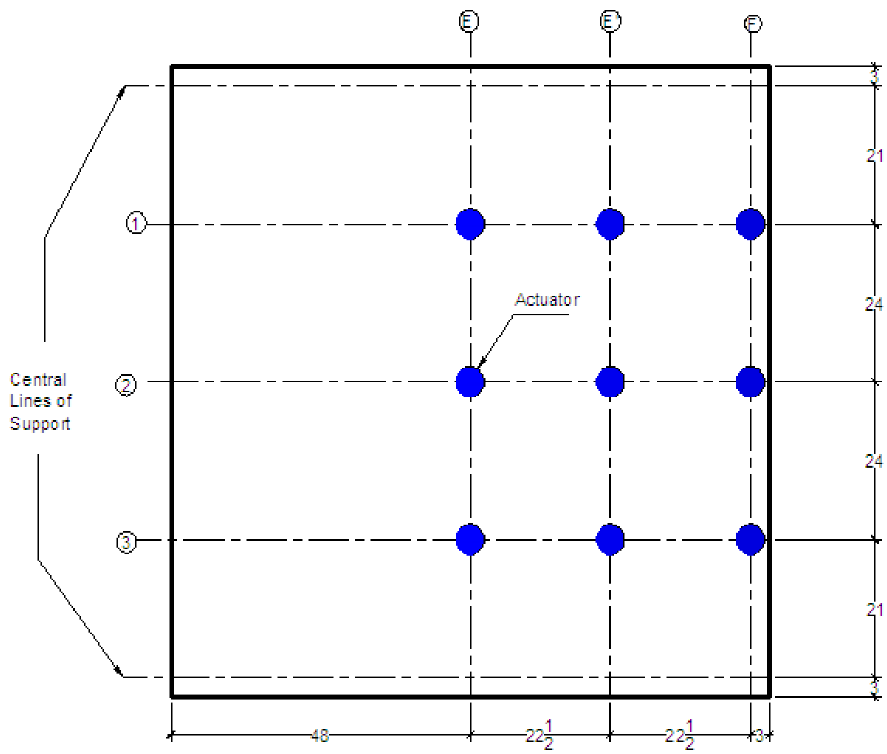

Figure D-18 Displacement Instrumentation Layout

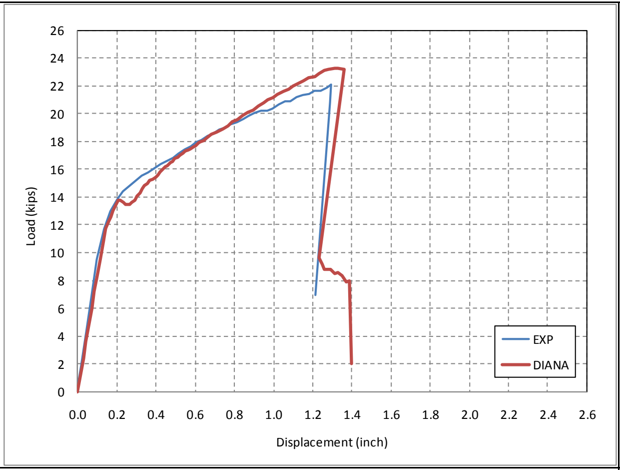

E-1

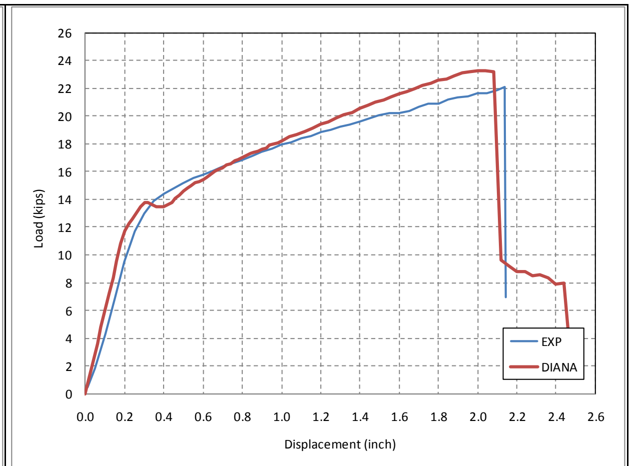

E-2

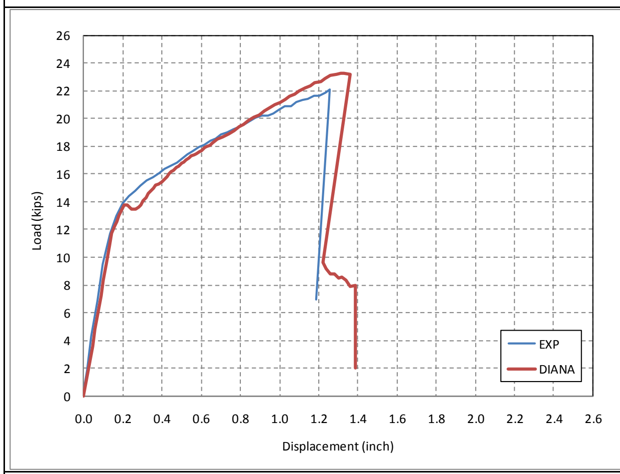

E-3

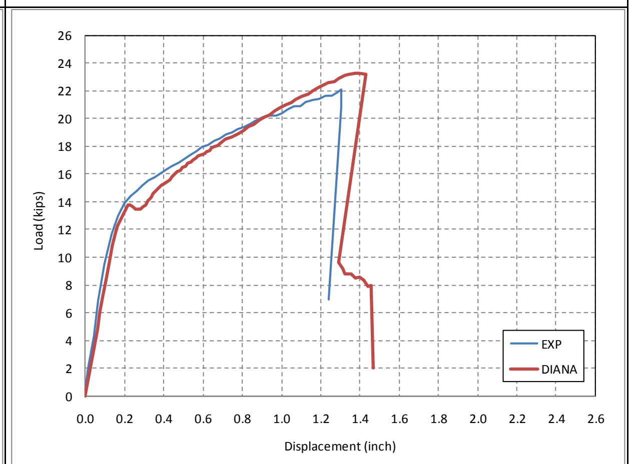

E’-1

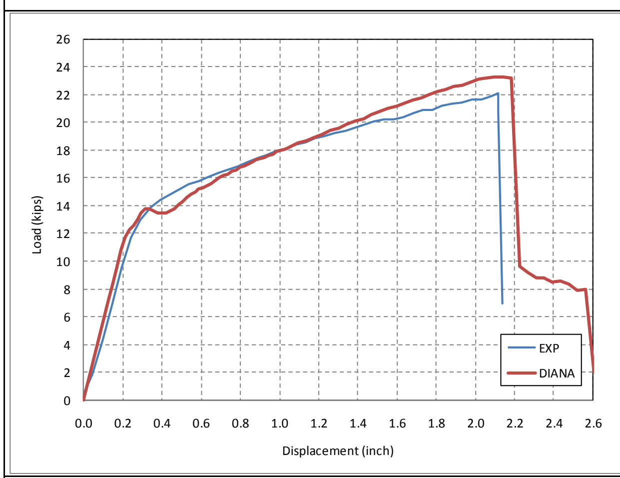

E’-2

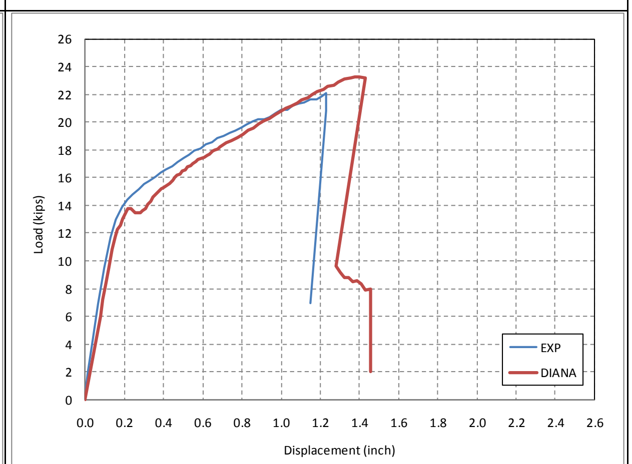

E’-3

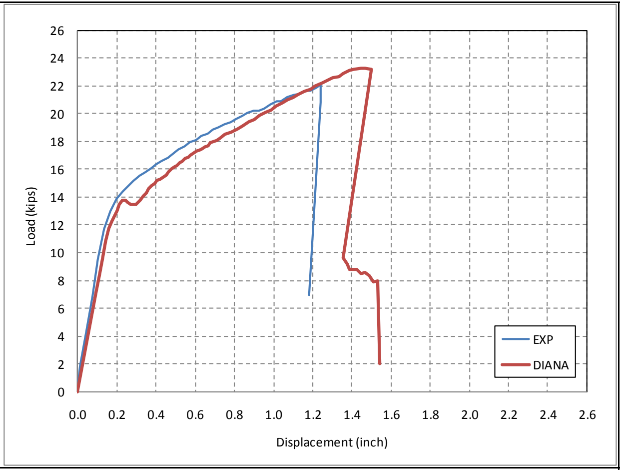

F-1

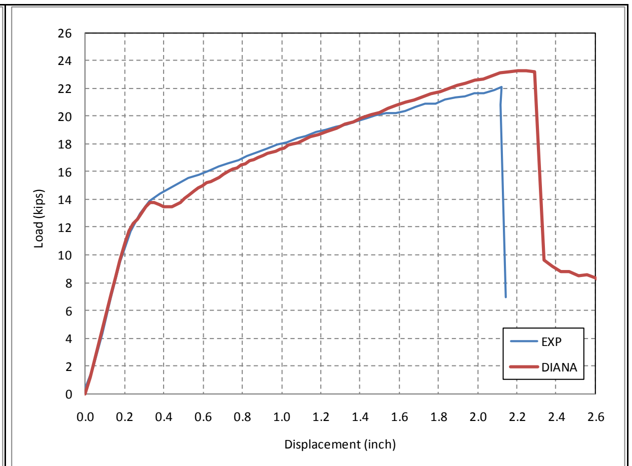

F-2

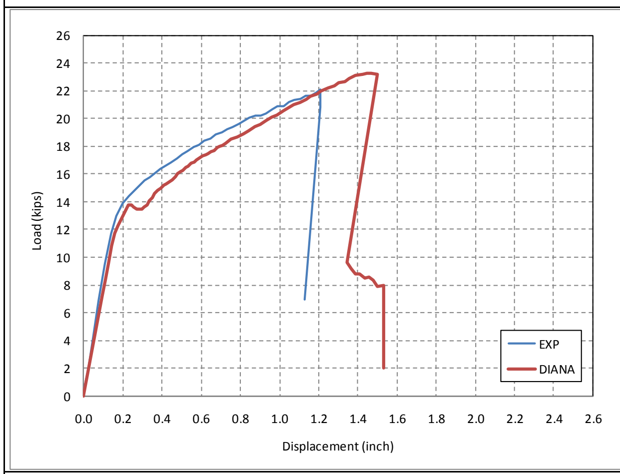

F-3

Figure D-19 Comparison of Load-Displacement for Panel ST-NC-SL

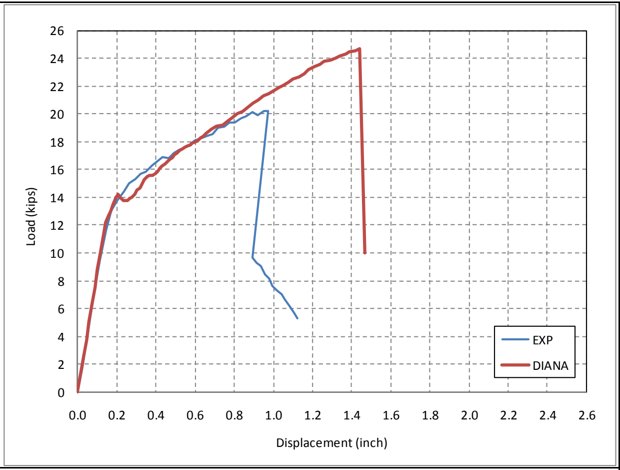

E-1

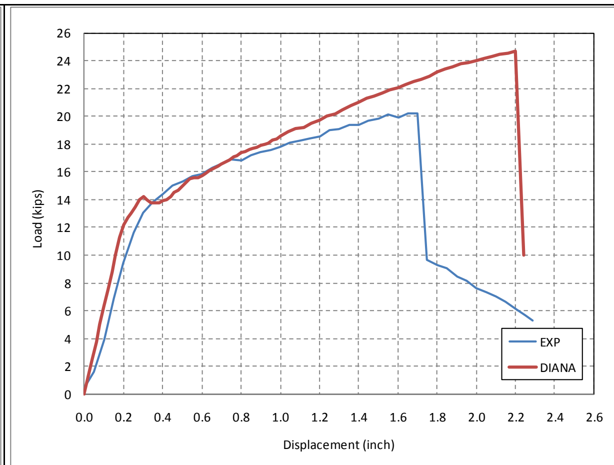

E-2

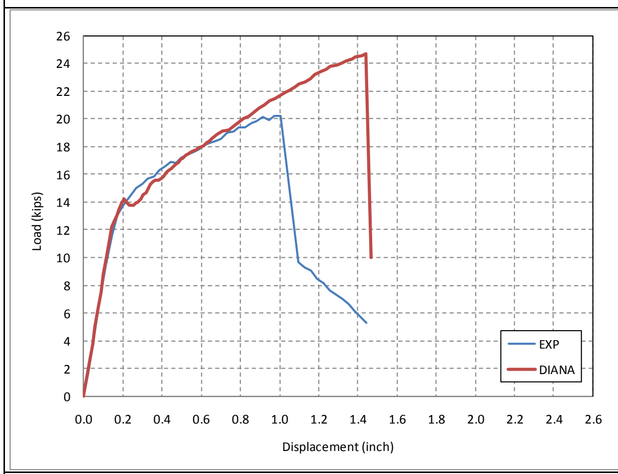

E-3

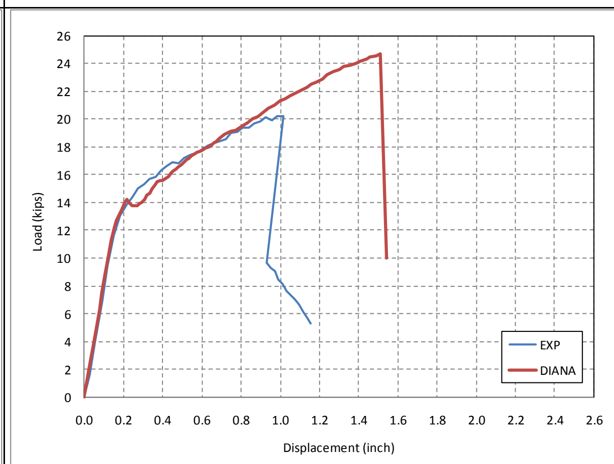

E’-1

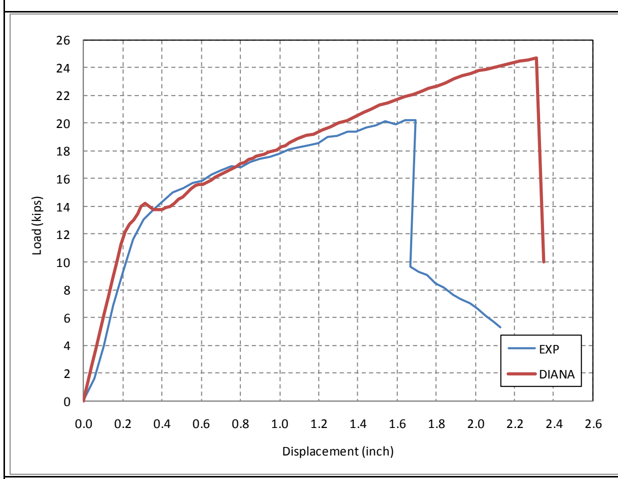

E’-2

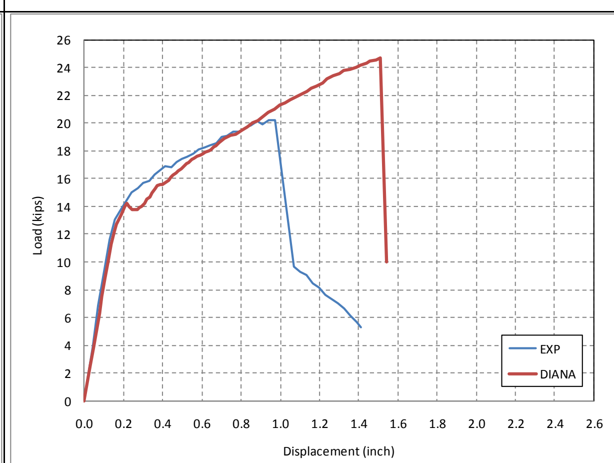

E’-3

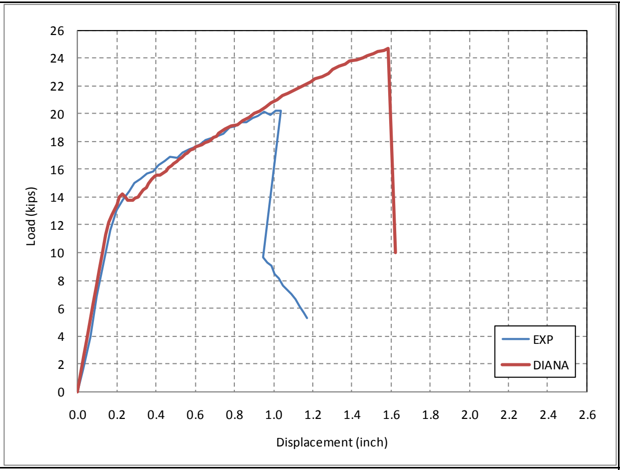

F-1

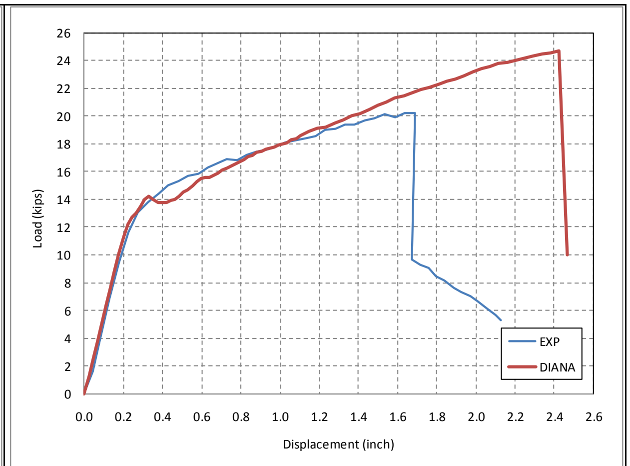

F-2

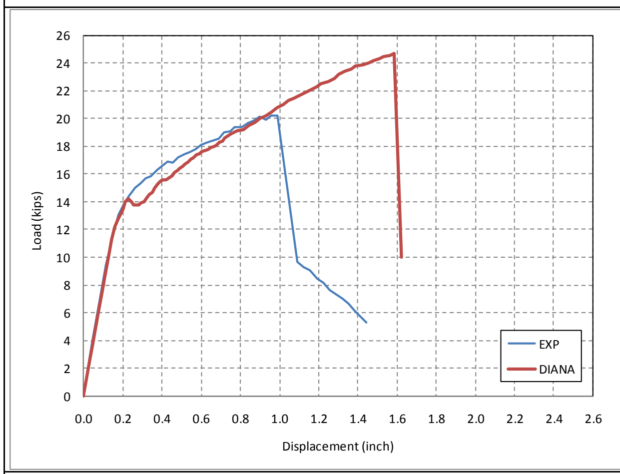

F-3

Figure D-20 Comparison of Load-Displacement for Panel ST-FRC-SL

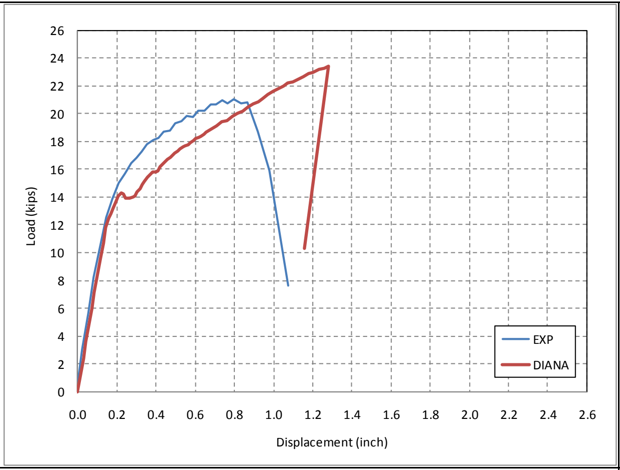

E-1

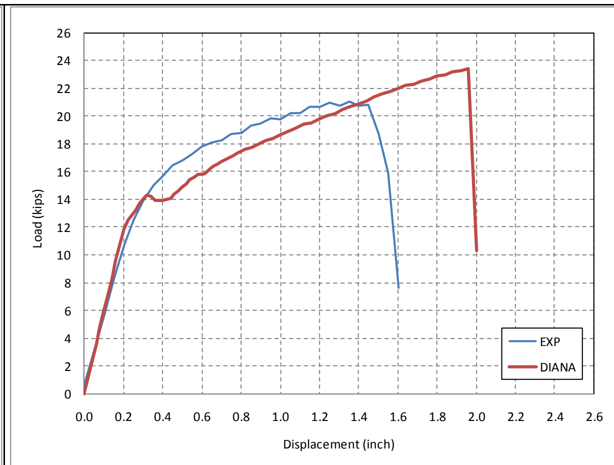

E-2

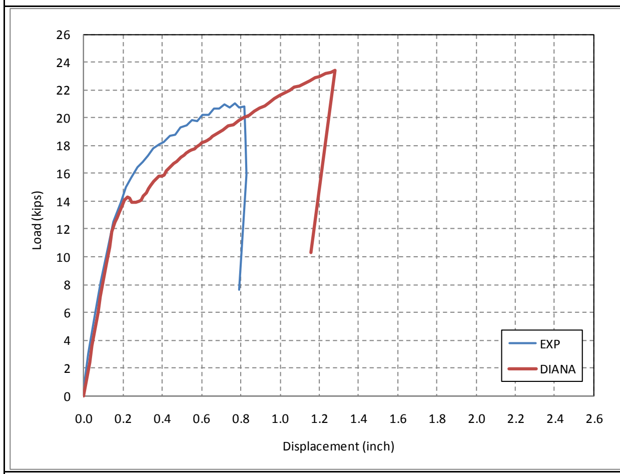

E-3

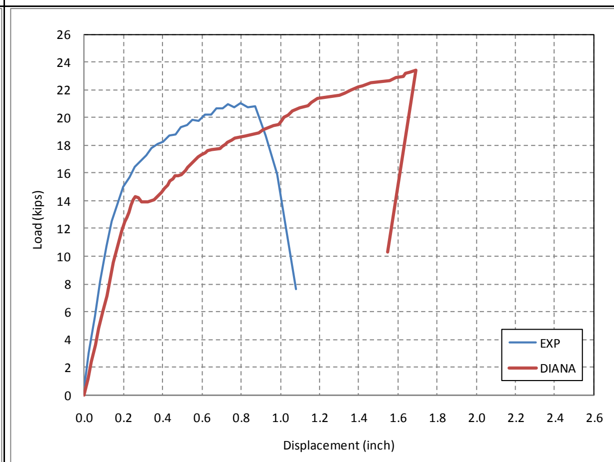

E’-1

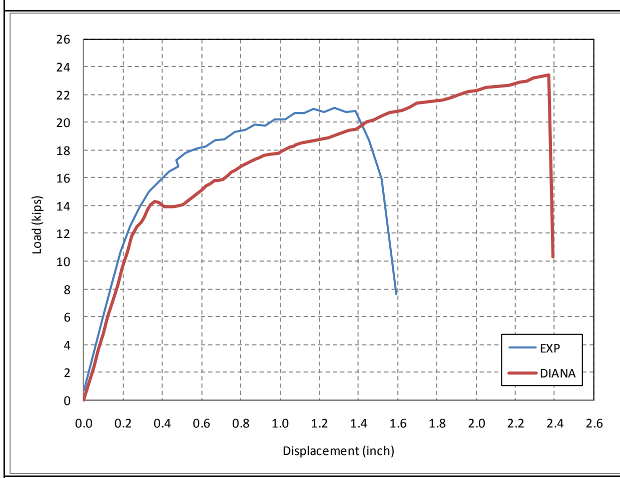

E’-2

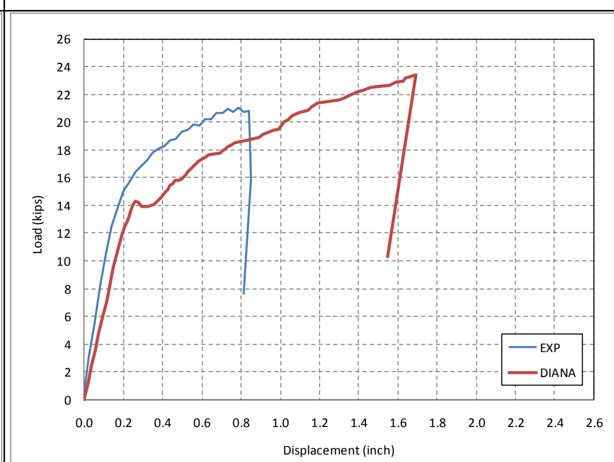

E’-3

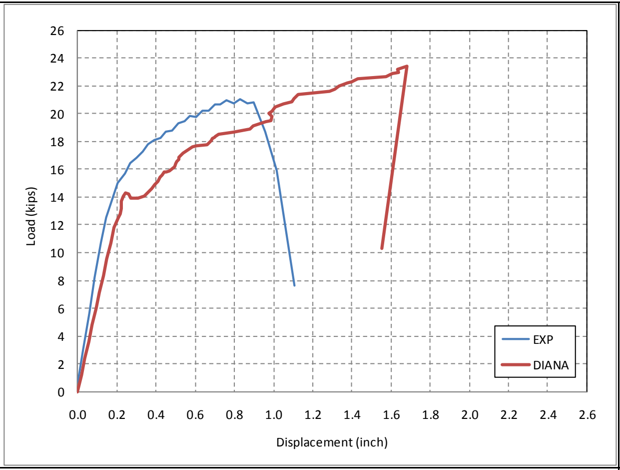

F-1

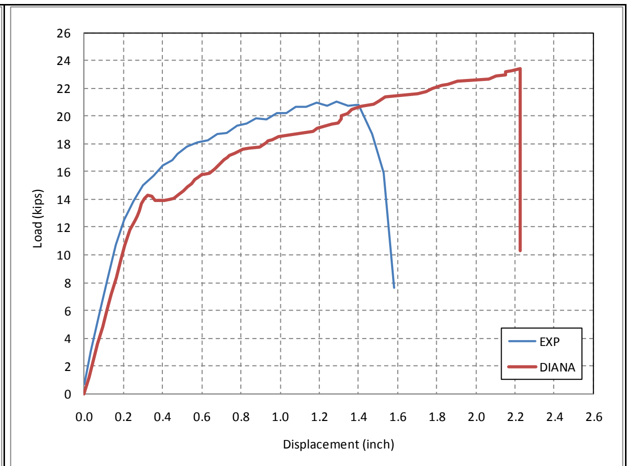

F-2

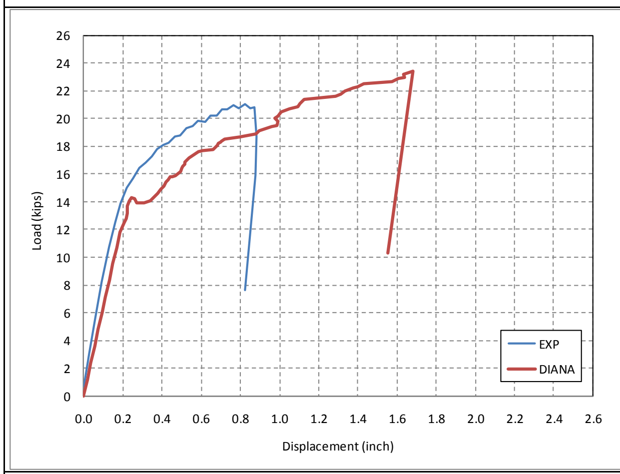

F-3

Figure D-21 Comparison of Load-Displacement for Panel CFRPT-NC-SL

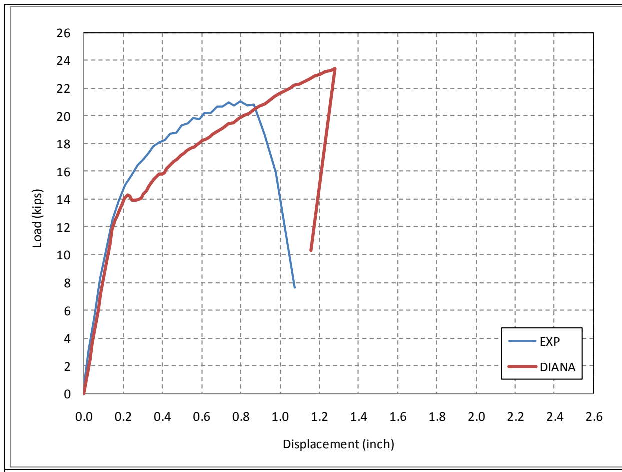

E-1

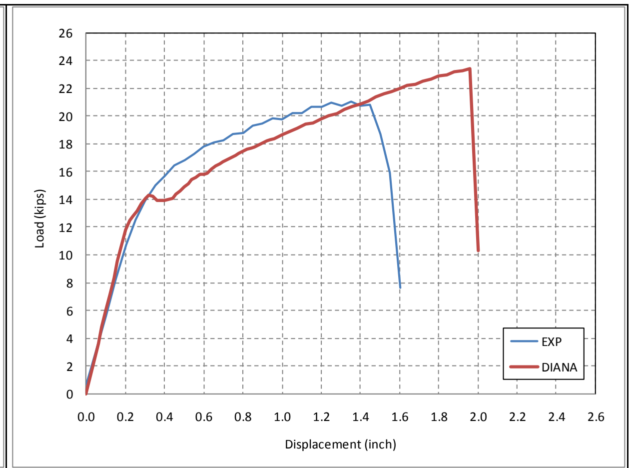

E-2

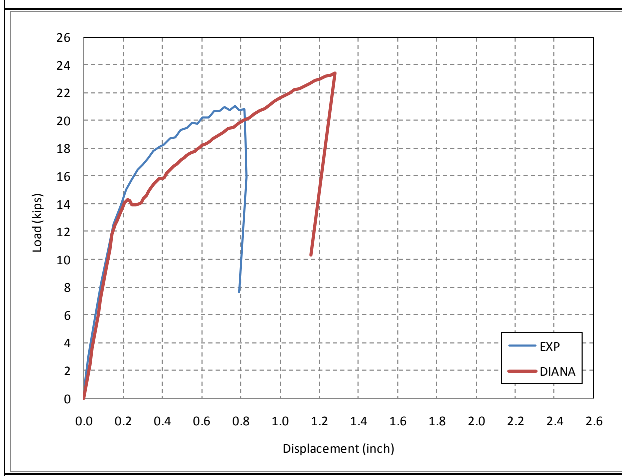

E-3

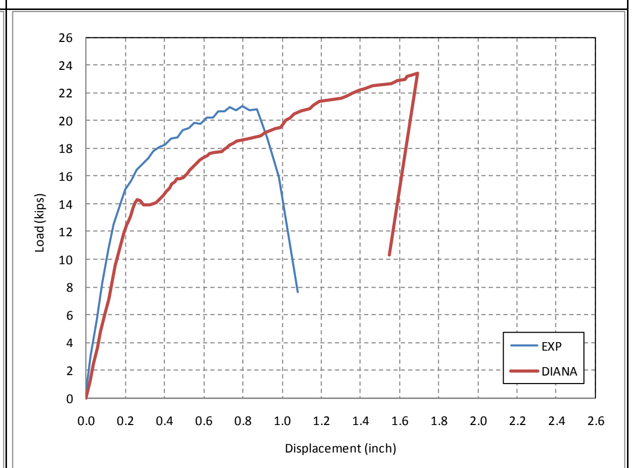

E’-1

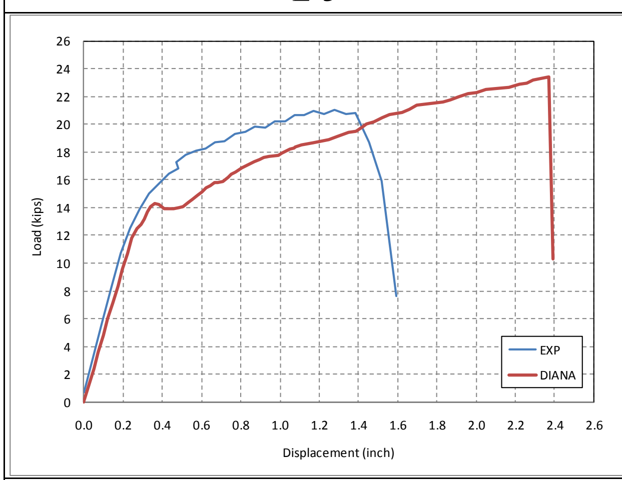

E’-2

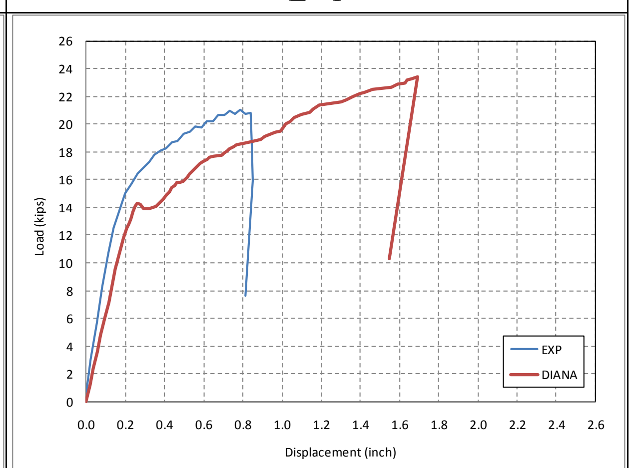

E’-3

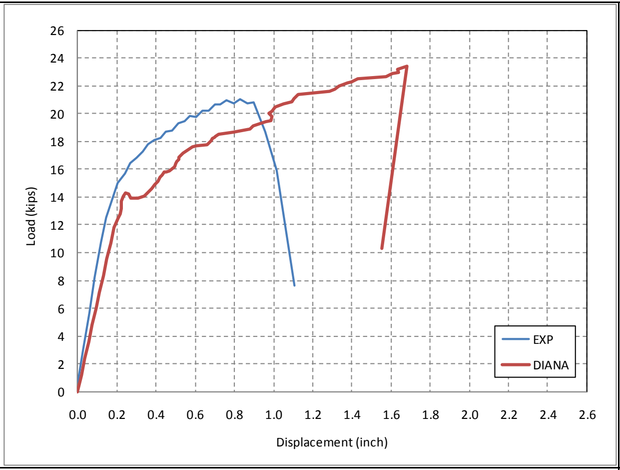

F-1

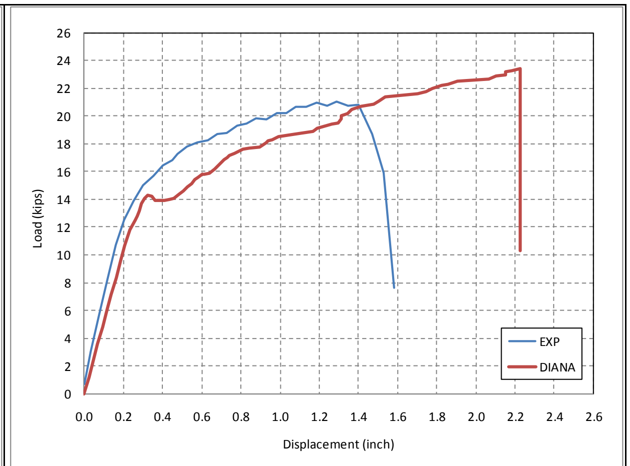

F-2

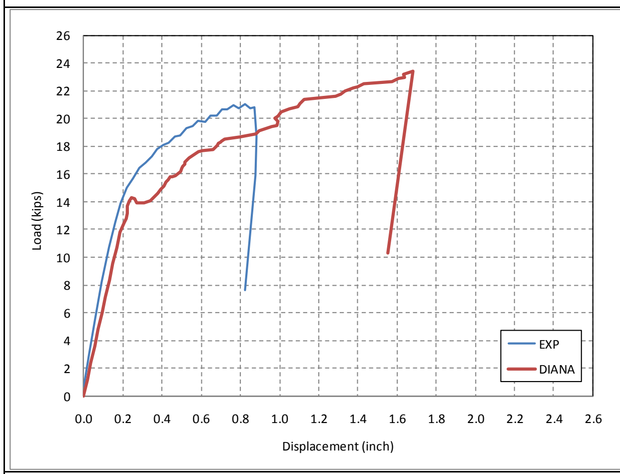

F-3

Figure D-22 Comparison of Load-Displacement for Panel CFRPT-NC-SL